Electrochemical Reduction of Trifluoroacetylpyridinium Salts for the Oxytrifluoromethylation of Styrenes

Isobel Wilson

A thesis submitted in partial fulfilment for the degree of Doctor of Philosophy

at

University College London

Christopher Ingold Building
University College London
20 Gordon Street
WC1H 0AJ

Declaration

I, Isobel Wilson, confirm that the work presented in this thesis is my own. Where information has been derived from other sources, I confirm that this has been indicated and acknowledged.

Abstract

New trifluoromethylation reactions are constantly being developed to keep up with the demand for fluorinated pharmaceuticals and agrochemicals. This PhD project was focused on developing an electrosynthetic trifluoromethylation reaction from cheap and readily available starting materials. The reasons for this were two-fold. One was to improve upon the current, traditional methods for trifluoromethylation that use harsh reaction conditions and toxic starting materials. The other was to demonstrate the ease and utility of electrosynthesis to the wider organic community. We focused our attention on using trifluoroacetylpyridinium salts as a source for the trifluoromethyl radicals, which we attempted to synthesise from trifluoroacetic anhydride and pyridine. Cyclic voltammetry showed that these salts underwent a single reduction process within the solvent window, making them good candidates for electrosynthesis. It was also demonstrated that upon reduction the trifluoroacetylpyridinium salts with electron withdrawing substituents on the pyridinium ring formed films on carbon-based electrodes. The films were studied to gain an insight into the fate of the radicals produced upon electron transfer with the trifluoroacetylpyridinium salts. Investigations involving x-ray photoelectron spectroscopy and redox probes revealed that the thickness and porosity of the films were dependent on the substituents on the trifluoroacetylpyridinium ring. This demonstrated a new method for attaching pyridine to an electrode. Once a detailed understanding of the electrochemical behaviour of the trifluoroacetylpyridinium salts had been established they were used for the successful electrosynthetic oxytrifluoromethylation of styrenes to afford trifluorophenylpropanone derivatives.

Impact Statement

Our investigations, which have focused on the electrochemical reduction of trifluoroacetylpyridinium salts, allowed us to develop methods for electrode modification and for producing trifluoromethyl radicals, both of which are novel (to the best of our knowledge). Inside academia, our new method of electrode coating allows for an alternative way to attach pyridine to an electrode surface. With further work, these modified electrodes could be used outside of academia for sensing, for example they could be used to detect contaminants in drinking water samples. Our new method for producing trifluoromethyl radicals uses cheaper starting materials than previous methods which is beneficial for further academic pursuits. The successful electrosynthetic oxytrifluoromethylation of styrene also contributes to the growing field of electrosynthesis and hopefully helps to demonstrate that electrosynthesis can be adopted with relatively little prior experience. This should help to encourage more people to adopt the technique, which can be cheaper and 'greener' than traditional methods. With future work and refinement of our technique for producing trifluoromethyl radicals electrochemically, this could eventually be incorporated into a multi-step synthesis. This would hopefully demonstrate the possibility for electrochemical trifluoromethylation being used in the pharmaceutical or agrochemical industries.

The best way for these impacts to be made possible, both outside and inside of academia, is through the communication of our findings in academic journals and via presentations at conferences. So far we have been able to present this work at two conferences (Electrochem, 2019 and RSC Organic Poster Symposium, 2020). We are also in the process of preparing some of our work to be published in an academic journal soon.

Table of Contents

Abbreviations

Abbreviation	Meaning
	Equation Symbols
[O]	Concentration of O
$[O]_0$	Concentration of O at Electrode Surface
$[O]_{bulk}$	Bulk Concentration of O
[R]	Concentration of R
$[R]_0$	Concentration of R at Electrode Surface
$[R]_{bulk}$	Bulk Concentration of R
A	Electrode Area
α	Transfer Coefficient
C	Concentration of Solution
C_0	Initial Concentration (Cottrell Equation)
D	Diffusion Constant
E	Potential
E_0	Cell Potential at Standard Conditions
E_A	Activation Energy
E_{eq}	Equilibrium Potential
E_p	Peak Potential
$E_{p/2}$	Half Peak Potential
F	Faraday's Constant
G	Gibb's Free Energy
i	Current
i_0	Exchange Current
i_p	Peak Current
j	Flux
k_0	Heterogeneous Rate Constant for Electron Transfer
k_{ox}	Oxidation Rate Constant
k_{red}	Reduction Rate Constant
η	Overpotential
n	Number of Electrons
O	Oxidised Species
Q	Charge
R	Gas Constant
R	Reduced Species
T	Temperature
v	Scan Rate (Cyclic voltammetry)
X'	Frequency Factor (Arrhenius Equation)

Abbreviation	Meaning
	Chemicals/materials
2-DHPP	2-Dihydropyridylpyridinium
4-DMAP	4-Dimethylaminopyridine
BDD	Boron doped diamond
CE	Counter electrode
CF_3	Trifluoromethyl
CF_3H	Fluoroform
CFCs	Chlorofluorocarbons
CsF	Caesium fluoride
DMF	Dimethylformamide
Fc	Ferrocene
FcMeOH	Ferrocene methanol
$[Fe(CN)_6]K_4$	Potassium ferrocyanide
H_2SO_4	Sulphuric acid
KHF_2	Potassium bifluoride
$LiClO_4$	Lithium perchlorate
MeCN	Acetonitrile
$MgCl_2$	Magnesium chloride
NaOH	Sodium hydroxide
Pyr	Pyridine
RE	Reference electrode
$RuCl_3$	Ruthenium chloride
$[Ru(NH_3)_6]Cl_3$	Hexaammineruthenium chloride
t-BuOK	Potassium *tert*-butoxide
TBAF	Tetra-n-butylammonium fluoride
$TBAPF_6$	Tetrabutylammonium hexafluorophosphate
TBHP	*tert*-Butyl hydroperoxide
TFAA	Trifluoroacetic anhydride
$TMSCF_3$	Trimethyl(trifluoromethyl)silane
TREAT-HF	Triethylamine trihydrofluoride
WE	Working electrode
ZnTFMS	Zinc trifluoromethanesulfinate
	Other
DFT	Density functional theory
et al.	*Et alia*
HSQC	Heteronuclear single quantum coherence
IR	Infrared
NMR	Nuclear magnetic resonance
SEM	Scanning electron microscopy
XPS	X-ray photoelectron spectroscopy

Acknowledgments

I would like to start by thanking my supervisors Prof. Katherine Holt and Prof. Michael Porter for their generous support and guidance over the last four years (or six years in Katherine's case). They have been kind and patient throughout this project and allowed me to explore and develop as a researcher in a positive environment. I would also like to thank Prof. Rob Palgrave for his guidance in all things XPS-related. I must thank James Strachan and Raif Mohamed for helping me find my way in the organic lab and never tiring from my constant stream of questions. A special thanks must be made to Emre Sener whose never ending supply of knowledge and baking has fuelled this PhD. I would also like to thank Hollie Packman who has always been at the end of the phone to discuss the highs and lows of pursuing a PhD. I cannot miss this opportunity to thank my parents, my Dad who visited me weekly for coffee in the Print Room Café and my Mum, who will always be an inspiration. Finally, I want to thank my boyfriend Nic Allen who has supported me throughout my entire academic journey at UCL and my dog Tag who has kept me company whilst I wrote this Thesis.

Chapter One - Introduction

The aim of this research project was to create a new, simple electrosynthetic trifluoromethylation reaction which is cheaper and more environmentally friendly compared to current techniques. By doing so, we hoped to highlight the benefits of electrosynthesis to the organic chemistry community, who can be somewhat sceptical of the technique. In an effort to find a cheap trifluoromethyl (CF_3) source, trifluoroacetic anhydride (TFAA) was reacted with pyridine in an attempt to create trifluoroacetylpyridinium salts, which are discussed in Chapter Three. We wanted to ensure that great care was taken to understand the electrochemistry involved in the electrosynthetic reaction, so the trifluoroacetylpyridinium salts were investigated using cyclic voltammetry and chronoamperometry. Through this it was discovered that some of the trifluoroacetylpyridinium salts modified the working electrode. It was thought that investigation of these modified electrodes would help us to gain an insight into the fate of the trifluoroacetylpyridinium salts after they had undergone electron transfer, and this work is discussed in Chapters Four and Five. The trifluoroacetylpyridinium salts were then used in an electrosynthetic oxytrifluoromethylation reaction of styrene, which is discussed in Chapter Six.

1.1 The Importance of Fluorine in Pharmaceuticals and Agrochemicals

Fluorine-containing compounds make up a very small proportion of natural products, despite this, it is estimated that approximately 25% of pharmaceuticals and 30-40% of agrochemicals contain at least one fluorine atom.[1] Moreover, 50% of blockbuster drugs (drugs that create more than $1 billion of global revenue, annually) are fluorinated. Clearly the demand for fluorinated products is high and these figures are predicted to increase, with the number of FDA approved, fluorine-containing drugs increasing year on year.[2, 3]

Fluorinated pharmaceuticals are highly popular due to the increased lipophilicity and metabolic stability that fluorination brings to a compound. Lipophilicity (LogP) is a measure of how likely a compound is to dissolve in a lipid (i.e. fat). Increasing the

lipophilicity of a drug makes it easier for the compound to pass through cell membranes, giving faster rates of absorption/transportation around the body. However, it is a common misconception that fluorinating a compound will *always* increase lipophilicity, in fact fluorination of alkanes has the opposite effect due to the strong electron withdrawing effects of fluorine.[4] For lipophilicity to increase, fluorination needs to occur on an aryl ring or adjacent to a π-system or heteroatom.[5] This is because the lipophilicity will only increase if introducing a fluorine atom reduces the overall polarizability of the molecule, making it more soluble in an organic medium than an aqueous one.

Increasing the metabolic stability of a drug means that it can survive for longer in the body and reach the designated site for drug delivery before it is broken down into alternative components.[6] The most common reason for incorporating fluorine into a molecule is to reduce the rate of oxidative metabolism.[7] Another common misconception in pharmacokinetics is to think that the replacement of a C-H bond with C-F prevents metabolic oxidation. In reality it is that the bond energy and heat of formation for a C-F bond are greater and so attack at that position is unfavourable.[7]

Clearly the incorporation of fluorine in drugs is highly beneficial, and so it is not a surprise that fluorine is found in a wide array of medicines used for: anticancer treatment, the central nervous system, the cardiovascular system, infectious diseases, diabetes and many more.[8, 9] Trifluoromethyl containing drugs are among the top 200 largest selling pharmaceutical products, with Prozac probably being the most widely known and sold.[10]

Pesticides contain fluorine for a similar reason as pharmaceuticals, an increase in lipophilicity improves the ability of the drug to traverse cell membranes in a plant. A large proportion of pesticides are used as enzyme inhibitors, and so it is important for the pesticide to be able to penetrate cell walls in order for them to be effective.[11]

Currently, the world is facing a growing population - it is estimated that the global population will reach 9.6 billion by 2050.[12] Thus, it is now more important than ever to

be able to keep up with demands for food and healthcare. In order to provide these necessities, it is foreseeable that the need for fluorinated compounds will increase. Thus, owing to the high demand and popularity of trifluoromethylated compounds a vast amount of research has gone into trifluoromethylation reactions over the last three decades.[13] The types of reactions focused on can largely be categorized into three areas: nucleophilic, electrophilic and radical trifluoromethylation reactions. Intuitively, they are classed as these types of reactions based on the character of the trifluoromethyl group during reaction, whether it is a nucleophilic CF_3^- anion, electrophilic CF_3^+ cation or radical $CF_3^\bullet$ species.

1.2 Nucleophilic Trifluoromethylation

Nucleophilic trifluoromethylation reactions are some of the most commonly used trifluoromethylation reactions. In nucleophilic trifluoromethylation reactions the trifluoromethyl source is reduced to give a CF_3^- anion. However, the free CF_3^- anion can be unstable, due to a lack of vacant orbitals available to delocalize the negative charge, and so it is quick to decompose to a single F^- anion and a $:CF_2$ carbene species.[14, 15] Thus, as will be seen in the following examples, additional reagents or reaction conditions are often required to stabilise the CF_3^- anion before it is transferred to the desired substrate.

1.2.1 Fluoroform

Fluoroform (CF_3H, **1**) is a by-product of the Teflon industry, it is a synthetic greenhouse gas (with an atmospheric lifetime of ~250 years) and has an estimated global warming potential 11,700 times greater than CO_2.[16] Thus, reactions which consume fluoroform are environmentally favourable. When fluoroform is used in trifluoromethylating reactions it is deprotonated to form a CF_3^- anion. The majority of fluoroform trifluoromethylations seen in the literature are carried out in dimethylformamide (DMF), as the CF_3^- anion reacts at the carbonyl C-atom to form a stable hemiaminolate adduct. However, this hemiaminolate species is also relatively unstable and so must be kept at low temperatures and used in reactions relatively quickly (1-2 h). The

implementation of this method can be seen in the work done by Saint-Jalmes *et al.* in the reaction of fluoroform with aldehydes, to form trifluoromethylated alcohols (**2**) (Scheme 1, a).[17]

An alternative reaction to the production of the hemiaminolate adduct is a method called 'cupration' which involves the formation of a Cu-CF_3 species. Cupration is advantageous over the hemiaminolate method as it can be performed at room temperature, and, when stabilized with triethylamine trihydrofluoride (TREAT-HF) the Cu-CF_3 species can be stored for 1-2 days at room temperature.[15] Grushin *et al.* has demonstrated this method in two reactions seen here (Scheme 1, b and c).[18, 15] In both examples, copper chloride (CuCl) and potassium *tert*-butoxide (*t*-BuOK) are reacted in the presence of phenanthroline to form a dialkoxy cuprate anion which is reacted with fluoroform, providing the desired Cu-CF_3 species. This acts as the CF_3 transfer agent towards the substrate, either an arylboronic acid (**3**) or an aryliodide (**4**), in order to obtain a trifluoromethylated aromatic product (**5**).

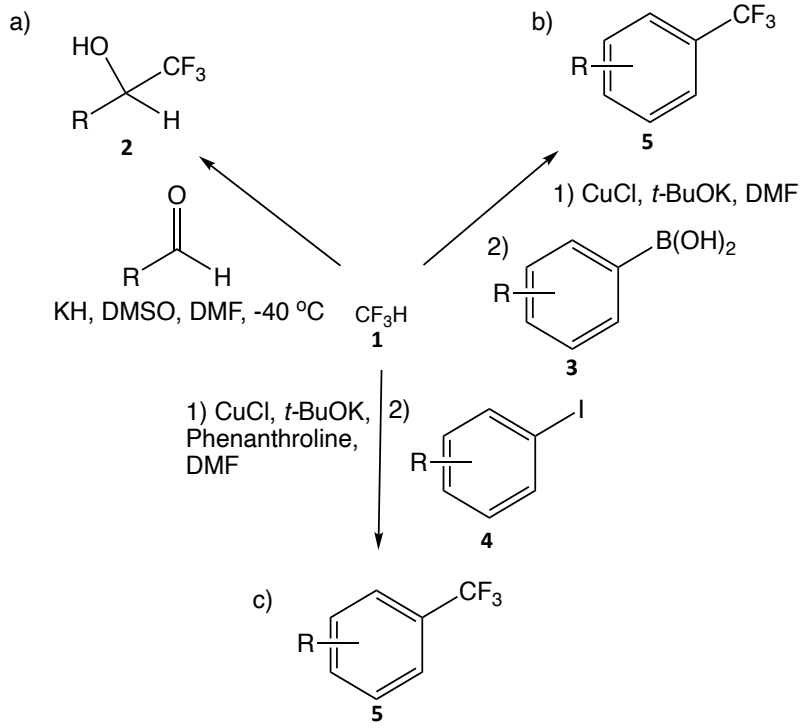

Scheme 1: Nucleophilic trifluoromethylation reactions using fluoroform as the CF_3 transfer reagent. Work carried out by: a) Saint-Jalmes et al.;[17] b) and c) Grushin et al.[18, 15]

1.2.2 Ruppert-Prakash Reagent

Trifluoromethyltrimethylsilane (i.e. $TMSCF_3$ or Ruppert-Prakash reagent, **6**) was originally synthesised by Ruppert's group in 1984 as part of a wide array of trifluoromethylated silanes.[19] It wasn't until 1989 when Prakash reported its use in the trifluoromethylation of carbonyl compounds that it became known as a nucleophilic trifluoromethylating reagent.[20] Since then, it has become very popular and can be applied to a wide variety of transformations.[21] Originally Ruppert synthesised $TMSCF_3$ using bromotrifluoromethane (Halon), a substance which was originally developed by the U.S Army as a fire suppressant, but this reagent is now banned due to its high toxicity. Recent syntheses of Ruppert-Prakash reagents use fluoroform and trimethylsilyl chloride as an alternative, less toxic reaction.

It is common for reactions using the Ruppert-Prakash reagent to be initiated by a fluoride species i.e. potassium bifluoride (KHF_2), caesium fluoride (CsF) or tetrabutylammonium fluoride (TBAF) (Scheme 2). These compounds provide fluoride ions which react with the Ruppert-Prakash reagent, cleaving the Si-CF_3 bond, to produce a CF_3^- anion.

For some of the reactions seen here (Scheme 2 a and b)[22,23] only a small amount of the initiator is needed to 'kick start' the reaction, making them highly efficient. In the case of the conversion of dinucleotide phosphorofluoridite compounds (**7**) to dinucleoside trifluromethylphosphonate compounds (**8**) (Scheme 2a), once the CF_3^- anion was produced it displaced the fluorine atom in the P-F bond. The displaced fluoride ions were then able to continue the catalytic cycle, generating CF_3^- anions from the Ruppert-Prakash reagent. Another trifluoromethylation reaction that uses CsF as an initiator is the reaction of carbonyl bonds, undertaken by Shreeve *et al.*, (Scheme 2, b).[23] Here, this group reacted esters, aldehydes and ketones with the Rupert-Prakash reagent to form trifluoromethylated alcohols (**9**). In these examples, after initiation by CsF, a trifluoromethylated oxyanion intermediate was formed which then catalysed the subsequent reactions.

For the reaction of imines (**10**, **11**) (Scheme 2, c)[24, 25] acidic conditions were required as well as KHF_2 as the fluoride ion initiator.[26] This was because unactivated imines will not react with the Ruppert-Prakash reagent alone and so they must first be transformed into the iminium cation. Following the formation of the iminium cation, the hydrodifluoride anion acted as a Lewis base activator with respect to the Ruppert-Prakash reagent which allowed concerted transfer of the CF_3 group to the iminium cation, yielding the desired trifluoromethyl-amines (**12**, **13**).

TBAF is also a common source of fluoride ions, and was used as an initiator in the work by Langlois *et al.* in the trifluoromethylation of aromatic thiones (**14**) using the Ruppert-Prakash reagent.[27] Unlike the previous examples that used catalytic amounts of the fluoride initiator, Langlois employed TBAF.H_2O in excess. This meant there was an abundant source of protons in solution to rapidly quench the intermediate anions formed from both thiophilic and carbophilic attack of the CF_3^- anion. The major product of the reaction was the trifluoromethyl sulfide (**15**). This was because during the reaction, a nucleophilic intermediate was formed between TBAF and the Ruppert-Prakash reagent that had both hard and soft characteristics, but, the soft character predominated which was why the trifluoromethyl sulfide was the major product and the trifluoromethylated thiol (**16**) was the minor product. However, despite using TBAF in excess the yields of both products were not substantially high.

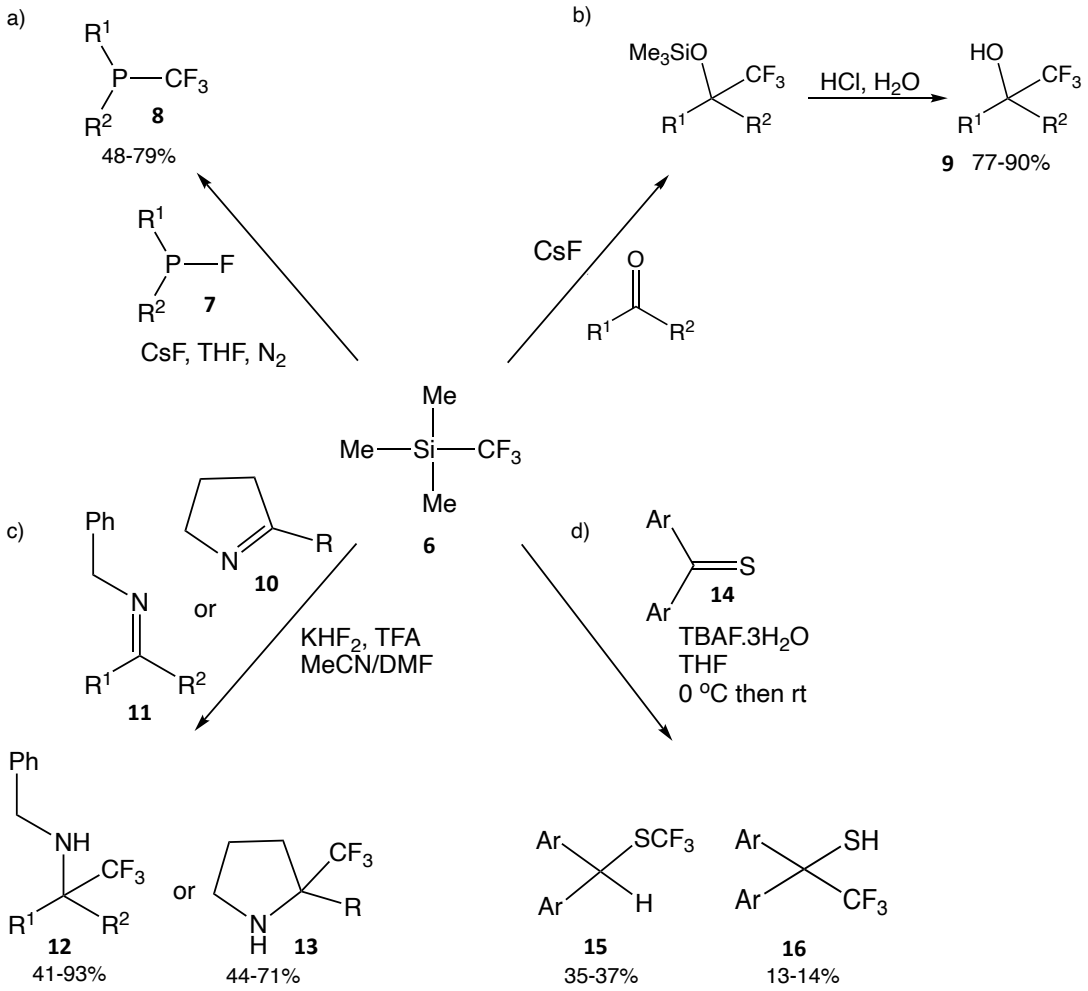

Scheme 2: Nucleophilic trifluoromethylation reactions using the Ruppert-Prakash reagent as a source of CF_3. Work carried out by: a) Michalski et al.;[22] b) Shreeve et al.;[23] c) Mikhailiuk et al.[24] and Röschenthaler et al.;[25] d) Langlois et al.[27]

1.3 Electrophilic Trifluoromethylation

As stated before, electrophilic trifluoromethylations involve the transfer of a 'CF_3^+' species. However, in reality it is very difficult to generate the CF_3^+ cation via a chemical reaction due to a lack of available electrons that would allow for hyperconjugation, and thus stabilise the CF_3^+ molecule. Hence, many reactions that are classed as electrophilic trifluoromethylations do not actually involve the CF_3^+ cation. Instead, the CF_3 group is thought to act as an electrophile when it is positively polarised by a more electronegative group.[13] There are two main types of electrophilic trifluoromethylation reagents, Togni's reagent (**17, 18**) and Umemoto's reagent (**19**).

1.3.1 Togni's Reagent

In 2006 Togni *et al.* developed a group of hypervalent iodine species that could be used as trifluoromethylation reagents. Of the many hypervalent iodine species synthesised the two that have dominated the most in terms of trifluoromethylation reactions are: 3,3-dimethyl-1-(trifluoromethyl)-1,2-benziodoxole (Scheme 3, **17**) and 1-trifluoromethyl-1,2-benziodoxol-3-(1H)-one (Scheme 3, **18**).[28] In the reaction of either species **17** or **18**, the I-O bond is broken to form a iodonium cation which is then reacted with the substrate before reductive elimination occurs, in which the CF_3 group is transferred to yield the trifluoromethylated product.

Togni demonstrated the ability for reagent **17** to act as an electrophilic trifluoromethylation reagent in the reaction of hydrogen phosphates (**19**) and S-hydrogen phosphorothioates (**20**), to yield trifluoromethyl phosphates (**21**) and S-(trifluoromethyl) phosphorothioates (**22**) (Scheme 3, a and b).[29, 30] Both reactions required activation of Togni's reagent **17** via protonation from the substrate. It can be seen that the S-hydrogen phosphorothioates reacted to give much higher yields than the hydrogen phosphates. This was because, typically, the S-hydrogen phosphorothioates are more acidic and so the initial protonation happened at a faster rate. These reactions are simple and effective in the sense that an additional initiator was not required to activate Togni's reagent, however the reaction is limited as isolation of a pure product was almost impossible due to decomposition of the compounds during chromatographic purification.

In the work done by MacMillan *et al.* for the trifluoromethylation of aldehydes to form α-CF_3 aldehydes (**23**) (Scheme 3, c)[31] Togni's reagent had to be activated by a Lewis acid in order for trifluoromethylation to be successful (without a Lewis acid present a yield of only 14% was seen). Activation occurred when the Lewis acid cleaved the I-O bond forming an electrophilic iodonium salt and an O-CuCl bond. Additionally, MacMillan was also able to include an imidazoline catalyst which reacted with the aldehyde substrates to form a chiral enamine. The formation of this chiral enamine

allowed for enantioselective C-CF_3 bond formation with up to 96% *ee* in the final products.

Togni also used a Lewis acid to activate reagent **18** for the trifluoromethylation of alcohols to form ethers (**24**) (Scheme 3, d).[32] In this strategy the Lewis acid formed a zinc dicarboxylato complex (coordinating between 2 molecules of reagent **18**). However, it is unclear whether the trifluoromethylation mechanism followed is similar to the previous examples, whereby the alcohol attacked at the iodine position before reductive elimination occurred, or whether it followed an S_N2 – type process.

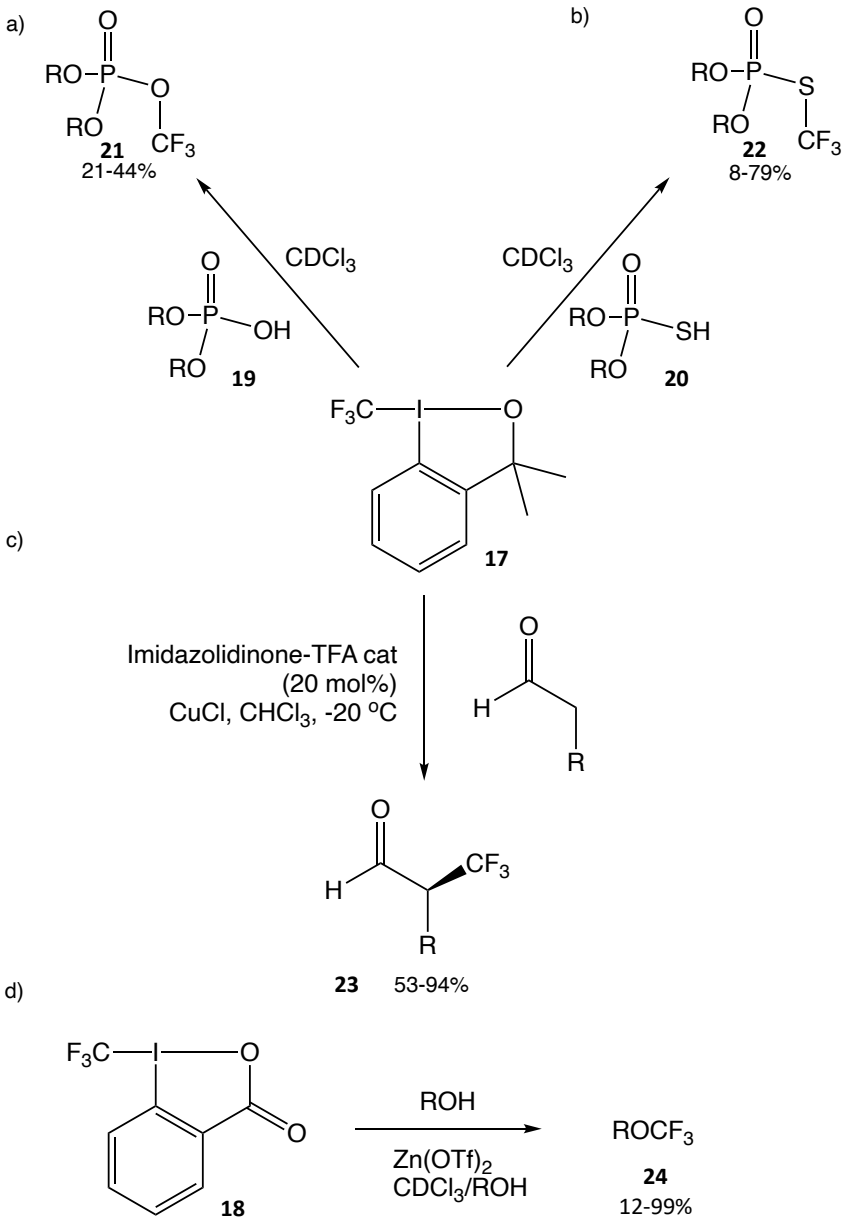

*Scheme 3: Electrophilic trifluoromethylation reactions using 3,3-dimethyl-1-(trifluoromethyl)-1,2-benziodoxole (**17**). Work done by: a) and b) Togni et al.*[29, 30] *c) MacMillan et al.*[31] *d) Electrophilic trifluoromethylation done by Togni et al. using 1-trifluoromethyl-1,2-benziodoxol-3-(1H)-one (**18**).*[32]

1.3.2 Umemoto's Reagent

In 1993 Umemoto *et al.* developed a series of (trifluoromethyl)dibenzothio-, -seleno- and -tellurophenium salts to be used as electrophilic trifluoromethylation reagents.[33] Later, in the early 2000's they also managed to develop O-(trifluoromethyl)dibenzofuranium salts (Figure 1).[34]

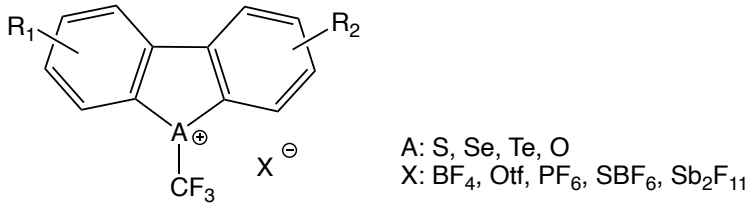

Figure 1: Series of trifluoromethyl)dibenzothio-, -seleno-, -tellurophenium- and -furanium salts developed by Umemoto to be used as electrophilic trifluoromethylating reagents.

Umemoto reported that the reactivity of the salt differed depending on the identity of the cationic species A, bonded to the CF_3 group. For example, when reacted with an alkyl amine, the furanium-salt produced a N-CF_3 product, whereas the thio-salt decomposed to form fluoroform. Thus, Umemoto proposed that the furanium-salt undertook a S_N2 type reaction mechanism in which a CF_3^+ or $CF_3^{\delta+}$ species was transiently formed; while the thio-salt undertook a single electron-transfer type mechanism to produce a $CF_3^{\bullet}$ radical.[34, 35] The reasons for these differences in the reaction mechanisms was thought to be due to the electronegativity of the hetero atom bonded to the CF_3 group. Thus, because oxygen is more electronegative than sulphur, it was capable of generating the CF_3^+ cation. This led to Umemoto claiming that O-(trifluoromethyl)dibenzofuranium salts are the only 'true' source of CF_3^+ cations.

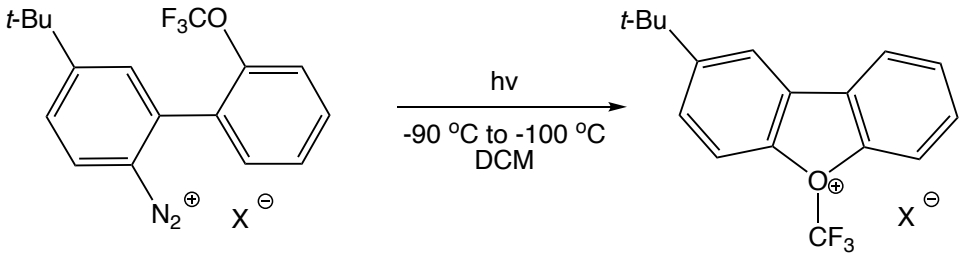

X = SbF_6, Sb_2F_{11}, PF_6, BF_4 32-93%

Scheme 4: Synthesis of O-(trifluoromethyl)dibenzofuranium salts via photodecomposition of diazonium salt in DCM with a high-pressure Hg lamp.[34, 35]

Synthesis of furanium-salts is not easy, they require low temperature and high pressure to be formed (Scheme 4) and once synthesised they must be reacted quickly at low temperatures as they are thermally unstable. It was observed that the reactivity of the furanium-salts increased as the nucleophilicity of the counterion decreased. For the counterions tested, the nucleophilicity decreased in order of BF_4^-<PF_6^-<SbF_6^-<$Sb_2F_{11}^-$. Based on these facts, SbF_6^- was chosen as the counterion, and the furanium-salt (**25**) was synthesised in situ before reacting with a range of amine and alcohol type substrates (Scheme 5). Reaction of this 'true' electrophilic trifluoromethylation reagent by Umemoto has provided O- and N-trifluoromethylation (**26**-**29**) (Scheme 5).[13]

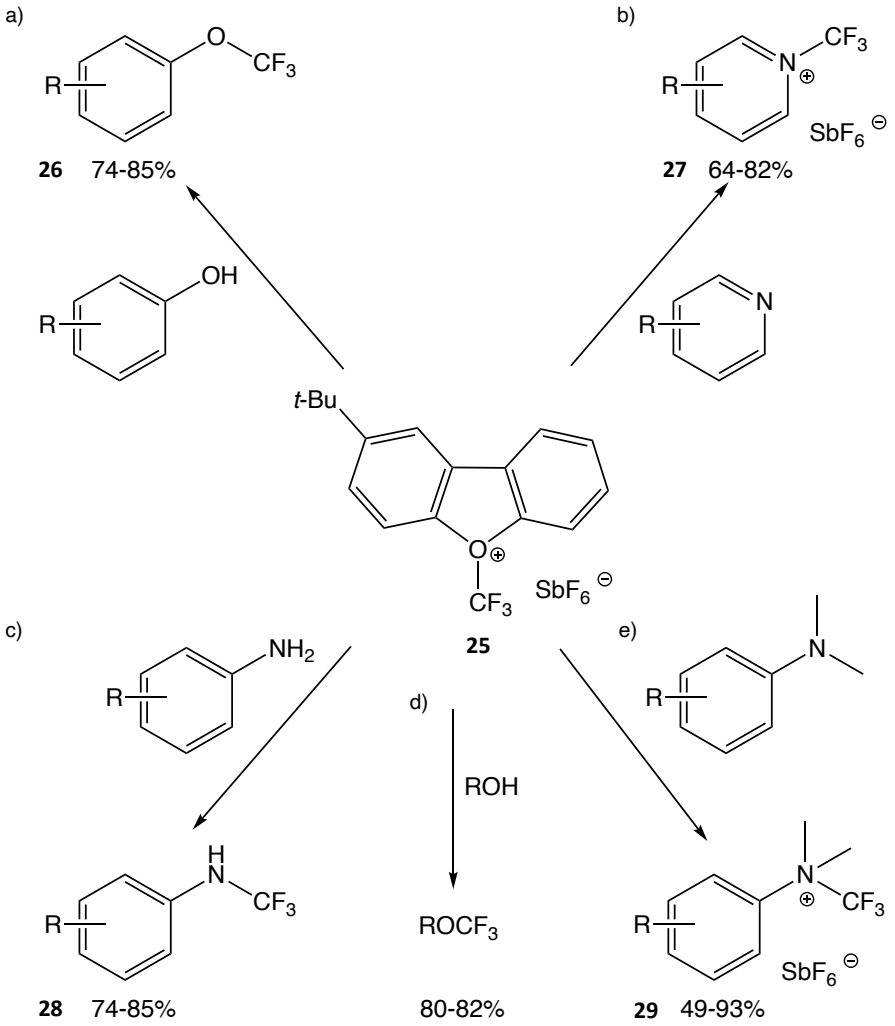

Scheme 5: Electrophilic trifluoromethylation using one of Umemoto's reagents, based on O-(trifluoromethyl)dibenzofuranium salts. All reactions were carried out in DCM at -90 to -10 °C.[34, 35]

1.4 Radical Trifluoromethylation: Photoredox Chemistry

A common approach to synthesising trifluoromethylated compounds via radical reactions has been to use high pressure and temperature conditions along with toxic metal reagents such as antimony trifluoride (SbF_3).[36] Not only is this non-ideal in terms of safety and environmental responsibility but these harsh conditions also led to poor functional group tolerance. As well as this, the conditions offer no control over the reaction, meaning that the $CF_3^{\bullet}$ radical is produced in high concentrations over a short time period which leads to undesirable radical propagation and side reactions.

Therefore, the need for a synthetic route which avoids such harsh conditions is needed. One response to this need has been to use photoredox chemistry, where the $CF_3^{\bullet}$ radicals can be generated from single electron transfer via a photoredox catalyst, which is excited using a light source.

1.4.1 Umemoto's Reagent

Although Umemoto's reagents are largely classed as electrophilic trifluoromethylating reagents, as discussed previously, the thio-salts can also undergo single electron transfer in order to cleave the S-CF_3 bond to produce the $CF_3^{\bullet}$ radical. Akita *et al.* have used Umemoto's thio-salt (**30**) to trifluoromethylate a range of alkenes, using photoredox catalysts to promote the radical reaction (Scheme 6).[37, 38, 39, 40]

The trifluoromethylation products reported by Akita were all formed regioselectively. This can be explained by the reaction mechanism, the $CF_3^{\bullet}$ radical was generated from single electron reduction of the thio-salt via the photoredox catalyst. The $CF_3^{\bullet}$ radical then attacked the terminal end of the alkene to form a radical intermediate. This intermediate was then oxidised to form a β-CF_3 carbocation which was attacked by a nucleophilic species to form the product. This is evidenced in Scheme 6 (reactions a and d) where the solvent (alcohol or acetonitrile) attacked the carbocation intermediate to from α-CF_3 esters (**31**) and amides (**32**). Alternatively, in the reaction of trisubstituted alkenes (Scheme 6, b), the olefinic proton was eliminated to reform the alkene bond (**33**).

This same regioselectivity is observed in the trifluoromethylation and subsequent lactonization of terminal (**34**) and internal (**35**) alkenes (Scheme 6, c). Once again, trifluoromethylation followed by oxidation formed the β-CF_3 carbocation intermediate, which is then attacked by the carboxylate to form 5, 6 or 7 membered rings (**36**). For the reaction of internal alkenes, diastereoselectivity was also observed, as the trans isomer (**37**) was the only product formed. Akita used density functional theory (DFT) methods to explore why this was and found that the most favourable conformation of the β-CF_3 carbocation was when the CF_3 and the aromatic group were arranged in an

anti-fashion. This was probably due to the repulsion between the groups causing them to be held far apart.

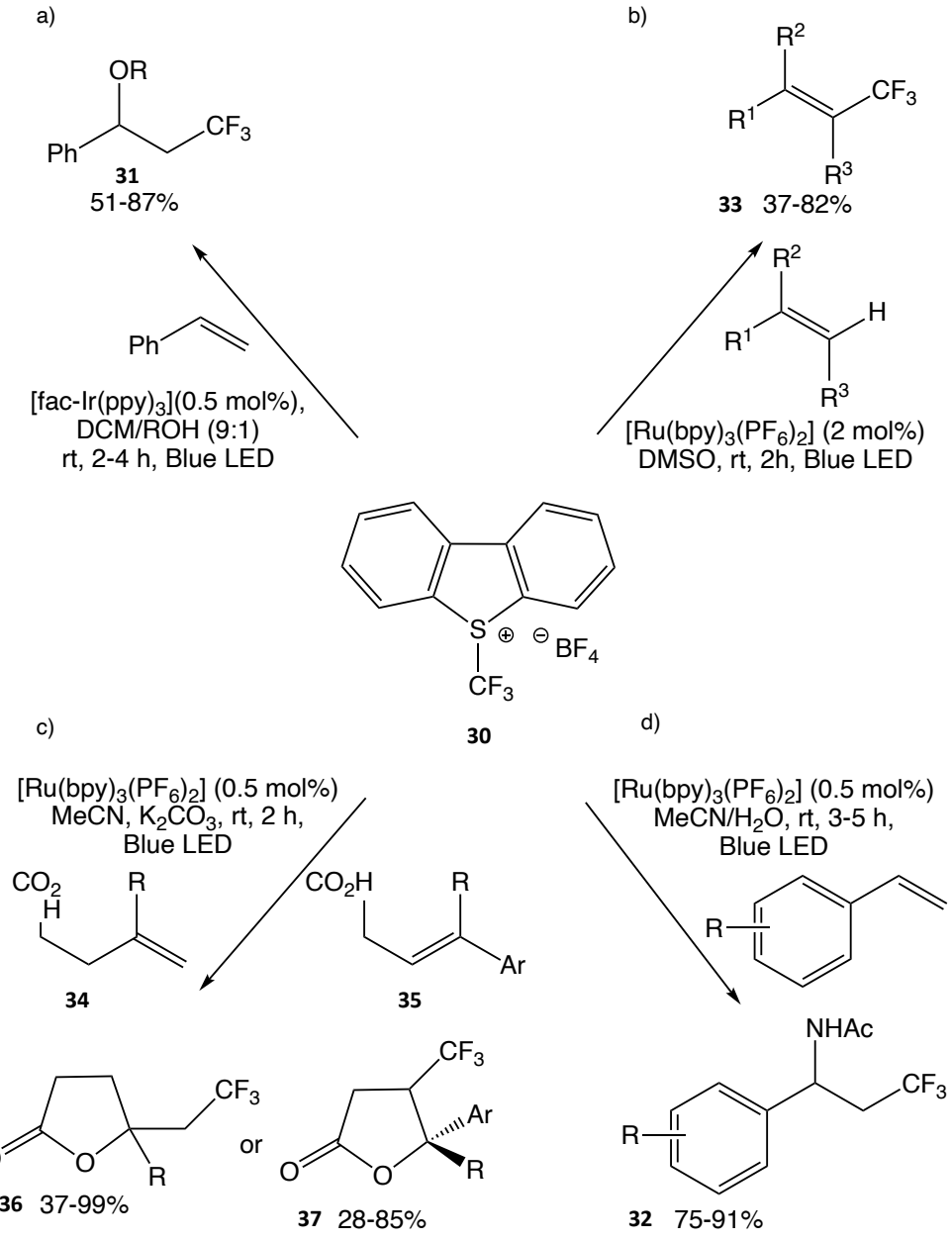

Scheme 6: Work done by Akita et al. in the photoredox trifluoromethylation of alkenes, using Umemoto's reagent as the CF_3 source.[37, 38, 39, 40]

1.4.2 Trifluoroiodomethane

Trifluoroiodomethane (**38**) was created as an alternative to chlorofluorocarbons (CFCs) and Halon ($CClBrF_2$), but can also be used as a nucleophilic[41, 42, 43] or radical trifluoromethylating reagent. Iqbal *et al.* were able to produce trifluoromethylated terminal alkenes (**39**) using a photoredox catalyst with visible light at room temperature (Scheme 7, right).[44] Such mild reaction conditions allowed for high regio- and stereoselectivity, producing trifluoromethylated terminal alkenes with E-stereochemistry only (78-95%). The mild conditions also accommodated a wide range of substrates, with functional group tolerance of alcohols, aldehydes, ketones, esters, carbamates, amides, silyl ethers, sulfonates, and halides (bromine and chlorine).

Once successful in trifluoromethylating alkenes, Iqbal *et al.* also used the same technique to generate trifluoromethylated heterocycles (**40**) (Scheme 7, left).[45] Many drug motifs include trifluoromethylated heterocycles,[46] however, preparation often involves a multistep synthesis and requires an activating group on the aromatic ring.[45] Iqbal *et al.* were able to produce trifluoromethylated aromatic compounds (71-95%) without pre-functionalisation due to the high reactivity of the $CF_3^{\bullet}$ radical. Again, the mild conditions also allowed for a high functional group tolerance of many compounds including bromides, aldehydes, esters and amides. Thus, this work carried out by Iqbal *et al.* has highlighted a simple yet effective route to the trifluoromethylation of substrates, which could be applied to the late stage modification of complicated pharmaceutical molecules.

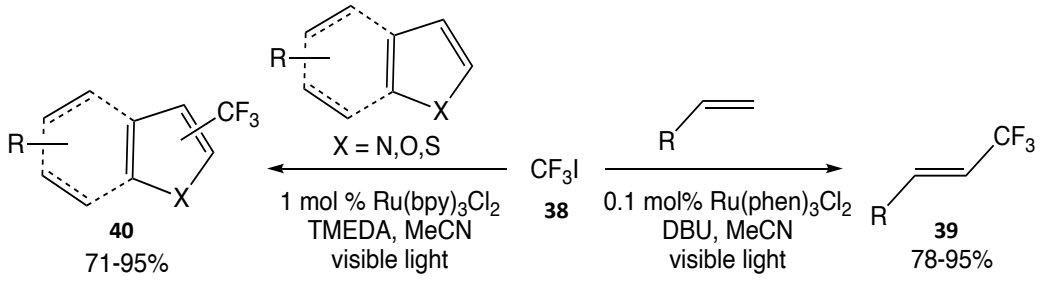

Scheme 7: Work undertaken by Iqbal et al. for the photochemical trifluoromethylation of, left: heterocycles,[45] *right: alkenes.*[44]

1.5 Electrosynthesis

Despite the clear benefits of using photoredox catalysis to generate trifluoromethyl radicals, the photoredox catalysts required for reaction can be very expensive (£104 - £3920 per gram, according to Merck). Electrosynthesis can be thought of as a much cheaper alternative to photoredox catalysis as the expensive catalyst is replaced by electricity which is barely considered a cost. Like photoredox catalysis, electrosynthesis can be carried out in mild conditions (room temperature and pressure) making it an ideal process for trifluoromethylation reactions as compared to traditional radical methods.

In simple terms, an electrosynthetic reaction can be thought of in the same way as an organic reaction but with electricity as one of the key reagents.[47] Electrons are transferred between an electrode and a species in solution to generate a redox agent, which is then used as part of a chemical reaction.

In 2018 a review paper published on electrosynthesis stated that we are "on the verge of a Renaissance" and "could head into a golden era of vibrant utility".[47] The method has been praised for the wide range of reagents available, the selectivity of the reactions that can be implemented and the inexpensive nature of electricity when compared to other reagents.[48] Thanks to the sustainability and stability of electrosynthetic reactions, paired with the ability to fine tune reaction conditions (such as redox potential and current) it could promise to become a fundamental tool used in organic labs.

However, the uptake of electrosynthesis as a widely used tool has yet to be seen.[49] Aspects which traditional electrochemists praise such as the variety of different electrolytes or electrodes available put off chemists from other backgrounds. Having so many options can be perceived as a complex setup with too many reaction variables, making it an inaccessible field for those without an electrochemical background. To remedy these concerns, it has been suggested[47] that a standardised database could be created to store information on which conditions are best suited to

the type of reaction being attempted. This would allow researchers to add optimal protocols and set parameters for various reaction conditions, so that those less experienced in the field can access them when needed. Recently, Baran *et al.* took steps to achieving this by publishing 'A Survival Guide for the "Electro-curious"' in which they explained the steps they took to promote successful electrosynthetic reactions.[50]

Overall, the general opinion on electrosynthesis seems to be that it has great potential as a tool in organic chemistry, especially when it comes to simple redox manipulations of functional groups (e.g., alcohol to ketone or ester to alcohol) that traditionally required super stoichiometric reagents.[49] However, for this technique to be taken on by the wider organic community, the idea that electrosynthesis is a 'black-box' needs to be debunked. For this to happen current researchers in electrosynthesis should take extreme care to make their work as reproducible as possible, describing their reaction setup in acute detail for future chemists to follow.

There are two main methods for generating the $CF_3^{\bullet}$ radical electrochemically, anodic oxidation or cathodic reduction. Anodic oxidation takes place when the CF_3 source donates an electron to the positively charged electrode (anode). The opposite is true for cathodic reduction, the CF_3 source receives an electron from the negatively charged electrode (cathode). In both cases, the loss or gain of an electron results in the production of a $CF_3^{\bullet}$ radical. Whether the production of a $CF_3^{\bullet}$ radical occurs via oxidation or reduction depends on the nature of the CF_3 source, whether it is nucleophilic or electrophilic. In the field of electrochemical trifluoromethylation it is much more common to find anodic oxidation reactions. This is because it is typically easier to utilise an inert reduction reaction (such as proton reduction to form hydrogen gas), to balance the cell, than it is to use an inert oxidation reaction.

1.5.1 Anodic Oxidation

One example of anodic trifluoromethylation is the work done by Baran *et al.* who compared a traditional method for radical generation using peroxide (TBHP) (Scheme

8, a) with electrosynthetic techniques (Scheme 8, b).[51] In both cases electron transfer resulted in the oxidation of zinc trifluoromethanesulfinate (ZnTFMS, **41**) to generate a $CF_3^{\bullet}$ radical which was then reacted with 1-methyl-1*H*-imidazole-4-carboxylate (**42**) to form 1-methyl-5-(trifluoromethyl)-1*H*-imidazole-4-carboxylate (**43**). Here, the yield from the electrosynthetic method (53%) was much higher than the yield from the peroxide method (25%). This was due to the rate at which the $CF_3^{\bullet}$ radical was produced. For the electrosynthetic method, the current and potential could be controlled so that the $CF_3^{\bullet}$ radical was produced at a steady rate which increased the window of time for a productive reaction. For the peroxide reaction, there was no control over the rate of production of the $CF_3^{\bullet}$ radical. Therefore, a high concentration of $CF_3^{\bullet}$ was produced quickly which led to side reactions and a diminished yield.

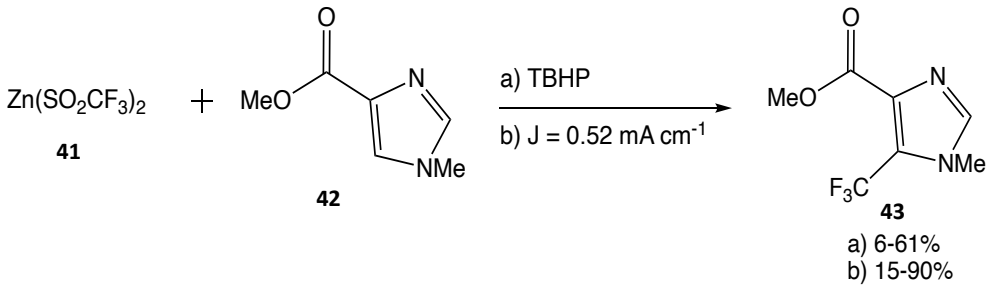

Scheme 8: Trifluoromethylation of heterocyclic substrates via a) traditional $CF_3^{\bullet}$ radical production using peroxide and b) electrochemical generation of $CF_3^{\bullet}$ radical.[51]

In the last few years a significant amount of research has been produced focusing on the electrochemical oxidation of sodium trifluoromethanesulfinate (NaTFMS, **44**) also known as Langlois' reagent. Oxidation of Langlois' reagent leads to the production of a $CF_3^{\bullet}$ radical which can then be reacted with an alkene to produce a range of trifluoromethylated products.

A growing area of research in the use of Langlois' reagent is the coupling of trifluoromethylation reactions with another electrosynthetic reaction to create difunctionalised products. An example of this is the paired electrolysis of Langlois' reagent and water in the presence of an alkene, undertaken by Kappe and Cantillo *et al.* (Scheme 9, a).[52] Initially Langlois' reagent was oxidised at the anode to produce a $CF_3^{\bullet}$ radical which attacked the alkene bond, forming a C-CF_3 bond on one side of the

alkene bond and a carbon radical on the other. This carbon radical was then oxidised at the anode to form a β-CF_3 carbocation. Meanwhile, at the cathode water was reduced to form hydrogen, alongside hydroxide ions which went on to attack the β-CF_3 carbocation to form a C-OH bond, thus creating 1-hydroxy-2-trifluoromethylated compounds (**45)** in moderate to excellent yields (27-96%). Lei *et al.* also used this technique, but instead replaced the water with alcohols. With the addition of an yttrium catalyst Lei was able to produce 1-oxy-2-trifluoromethylated compounds (**46**) (49-89%) (Scheme 9, b).[53]

Lin *et al.* used a similar technique to produce 1-chloro-2-trifluoromethyl compounds (**47**) (46-85%) (Scheme 9, c).[54] This group used Langlois' reagent alongside magnesium chloride ($MgCl_2$) as the $CF_3^{\bullet}$ and $Cl^{\bullet}$ donors respectively. Langlois' reagent reacted with the alkene in the same way as Kappe and Cantillo *et al.* to attach the CF_3 group to one side of the alkene bond, forming a radical at the other side. $MgCl_2$ was then reacted with a Mn(II) catalyst to form Mn(II)-Cl which was then oxidised at the anode to form Mn(III)-Cl. The Mn(III)-Cl acted as a radical transfer agent to donate the chlorine radical to the alkene and regenerate the Mn(II) catalyst.

One group, Zeng *et al.*, managed to combine both anodic oxidation and cathodic reduction (Scheme 9, d).[55] In this synthesis, a bromide catalyst was oxidised at the anode to produce bromine. The bromine then reacted with Langlois' reagent, to form an O-Br bond. This brominated intermediate was then reduced at the cathode to produce a $^{\bullet}CF_3$ radical. The radical was reacted with N-acrylamides (**48**), resulting in a cyclisation reaction to produce oxindoles (**49**) in good to excellent yields (59-90%).
All four groups used a carbon cathode and a platinum (or steel)[52] anode. The researchers highlighted the simplicity of using Langlois' reagent, complimenting the cheap price and availability. They also commented on the ease of reaction and functional group tolerance. Lei *et al.* in particular referenced the ease in which the reaction could be scaled up due to the utility and applicability of the reaction.

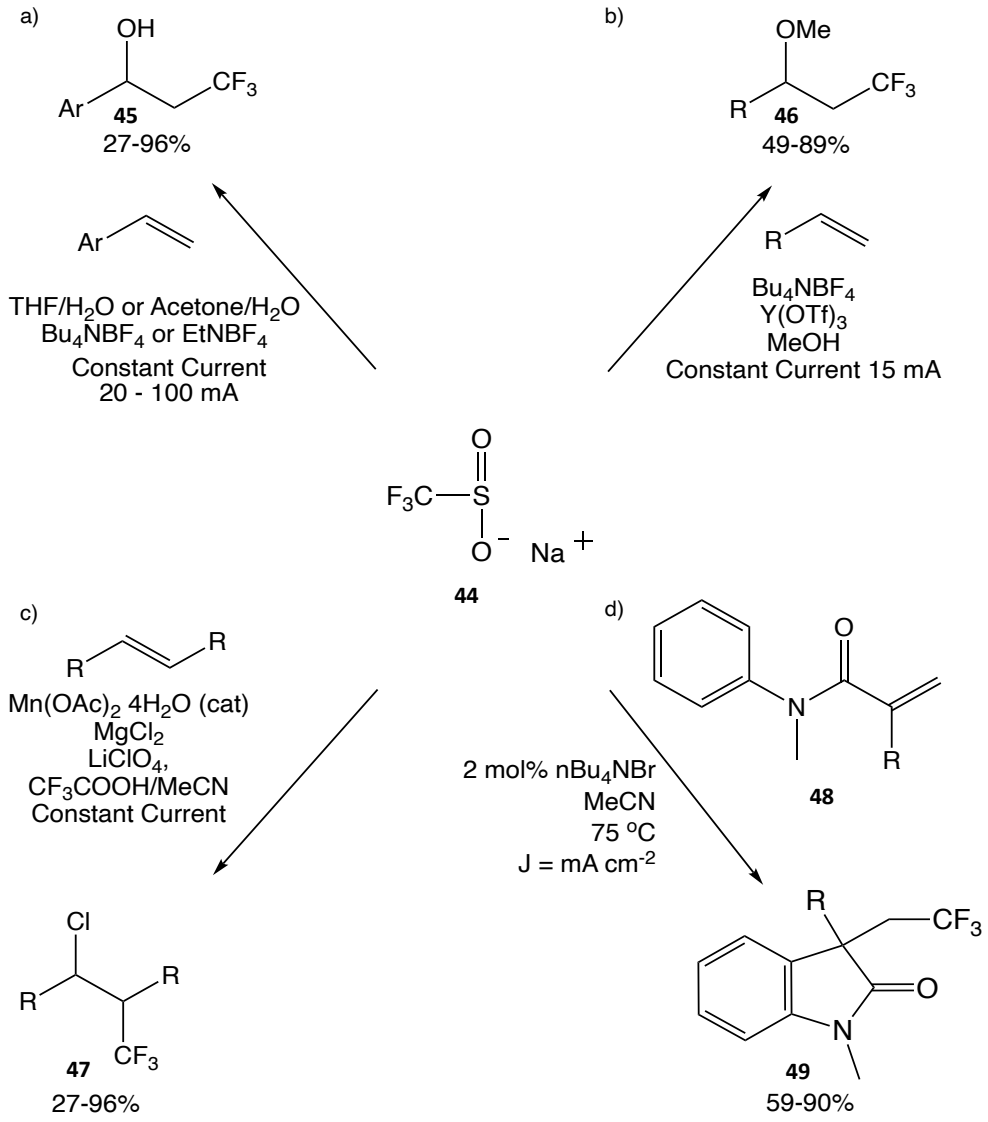

Scheme 9: Electrochemical trifluoromethylation of various substrates using Langlois' reagent as the source of the CF_3 radicals. Work done by a) Kappe and Cantillo et al.,[52] b) Lei et al.,[53] c) Lin et al.,[54] d) Zeng et al.[55]

1.5.2 Cathodic Reduction

Kappe and Cantillo claim to be the first group to report the cathodic trifluoromethylation of arenes and heteroarenes (Scheme 10).[56] This reaction was based on the reduction of a triflylammonium complex (**50**) which was generated in situ from trifluoromethanesulfonyl chloride and triethylamine. This synthesis had to be done in situ as the triflylammonium cation was unstable and would readily decompose into electrochemically inert by-products. In fact, the triflylammonium complex was so unstable that the group were unable to obtain a reduction potential of the species using

cyclic voltammetry. The group were able to control the rate of reaction, using a high constant current (40 mA) to force the reaction to occur quickly, before the triflylammonium complex decomposed. Remarkably, despite the unfavourable stability of the triflylammonium complex the group were still able to report yields of trifluoromethylated heterocycles (**5**) up to 89%. Despite the instability of the triflylammonium complex, one benefit to this method was that the triethylamine used to form the triflylammonium cation could also be oxidised at the anode generating diethylamine, and this reaction balanced the cell.

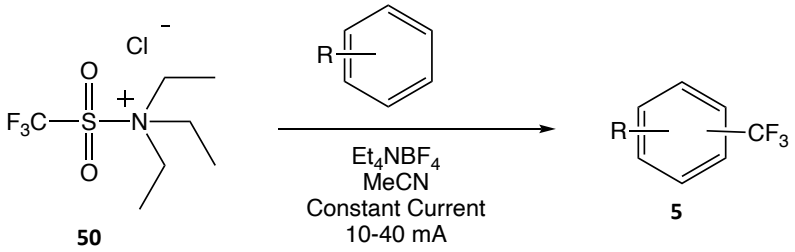

Scheme 10: Cathodic reduction reaction to trifluoromethylate arenes and heteroarenes.[56]

Chapter Two – Theory and Experimental

2.1 Electrochemistry Theory

Electrochemistry involves the movement of electrons between an electrode and a species in solution, and the chemical changes which accompany them, reduction and oxidation. There are many types of analytical tools that electrochemists can use to study a material (typically referred to as a substrate). In order for electrochemical analysis to be successful one must have carefully considered the type of electrodes, electrolyte, solvent and cell parameters.

The electrode at which the flow of electrons is measured is known as the working electrode, and can either be an anode or a cathode. A second electrode is required to complete the circuit and this is called the counter electrode, thus if a substrate is oxidised at the working electrode this will be balanced by reduction at the counter electrode. A third electrode, a reference electrode, is also used. The working electrode should have a potential window (range between the potentials at which oxidation and reduction of the solvent occur) large enough to accommodate for the redox potential of the chosen substrate. The potential window will differ depending on the electrode-electrolyte-solvent combination. For example, a platinum electrode can have a potential window of +1.5 V to 0 V in water (pH=0) or 3.0 V to -2.5 V in acetonitrile.[57]

For the purpose of clarity, all examples of a redox process in this chapter will discuss the reduction of a substrate, O, to produce a new species, R (Equation 1). Furthermore, the theory discussed in this chapter is in reference to Electrochemical Methods: Fundamentals and Applications by Bard & Faulkner.[58]

$$O + ne^- \rightarrow R \qquad \textit{Eq. 1}$$

When O and R are in equilibrium no net current will flow. The equilibrium potential (E_{eq}) of this reaction can be determined from the Nernst equation – one of the most important equations used in electrochemistry.

$$E_{\mathrm{eq}} = E_0 + \frac{RT}{nF}\ln\frac{[\mathrm{O}]}{[\mathrm{R}]} \qquad \textit{Eq. 2}$$

Here, E_0 is the standard potential, R is the universal gas constant, T is the temperature in Kelvin, n is the number of electrons, F is the Faraday constant and [O]/[R] is the reaction quotient. In an electrochemical cell, if a potential more negative than E_{eq} is applied to the system then the electrons in the electrode will increase in energy. At a certain point the energy of the electrons in the electrode will be higher than that of the electrons in the LUMO of the substrate O. Electrons will then be transferred from the electrode to substrate O, resulting in the production of species R. This transfer of electrons will also result in a reductive current (a negative current produced as electrons flow from the electrode to the species in solution). The magnitude of this current, i, can be described using the equation:

$$i = AFj \qquad \textit{Eq. 3}$$

Here, A represents the area of an electrode, and j represents the flux i.e. the total mass transport of a material. The flux can be described in terms of the rate of electron transfer, k, and the concentration of the species being reduced [O]:

$$j = k_0[\mathrm{O}]_0 \qquad \textit{Eq. 4}$$

Equations 3 and 4 can be combined to describe the amount of current passed at an electrode in terms of the rate of electron transfer:

$$i = FAk_{\mathrm{red}}[\mathrm{O}]_0 \; or \; i = FAk_{\mathrm{ox}}[\mathrm{R}]_0 \qquad \textit{Eq. 5}$$

Combining the oxidative and reductive currents will provide the overall net current:

$$i = -FAk_{\mathrm{red}}[\mathrm{O}]_0 + FAk_{\mathrm{ox}}[\mathrm{R}]_0 \qquad \textit{Eq. 6}$$

From this equation it can be seen that the current is dependent on two factors, the rate of electron transfer and the concentration of species at the electrode surface.

2.1.1. Rate of Electron Transfer

The Arrhenius equation is often used to describe the rate constant for a solution-phase reaction, therefore it is appropriate to apply it in terms of the rate of electron transfer between an electrode and species in solution.

$$k = X' \exp\left(\frac{-E_A}{RT}\right) \qquad \textit{Eq. 7}$$

Here, *X'* represents the pre-exponential factor, and E_A represents the activation energy. For a chemical reaction the activation energy is needed to overcome the energy barrier and allow the reaction to happen. In terms of electron transfer the activation energy can be thought of as the Gibbs Free Energy, *G*.

$$E_A = G = -nFE \qquad \textit{Eq. 8}$$

Equation 8 equates the free energy associated with the amount of work undertaken by the system during the electron transfer step. As discussed previously, when the system is in equilibrium (E=E_{eq}) no net current will flow. Therefore for electron transfer to occur a potential greater or smaller than E_{eq} will need to be applied to the electrode. This is known as the overpotential, η.

$$\eta = E - E_{eq} \qquad \textit{Eq. 9}$$

The rate of electron transfer for the reduction or oxidation of a species, in terms of overpotential, can be given by:

$$k_{red} = k_{red_0} \exp\left(\frac{-\alpha F \eta}{RT}\right) \qquad \textit{Eq. 10}$$

$$k_{ox} = k_{ox_0} \exp\left(\frac{(1-\alpha) F \eta}{RT}\right) \qquad \textit{Eq. 11}$$

α represents the charge transfer coefficient (with a value between 0 and 1), it can be thought of as the reflection of the transition state symmetry of the species during the electron transfer step. If α = 0 then the transition state resembles the reactants, in its potential dependence. If α = 1 the transition state is a closer resemblance of the products, in its potential dependence. Typically α = 0.5 is an appropriate approximation for a simple one electron transfer.

Equations 10 and 11 can be substituted into equation 6 to give the Butler-Volmer equation:

$$i = i_0 \left[\exp\left(\frac{(1-\alpha) F \eta}{RT}\right) - \exp\left(\frac{-\alpha F \eta}{RT}\right)\right] \qquad \textit{Eq. 12}$$

i_0 is known as the exchange current. It can be described by the following equation (if [O]=[R]):

$$i_0 = FAk_0[\mathrm{O}]_{\mathrm{bulk}} = FAk_0[\mathrm{R}]_{\mathrm{bulk}} \qquad \textit{Eq. 13}$$

The equations detailed above are important as the kinetics of the electron transfer step can reveal a lot about a reaction. If the kinetics are fast the electron transfer between the electrode and substrate will be reversible. If the kinetics are slow the electron transfer will be irreversible. This can be explained in more detail by considering Marcus theory. That is, if the electron transfer is quick, species O and R must have the same geometries, whereas if the electron transfer is slow the O and R will have different geometries. This is due to two factors governing the electron transfer step. The first is the Franck Condon Principle. Due to the quick nature of electron transfer (10^{-15} – 10^{-16} s)[58] compared to that of nuclear vibrations (10^{-13} s)[58] it is assumed that there is no change in geometry of the substrate during the electron transfer step. The second is that there can be no loss or gain of energy during the electron transfer step. Therefore if electron transfer is quick, R must have the same geometry as O before it was reduced.

2.1.2. Rate of Mass Transport

Electron transfer between an electrode and a substrate occurs directly at the electrode surface. As substrate O is converted to R, a constant supply of fresh O needs to reach the electrode surface in order to maintain electron transfer. If substrate O cannot reach the surface the concentration of O available for electron transfer will decrease, and so the current will drop. The rate at which O can reach the electrode can be controlled through three mass transport processes known as convection, migration and diffusion.

Convection occurs naturally due to thermal or density differences in a solution. Currents caused by convection can be controlled by ensuring that the solution is stable before a measurement is taken. Alternatively, the convection current can be managed by applying a known convection rate to the solution. This is commonly achieved by using a rotating disk electrode.

Migration of the substrate occurs when an external force is applied to the solution, i.e. when a potential difference is applied at the electrode the charged substrate will move through the solution. Migration currents are controlled by the addition of an inert electrolyte (a salt which can be dissolved in a solvent), in excess of the concentration of R or O. The electrolyte is used to promote conductivity and decrease the resistance in the solution. The excess of electrolyte ions shield R or O from the potential gradient from the electrode and prevent their movement by migration. As electron transfer occurs at the electrodes, the supporting electrolyte will migrate to balance the charge and complete the electrical circuit.[59]

Diffusion is the movement of the substrate caused by concentration gradients. The diffusion of a substrate in solution can be described by Fick's laws of diffusion, where *D* is the Diffusion Coefficient.

$$J = -D\left(\frac{\mathrm{d}[\mathrm{O}]}{\mathrm{d}x}\right) \qquad \textit{Eq. 14}$$

$$\frac{\mathrm{d}[\mathrm{O}]}{\mathrm{d}t} = D\left(\frac{\mathrm{d}^2[\mathrm{O}]}{\mathrm{d}x^2}\right) \qquad \textit{Eq. 15}$$

Fick's first law, given in Equation 14, describes the flux in terms of the diffusion coefficient and the concentration gradient of a species in solution. It states that the flux due to diffusion is proportional to the concentration gradient. Fick's second law (Equation 15) is a partial differential of the concentration with respect to time. The second law can be used to describe how the concentration of a substrate will change due to diffusion.

As convection and migration can be easily controlled their effects commonly have negligible effect on the current. Therefore, diffusion is the major contributor to the mass transport of a substrate. According to Fick's laws, as substrate O at the electrode surface is consumed the concentration of O will decrease. Therefore, more of the substrate will move through the solution to balance the drop in concentration. Typically, the rate at which the substrate O can reach the electrode surface will be less

than the rate it is converted to R, which will limit the amount of current produced. Thus, in these cases, the current will be described as diffusion limited currents.

2.2 Electrochemical Analytical Tools

2.2.1. Cyclic Voltammetry

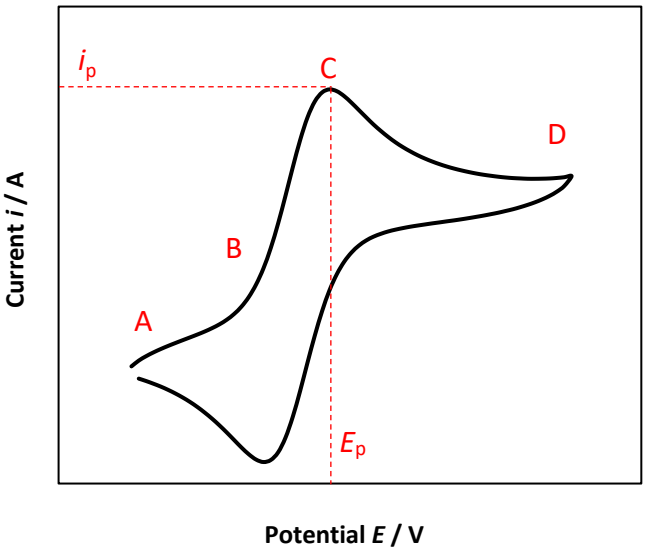

Figure 2: Typical response for a cyclic voltammogram.

Cyclic voltammetry is one of the most common analytical tools used throughout the field of electrochemistry and is discussed throughout this thesis. Cyclic voltammetry can provide information on redox reactions including redox potentials, reversibility and the kinetics of a reaction. For these measurements to be taken the potential is swept between high and low potentials via the working electrode and the resulting current is measured. A typical voltammogram can be seen in Figure 2.

The voltammogram is started at point A, a potential where no net current will flow and the potential is then swept in the positive direction. As this happens, the potential reaches a point (B) at which electron transfer occurs from R to the electrode to produce O and an oxidation current is observed. From Equation 5 we know that the current is proportional to the rate of electron transfer, k_{ox}. From Equation 11 we know that k_{ox} increases exponentially with overpotential. Thus, as the potential is swept to

increasingly positive values the overpotential increases (according to equation 9) and so the current increases exponentially.

At point C the current reaches a maximum value, i_p, with a corresponding potential, E_p. This is the point at which diffusion of fresh R can no longer keep up with the rate of electron transfer – R is being consumed faster than it can be replaced. Therefore, the current observed before point C is dependent on the rate of electron transfer and the current beyond point C is diffusion limited.

When the potential reaches point D it is reversed and swept back to point A. As the potential is reversed R is regenerated as O is reduced, which produces a reduction current. The same response in current is observed for the reduction of O, however this time as electrons are passed from the electrode to the substrate a negative current is seen. The current response due to the first potential sweep is referred to as the forward scan or forward peak. The peak due to the second potential sweep is referred to as the reverse scan or reverse peak. The forward/reverse scans can either show oxidation or reduction depending in what direction the potential was swept first. In this report it will always be clearly explained in which direction the potential was swept.

One of the key details of a voltammogram is the peak current, i_p, which can be described using the Randles- Ševčík equation.

$$i_p = 0.4463nFA[O]\sqrt{\frac{nFvD}{RT}} \qquad \textit{Eq. 16}$$

Here, v represents the scan rate the cyclic voltammogram was taken at. Equation 16 shows how the peak current is proportional to the scan rate. Plots of i vs $v^{1/2}$ should be linear and pass through the origin. If this is true then the gradient can be used to predict the diffusion coefficient of a substrate.

3.2.1 Chronoamperometry

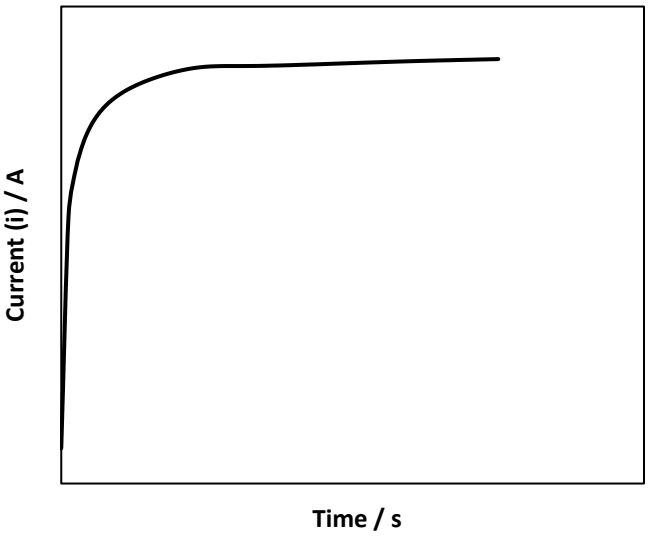

Figure 3: Typical response for a chronoamperogram in which O is converted to R.

Chronoamperometry is a classical electrochemical experiment whereby the current-time behaviour of an electrochemical system is observed. During a chronoamperometry experiment, at a time of t_0 the electrode potential is stepped from a potential at which no electron transfer would occur, to one where electrons are transferred to O in solution to generate R, with no limitation in electron transfer kinetics (i.e. large k^0). As the potential is constant and electron transfer is not rate limiting, the current is governed by diffusion-controlled mass transport. As time progresses the concentration of R increases and forms a diffusion layer at the electrode surface. Thus, for more O to reach the electrode surface it will need to diffuse through the diffusion layer. The diffusion layer will grow till it reaches a point where further growth is halted by the mixing of solution due to natural convection.

The behaviour of the observed current at a fixed potential, over time, for a reversible redox reaction can also be described by the Cottrell Equation:

$$i = \frac{nFAC_0\sqrt{D}}{\sqrt{\pi t}} \qquad \textit{Eq. 17}$$

A plot of i vs $t^{1/2}$ can be used to find unknown values such as the diffusion coefficient, D, or the number of electrons transferred, n.

Chronoamperometry experiments can also be used to calculate the number of electrons transferred between an electrode and a substrate. The charge passed through the electrode, Q, is proportional to current and time:

$$Q = it \qquad \textit{Eq. 18}$$

Therefore, integration of a current-time plot (Figure 3) would give the total amount of charge passed during the experiment. This can then be divided by the charge of an electron to determine how many electrons were transferred, which can then be converted into a molar quantity using Avogadro's number.

In the chronoamperometry experiments in this report, the current-time graphs were integrated using the trapezia theorem:

$$\int f(x)\,dx = \sum_{k=1}^{\mathrm{N}} \frac{f(x_{\mathrm{k}-1}) + f(x_{\mathrm{k}})}{2}(x_{\mathrm{k}} - x_{\mathrm{k}-1}) \qquad \textit{Eq. 19}$$

The trapezia theorem approximates the area under the curve to be a series of trapezoids. The area of each trapezoid is calculated and summed together to give a total value for the area under the curve. Chronoamperometry was also used for electrosynthesis, where the potential of the working electrode was held at a known reduction potential in order to generate radicals that could react with a radical trap also in solution. Integration of the current-time graph generated during the electrosynthesis process was used to calculate the equivalent number of electrons per mol of substrate passed during an electrosynthetic reaction.

2.2.3 Experimental

Cyclic voltammetry and chronoamperometry were used for several purposes for the research presented in this thesis. The same reaction conditions for the cyclic voltammetry experiments were used for chronoamperometry experiments, with the working electrode varying from a glassy carbon electrode to platinum, gold or boron

doped diamond depending on the experiment. (More information on this to follow in the results section of the report).

Cyclic voltammetry and chronoamperometry were used to observe the electrochemical behaviour and discover the reduction potentials of trifluoroacetylpyridinium salts. These experiments were performed in acetonitrile (MeCN) with 0.1 M tetrabutylammonium hexafluorophosphate ($TBAPF_6$) supporting electrolyte. A 20 ml glass cell, containing a lid with three holes was set up with a glassy carbon working electrode (3 mm diameter), a nickel counter electrode and a silver wire quasi-reference electrode. The use of a quasi-reference electrode meant that we also had to reference the potentials to ferrocene (Fc/Fc^+). The 10 mM solutions of trifluoroacetylpyridinium salts were prepared by adding TFAA (15 mM) to pyridine (10 mM in $MeCN/TBAPF_6$. If the solutions needed to be deoxygenated then argon was bubbled through the solution for 20 min before any measurements were taken, then an argon atmosphere was maintained in the cell whilst cyclic voltammetry was performed. Using the same conditions, cyclic voltammetry was also implemented to modify the clean glassy carbon electrode. This was usually performed by cycling the clean electrode from 0 V to – 2 V over 9 consecutive cyclic voltammograms, in a 10 mM solution of the trifluoroacetylpyridinium salt.

Cyclic voltammetry was also used to determine the blocking effects of modified electrodes towards a series of redox probes: potassium ferrocyanide ($K_4[Fe(CN)_6]$), hexaammineruthenium chloride ($Cl_3[Ru(NH_3)_6]$) and ferrocenemethanol (FcMeOH). Each solution was prepared with 1 mM of the redox probe in an aqueous solution of 0.1 M sodium chloride (NaCl) with deionised water. For these experiments, a glassy carbon working electrode, nickel counter electrode, and silver/silver chloride reference electrode were used. All cyclic voltammograms were performed at a scan rate of 0.1 V s^{-1} unless stated otherwise. Before any electrochemical techniques took place the glassy carbon working electrode was polished with a 0.3 μm alumina solution on a Buehler Microcloth polishing pad, then rinsed. All electrochemical measurements were taken on an Autolab potentiostat (EcoChemie, Netherlands), controlled by GPES version 4.7.

2.3 Surface Analysis

2.3.1 XPS

X-ray photoelectron spectroscopy (XPS) was used in this thesis to characterise the surfaces of modified electrodes. XPS is a technique used to characterise the elements present on the surface of a material. In order to obtain a spectrum of the surface, a sample is irradiated with a beam of X-rays. The atoms within the sample will absorb the X-ray and in turn release an electron. Electrons from the top 1-10 nm of the sample are emitted. The electrons are then detected by a monitor and the kinetic energy of each electron is measured and analysed. The kinetic energy measured is dependent on the binding energy of the electron, which in turn is dependent on the element, orbital and chemical environment from which it originated. Thus, by counting the electrons and measuring the kinetic energy of each one, a spectrum can be created from which one is able to identify which elements are present at the surface, how they are bonded and quantify how much of each element there is.

2.3.2 Experimental

In this thesis, samples for XPS were prepared using graphite that had been polished using sandpaper. The graphite electrodes were modified either via cyclic voltammetry or chronoamperometry in a 10 mM solution of the given trifluoroacetylpyridinium salt, with 0.1 M $TBAPF_6$/ MeCN. They were then cleaned via sonication in MeCN for 2 min, before being dried in a vacuum desiccator overnight. XPS measurements were taken using a Thermo Scientific K-Alpha instrument with a monochromated microfocused Al Kα Xray source (1486.6 eV). These measurements were performed under ultrahigh vacuum conditions with a 400 µm spot size. The spectral data acquired from the XPS experiment was then analysed using CASA XPS and Origin to identify what species were present on the surface of the graphite electrodes and in what quantities.

2.4 Electrochemical Synthesis

2.4.1 Theory

Electrochemical synthesis can be performed in a divided cell or an undivided cell. Divided cells hold the working electrode and the counter electrode in separate chambers connected by a permeable membrane or a glass frit, which allows for the passing of charged species only. Divided cells can be useful for keeping the oxidation and reduction reactions separate, for example, if the product formed via reduction is easily oxidised a divided cell can prevent such a reaction from happening. However, divided cells can have some limitations. Electrodes are normally held very far apart, and together with the presence of the frit/membrane, this can cause high resistance and low currents in the cell. Thus, undivided cells are seen more commonly in the literature. An alternative electrochemical synthesis set-up involves the use of an electrochemical flow cell. Here, the reaction solution is passed over a working electrode to produce the desired product. These types of cells are most popular for large scale synthesis, as there is no limit on how much solution can pass over the working electrode, whereas if the same reaction were to be performed in an undivided cell there the reaction would be limited by the mass transport of the reagents.

There are two ways to control the electron transfer in electrochemical synthesis, constant current or constant potential methods. During constant current methods the current in the working electrode is set to a given value and the potential of the electrode changes so that this current is maintained. This can be useful for driving the rate of reaction, for instance a high current would lead to quicker reactions and vice versa for low currents. Yet, constant current methods are not reaction-specific and any electron transfer reaction will occur to maintain the set current, which could lead to large numbers of side products. Alternatively, constant potential methods allow you to select the potential of a specific electron transfer reaction between the electrode and the reagents in solution. Here, the working electrode is set to a specific potential and the current that is recorded will be determined by the rate of electron transfer and the mass transport of the reagents in solution. This allows you to control which reactions take place in solution but not the rate of reaction. Some parameters can be set when

using the potentiostat so that the reaction will stop if a certain potential or current is reached.

2.4.2 Experimental

For the research presented in this thesis many different combinations of solvents, electrolytes, electrodes and cells were employed to try to discover the optimum reaction conditions. However, there was a general procedure all reactions followed. First, in a clean cell that had been dried overnight in the oven, the electrolyte was dissolved in the solvent to make a 0.1 M solution. If a certain atmosphere was required, this gas was connected to the cell via a needle attached to a gas cylinder, or a balloon containing the gas. Next, with constant stirring from a stir bar, the radical trap was added to the solution, followed by the pyridine or pyridine-like species. Finally, the trifluoroacetic anhydride was added. The electrodes were then placed in solution and the reaction proceeded via the conditions set in the potentiostat. The progress of the reaction was monitored via ^{19}F NMR. At the end of the reaction, the crude reaction mixture was analysed via ^{1}H and ^{19}F NMR. The crude solution was then washed with water and the organic layer was condensed. The products were purified via column chromatography using an ethyl acetate/hexane (6:94) solvent mixture.

2.5 Product Characterisation

2.5.1 Nuclear Magnetic Resonance

Nuclear magnetic resonance (NMR) is used to characterise the nuclei of molecules which can be related to the chemical environments in a compound. NMR is performed by placing a sample into a strong magnetic field. The atomic nuclei in the sample will each have a unique magnetic moment, and the presence of the external magnetic field will cause the nuclear spins to align. A radio pulse, made up of a broad spectrum of radio frequencies, is then emitted which disrupts the nuclear spins, and when they realign they resonate at a specific frequency unique to the individual nuclei. The frequency at which the nucleus resonates at will give information about what

environment it is in, such as what it is bonded to and what the nuclei around it are. The resonant frequencies of the nuclei are then converted to a spectrum which is displayed as peaks on a graph. The height of each peak will be representative of how many nuclei resonated at that specific frequency, indicating how many atoms in that specific environment are present in a sample. The peaks may also be coupled together, and this coupling is caused by the spin states of neighbouring nuclei interacting.

2.5.2 Infrared Spectroscopy

Infrared (IR) spectroscopy also provides information on the chemical environments present in a molecule, according to the stretching and bending frequencies of the bonds within the molecule. To gather this information, an IR spectrometer will pass a beam of IR radiation through a sample, at a range of frequencies. Some of the IR radiation will be absorbed by the sample, depending on what frequency the bonds inside the sample are vibrating at. The amount of absorbance is then plotted against the corresponding wavenumber.

For a specific vibration to be seen in the IR spectrum it must be 'IR active', i.e. the absorption of IR radiation must coincide with a change in dipole moment. This usually coincides with the polarity of a bond, where very polar bonds will adsorb a lot of IR radiation and be 'IR active'. Weakly polar bonds will not undergo a change in dipole moment, and so only weakly absorb IR radiation, meaning they are not 'IR active'.

There are six possible vibrational modes in a molecule. They can be stretching (symmetric and antisymmetric) or bending (scissoring, rocking, wagging and twisting). Linear molecules will contain $3N-5$ vibrational modes and non-linear molecules will contain $3N-6$ vibrational modes, where N represents the number of atoms in the molecule.

2.5.3 Mass Spectrometry

Mass spectrometry is used to determine the mass of a molecule when it has been split into its gas-phase ions. To do this, the mass spectrometer vaporises the sample to turn it into a gas, and then ionises the gas to create charged species. The gaseous ions then travel through magnetic and electric fields. The magnetic field will deflect the ions, and the magnitude of deflection will depend on the mass-to-charge ratio of the ion. This then sorts the ions into 'streams' where the lighter ions will have experienced a greater magnetic force than the heavier ions, and so will have been deflected more. The streams of ions are then detected and a plot of % ions detected versus the mass-to-charge ratio (m/z) is created.

2.5.4 Experimental

NMR, IR and mass spectrometry were used to characterise the final products synthesised from electrochemical synthesis, after they had been purified via column chromatography. To do this, small amounts of each sample (~1-2 mg) were dissolved in an appropriate solvent. For NMR this was deuterated chloroform ($CDCl_3$), for IR this was petroleum ether (PET, then a drop of the dissolved sample was placed on the IR prism and the PET was allowed to evaporate, leaving a neat sample on the IR prism) and for mass spectrometry this was acetonitrile (MeCN). For mass spectrometry, samples were submitted and run by the mass spectrometry team at UCL, on a Thermo Orbitrap Exactive Plus mass spectrometer. NMR samples were run on a Bruker NMR Avance Neo 700/ Avance III 600/ Avance III 400/ Avance 300. IR samples were run on an ALPHA Bruker ATR using OPUS software.

Chapter Three – Preparation of Trifluoroacetylpyridinium salts

3.1 Motivation for this Work

The work in this chapter describes the attempts made to synthesise and characterise a $CF_3^{\bullet}$ radical source that could be used for electrosynthetic trifluoromethylation reactions. The main objective of this PhD project was to develop an electrosynthetic trifluoromethylation reaction that is cheaper and 'greener' than alternative methods currently employed, in the hope that this would demonstrate the benefits of electrosynthesis to the organic chemistry community. To do this, our trifluoromethyl radical source needed to be cheap and readily available. In terms of the practicality of performing an electrosynthetic reaction we desired a radical source that was 'easy' to oxidise or reduce. Here, 'easy' refers to a compound that is electrochemically active within the solvent window (the potential range between the oxidation and reduction of the solvent) and has a clearly defined reduction/ oxidation potential. The most ideal synthesis conditions would be where only one electrochemical reaction (the desired reaction) is happening. Thus, we needed a radical source with a potential that doesn't overlap with any other electrochemically active species in solution.

With this in mind, our attention turned to using pyridinium salts as $CF_3^{\bullet}$ radical sources. Pyridinium salt is an umbrella term that covers a wide array of compounds, from natural products[60, 61, 62] to liquid electrolytes,[63] that all contain a pyridine N^+-R X^- motif. Over the past few decades several methods for the synthesis of pyridinium salts have been highlighted, the most common method being an S_N2 type reaction of pyridine and alkyl halides.[64] Other methods include the formation of Katritzky Salts from pyrylium,[65, 66, 67] the Zincke reaction[68, 69] and the Mitsunobu reaction.[70]

Pyridinium salts are very versatile. They are commonly used as radical donors, allowing for the formation of O-, N- and C-centred radicals.[71, 72, 73, 74, 75, 76] But they can also act as radical acceptors and are involved in a wide array of nucleophilic radical reactions. Examples include ortho-selective attack from alkyl radicals,[77, 78] cyclisation reactions and pyridylation of sulfonamides and carboxamides.[79] N-

acylpyridinium salts are also used to study the regioselectivity of nucleophilic addition. Generally, following the Hard-Soft-Acid-Base (HSAB) principle, hard nucleophiles add to N-acylpyridinium salts at the 2-position, whereas soft nucleophiles add at the 4-position.[80, 81, 82, 83]

For this project, we reacted TFAA (**51**) with pyridine (**52a**) in an attempt to synthesise a trifluoroacetylpyridinium salt (**53a**), with the intention to use it as a radical source (Scheme 11). The chemicals required to form this trifluoroacetylpyridinium salt are straightforward to acquire and store, and TFAA is one of the cheapest CF_3 sources available (see Table 1). We theorised that the trifluoroacetylpyridinium salt should readily accept an electron, forming a pyridine radical (**54**) that would readily decompose to produce a trifluoroacetyl radical (**55**). The trifluoroacetyl radical should then rapidly undergo decarbonylation to produce carbon monoxide and a $CF_3^{\bullet}$ radical (**56**).[84, 85, 86]

Our proposed synthesis:

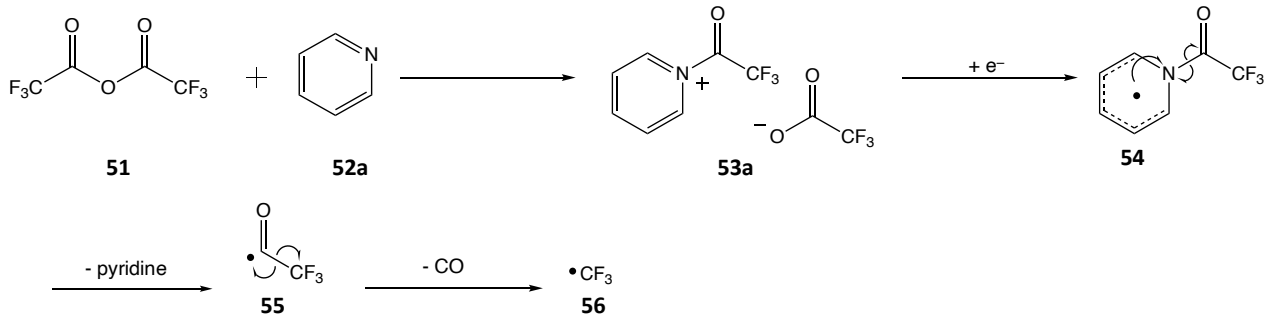

Previous work:

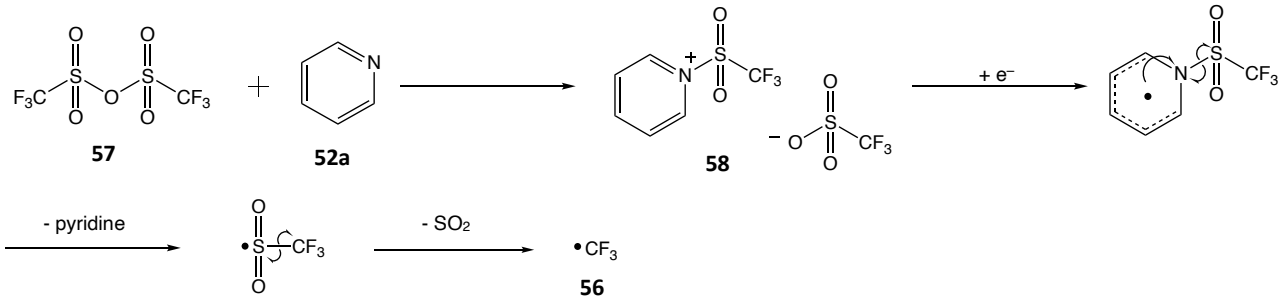

Scheme 11: Our proposed synthesis of the trifluoroacetylpyridinium salt and the synthesis of a pyridinium complex, as a source of trifluoromethyl radicals by Qing et al.; [87]

Recently, Katayev *et al.* commented on the equilibrium between the trifluoroacetyl radical and the $CF_3^{\bullet}$ radical, during the photochemical reduction of TFAA. Here, the group had to implement a high pressure (10 bar) carbon monoxide environment to suppress the formation of any trifluoromethylated products, as this shifted the equilibrium to favour the production of the trifluoroacetyl radical. We predicted that without such reaction conditions the formation of the $CF_3^{\bullet}$ radical would be favoured, and so, the reduction of a trifluoroacetylpyridinium salt should lead to the formation of trifluoromethylated products. To the best of our knowledge, this method of electrochemically reducing a trifluoroacetylpyridinium salt to produce a $CF_3^{\bullet}$ radical has not been reported on before. However, during the course of this project, Qing *et al.* reported on the reaction of pyridine and trifluoromethanesulfonic anhydride (**57**) to form a pyridinium complex (**58**) that was reduced photochemically to produce sulfur dioxide and a $CF_3^{\bullet}$ radical (Scheme 11).[87] To the best of our knowledge, there is no prior evidence of the reduction of acylpyridinium salts, but there is some precedence for the electrochemical reduction of pyridinium salts demonstrated by Ames, who reported on the reduction potentials of styrylpyridinium salts which were in the range of -0.89 – -1.21 V.[88]

Table 1: List of possible CF_3 radical sources associated with costs (according to Merck UK August 2021).

CF_3• Radical Source	Price £/mmol
Trifluoroacetic Anhydride (**51**) 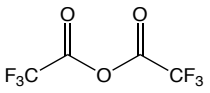	0.09
Trifluoromethanesulfonyl Chloride (**59**) 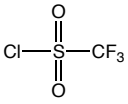	1.80
Trifluoromethanesulfonic Anhydride (**57**) 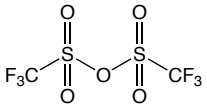	1.90
Langlois' Reagent (**44**) 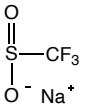	2.64
Ruppert-Prakash Reagent (**6**) 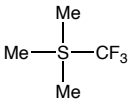	3.60
Trifluoroiodomethane (**38**) CF_3I	14.20
Umemoto's Reagent (**25**) 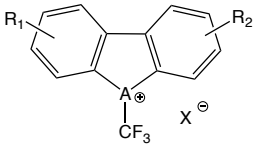 A: S, Se, Te, O X: BF_4, Otf, PF_6, SBF_6, Sb_2F_{11}	51.50
Togni's Reagent (**17**) 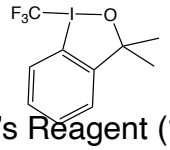	100.00

3.2 Characterisation of Pyridinium Salts

There has been little information reported on trifluoroacetylpyridinium salts, perhaps because the formation and characterisation of this type of salt appears to be elusive. In 1988 King reported the synthesis of the trifluoroacetylpyridinium salt (**53a**) which could undergo addition of a second pyridine to form the 2-dihydropyridinylpyridinium (2-DHPP, **60**) species (Scheme 12a).[89] This process was reversible, with the 2-DHPP product being favoured at temperatures lower than -50 °C, whereas at room

temperature, the equilibrium favoured pyridine and TFAA as individual components (performed in a non-polar solvent). The group were able to prove the reversibility of this reaction through cycling the temperature between room temperature and -90 °C whilst observing the products formed. The addition of the second pyridine was suggested to be due to the large charge-dipole destabilisation effect caused by the formation of the pyridinium salt. Through ^{13}C NMR studies, the 2-DHPP species could be identified via an indicative peak at 62-70 ppm corresponding to the carbon nucleus in the N^+-C bond, where the pyridinium nitrogen bound to the dihydropyridinyl ring. IR studies were also used, where the carbonyl bond in the 2-DHPP structure shifted to lower energies, whereas the carbonyl bond in the trifluoroacetylpyridinium salt shifted to higher energies, compared to the carbonyl bond in TFAA. King also reported the influence of substituents on the pyridine ring, where substitution of electron donating groups on the 3- or 4- position led to formation of species analogous to the trifluoroacetylpyridinium salt (**53a**), whereas substitution of electron withdrawing groups led to the formation of species analogous to the 2-DHPP species (**60**).

Later in 1995, Christophersen *et al.* attempted to prepare the trifluoroacetylpyridinium salt **53a** but were unable to do so, and instead reported that structure **61** was formed at room temperature, in deuterated chloroform ($CDCl_3$) and upon cooling the 2-DHPP (**60**) species was formed (Scheme 12b).[90] Christophersen *et al.* suggested that structure **53a** would have been formed transiently at cold temperatures, as an intermediate between structures **61** and **60**, however they were unable to obtain any structural data as proof that it was formed. The presence of structure **60** at room temperature was determined by Raman spectroscopy, where upon addition of pyridine to TFAA the C=O bond decreased in intensity.

The only other trifluoroacetylpyridinium-type salt to be reported is the trifluoroacetyl-4-dimethylaminopyridinium salt **53b** (Scheme 12c) formed from TFAA and 4-dimethylaminopyridine (4-DMAP, **52b**), which has been used to synthesise trifluoroacetylated heterocycles.[91, 92] The structure of **53b** was assigned using NMR and IR spectroscopy, where the dimethyl group protons were shifted upfield compared to unreacted 4-DMAP.

For the work discussed in this thesis, a wide range of pyridines (**52a-52n**, Figure 4) were reacted with TFAA in an effort to produce trifluoroacetylpyridinium salts. To do this, TFAA (1.5 mmol) was added dropwise to a solution of pyridine (1 mmol) and anhydrous acetonitrile (10 ml), in a 20 ml sample vial with an argon atmosphere. An excess of TFAA was used to ensure all of the pyridine was reacted. The acetonitrile was dried and degassed for 30 min before the TFAA or pyridine was added. It was believed that the trifluoroacetylpyridinium salts would be susceptible to hydrolysis of the N^{+}-$COCF_3$ bond if water was present, hence the need for the dry solvent and inert atmosphere. Acetonitrile was chosen as the solvent as it is polar, has a large dielectric constant and one of the broadest solvent windows, making it ideal for electrosynthesis. The work in this chapter will discuss the structural assignment and electrochemical behaviour of the salts.

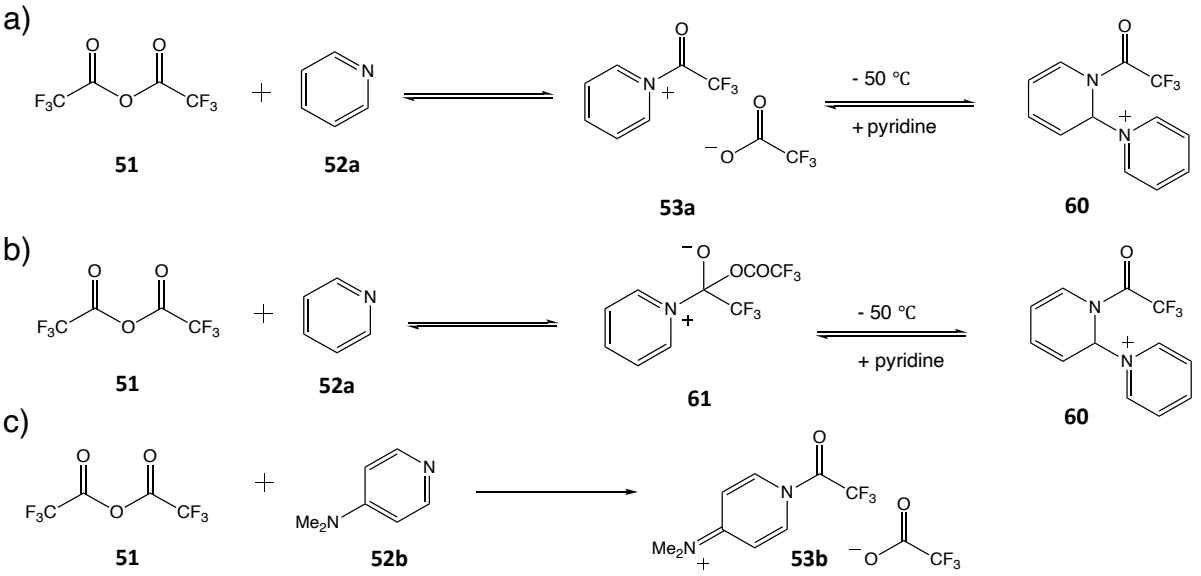

Scheme 12: a) reported attempts at syntheses of the trifluoroacetylpyridinium salt by King;[89] *b) reported attempts at syntheses of the trifluoroacetylpyridinium salt by Chrisophersen et al.* [90] *and c) the reported synthesis of a trifluoroacetyl-4-dimethylaminopyridinium salt.*[91, 92]

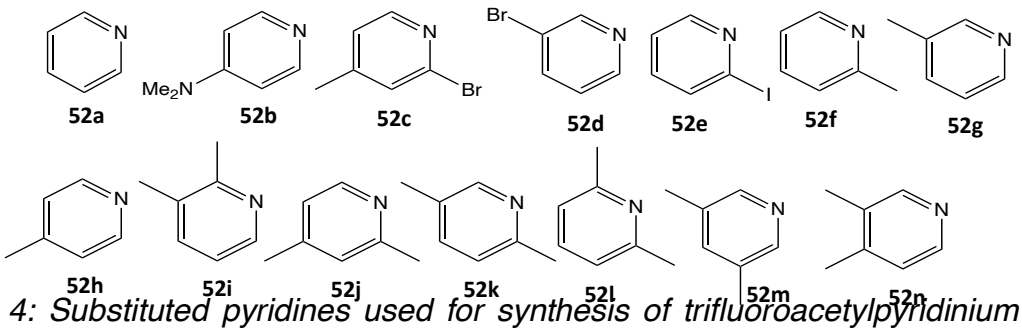

Figure 4: Substituted pyridines used for synthesis of trifluoroacetylpyridinium salts: 52a) pyridine; 52b) 4-dimethylaminopyridine; 52c) 2-bromo-4-methylpyridine; 52d) 3-bromopyridine; 52e) 2-iodopyridine; 52f) 2-methylpyridine; 52g) 3-methylpyridine; 52h) 4-methylpyridine; 52i) 2,3-dimethylpyridine; 52j) 2,4-dimethylpyridine; 52k) 2,5-dimethylpyridine; 52l) 2,6-dimethylpyridine; 52m) 3,5-dimethylpyridine; 52n) 3,4-dimethylpyridine.

3.2.1 NMR Characterisation

The species formed upon addition of TFAA and pyridine were characterised via NMR studies. For these investigations ^{1}H and ^{13}C NMR spectroscopy were performed on samples of the unreacted pyridines (**52a-52n**). Then, to these samples TFAA (1.5 molar equivalents) was added and the ^{1}H and ^{13}C NMR spectroscopy were performed again. The samples were run in dry MeCN so that the reaction conditions would be the same as when the pyridinium salts were used for electrochemical synthesis. The chemical shifts of the pyridine species (unreacted and reacted with TFAA) are listed in Tables 2 and 3. The proton chemical shifts were assigned based on splitting patterns and the carbon chemical shifts were assigned based on the Heteronuclear Single Quantum Coherence (HSQC)*[1]spectra, i.e. the proton-carbon single bond correlations. The full spectra for each compound can be seen in Appendix A. For clarity, Figure 5 shows the positions within the pyridinium structure which correspond to the labelled shifts in Tables 2 and 3, i.e. $C_{pyr\text{-}2}$ and $H_{pyr\text{-}2}$ correspond to the carbon and hydrogen atoms at the 2-position of the ring. Similarly, the $C_{Me\text{-}2}$ and $H_{Me\text{-}2}$

*HSQC spectra were obtained for the TFAA+pyridine, TFAA+2-iodopyridine, TFAA+3-methylpyridine, TFAA+4-methylpyridine mixtures supporting the assignment shown. For the other mixtures we were unable to obtain data from which definitive assignments could be made. The reason for this is not clear.

correspond to the carbon and hydrogen atoms of the methyl group substituted at the 2-position of the ring.

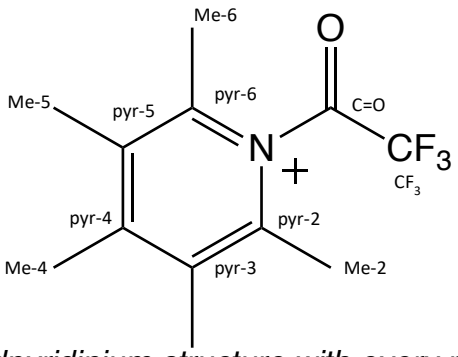

Figure 5: Trifluoroacetylpyridinium structure with every possible carbon or hydrogen position labelled, which corresponds to the shifts in Tables 2 and 3.

Comparing the proton environments (Table 2) of the unreacted pyridine and when TFAA was added, we saw that the addition of TFAA caused all the proton environments to be shifted downfield, for every pyridine species tested. Generally, the protons at the 3-, 4- and 5- positions were shifted more (0.1-0.8 ppm) than the protons at the 2- and 6-positions (0.1-0.3 ppm). This downfield shift could be evidence that the nitrogen atom had become cationic. Thus, the positive charge introduced to the ring attracted the electron density away from the hydrogen nuclei. These nuclei were then deshielded and experienced a greater effect of the magnetic field applied during the NMR measurements which was why the environments shifted downfield. These results are in contrast to the results reported by Christophersen *et al.*, who saw upfield shifts of the protons on addition of TFAA to pyridine in $CDCl_3$. Instead, these results are similar to the pyridinium trifluoroacetate (**61**) structure they reported, where upon formation of this structure the protons shifted downfield.

Looking at the carbon environments (Table 3), for all the pyridine species investigated the $C_{pyr\text{-}2}$ and $C_{pyr\text{-}6}$ environments shifted upfield upon the addition of TFAA. Conversely, the $C_{pyr\text{-}3}$, $C_{pyr\text{-}4}$ and $C_{pyr\text{-}5}$ environments all shifted downfield. In most cases, the $C_{pyr\text{-}4}$ showed the largest change in chemical shift, except for when methyl groups were present on the $C_{pyr\text{-}3}$ or $C_{pyr\text{-}5}$ positions. In these cases, the $C_{pyr\text{-}3}$ or $C_{pyr\text{-}5}$ carbons showed the largest change in chemical shift. Again, from comparison of

these results to those reported by Christophersen, it would appear that the pattern of results we see is more in line with the formation of the pyridinium trifluoroacetate structure. Christophersen reported that upon formation of the pyridinium trifluoroacetate structure; the carbon at the 2-position shifted upfield whilst the carbons at the 3- and 4- position shifted downfield.

The C=O and CF_3 peaks were easy to identify as the presence of the three fluorine atoms caused these peaks to be split into quartets. For TFAA the C=O environment was found at 158.3 ppm and the CF_3 environment was found at 115.8 ppm. When the TFAA was added to each pyridine both of these environments shifted downfield to approximately 160-162 ppm and 117-118 ppm. This downfield shift was most likely caused by the electron density being pulled towards the positively charged nitrogen atom which deshielded the carbon nuclei. However, there were two examples where this was not the case – when TFAA was added to 2-bromo-4-methylpyridine and 2-iodopyridine (Table 2, entries 7 and 11). In these examples, no C=O environment was seen and the CF_3 peak was shifted upfield to 114.9-115.0 ppm. The reason for this is unclear, but it could have something to do with the halogen group at the 2-position of the pyridine ring. It was also surprising that only one C=O and CF_3 environment was found in each of the solutions where the pyridine species had been reacted with TFAA. If the trifluoroacetylpyridinium species had been formed we would expect to see two C=O and CF_3 environments, corresponding to the trifluoroacetylpyridinium and trifluoroacetate ions respectively. The reason for the absence of peaks corresponding to a counter ion is unknown.

The spectra for each pyridine species after TFAA was added showed no evidence of a peak at 62-70 ppm which indicated that the 2-DHPP reported by King was not formed. Due to the lack of C=O and CF_3 peaks that would allow for the definitive identification of the trifluoroacetylpyridinium ion and the corresponding counterion an exact structure for the product formed upon addition of pyridine and TFAA cannot be given based on the NMR data presented here. However, the shifts in the ^{13}C and ^{1}H NMR suggest strongly that the pyridine had been reacted to form some sort of pyridinium species. One possible reason why separate C=O and CF_3 peaks for the

counterion and trifluoroacetylpyridinium species weren't seen could be that the pyridine, TFAA and trifluoroacetylpyridinium species were in a dynamic equilibrium which was rapid on the NMR timescale. Thus, we only saw a chemical shift averaged between the three possible environments. Future work could focus on variable temperature NMR to see if a cooler temperature allowed for a more definitive structure to be seen. Although the structures of these adducts have not been fully ascertained they are referred to as trifluoroacetylpyridinium salts for the remainder of this thesis.

	Species	NMR Shifts (ppm)									
		H_{pyr-2}	H_{pyr-3}	H_{pyr-4}	H_{pyr-5}	H_{pyr-6}	H_{Me-2}	H_{Me-3}	H_{Me-4}	H_{Me-5}	H_{Me-6}
1	Pyridine (**52a**)	8.56	7.32	7.72	-	-					
2	TFAA (**51**) + Pyridine (**52a**)	8.79	7.88	8.39	-	-					
3	DMAP (**52b**)	7.99	6.43		-	-	2.86 (N-Me)				
4	TFAA (**51**)+ DMAP (**52b**)	8.44	7.10		-	-	3.43 (N-Me)				
5	2-bromo-4-methylpyridine (**52c**)		7.38		7.16	8.17			2.30		
6	TFAA (**51**) + 2-bromo-4-methylpyridine (**52c**)		7.51		7.29	8.27			2.23		
7	3-bromopyridine (**52d**)	8.66		7.98	7.28	8.52					
8	TFAA (**51**) + 3-bromopyridine (**52d**)	8.83		8.35	7.65	8.68					
9	2-iodopyridine (**52e**)		7.78	7.41	7.34	8.33					
10	TFAA (**51**) + 2-iodopyridine (**52e**)		7.93	7.61	7.51	8.46					
11	2-methylpyridine (**52f**)		7.19	7.60	7.11	8.43	2.47				
12	TFAA (**51**) + 2-methylpyridine (**52f**)		7.79	8.38	7.77	8.61	2.75				
13	3-methylpyridine (**52g**)	8.40		7.54	7.21	8.35		2.30			
14	TFAA (**51**) + 3-methylpyridine (**52g**)	8.62		8.31	7.85	8.60		2.50			
15	4-methylpyridine (**52h**)	8.40	7.15		-	-			2.32		
16	TFAA (**51**) + 4-methylpyridine (**52h**)	8.52	7.44		-	-			2.45		
17	2,3-dimethylpyridine (**52i**)			7.42	7.04	8.25	2.43	2.24			
18	TFAA (**51**) + 2,3-dimethylpyridine (**52i**)			8.14	7.64	8.52	2.41	2.68			

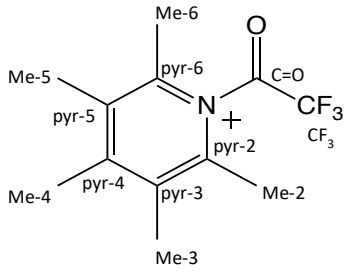

19	2,4-dimethylpyridine (**52j**)		7.01		6.94	8.28	2.42		2.26		
20	TFAA (**51**) + 2,4-dimethylpyridine (**52j**)		8.71		7.98	8.72	2.76		2.65		
21	2,5-dimethylpyridine (**52k**)		7.07	7.41		8.27	2.42			2.25	
22	TFAA (**51**) + 2,5-dimethylpyridine (**52k**)		7.68	8.19		8.43	2.69			2.44	
23	2,6-dimethylpyridine (**52l**)		6.97	7.48	-		2.42				2.42
24	TFAA (**51**) + 2,6-dimethylpyridine (**52l**)		7.08	7.67	-		2.48				2.48
25	3,4-dimethylpyridine (**52m**)	8.24			7.06	8.27		2.21	2.23		
26	TFAA (**51**) + 3,4-dimethylpyridine (**52m**)	8.46			7.73	8.46		2.51	2.39		
27	3,5-dimethylpyridine (**52n**)	8.20		7.34		-		2.25			
28	TFAA (**51**) + 3,5-dimethylpyridine (**52n**)	8.28		7.58		-		2.33			

Table 2: ^{1}H NMR shifts (ppm) of the different substituted pyridine species alone and when reacted with TFAA; including an insert of structure from Figure 5 to illustrate the hydrogen and carbon positions. All NMR frequencies are reported with an error range of +/- 0.04 ppm.

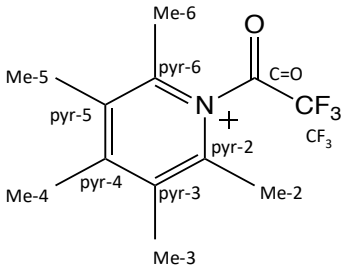

	Species	NMR Shifts (ppm)											
		C_{pyr-2}	C_{pyr-3}	C_{pyr-4}	C_{pyr-5}	C_{pyr-6}	C_{Me-2}	C_{Me-3}	C_{Me-4}	C_{Me-5}	C_{Me-6}	C=O	CF_3
1	TFAA (**51**)											158.3	115.8
2	Pyridine (**52a**)	150.8	124.8	136.9	-	-							
3	TFAA (**51**) + Pyridine (**52a**)	143.9	127.2	145.2	-	-						162.3	118.0
4	DMAP (**52b**)	149.7	106.5	154.1	-	-	38.9						
5	TFAA (**51**) + DMAP (**52b**)	145.2	107.7	157.0	-	-	39.8					161.5	118.5
6	2-bromo-4-methylpyridine (**52c**)	142.7	129.5	150.7	125.2	152.1			20.7				
7	TFAA (**51**) + 2-bromo-4-methylpyridine (**52c**)	140.8	130.7	154.9	126.0	149.4			21.2				115.0
8	3-bromopyridine (**52d**)	151.7	121.5	139.6	126.2	149.1							
9	TFAA (**51**) +3-bromopyridine (**52d**)	146.4	122.4	143.9	128.1	146.4						160.7	116.0
10	2-iodopyridine (**52e**)	118.8	136.0	139.1	124.3	151.8							
11	TFAA (**51**) + 2-iodopyridine (**52e**)	115.7	137.3	141.4	125.3	150.4							114.9
12	2-methylpyridine (**52f**)	159.4	124.1	137.2	121.7	150.0	24.5						
13	TFAA (**51**) + 2-methylpyridine (**52f**)	155.9	128.1	143.3	124.7	145.1	20.4					162.1	118.1
14	3-methylpyridine (**52g**)	150.8	134.1	137.0	123.9	147.5		18.2					
15	TFAA (**51**) + 3-methylpyridine (**52g**)	142.5	147.4	139.6	127.6	140.1		18.5				161.8	117.7

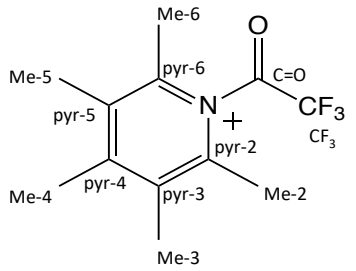

16	4-methylpyridine (**52h**)	150.4	125.6	148.2	-	-			21.0				
17	TFAA (**51**) + 4-methylpyridine (**52h)**	146.3	127.1	154.3	-	-			21.7			162.3	118.2
18	2,3-dimethylpyridine (**52i**)	158.1	132.4	137.7	122.2	147.3	22.8	19.2					
19	TFAA (**51**) + 2,3-dimethylpyridine (**52i**)	154.3	138.4	146.5	125.2	139.4	18.4	18.2					117.7
20	2,4-dimethylpyridine (**52j**)	159.1	124.8	148.3	122.6	149.8	24.4		20.2				
21	TFAA (**51**) + 2,4-dimethylpyridine (**52j**)	154.2	129.2	160.6	126.0	141.1	19.6		22.2				
22	2,5-dimethylpyridine (**52k**)	156.2	123.5	137.6	131.0	150.3	24.0			18.0			
23	TFAA (**51**) + 2,5-dimethylpyridine (**52k**)	152.3	128.3	141.2	136.5	147.6	19.4			18.0		161.5	117.5
24	2,6-dimethylpyridine (**52l**)	158.7	121.0	137.6	-	-	24.7						
25	TFAA (**51**) + 2,6-dimethylpyridine (**52l**)	154.6	125.9	146.9	-	-	19.6					161.1	118.2
26	3,4-dimethylpyridine (**52m**)	150.9	133.4	148.3	125.4	146.6		16.4	19.1				
27	TFAA (**51**) + 3,4-dimethylpyridine (**52m**)	141.0	138.6	161.4	128.5	139.2		16.9	20.7			161.4	117.5
28	3,5-dimethylpyridine (**52n**)	147.9	133.6	137.7	-	-		18.1					
29	TFAA (**51**) + 3,5-dimethylpyridine (**52n**)	139.5	148.4	139.0	-	-		18.3				161.5	118.4

Table 3: [13]C NMR shifts (ppm) of the different substituted pyridine species alone and when reacted with TFAA; including an insert of structure from Figure 5 to illustrate the hydrogen and carbon positions.

All NMR frequencies in this table are reported with an error range of +/- 0.2ppm

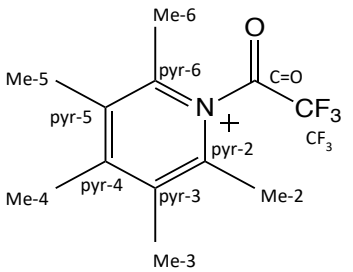

3.2.2 Electrochemical Characterisation

Following on from the NMR investigations, cyclic voltammetry was used to establish which trifluoroacetylpyridinium salts would be suitable $CF_3^{\bullet}$ radical precursors, according to the criteria discussed previously:

- Can be reduced within the solvent window
- Single reduction process is seen that does not overlap with other redox processes

Before the pyridinium salts were investigated, a cyclic voltammogram of TFAA alone was taken, seen in Figure 6.

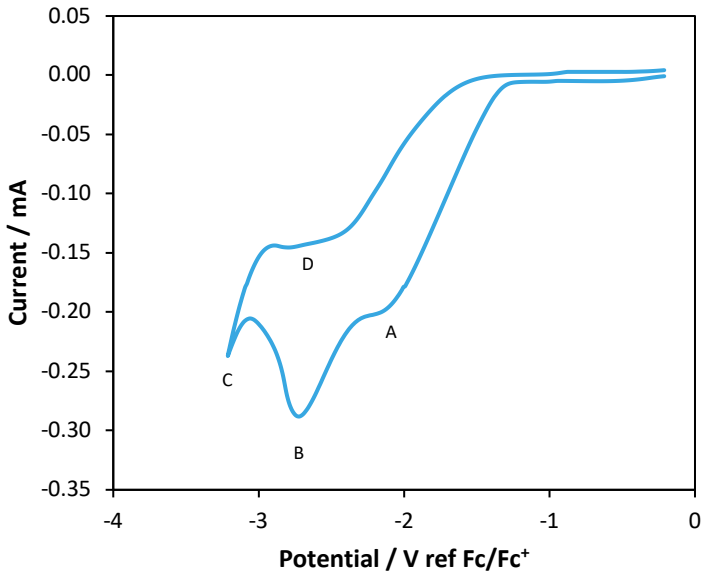

Figure 6: Cyclic voltammogram of TFAA (10 mM) in MeCN with $TBAPF_6$ electrolyte.

The cyclic voltammogram of TFAA showed three reduction processes in the forward scan, each labelled in Figure 6 (A, B and C). The first reduction process (position A) was seen as a 'shoulder' at -2.15 V. A second reduction current was then seen, resulting in a peak current of -28.7mA at -2.70 V (position B). These results suggest that two different reduction processes were taking place, but the two processes occurred in a small range of potential, causing the peaks to overlap and hence only a shoulder was seen for one of them. The onset reduction of MeCN was then seen directly after this reduction peak, at -3.16 V (position C).

It was proposed that during the initial reduction (A), the TFAA (**51**) was reduced to produce an acyl radical and a carboxylate. Directly after the reduction of TFAA a second reduction occurred, which resulted in the peak seen at -2.70 V. This second reduction led to the formation of an adsorbed layer on the surface of the electrode which blocked further reduction and so the electrode surface was passivated. This passivation is clear from the sharp decrease in current, as a more gradual decrease in the current would be seen if the current was diffusion limited only. Then, either due to the reduction of the solvent or the passing of time, the film was removed from the surface of the electrode. When the potential was reversed on the backward scan the species that was reduced at –2.70 V remained in the diffusion layer surrounding the electrode as not all of it had been reduced in the forward scan. In the absence of the adsorbed layer, the species was able to be reduced, leading to the current seen at position D. It was speculated that the identity of the species that was reduced at points B and D in Figure 6 was that of a trifluoroacetyl radical (**55**), which was reduced to form a trifluoroacetyl anion (**62**). Work done by Lund *et al.* reported the theoretical reduction potentials of acyl radicals, estimated using a rotating disk electrode. They found that the electrochemical reduction of acetic anhydride resulted in the formation of an acyl radical, and the subsequent reduction of this newly formed acyl radical was estimated to be -2.03 V (vs SCE).[93] We believed this to be a reasonable comparison to the experimental value of -2.70 V (vs Fc/Fc^{+}) that we observed. Lund *et al.* also reported that the reduction of the acyl radical would happen at a faster rate than decarbonylation to form a $CF_3^{\bullet}$ radical (**56**). We believe this work supports our claim that the species reduced at points B and D in Figure 6 is a trifluoroacetyl radical.

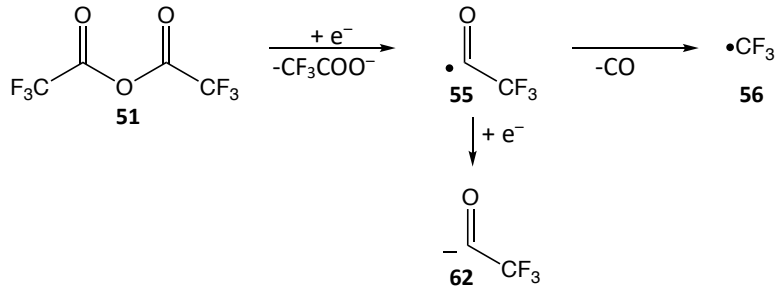

Scheme 13: Proposed mechanism for the reduction of TFAA

It was clear from the reduction currents seen in Figure 6 that TFAA alone would not be an ideal reagent to use for the electrochemical production of $CF_3^{\bullet}$ radicals. This was because the reduction of TFAA occurred at a position very close to the solvent window (reduction of the solvent was seen right after the reduction of the acyl radical). Reduction processes so close to the solvent window are non-ideal as the highly negative voltage could reduce other reactants in the solution, causing side reactions and contaminants. The evidence that multiple electron transfer process were occurring in a small potential range was also off-putting, as this could cause possible side reactions.

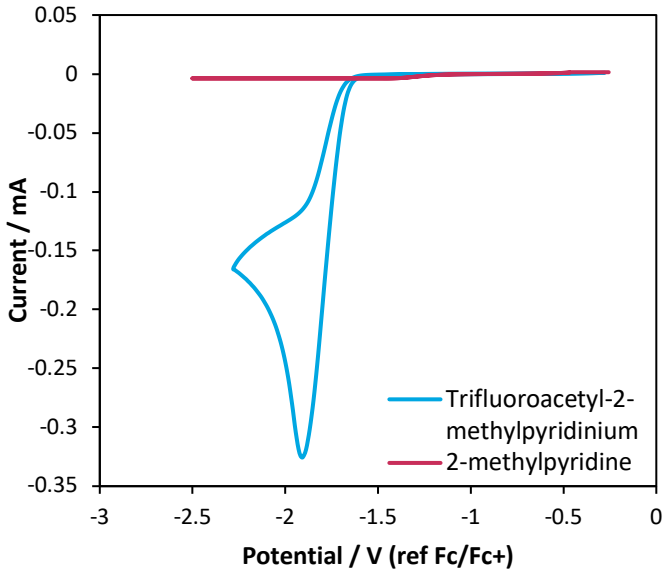

Figure 7: Cyclic voltammogram of: blue - trifluoroacetylpyridinium (10 mM) and red – 2-methylpyridine (10 mM) in MeCN with $TBAPF_6$ electrolyte.

Figure 7 shows the cyclic voltammogram of trifluoroacetyl-2-methylpyridinium (blue), prepared by adding TFAA (1.5 mmol) to 2-methylpyridine (1 mmol). The cyclic voltammogram of 2-methylpyridine is also given (red), which does not display any electrochemical activity in the potential range tested. Quite clearly, the electrochemical behaviour of the trifluoroacetyl-2-methylpyridinium was very different to the behaviour of TFAA. Here, one reduction peak was seen at -1.91 V with a reduction current of -0.33 mA. This peak most likely corresponds to the addition of an electron into the pyridine ring which then resulted in the cleaving of the N^+-$COCF_3$ bond to produce an

acyl radical. No other peaks were seen in the forward or backward scan, which suggests that the acyl radical was not reduced, unlike in the cyclic voltammogram of TFAA. This difference could be because the electron transfer between the electrode and the trifluoroacetylpyridinium salt did not directly cleave the N^{+}-$COCF_3$ bond. Whereas, when TFAA was reduced, the electron transfer from the electrode did result in the immediate cleaving of the O-$COCF_3$ bond. Hence, when TFAA was reduced the acyl radical was in close proximity to the electrode so could adsorb to the electrode and be reduced. When the trifluoroacetyl-2-methylpyridinium was reduced the additional step required for the acyl radical to be produced could have allowed enough time for the radical pyridinium species to diffuse away from the electrode surface and so the acyl radical was not reduced.

The electrochemical behaviour of the trifluoroacetylpyridinium salts is discussed in further detail in Chapter Four. For now, it is sufficient to say that the voltammograms of TFAA alone and when it had been reacted with a pyridine species show different electrochemical behaviours. This is further evidence that a new species had been formed when TFAA was reacted with pyridine. The cyclic voltammograms of all the trifluoroacetylpyridinium species can be found in Chapter 3 and Appendix B, and the reduction potentials of each one have been listed in Table 4.

Overall, the reduction peaks of the trifluoroacetylpyridinium salts were seen at approximately -2 V. The only trifluoroacetylpyridinium salts that did not show a reduction current at -2 V were trifluoroacetyl-2-iodopyridinium, trifluoroacetyl-3-bromopyridinium and trifluoroacetyl-4-dimethylaminopyridinium. The reasons for this were thought to be due to the substituents on the pyridine ring. These effects are discussed in further detail in Chapter Four.

	Species	Peak potential / V (ref Fc/Fc^+)
1	Trifluoroacetylpyridinium (**53a**) 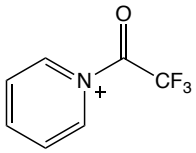	-1.98
2	Trifluoroacetyl-4-dimethylaminopyridinium (**53b**) 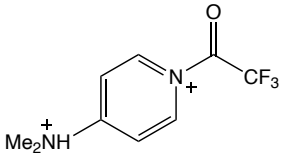	-2.29, -2.61
3	Trifluoroacetyl-2-bromo-4-methylpyridinium (**53c**) 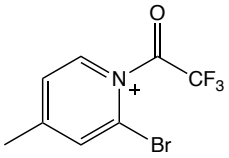	-2.06
4	Trifluoroacetyl-3-bromopyridinium (**53d**) 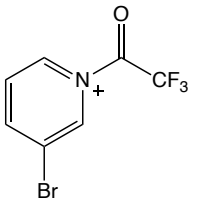	-1.62
5	Trifluoroacetyl-2-iodopyridinium (**53e**) 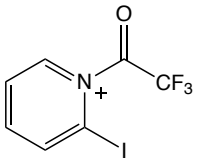	-1.67
6	Trifluoroacetyl-2-methylpyridinium (**53f**) 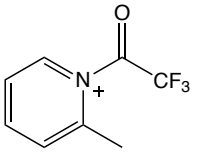	-1.91
7	Trifluoroacetyl-3-methylpyridinium (**53g**) 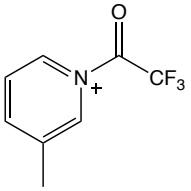	-1.95
8	Trifluoroacetyl-4-methylpyridinium (**53h**) 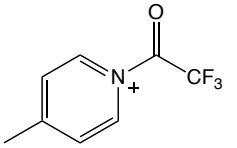	-2.02

9	Trifluoroacetyl-2,3-dimethylpyridinium (**53i**) 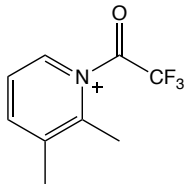	-2.05
10	Trifluoroacetyl-2,4-dimethylpyridinium (**53j**) 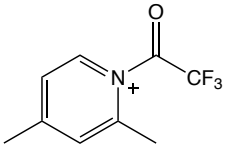	-1.97
11	Trifluoroacetyl-2,5-dimethylpyridinium (**53k**) 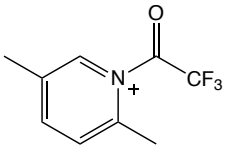	-2.06
12	Trifluoroacetyl-2,6-dimethylpyridinium (**53l**) 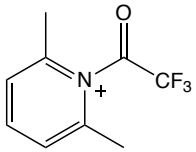	-2.00
13	Trifluoroacetyl-3,4-dimethylpyridinium (**53m**) 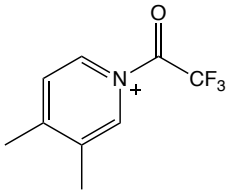	-2.07
14	Trifluoroacetyl-3,5-dimethylpyridinium (**53n**) 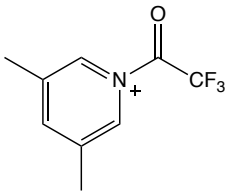	-2.06

Table 4: The proposed structures of the trifluoroacetylpyridinium salts and the corresponding peak potentials, determined from cyclic voltammetry.

3.3 Conclusions

The purpose of the experiments discussed in this chapter were to synthesise trifluoroacetylpyridinium salts and test if they would be suitable for electrochemical synthesis. Although the structures of the salts couldn't be assigned definitively from

the NMR spectra it was clear that a new product had been formed. Electrochemical analysis of this new product showed that a single reduction process occurred at a potential less negative than the reduction of MeCN, making it a suitable candidate to act as a prospective $CF_3^{\bullet}$ radical source. The remaining chapters of this thesis will further discuss the electrochemical behaviour of the trifluoroacetylpyridinium salts and their use in the oxytrifluoromethylation of styrene.

Chapter Four – Electrode Modification

4.1 Introduction to Electrode Modification

4.1.1 Motivation for this Work

As stated previously, the main objective of this project was to develop an electrosynthetic trifluoromethylation reaction. It was hoped that electrochemical investigation of the trifluoroacetylpyridinium salts would allow for a deeper understanding of the fate of the radicals formed upon electron transfer. Thus this would help our efforts to demonstrate that electrosynthesis is not a 'black box'. During the initial cyclic voltammetry studies of the trifluoroacetylpyridinium salts, discussed in Chapter Three, it was found that some of the salts passivated the electrode surface (shown by the peak current decreasing upon successive scans). It was thought that further examination of this behaviour may help to provide information on what happened to the trifluoroacetylpyridinium salts following reduction at the electrode. It was quickly established that the pyridinium salts were forming a film attached to the electrode surface after reduction had occurred. The presence of this film then modified the behaviour of the electrode. From herein the formation of the film on the electrode surface will be referred to as electrode modification. The work in this chapter describes how the electrodes were modified and what influenced the modification process.

4.1.2 Electrode Modification Background

Broadly speaking, the research field of surface modification is focused on the binding of one material onto another, for instance, the formation of a polymer on a metal surface.[94] There are varying reasons to change the surface properties of a material, for example: coating of biomedical implants,[95] antibacterial coatings,[96] nanotechnologies[97] or sensors.[98] In most cases, the success of a surface coating is judged on stability, adhesion and lifetime. There are many techniques available to produce a layer on a surface. Layers can be deposited in a gaseous state using techniques such as vapour deposition,[99] or ion beam assisted deposition.[100] They can

also be deposited in a molten state using plasma deposition,[101] or as is the case with the work presented here, they can be deposited from a solution state.

Looking specifically at electrode modification, electrodes can be modified in different ways such as self-assembly,[102] drop coating,[103] electrode doping or electrodeposition/electrografting, to name a few.[104, 105, 106, 107] Electrodeposition can take place when a species in solution undergoes electron transfer at the electrode surface, which then reacts with the electrode to form a covalent bond. Initially, a monolayer forms on the electrode surface. As time continues, fresh reactants attach to the existing monolayer, forming polymer chains. Depending on the intended use of the surface coating, it can be beneficial to only produce a monolayer, or allow polymerisation to occur, creating multilayers. As the formation of the coating relies on radical formation it is often harder to stop the process at the monolayer stage. Thus, much work has been done to control monolayer formation. These efforts have included using redox mediators, protection-deprotection strategies or bulky substituents.[108]

Diazonium salts are commonly used to create organic films made up of benzene or benzene-like layers at electrode surfaces.[109, 110, 111, 112] The diazonium salts easily undergo reduction at the electrode, accepting an electron which triggers the loss of dinitrogen (known as dediazonation), forming an aromatic radical which attaches onto the electrode surface. This is a popular method as the diazonium salts are cheap and readily available. However, diazopyridinium cannot be isolated as a stable salt and so it must be prepared in situ from a corresponding aminopyridine precursor before electrografting can commence.[113] The preparation of diazopyridinium also leads to the production of hydroxypyridine as one of the major products, creating unideal electrodeposition conditions, hence why comparatively little work has been done with diazopyridinium compared to other diazonium salts.

Despite this, Agullo *et al.*[114] have been successful in the electrografting of pyridine to the surface of glassy carbon electrodes using a diazonium salt. The group reacted sodium nitrite with 3-aminopyridine to form 3-diazopyridinium cations which were then analysed using cyclic voltammetry. When the cyclic voltammetry was performed, the

reduction of the 3-diazopyridinium cations resulted in the electrografting of pyridinium onto the glassy carbon surface. The first voltammogram recorded by the group showed a broad reduction peak at –0.4 V corresponding to the dediazonation of the cation. Consecutive voltammograms showed a decrease in the peak current, indicative of an electrografting process. As the pyridine attached to the electrode it passivated the electrode surface and blocked further electron transfer between the electrode and the remaining diazopyridinium, resulting in the drop in current.

Agullo *et al.* only attempted to electrograft 3-aminopyridine to the electrode surface as it was believed that the 4- and 2-diazopyridinium salts were highly unstable. However, using a similar method to Agullo *et al.*, in 2017 Smida *et al.* were able to electrograft 2-, 3- and 4- aminopyridine to a glassy carbon electrode.[115] Smida *et al.* saw the same distinctive passivation of the electrode surface as Agullo *et al.* when conducting cyclic voltammograms for all three diazopyridinium salts. The X-ray photoelectron spectroscopy (XPS) data taken for the three electrografted salts was also in agreement with that of Agullo's group. Interestingly though, they reported that the surface concentration of carbon and nitrogen within the layer grafted from 3-aminopyridine was higher than that of the 2- or 4-aminopyridine indicating that 3-aminopyridine formed thicker, more compact multilayers. Smida *et al.* tested the blocking properties of the deposited pyridine layers by evaluating the redox behaviour of ferricyanide towards the electrografted electrodes. For bare glassy carbon electrodes, ferricyanide exhibited quasi reversible redox behaviour. The group found that the peak current decreased and the peak separation increased in the presence of the deposited pyridine layers as compared to the bare glassy carbon electrode. This indicated that the presence of pyridine on the electrode surface blocked electron transfer between the electrode and the ferricyanide species in solution. The blocking effect was strongest for the layer formed from 3-aminopyridine, followed by 4-aminopyridine, with layers formed from 2-aminopyridine showing very small amounts of blocking. After gathering this information, Smida *et al.* used pyridine-modified-graphite-electrodes electrografted from 4-aminopyridine to grow electroactive biofilms. 4-aminopyridine was chosen as the electrografting material as it formed a thin homogenous film that did not completely block electron transfer. The

pyridine-modified- electrodes showed improved hydrophilicity (the static contact angle of a water droplet decreased from 97° to 52°) and better catalytic performance toward the growth of the biofilm compared to the bare glassy carbon electrodes.

Another work which showcases the advantages of pyridine based electrografted films is that of Yeşildağ *et al.*[116] This group were successful in electrografting films from 3-aminopyridine, 6-aminoquinoline and 5-aminophenanthroline onto glassy carbon, using the same techniques as Agullo and Smida. Once the films were established the group then reacted them with ruthenium trichloride ($RuCl_3$) to form ruthenium complexes. Ruthenium-pyridine based films are highly popular organometallic materials,[117] as they exhibit desirable optical properties in the visible light spectrum such as: long excited state lifetimes, high luminescence quantum yields and high stability.[118] Thus, the simple and reproducible synthesis of these films by Yeşildağ was highly effective and the method has the potential to be extended for other metals with possible applications for electronic and photonic devices.

So far, all the examples given of using diazopyridine for electrografting have shown the deposition onto glassy carbon, however Li *et al.* used the same technique to deposit pyridine onto silicon substrates.[119] Silicon is a popular material used for solar energy converting devices as it has a band gap of 1.12 eV which is ideal for adsorbing solar light, whilst also being cheap and readily available.[120, 121] As such, it has been used widely as a photocathode material in the water splitting reaction to generate renewable hydrogen gas.[122] However, a drawback with using silicon is that an oxide layer will readily form on the surface of silicon in the presence of water or oxygen creating a passivating layer which decreases the photochemical activity. Due to this problem, much research has been done into modifying the silicon surface to stop it from oxidising. The work done by Li *et al.* deposited pyridinium onto silicon from 3-aminopyridine, via the same diazonium method used by other groups. They then reduced the deposited pyridinium molecules which led to the formation of pyridyl radicals. The radicals then acted as a source of easily cleaved H_2 gas, with the hydrogen evolution occurring at an overpotential of 400 mV less than with hydrogen-terminated silicon.

A different method from the diazonium approach to attach pyridine moieties to the electrode surface is the electrodeposition of pyridine-2-sulfonic acid and pyridine-2-carboxylic acid.[123, 124] Here, pyridine is reacted with the acids to form a substituted pyridinium ion, which they claim forms a pyridine radical upon reduction which then binds to the electrode surface. This method is less established than the diazonium method, only being reported by one group. It is also less clear as to how the pyridine radical is formed, as there is no obvious leaving group such as the dediazonation step in the diazonium method. However, they do manage to attach pyridine (or pyridine like molecules) to the electrode surface which they then use for anodic stripping voltammetry, in the analysis of toxic heavy metals in drinking water.

It has been shown here that there are various applications for the use of electrodeposited materials, and the ease with which the electrodes can be modified makes it an attractive technique. Although individual research groups have used the electrografting technique for different outcomes their approaches were almost always identical. The electrografting step was controlled either through a fixed potential method using chronoamperometry, or, a sweeping potential method using cyclic voltammetry. An elemental picture of the electrografted layer was then built up using a combination of XPS, infrared spectroscopy (IR), Raman spectroscopy and scanning electron microscopy (SEM), whilst the blocking effect was typically explored with redox probes such as potassium ferricyanide.

4.2 Modification via Cyclic Voltammetry

It is well established in the literature that the passivation of current during cyclic voltammetry is an indication that a process is occurring at the electrode surface to block electron transfer. This passivation is also commonly taken as a sign that the electrode has been modified. During many investigations that will be discussed throughout Chapter Four and Chapter Five of this thesis it was established that a film built up at the electrode surface caused by the reduction of certain trifluoroacetylpyridinium salts. In this section I will discuss the behaviour of various trifluoroacetylpyridinium salts during the cyclic voltammetry process and how this

corresponds to the modification of the electrode surface. For all cyclic voltammograms discussed a glassy carbon working electrode was used, apart from in the 'Different Electrodes' sub-chapter.

4.2.1 Trifluoroacetylmethylpyridinium and Trifluoroacetyldimethylpyridinium Salts

The electrochemical behaviour of the trifluoroacetylpyridinium salts that contained methyl groups on the pyridine ring were investigated by carrying out nine consecutive cyclic voltammograms. The behaviour of all the trifluoroacetylmethylpyridinium and trifluoroacetyldimethylpyridinium salts were very similar, so two examples are highlighted below and the remaining cyclic voltammograms can be seen in Appendix B.

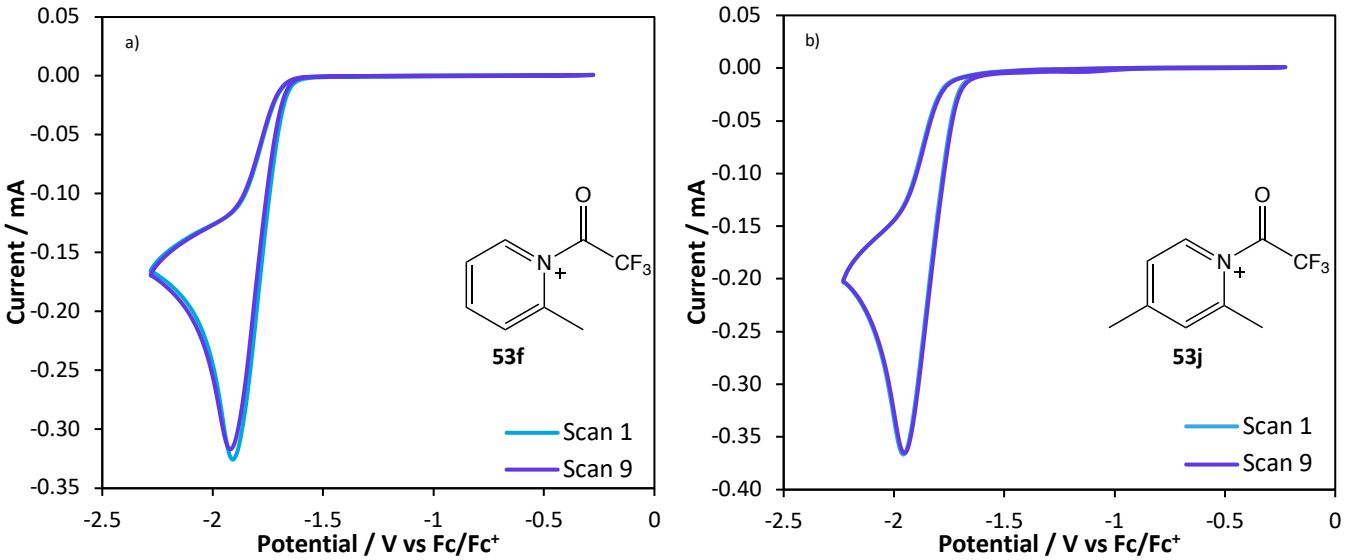

Figure 8: Cyclic voltammograms of the 1st and 9th scans of a 10 mM solution of a) trifluoroacetyl-2-methylpyridinium and b) trifluoroacetyl-2,4-dimethylpyridinium, both referenced to ferrocene, taken in degassed MeCN with $TBAPF_6$ supporting electrolyte, scan rate 0.1 V s^{-1}.

Figure 8 shows the 1st and 9th cyclic voltammogram for trifluoroacetyl-2-methylpyridinium (Figure 8a) and trifluoroacetyl-2,4-dimethylpyridinium (Figure 8b). For the trifluoroacetyl-2-methylpyridinium salt, in the 1st scan onset reduction began at -1.61 V with a peak reduction current of -0.33 mA occurring at -1.91 V. The 9th cyclic voltammogram shows a similar behaviour, where onset reduction began at -1.61 V

and reached a peak reduction current of -0.32 mA at -1.92 V. The minor shift in potential seen here was due to using a quasi-reference electrode, which is not as accurate as an internal reference electrode. The small decrease in current is negligible. The cyclic voltammograms for trifluoroacetyl-2,4-dimethylpyridinium show a similar behaviour. In the 1st scan the reduction current began at -1.66 V, with a peak reduction current of -0.39 mA occurring at -1.97 V. In the 9th scan a peak reduction current of -0.37 mA was seen at -1.96 V. Again these very minor differences in the current and potential between the 1st and 9th scan are negligible.

The reproducible behaviour shown here from the 1st to the 9th cyclic voltammogram for both salts evidences that no electrode modification had taken place, as the electron transfer between the salts in solution and the electrode surface did not change over time. This reproducible behaviour was identical for all methyl and dimethyl substituted trifluoroacetylpyridinium salts tested.

4.2.2 Trifluoroacetylpyridinium

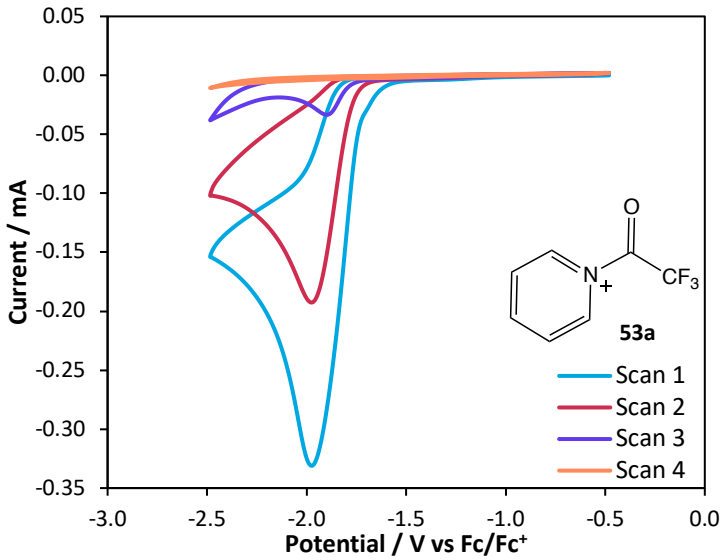

Figure 9: Cyclic voltammograms of trifluoroacetylpyridinium (10 mM) in degassed, anhydrous MeCN with $TBAPF_6$ electrolyte (0.1 M). Scan rate 0.1 V s^{-1}. Potentials are referenced to ferrocene. Four consecutive scans can be seen, indicated by different colours: scan 1 – light blue; scan 2 – red; scan 3 – purple; scan 4 – orange.

The electrochemical behaviour of trifluoroacetylpyridinium over the course of four cyclic voltammograms can be seen in Figure 9. In the 1st scan, reduction began at -1.52 V and a peak reduction current of -0.33 mA was seen at -1.98 V. The peak current decreased on the 2nd scan to -0.19 mA at -1.97 V. On the 3rd scan the peak current had further decreased to -0.03 mA at -1.90 V. In the 4th scan no reduction peaks were seen. This decrease in the reduction peak current is clear evidence that the electrode surface had been passivated, and that the reduction of trifluoroacetylpyridinium caused electrode surface modification.

4.2.3 Trifluoroacetyl-2-iodopyridinium

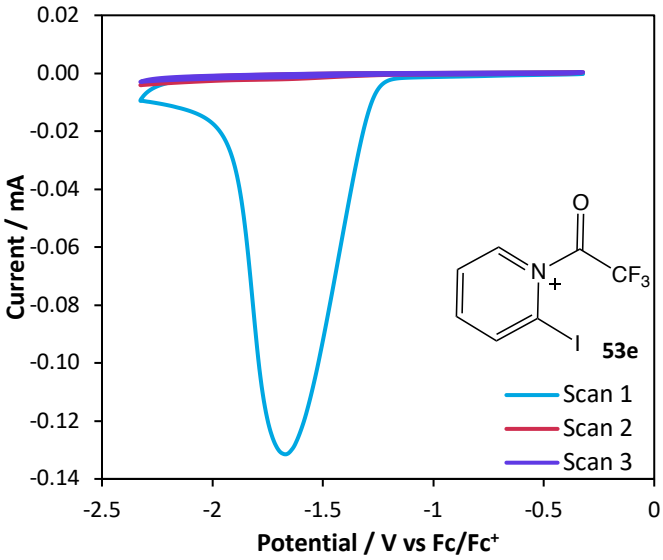

Figure 10: Cyclic voltammograms of trifluoroacetyl-2-iodopyridinium (10 mM) in degassed, anhydrous MeCN with $TBAPF_6$ electrolyte (0.1 M). Scan rate 0.1 V s^{-1}. Potentials are referenced to ferrocene. Four consecutive scans can be seen, indicated by different colours: scan 1 – light blue; scan 2 – red; scan 3 – purple.

The electrochemical behaviour of trifluoroacetyl-2-iodopyridinium (Figure 10) is quite different to that of trifluoroacetylpyridinium, despite both of them showing electrode passivation. For trifluoroacetyl-2-iodopyridinium, in the 1st scan onset reduction begins at -1.16 V and a peak current of -0.13 mA was reached at -1.67 V. After this scan no further reduction peaks were seen. Comparing this to trifluoroacetylpyridinium, we see that the iodine substituted salt had a much smaller peak reduction current and a more

positive peak potential. The shape of the 1st voltammogram for each salt was different too. For the trifluoroacetylpyridinium salt the peak shape followed a typical cyclic voltammogram response, where the current was dependent on the rate of electron transfer and increased rapidly until it reached a maximum. At this point the current became diffusion limited and slowly decreased giving the 'tail' to what is often referred to as the 'duck' shape of cyclic voltammograms. Conversely, for the trifluoroacetyl-2-iodopyridinium salt the response showed a rapid increase in current until it reached a maximum, before the current rapidly decreased, forming a 'V' shaped peak. This rapid decrease in current was not in accordance with diffusion limited currents, suggesting that a different process was responsible for limiting the electron transfer. It was believed that this rapid decrease in current was caused by the fast formation of the film on the electrode surface. Hence, this explains why the peak reduction current was much smaller for the trifluoroacetyl-2-iodopyridinium salt (as compared to the trifluoroacetylpyridinium salt) the electron transfer was blocked by the film before mass transport of the pyridinium salt could become the limiting factor in electron transfer.

4.2.4 Trifluoroacetyl-2-bromo-4-methylpyrindium

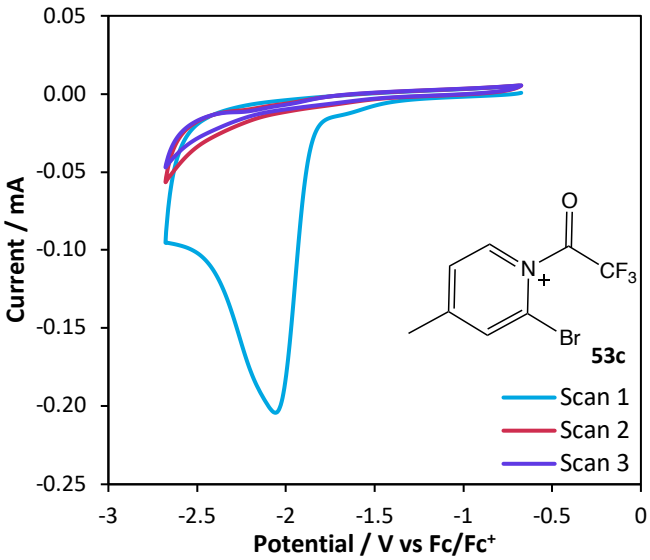

Figure 11: Cyclic voltammograms of trifluoroacetyl-2-bromo-4-methylpyridinium (10 mM) in degassed, anhydrous MeCN with TBAPF$_6$ electrolyte (0.1 M). Scan rate 0.1 V s^{-1}. Potentials are referenced to ferrocene. Four consecutive scans can be seen, indicated by different colours: scan 1 –light blue; scan 2 – red; scan 3 – purple.

The cyclic voltammograms for trifluoroacetyl-2-bromo-4-methylpyridinium (Figure 11) showed some similarities in behaviour to both the trifluoroacetylpyridinium and trifluoroacetyl-2-iodopyridinium salts. For trifluoroacetyl-2-bromo-4-methylpyridinium, onset reduction began at -1.31 V and the reduction peak occurred at -2.06 V with a peak current of -0.20 mA. Similarly to the tirlfuoroacetyl-2-iodopyridinium salt, no reduction peaks were seen after the 1st scan. Despite this, the behaviour in the 1st scan is more similar to that of trifluoroacetylpyridinium, where the current increases rapidly before the peak potential, but then decreased gradually after the peak potential. However, once the potential was reversed and swept in the positive direction the current immediately decreased to near 0 mA currents. The peak potential of trifluoroacetyl-2-bromo-4-methylpyridine was similar to that of trifluororacetylpyridine, whilst the peak current appeared mid-way between that of trifluoroacetylpyridinium and trifluoroacetyl-2-iodopyridinium. Overall these results suggest that the behaviour of trifluoroacetyl-2-bromo-4-methylpyridine contained a mixture of characteristics from both the trifluoroacetylpyridinium and trifluoroacetyl-2-iodopyridinium salts, and that the rate of formation of the film was also somewhere between the rapid formation of trifluoroacetyl-2-iodopyridinium film and the more gradual formation of the trifluoroacetylpyridinium film.

4.2.5 Trifluoroacetyl-4-dimethylaminopyridine

Figure 12 shows three cyclic voltammograms of trifluoroacetyl-4-dimethylaminopyridinium. In the 1st scan we saw two peaks, peak A at -2.29 V with a peak current of -0.19 mA, and the second peak, peak B at -2.61 V with a peak current of -0.28 mA. In the backward scan another reduction peak was seen at -2.62 V, -0.03 mA. This small peak was probably caused by the species responsible for peak B adsorbing to the surface of the electrode and so was still present at the electrode surface during the backward scan. In the 2nd scan only one peak occurred at -2.46 V with a peak current of -0.12 mA. Finally, in the 3rd scan there was a single peak at -2.45 V with a corresponding peak current of -0.06 mA. No reduction peaks were seen in the 4th scan.

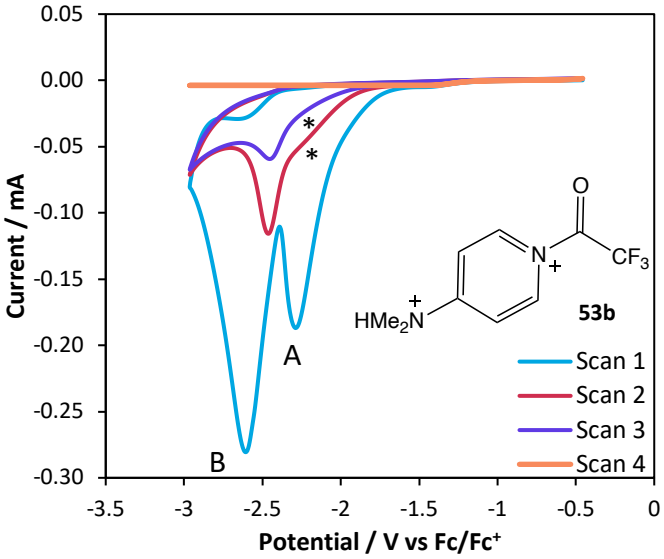

Figure 12: Cyclic voltammograms of trifluoroacetyl-4-dimethylaminopyridinium (10 mM) in degassed, anhydrous MeCN with $TBAPF_6$ electrolyte (0.1 M). Scan rate 0.1 V s^{-1}. Potentials are referenced to ferrocene. Four consecutive scans can be seen, indicated by different colours: scan 1 – light blue; scan 2 – red; scan 3 – purple.

It was surprising that two peaks were only seen in the 1st scan, but not in the others. In the 2nd and 3rd scans a small shoulder was seen in the forward scans before the reduction peak occurred (marked with an asterisk in both scans). This shoulder could be caused by the same reduction process that was responsible for peak A (at -2.29 V) in the first scan. It is well established that when the electrode was modified a passivating film was created on the electrode surface. It is possible that in the 1st scan, when the electrode was clean, both species A and B were reduced at the electrode surface. Then in the 2nd scan, when the film had partially formed, the process responsible for peak A was passivated more than the process responsible for peak B. Hence, peak B was the only peak seen. In the 2nd scan peak B was seen at a more positive peak potential (-2.46 V) than in the 1st scan (-2.61 V). This shift towards more positive peak potentials was also seen for the cyclic voltammograms taken of trifluoroacetylpyridinium (Figure 9), and is additional evidence that the electrode surface has been modified. The shape of the reduction peaks seen in the 1st and 2nd scans were very sharp in the way the current rapidly increased then decreased. Again, this suggests that the film formed quickly and passivated the electrode surface before mass transport became the limiting factor in electron transfer.

4.2.6 Trifluoroacetyl-3-bromopyridinium

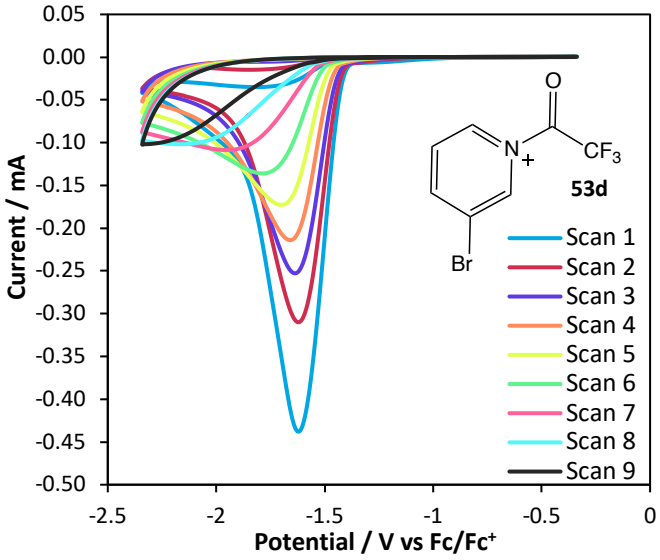

Figure 13: Cyclic voltammograms of trifluoroacetyl-3-bromopyridinium (10 mM) in degassed, anhydrous MeCN with $TBAPF_6$ electrolyte (0.1 M). Scan rate 0.1 V s^{-1}. Potentials are referenced to ferrocene. Four consecutive scans can be seen, indicated by different colours: scan 1 – light blue; scan 2 – red; scan 3 – purple; scan 4 – orange; scan 5 – yellow; scan 6 – green; scan 7 – pink; scan 8 – electric blue; scan 9 – black.

In the case of trifluoroacetyl-3-bromopyridinium (Figure 13), even after nine scans some reduction currents were still seen, although there was not a distinct reduction peak in the 9th scan. In the 1st scan the peak reduction current was -0.44 mA at -1.62 V, this shifted to -0.31 mA at -1.63 V in the 2nd scan, and -0.25 mA at -1.64 V in the 3rd scan. This pattern of peak current decreasing and peak potential shifting to more negative values continued, with the final reduction peak seen in the 8th scan occurring at -0.10 mA at -2.17 V. The peaks also appeared to get broader as successive scans were taken.

Once again, we see that the peak current decreased per scan, evidencing that the electrode surface had been modified and electron transfer between the electrode and the pyridinium salt was impeded. In previous cases, when the reduction peak shifted in potential over successive scans (trifluoroacetylpyridinium and trifluoroacetyl-4-dimethylaminopyridinium) the reduction peak shifted to more positive potentials. For

trifluoroacetyl-3-bromopyridinium, the peak shifted to more negative values. The reason for this is unclear, but could be due to the rate at which the passivating film is formed. For the trifluoroacetylpyridinium and trifluoroacetyl-4-dimethylaminopyridinium salts the reduction peak had disappeared by the 4th voltammogram, whereas for the trifluoroacetyl-3-bromopyridinium the reduction peak disappeared by the 9th scan. Hence, the rapid formation of the film caused a positive shift in the reduction potentials, whereas the slower formation resulted in a shift towards more negative potentials.

4.2.7 Different Electrodes

A series of cyclic voltammograms were taken in a solution of the trifluoroacetylpyridinium salt with various different working electrodes, to test if the material of the electrode surface influenced whether the electrode was modified. Three working electrodes were tested and the results can be seen below, the electrodes were a) Gold (Au); b) Platinum (Pt); c) boron doped diamond (BDD) and d) glassy carbon.

For the cyclic voltammograms taken with a Au working electrode (Figure 14a), in the 1st scan the reduction peak occurred at -1.64 V with a peak current of -0.31 mA. In the 9th scan the peak occurred at -1.65 V with a peak current of -0.30 mA. For the cyclic voltammograms taken with a Pt working electrode (Figure 14b), in the 1st scan the reduction peak occurred at -1.20 V with a peak current of -0.50 mA, and in the 9th scan the reduction peak occurred at the same peak potential, with a current of -0.49 mA. These results show that no electrode modification took place for either the Au or the Pt working electrodes, as the peak current and peak position were maintained over the course of nine cyclic voltammograms. When BDD was used as the working electrode (Figure 14c), a peak current of -0.71 mA was seen at -2.13 V and by the time the 9th scan was conducted the peak current had dropped to -0.11 mA and the peak had shifted to -1.89 V. Once again, this passivation of the electrode surface and resulting decrease in current are strong evidence that a film had formed at the electrode surface.

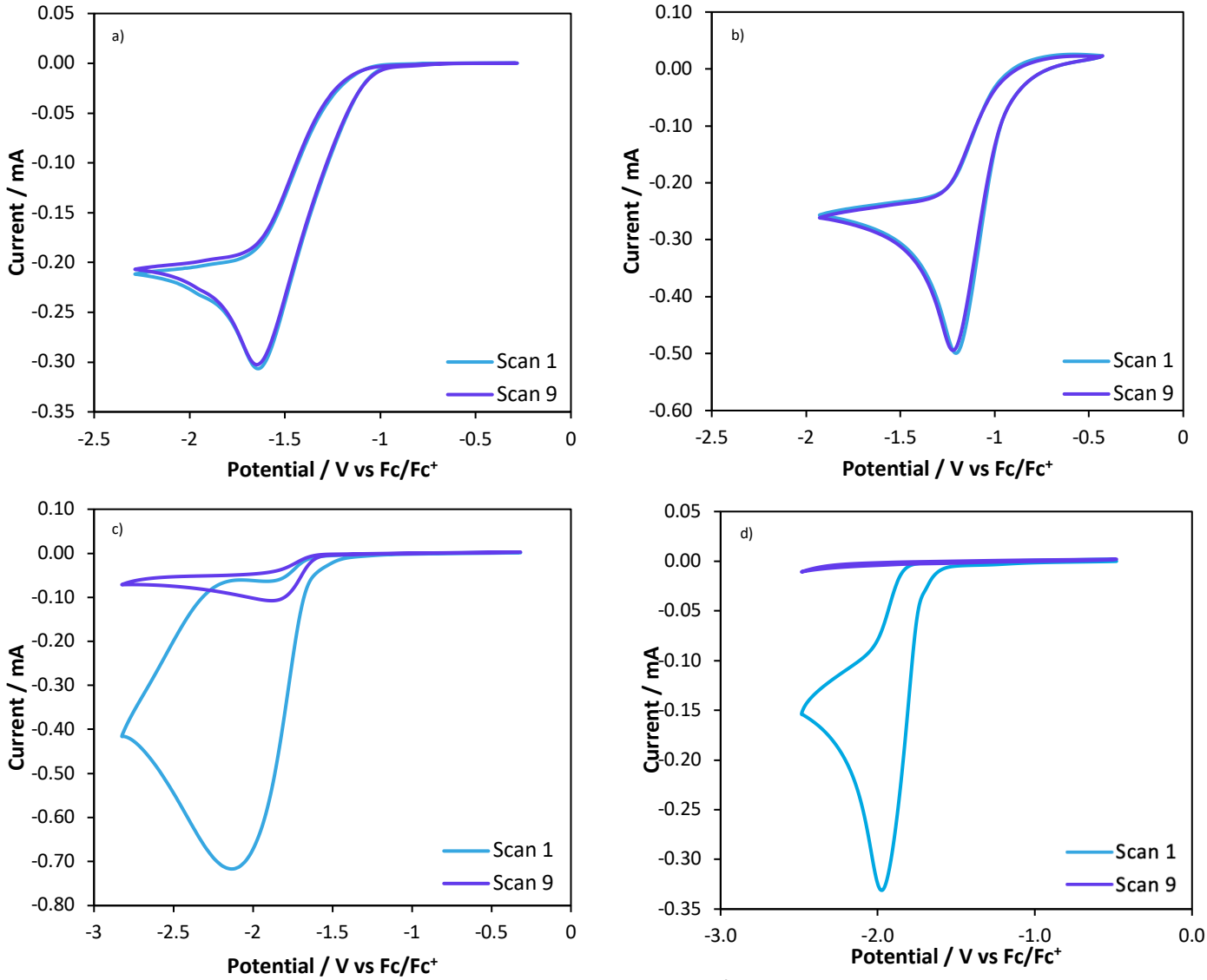

Figure 14: Cyclic voltammograms of the 1st and 9th scans of a 10 mM solution of trifluoroacetylpyridinium in degassed MeCN with $TBAPF_6$ supporting electrolyte, scan rate 0.1 V s^{-1} with different working electrodes: a) gold; b) platinum; c) boron doped diamond and d) glassy carbon.

Overall, comparing the behaviour of the Au, Pt, BDD and glassy carbon electrodes, it was clear that the carbon based electrodes (glassy carbon and BDD) allowed for film formation when the trifluoroacetylpyridinium salt was reduced. Whereas, the metal based electrodes (Au and Pt) did not allow for film formation. This suggests that a carbon-carbon bond was needed for the film to attach to the electrode surface upon reduction.

4.2.8 Summary of all Pyridinium Salts

Comparing the overall behaviour of all the pyridinium salts discussed in this sub-chapter there are some general conclusions that can be made. First of all, it would appear that the substituents on the pyridinium ring influenced whether electrode modification took place. When methyl- and dimethylpyridinium salts were used no electrode modification occurred, however, when no substituents or halogen/dimethylamino groups were used electrode modification did take place (evidenced by decreasing reduction currents/no reduction currents after the 1st scan). It can be said that the position of the substituent on the pyridine ring did not influence whether electrode modification ensued, as pyridinium salts with methyl groups on every possible ring position, specifically the 2-, 3- and 4-position were tested without any signs of electrode modification taking place. However, when the 2-, 3- and 4-positons were substituted with halogen or dimethylamino groups, modification did take place. This clarified that the reason for no electrode modification seen for the methyl/dimethyl substituted pyridinium salts was not due to a specific position on the pyridine ring being blocked. Nor was it due to the bulkiness or steric hindrance of the substituents, as the halogen and dimethylamino groups would be equally or more bulky than the methyl groups. With this in mind, it would appear that the electron density in the pyridine ring could be what influenced whether electrode modification took place. Methyl groups are electron donating so will increase the electron density in the pyridine ring, whereas halogen groups are electron withdrawing so will decrease the electron density. The one exception to this would be the case for the trifluoroacetyl-4-dimethylamino group, as the dimethylamino group should act as a strong electron donating group. It could be possible that the reaction solution contained some acid, as TFAA readily oxidises to trifluoroacetic acid (TFA) in the presence of water. This would mean that the dimethylamino group would be protonated, creating an $N^{+}Me_2$ group, that would be strongly electron withdrawing. Hence, it would seem that increasing the electron density in the pyridine ring influenced the behaviour of the pyridinium salts. It could be the case that when the pyridinium salts containing electron donating substituents were reduced at the electrode, the high electron density in the ring led to a quick decomposition of the radical, to cleave the N^{+}-$COCF_3$ bond. This quick process

meant that the radical did not 'hang around' long enough to form a film on the electrode surface. When the pyridinium salts with electron withdrawing groups were reduced, the radical formed was more stable and so the there was enough time for it to form a film on the electrode surface.

Although the ring position of the substituent on the pyridine ring did not influence whether electrode modification took place, for the pyridinium salts that did form films at the electrode surface, the ring position influenced the speed at which the film was formed. This is evidenced through the cyclic voltammograms taken of the pyridinium salts. If we compare the cyclic voltammograms for trifluoroacetyl-2-iodopyridinium (Figure 10) and trifluoroacetyl-2-bromo-4-methylpyridinium (Figure 11) we see that no reduction peaks were seen after the 1st scan, for both these salts. This suggests that maximum passivation of the electrode surface was accomplished in one scan, i.e. the film reached a point in which no further growth occurred. For the trifluoroacetyl-4-dimethylaminopyridinium salt, maximum passivation is seen after the 3rd scan (Figure 12), whilst for the trifluoroacetyl-3-bromopyridinium salt (Figure 13) maximum passivation was not seen until after the 8th scan. It is difficult to draw full conclusions from these results as we are comparing different substituents for each pyridinium salt (iodine, bromine and dimethylamino groups). However, looking at the position of the groups it could be said that the rate of passivation is fastest when the electron withdrawing substituent is at the 2-position (trifluoroacetyl-2-iodopyridinium and trifluoroacetyl-2-bromo-4-methylpyridinium) followed by electron withdrawing substituents at the 4-position (trifluoroacetyl-4-dimethylaminopyridinium) and finally it is slowest for electron withdrawing substituents at the 3-position (trifluoroacetyl-3-bromopyridinium). The rate of passivation of the electrode surface is further explored using chronoamperometry, in the next section.

4.3 Modification via Constant Potential

In this section, chronoamperometry was used to further investigate the rate of electrode passivation when the trifluoroacetylpyridinium salts were reduced. Trifluoroacetyl-2-methylpyridinium was used to compare the electrode-modifying pyridinium salts to the behaviour of a salt that was known to not passivate the electrode surface. For the results presented here, 10 mM solutions of each salt were prepared in a degassed solution of MeCN/0.1M $TBAPF_6$. Each salt was held at the relevant reduction peak potential (discovered via cyclic voltammetry) for 50 s. The starting and ending currents for each pyridinium salt, as well as the total amount of charge passed over the 50 s interval are summarised in Table 5.

The chronoamperogram for trifluoroacetyl-2-methylpyridinium can be seen by the yellow-green line in Figure 15. For this chronoamperogram we saw the highest starting current (-1.66 mA) and the most amount of charge passed (-14.72 mC). We know from the studies using cyclic voltammetry that reduction of trifluoroacetyl-2-methylpyridinium did not cause passivation of the electrode surface, as the peak current was unchanged after several scans. It was assumed that as no modification of the electrode surface took place during cyclic voltammetry, nor would it for chronoamperometry studies. Therefore the decrease in current seen here was caused by a build-up of a diffusion layer that limited the amount of fresh trifluoroacetyl-2-methylpyridinium that could reach the electrode surface. The greater amount of charge passed for this pyridinium salt that did not modify the electrode surface as compared to the pyridinium salts that did modify the electrode surface (all other salts presented in Figure 15) shows that the formation of the trifluoroacetylpyridinium-film at the electrode surface limited the electron transfer more than the build-up of the diffusion layer.

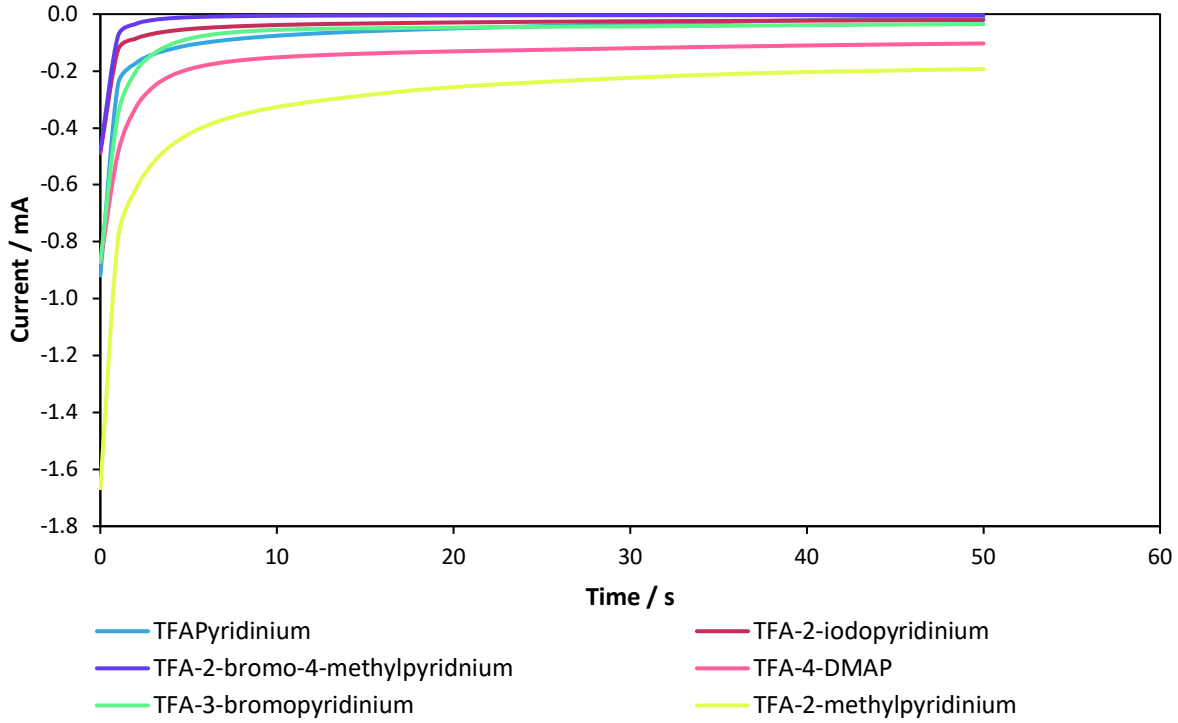

Figure 15: Chronoamperometry graphs taken for each of the pyridinium salts. Blue – trifluoroacetylpyridinium; red – trifluoroacetyl-2-iodopyridinium; purple – trifluoroacetyl-2-bromo-4-methylpyridinium; pink – trifluoroacetyl-4-dimethylaminopyridinium; green – trifluoroacetyl-3-bromopyridinium; yellow – trifluoroacetyl-2-methylpyridinium. Each of the scans were taken in a 10 mM solution of the pyridinium salt, in degassed, anhydrous MeCN, with 0.1 M $TBAPF_6$ supporting electrolyte. Each salt was held at the corresponding peak potential, derived from cyclic voltammetry.

	Pyridinium Salt	Start Current / mA	End Current / mA	Total Charge Passed / mC
1	TFApyidinium	-0.92	-0.012	-3.13
2	TFA-2-iodopyridinium	-0.49	-0.021	-1.90
3	TFA-2-bomo-4-methylpyridinium	-0.48	-0.004	-0.59
4	TFA-4-dimethylaminopyridinium	-0.88	-0.103	-7.58
5	TFA-3-bromopyridinum	-0.87	-0.035	-3.36
6	TFA-2-methylpyridinium	-1.66	-0.193	-14.72

Table 5: Table of the start and end currents, and the total amount of charge passed for the chronoamperometry scans taken in Figure 15.

Comparing all of the chronoamperograms in Figure 15, it can be seen that for the trifluoroacetyl-4-dimethylaminopyridinium, trifluoroacetyl-3-bromopyridinium and trifluoroacetyl-2-methylpyridinium salts the current decreased in an exponential-like way. Alternatively, for the trifluoroacetylpyridinium, trifluoroacetyl-2-iodopyridinium and trifluoroacetyl-2-bromo-4-methylpyridinium the current decreased rapidly and then tailed off. For the salts that are known to modify the electrode surface, the rapid decrease in current is evidence of a fast passivation of the electrode surface, i.e. a fast formation of the trifluoroacetylpyridinium film, whereas the gradual decrease in current shows a slower passivation/ formation of the film. The slower film formation also allowed for more electron transfer to occur, hence the higher amounts of charge passed for trifluoroacetyl-4-dimethylaminopyridinium and trifluoroacetyl-3-bromopyridinium salts. It should also be noted that not all of the electrons transferred from the electrode to the species in solution would have directly contributed to the formation of the trifluoroacetylpyridinium film. A proportion of the electrons transferred would have reduced the pyridinium salts, cleaving of the N^{+}-$COCF_3$ bond. Thus, for the pyridinium salts that passivated the electrode surface at a slower rate, a diffusion layer of the reduced (but not grafted) pyridinium salt would build up. Therefore, the decrease in current was caused by both passivation of the electrode surface and the presence of a diffusion layer.

Overall, it would appear that the chronoamperometry results largely agree with the results from the cyclic voltammetry experiments. The trifluoroacetyl-2-iodopyridinium salts rapidly formed a passivating film at the electrode surface, shown by the smaller amounts of charge passed and the quick decrease in current. The trifluoroacetyl-3-bromopyridinium and trifluoroacetyl-4-dimethylaminopyridinium were slower to form the passivating film, which allowed for more reduction of the salt, leading to more charge passed and the build-up of a diffusion layer.

A slight difference in results between the chronoamperometry experiments and the cyclic voltammetry experiments was seen for the reduction of trifluoroacetylpyridinium. During cyclic voltammetry the electrode was passivated relatively slowly (after 3 scans) whereas during chronoamperometry it was passivated quickly (rapid decrease

in current). The reason for this is not clear, but could be due to the mechanism in which the film is formed at the electrode surface.

4.4 X-Ray Photoelectron Spectroscopy

X-Ray Photoelectron Spectroscopy (XPS) was used to confirm that the passivation of current during CV was caused by a film forming at the electrode surface. It was also hoped that detailed analysis of a possible film would help to determine the nature of the trifluoroacetylpyridinium radical, therefore, XPS was chosen as it would give detailed chemical composition of the modified electrodes. For these studies, graphite electrodes were used instead of glassy carbon electrodes due to practicalities of placing large objects in the XPS chamber. The electrodes were all modified via 9 cyclic voltammograms in a 10 mM solution of each pyridinium salt. They were then washed via sonication in MeCN for 2 min before being air dried and kept in a vacuum for 12 hours before being transferred to the XPS chamber. The XPS spectra were then run using Avantage and were analysed using CasaXPS and Origin. As the spectra for each film were very similar, examples and noteworthy spectra are shown below, while full spectra for each modified electrode can be found in Appendix C.

Reviewing the literature, it would appear that formation of a trifluoroacetylpyridinium-type film on the surface of an electrode has not been reported on before. However, some groups have used TFAA as a derivatization tool for identifying nitrogen in complex polymers, via XPS.[125], [126]. To do this, the research groups would react TFAA with the polymers, forming a trifluoroacetamide group. This trifluoroacetamide group would then give identifiable XPS markers such as the CF_3 and N-C=O environments that would help to determine the amide concentration in these complex polymer structures. The XPS spectra reported by the research groups who investigated the TFAA derivatized polymers were very similar to the XPS spectra obtained for the modified electrodes discussed in this thesis, and so their results were helpful in identifying and clarifying the surface composition of the modified electrodes. It should be noted that the XPS spectra reported by these groups contained a neutral nitrogen

trifluoroacetamide species whereas we believe our reported spectra to contain cationic nitrogen, however we still believe the similarity in our spectra to be accurate.

4.4.1 Survey Spectrum

		C1s total at.%	N1s total at.%	O1s total at.%	F1s total at.%	I3d total at.%	Br3d total at.%
1	Clean	93	-	7	-	-	-
2	TFAPyridinium	69	8	8	15	-	-
3	TFA-2-iodopyridinium	77	7	9	6	< 1	-
4	TFA-2-bromo-4-methylpyridinium	75	5	11	6	-	< 1
5	TFADMAPyridinium	69	7	16	5	-	-
6	TFA-3-bromopyridinium	73	9	11	5	-	2

Table 6: Chemical composition of the clean (1) and modified graphite electrodes (2-6) determined from the XPS survey spectra.

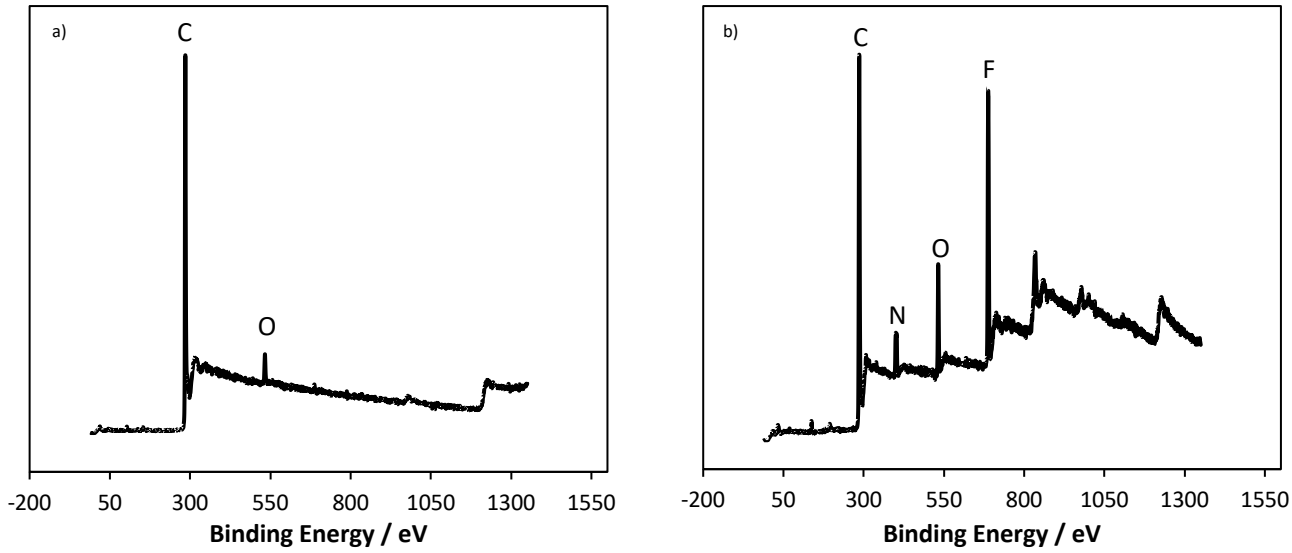

Figure 16: Survey spectrum of a) clean graphite electrode; b) electrode modified with trifluoroacetylpyridinium.

The survey spectrum shows the overall total atomic % for each element that was detected on the surface of the electrodes. Comparison of the clean and modified electrodes gave clear evidence that the surface composition of the electrode changed after electrode modification. When the graphite electrode was clean (Table 6, entry 1),

only electrons from the C1s (284.8 eV, 286.4 eV) and O1s (532.1 eV) orbitals were detected from the surface, which showed that carbon and oxygen were the only elements present. This was to be expected for a clean graphite surface.[127] After the electrodes were modified (Table 6, entries 2-6) electrons from N1s (399 eV, 402 eV) and F1s (688 eV) orbitals were detected, and the total atomic % of electrons arising from the O1s orbital increased. Thus, nitrogen and fluorine were present, and the amount of oxygen on the surface had increased. The presence of nitrogen indicates that pyridine had bonded to the electrode surface. The increase in oxygen, paired with occurrence of fluorine signifies that the trifluoroacetyl group was also present on the electrode surface.

It can be seen that the C1s atomic % varied slightly for each of the modified electrodes (Table 6). When the electrodes were modified with trifluoroacetylpyridinium or trifluoroacetyldimethylaminopyridinium the C1s total atomic % was 69%, but when the electrode was modified with trifluoroacetyl-2-iodopyridinium, trifluoroacetyl-2-bromo-4-methylpyridinium or trifluoroacetyl-3-bromopyrindium the C1s total atomic % was between 73-77%. This is a small increase but suggests that the surface coverage of the film on the electrode surface differs. For the electrodes modified with trifluoroacetylpyridinium or trifluoroacetyldimethylaminopyridinium the film was thicker/denser and so there is less contribution from the graphite beneath the film, causing less C1s contribution. Alternatively, when the electrode was modified with trifluoroacetyl-2-iodopyridinium, trifluoroacetyl-2-bromo-4-methylpyridinium or trifluoroacetyl-3-bromopyrindium the film was thinner/less densely packed, meaning there was a greater C1s contribution. This is illustrated below in Figure 17. When XPS was carried out photons were released from the top 1-10 nm of the surface. In Figure 17, we see that when the film on the electrode is thin there will be more photon contribution from the graphite electrode, and when the film is thicker there will be more photon contribution from the film.

Close inspection of the electrodes modified with the pyridinium salts that contain substituents on the pyridine ring gave an insight into the mechanism behind the modification step. Firstly, the electrodes modified with trifluoroacetyl-2-iodopyridinium,

trifluoroacetyl-3-bromopyridinium and trifluoroacetyl-2-bromo-4-methylpyridinium show very little iodine or bromine, respectively, on the modified surface. Comparing the atomic % in Table 6 there is more nitrogen present than bromine or iodine, when bromine or iodine were substituents on the ring. If these pyridinium salts attached to the electrode without loss of substituents then you would expect the ratio of nitrogen:halogen to be 1:1. Likewise, when comparing the amount of nitrogen present on electrode modified with trifluoroacetyl-4-dimethylaminopyridinium, the atomic % of nitrogen remains similar to the other modified electrodes. If the dimethylamino group was present on the pyridine ring it would be expected that the nitrogen atomic % would be twice as much as compared to the other modified electrodes, which it is not. Thus, these results signify that the substituents on the pyridine ring have acted as leaving groups during the electrode modification process. As discussed previously, when diazonium salts are reduced the dinitrogen substituent was removed to form a radical on the pyridine ring. If the mechanism of modification via reduction of trifluoroacetylpyridinium salts is similar to that of diazonium salts, it could be possible that these halogen/dimethylammonium groups are being removed to produce pyridine radicals that then react with the electrode surface.

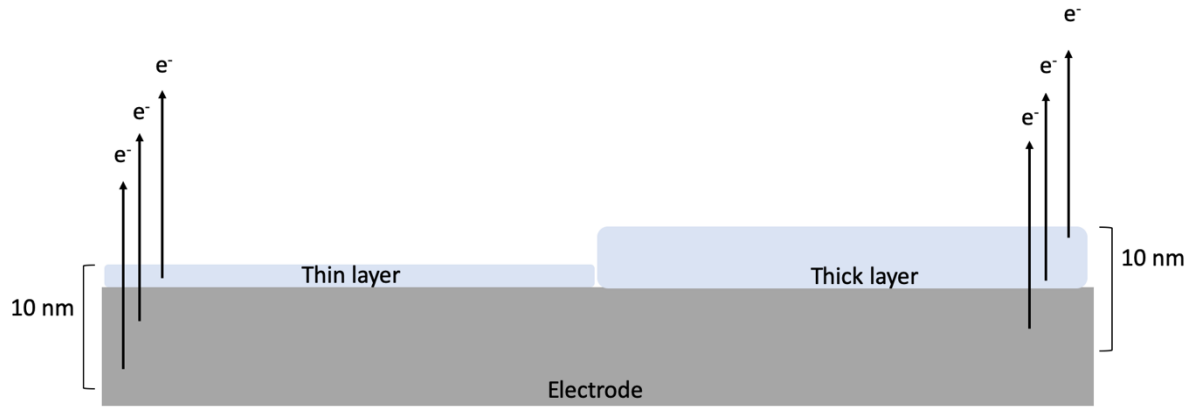

Figure 17: Illustration of the contribution of electrons from the graphite electrode and the film on the electrode surface, when the film is thick and when it is thin.

4.4.2 C1s Region

		C1s Peak Centre / eV (*Area %*)					
		284.8	285.5	286.4	287.0	288.5	292.1
1	Clean	*86*	-	*14*	-	-	-
2	TFAPyridinium	*47*	*28*	*6*	*10*	*5*	*4*
3	TFA-2-iodopyridinium	*60*	*18*	*11*	*6*	*3*	*2*
4	TFA-2-bromo-4-methylpyridinium	*61*	*17*	*9*	*8*	*3*	*2*
5	TFADMAPyridinium	*49*	*24*	*8*	*10*	*5*	*4*
6	TFA-3-bromopyridinium	*61*	*19*	*9*	*6*	*3*	*2*

Table 7: Peak centre and the associated area for peaks in the C1s region of the clean (1) and modified graphite electrodes (2-6).

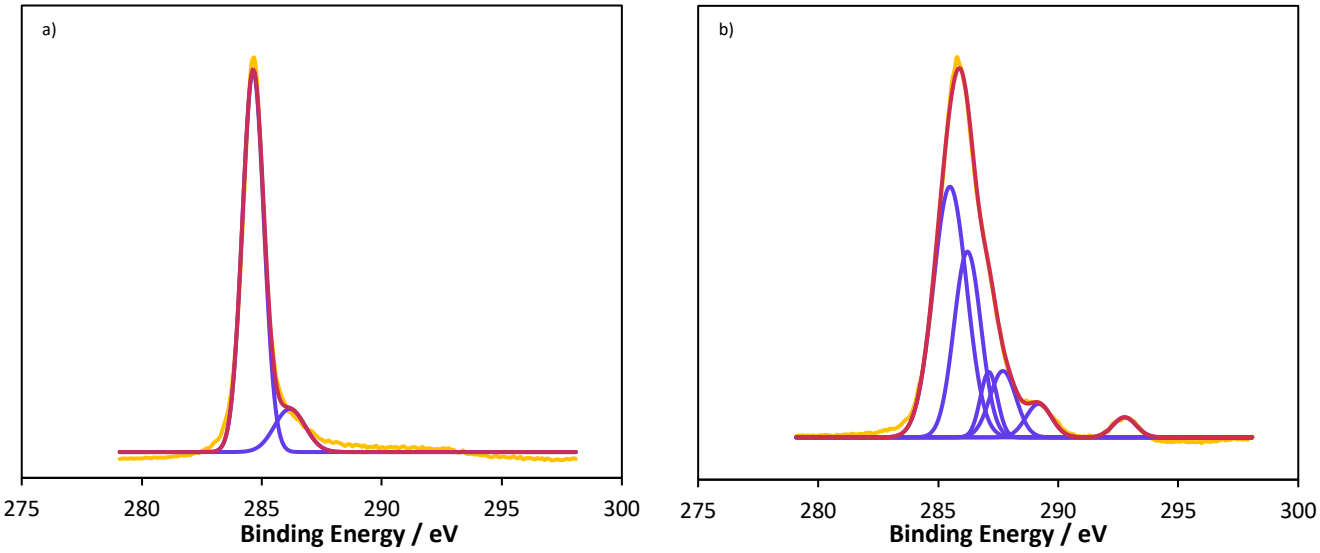

Figure 18: C1s region of a) clean graphite electrode; b) electrode modified with trifluoroacetylpyridinium. Red line – cumulative fitted peak; blue line – independent fitted peaks; yellow line – raw data.

Analysis of the clean graphite electrode (Figure 18 and Table 7, entry 1) revealed peaks at 284.8 eV and 286 eV corresponding to C-C (sp^3) and C-O bonds respectively, which agree with literature results for bare carbon electrodes.[114] The peaks corresponding to C-O bonds are due to a reaction between the graphite and oxygen or water in the air.[128, 129]

All of the modified electrodes showed five peaks that could be fitted to the C1s spectrum (Figure 18b and Table 7, entries 2-6). It can be assumed that the peaks at 284.8 eV and 286 eV originate from the graphite electrode beneath the film on the surface of the electrode, as the same peaks are seen for the clean graphite electrode. The peak at 285.5 eV was associated with pyridine carbon.[130] The peaks at 288 eV and 292 eV were attributed to C=O bonds and C-F bonds respectively, which is in accordance to other values recorded of trifluoroacetamide groups.[125] The peak at 287 eV corresponds to C-N bonds, attributed to bonds within the pyridine ring.[131] The presence of these C=O and CF_3 bonds with very similar binding energies to previously reported trifluoroacetamide bonds[125, 126, 132] are a clear indication that the pyridinium cation has attached to the electrode surface with the N-trifluoroacetyl bond still intact.

Comparison of the two C-C environments, graphite C-C (284.4eV) and pyridine C-C (285.5 eV) showed that the XPS signal of the electrodes modified from trifluoroacetylpyridinium or trifluoroacetyl-4-dimethylaminopyridinium have a greater pyridine contribution (24-28%) than the electrodes modified from trifluoroacetyl-2-iodopyridinium, trifluoroacetyl-2-bromo-4-methylpyridinium or trifluoroacetyl-3-bromopyrindium (17-19%). Likewise, the contribution from graphite is greater for the electrodes modified from trifluoroacetyl-2-iodopyridinium, trifluoroacetyl-2-bromo-4-methylpyridinium or trifluoroacetyl-3-bromopyrindium (60-61%) than for the electrodes modified from trifluoroacetylpyridinium and trifluoroacetyldimethylaminopyridinium (47-49%). This is further evidence that electrodes modified from trifluoroacetyl-2-iodopyridinium, trifluoroacetyl-2-bromo-4-methylpyridinium or trifluoroacetyl-3-bromopyrindium form thinner films. Hence why a greater graphite and smaller pyridine contribution is seen for these modified electrodes.

4.4.3 N1s Region

		N1s Peak Centre / eV (*Area %*)	
		399	402
1	Clean	-	-
2	TFAPyridinium	48	52
3	TFA-2-iodopyridinium	70	30
4	TFA-2-bromo-4-methylpyridinium	52	48
5	TFADMAPyridinium	51	49
6	TFA-3-bromopyridinium	63	37

Table 8: Peak centre and the associated area for peaks in the N1s region of the clean (1) and modified graphite electrodes (2-6).

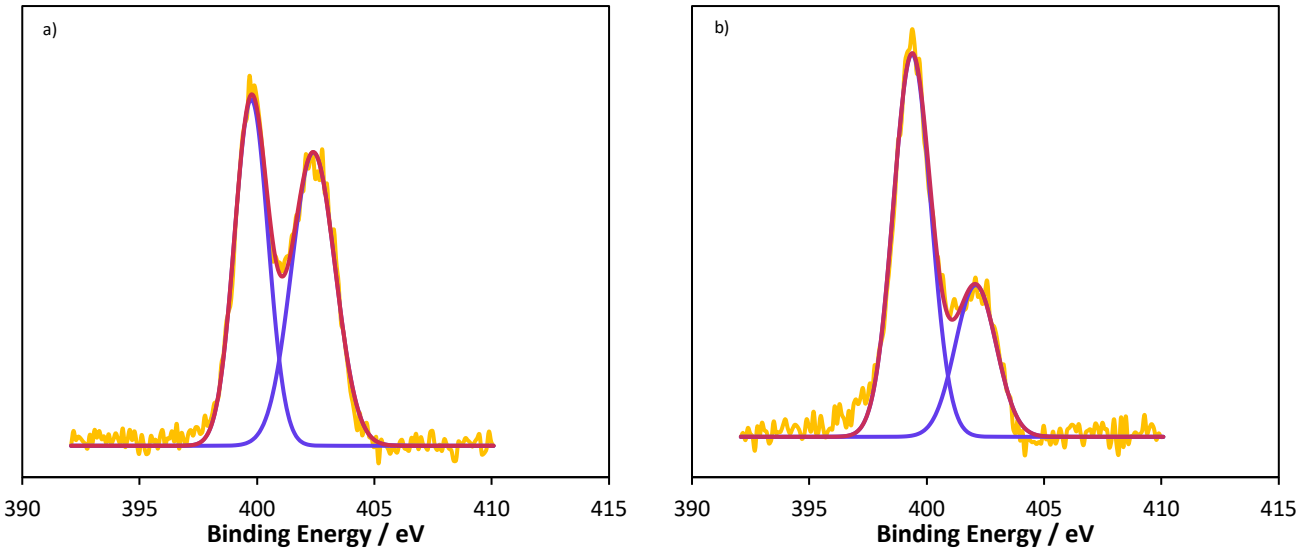

Figure 19: N1s region of a) electrode modified with trifluoroacetylpyridinium; b) electrode modified with trifluoroacetyl-2-iodopyridinium. Red line – cumulative fitted peak; blue line – independent fitted peaks; yellow line – raw data.

Table 8 details the N1s spectra for the clean and modified electrodes and the XPS spectra in Figure 19 show the typical response seen for a modified electrode. The clean graphite electrode showed no nitrogen environments, but the N1s region for the modified electrodes contained two peaks, one at 399 eV corresponding to neutral pyridine-nitrogen (pyrN) and the other at 402 eV which corresponded to cationic pyridine-nitrogen ($pyrN^+$). From our investigations into electrosynthetic trifluoromethylation, we knew that the reduction of trifluoroacetylpyridinium salts could cleave the N^+-trifluoroacetyl bond to produce a trifluoroacetyl radical which then

dealkylated to form a trifluoromethyl radical. This is evidenced through the production of trifluoromethylated products synthesised from the electrochemical reduction of pyridinium salts and is covered in more detail in Chapter Six. The cleaving of the N^+-$C(O)CF_3$ bond also reduced the cationic nitrogen to neutral nitrogen. Thus, it was thought that when the trifluoroacetylpyridinium salts (discussed here) were reduced they formed a radical which reacted with the electrode, forming a bond and attaching a trifluoroacetylpyridinium molecule to the surface. Then, as electron transfer continued some of the electrons transferred contributed to the reduction of the trifluoroacetylpyridinium salts in solution, and some contributed to the reduction of the trifluoroacetylpyridinium bound to the electrode surface. Consequently the film on the electrode surface would be made up of a combination of the cationic trifluoroacetylpyridinium and the reduced, neutral pyridine. This is illustrated in Scheme 14 below.

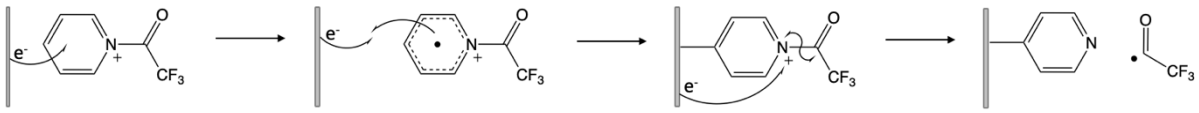

Scheme 14: Proposed mechanism showing the reduction of the trifluoroacetylpyridinium salt to form a bond on the electrode surface, followed by further reduction of the bonded trifluoroacetylpyridinium salt to form a free acyl radical and neutral pyridine bonded to the electrode surface.

For the electrodes modified from trifluoroacetylpyridinium, trifluoroacetyl-2-bromo-4-methylpyridinium and trifluoroacetyl-4-dimethylaminopyridinium the ratio of pyrN:pyrN$^+$ was roughly 50:50. Whereas, for the electrode modified from trifluoroacetyl-3-bromopyridinium the ratio of pyrN:pyrN$^+$ was 60:40 and when the electrode was modified from trifluoroacetyl-2-iodopyridinium the ratio was 70:30. The reasoning behind the different concentrations of pyrN and pyrN$^+$ could be due to the reactivity of the pyridinium salts, where the surface bound trifluoroacetyl-3-bromopyridinium and trifluoroacetyl-2-iodopyridinium are more likely to accept an electron to cleave the N^+-$C(O)CF_3$ bond.

For the modified electrodes in Table 7, (entries 2-6) we see that the area % for the peak corresponding to the C-N environment (peak 287.0 eV) is larger than for the area % for C=O and CF_3 environments (peaks 288.5 eV and 292.1 eV respectively). The smaller concentration of the trifluoroacetyl group compared to that of the pyridine nitrogen is further evidence that the N^+-$C(O)CF_3$ bond has been cleaved, removing the $C(O)CF_3$ group.

4.4.5 O1s Region

		O1s Peak Centre / eV (Area %)	
		532	533
1	Clean	100	-
2	TFAPyridinium	88	12
3	TFA-2-iodopyridinium	93	7
4	TFA-2-bromo-4-methylpyridinium	95	5
5	TFADMAPyridinium	85	15
6	TFA-3-bromopyridinium	95	5

Table 9: Peak centre and the associated area for peaks in the O1s region of the clean (1) and modified graphite electrodes (2-6).

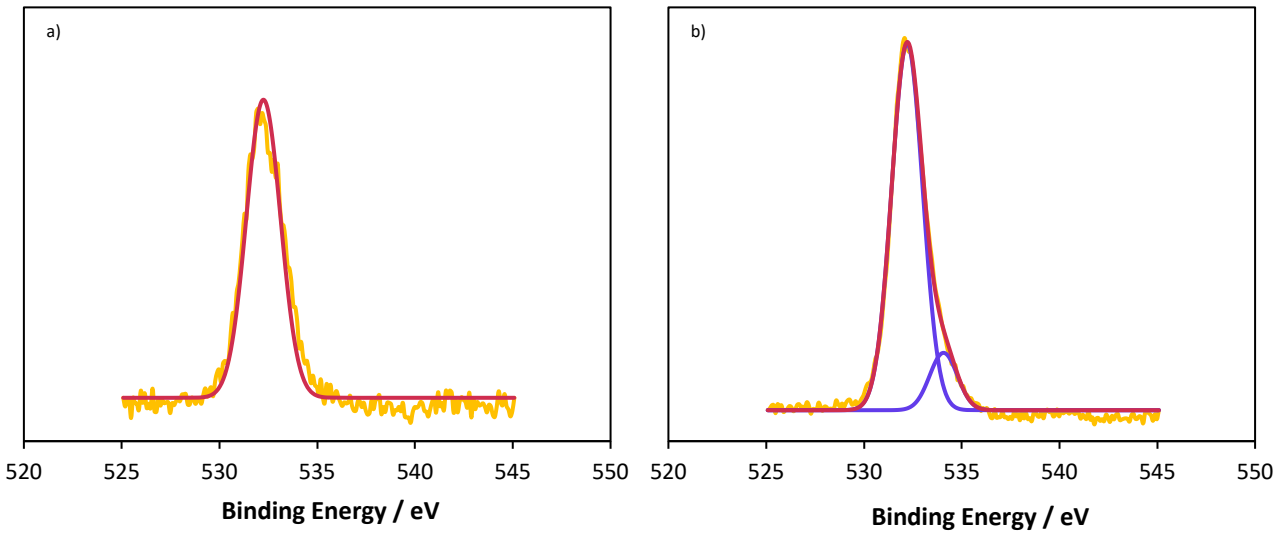

Figure 20: O1s region of a) clean graphite electrode; b) electrode modified with trifluoroacetylpyridinium. Red line – cumulative fitted peak; blue line – independent fitted peaks; yellow line – raw data.

Analysis of the O1s region of the clean graphite electrode (Figure 20a and Table 9, entry 1) revealed a single peak at 532 eV corresponding to C-O bonds in graphite

oxide.[133] The spectra for the modified electrodes were similar to that of the clean electrode, but they contained an additional peak at 533 eV corresponding to the carbonyl C=O group as part of the trifluoroacetylpyridinium that makes up the film on the electrode surface.[126] The C-O peak seen in the modified electrode could be due to oxygen in the graphite electrode, beneath the film formed during the modification step. It could also be due to a reaction between the film and water or oxygen in the atmosphere when the modified electrode was handled between the modification and XPS analysis steps.

The area % for carbonyl oxygen was greater for the electrodes modified with trifluoroacetylpyridinium and trifluoroacetyl-4-dimethylaminopyridinium than the electrodes modified with trifluoroacetyl-2-iodopyridinium, trifluoroacetyl-2-bromo-4-methylpyridinium or trifluoroacetyl-3-bromopyrindium. This again shows a trend in thicker or denser films formed from trifluoroacetylpyridinium and trifluoroacetyl-4-dimethylaminopyridinium than the other pyridinium salts.

4.4.6 F1s Region

		F1s Peak Centre / eV (Area %)	
		686	688
1	Clean	-	-
2	TFAPyridinium	44	56
3	TFA-2-iodopyridinium	48	52
4	TFA-2-bromo-4-methylpyridinium	33	67
5	TFADMAPyridinium	43	57
6	TFA-3-bromopyridinium	80	19

Table 10: Peak centre and the associated area for peaks in the F1s region of the clean (1) and modified graphite electrodes (2-6).

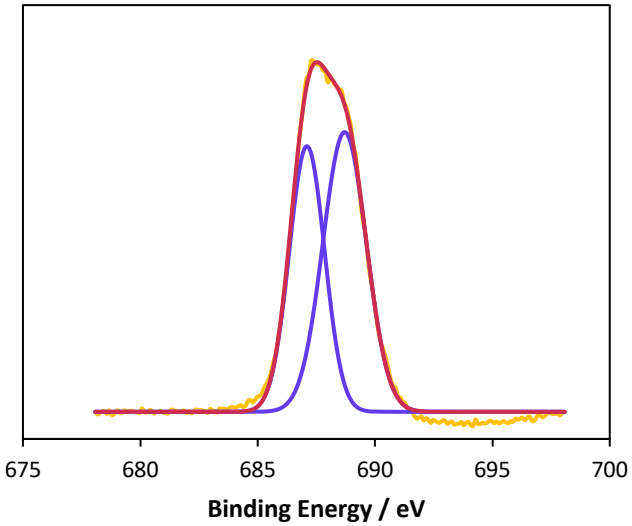

Figure 21: F1s region of an electrode modified with trifluoroacetylpyridinium. Red line – cumulative fitted peak; blue line – independent fitted peaks; yellow line – raw data.

Analysis of the F1s region of the modified electrodes showed two peaks (Figure 21 and Table 10). The peak at 688 eV corresponds to the CF_3 group as part of the trifluoroacetylpyridinium bound to the electrode surface.[126] The peak at 686 eV corresponds to PF_6 anions adsorbed to the surface from the $TBAPF_6$ electrolyte in solution.[134] The ratio of PF_6:CF_3 differs between each sample, however this is difficult to analyse as the amount of electrolyte adsorption is relatively unknown and not controlled between the samples. The effects of the supporting electrolyte on the modified electrode surfaces is explored more in the next section.

4.5 Effect of Electrolyte

		C1s total at.%	N1s total at.%	O1s total at.%	F1s total at.%
1	No Electrolyte	65	10	12	13
2	$LiClO_4$	59	9	20	12

Table 11: Chemical composition of graphite electrodes modified via cyclic voltammetry with 10 mM trifluoroacetylpyridinium, in degassed MeCN when no electrolyte was used (1) and when $LiClO_4$ was used as electrolyte (2) determined from the XPS survey spectra.

		C1s Peak Centre / eV (Area %)					
		284.8	285.5	286.4	287.0	288.5	292.1
1	No Electrolyte	54	20	7	8	7	4
2	$LiClO_4$	51	25	10	7	4	3

Table 12: Peak centre and the associated area for peaks in the C1s region of graphite electrodes modified via cyclic voltammetry with 10 mM trifluoroacetylpyridinium, in degassed MeCN when no electrolyte was used (1) and when $LiClO_4$ was used as electrolyte (2).

		N1s Peak Centre / eV (Area %)		F1s Peak Centre / eV (Area%)	
		399	402	686	688
1	No Electrolyte	55	45	-	100
2	$LiClO_4$	46	54	-	100

Table 13: Peak centre and the associated area for peaks in the N1s and F1s regions of graphite electrodes modified via cyclic voltammetry with 10 mM trifluoroacetylpyridinium, in degassed MeCN when no electrolyte was used (1) and when $LiClO_4$ was used as electrolyte (2).

Analysis of the modified electrodes revealed peaks belonging to cationic nitrogen and fluoride ions. The cationic nitrogen had been assigned to the pyridinium attached to the electrode surface, whereas the fluoride had been assigned to the supporting electrolyte, $TBAPF_6$. However, the supporting electrolyte also contained cationic nitrogen ions, i.e. the tetrabutylammonium ion (TBA). Therefore, investigations were undertaken to ascertain whether the peaks for cationic nitrogen and fluoride ions present in the previous XPS spectra of the modified electrodes were due to the $TBAPF_6$ electrolyte or the pyridinium salt. To do this, the electrodes were modified via 9 cyclic voltammograms in a solution of 10 mM trifluoroacetylpyridinium with: 1) no supporting electrolyte and 2) lithium perchlorate ($LiClO_4$) electrolyte.

The results seen in the survey spectrum and C1s region of the modified electrodes (Tables 11 and 12) are in accordance with the results seen for the electrode modified with trifluoroacetylpyridinium when $TBAPF_6$ was used as the background electrolyte

(Table 7, entry 2). Analysis of the N1s region (Table 13) revealed that cationic nitrogen was still present when no electrolyte or $LiClO_4$ was used, confirming that the cationic nitrogen seen in all of the modified electrodes originated from the pyridinium species. Similarly, the absence of a peak at 686 eV in the F1s region seen here (Table 13) also confirmed that the presence of fluoride ions in the previous studies (Table 10) originated from the PF_6^- anion. It is worth noting that the PF_6^- anion from the supporting electrolyte was incorporated into the film on the modified electrodes, but the TBA^+ cation was not. This was because a film containing pyridinium ions was attached to the modified electrode that would have attracted the negatively charged PF_6^- anions and repelled the TBA^+ cations.

One other point to note is that when $LiClO_4$ was used as the electrolyte a higher presence of oxygen was detected in the survey spectra (Table 11, entry 2) and the C-O peak at 286.4 increased in area % (Table 12, entry 2), as compared to no electrolyte, or $TBAPF_6$. $LiClO_4$ is known to be an oxidising agent, so it is possible that it oxidised the film, or, the bare graphite electrode when it was in solution, increasing the amount of oxygen present. Alternatively, the ClO_4^- ion may have been attracted to the surface of the pyridinium film, and the adsorption of the ClO_4^- may have led to the formation of C-O bonds between the pyridinium film and the anion.

Overall it can be said that the electrolyte had a small effect over the composition of the films formed during the modification step, such as oxidation by $LiClO_4$ or adsorption/incorporation of the anionic supporting electrolyte ions. However, comparison of the spectra when no electrolyte was used compared to when $TBAPF_6$ or $LiClO_4$ was used only show minor differences, suggesting any effect the electrolyte had on the pyridinium film is minimal.

4.6 Effect of Oxygen Presence During Electrode Modification

4.6.1 Why is Oxygen Relevant?

While experiments were being conducted on the formation of organic layers at the electrode surface, electrosynthetic investigations using pyridinium salts were also being conducted in parallel. Full details of the electrosynthetic investigations are given in Chapter Six, however some discoveries from that work are relevant here. During the electrosynthetic oxytrifluoromethylation of styrene it was discovered that oxygen played a key role in the reaction. Prior to this, all experiments (electrode modification and electrosynthetic reactions) were only conducted with degassed solutions of the pyridinium salts. After the realisation that oxygen was necessary for the oxytrifluoromethylation of styrene it was thought that the role it played in electrode modification should also be explored.

4.6.2 Redox Behaviour of Oxygen

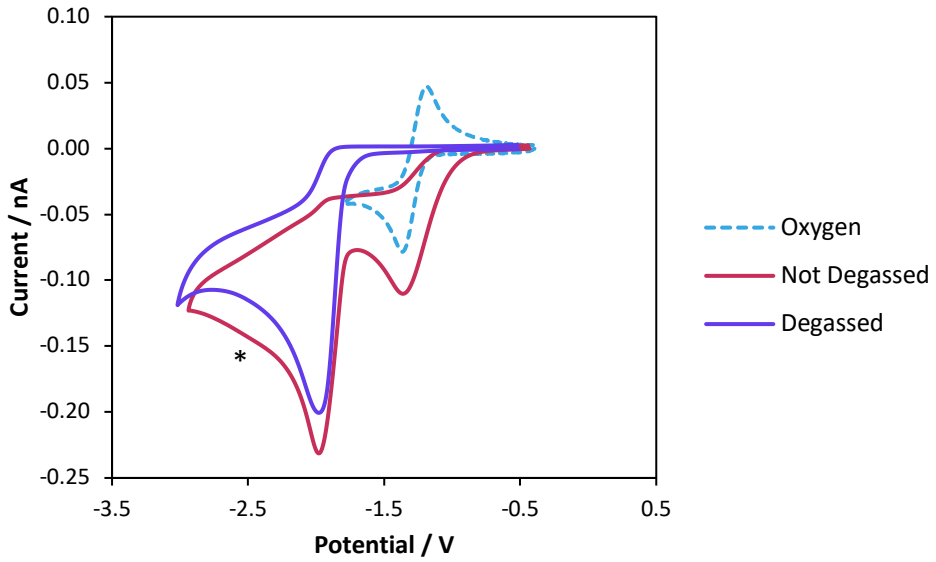

Figure 22: Cyclic voltammograms taken in 0.1 M $TBAPF_6$ in dry MeCN, scan rate 0.1 V s^{-1}. Blue dotted line – oxygen redox peaks in a solution of non-degassed electrolyte. Red – 10 mM trifluoroacetylpyridinium in a non-degassed solution. Purple – 10 mM trifluoroacetylpyridinium in a degassed solution. The asterisk marks a notable difference in the behaviour of the non-degassed solution of trifluoroacetylpyridinium.

Cyclic voltammograms were taken in degassed (purple line) and non-degassed (red-line) solutions of trifluoroacetylpyridinium, presented in Figure 22. A cyclic voltammogram was also taken in a non-degassed solution of just the supporting electrolyte, which shows the redox peaks of atmospheric oxygen dissolved in solution (light blue dotted line).[135] Here, oxygen undergoes a reversible redox reaction where it is reduced from oxygen to superoxide, and then oxidised back to oxygen. The redox equation for this is seen below:

$$O_2 + e^- \rightleftharpoons O_2^{\bullet -} \qquad \textit{Eq. 20}$$

When oxygen was the only species present in solution (light blue dotted line) clear reversible redox behaviour can be seen, with a peak reduction current of -0.08 nA at -1.37 V and a peak oxidation current of 0.05 nA at -1.19 V. When the solution of trifluoroacetylpyridinium was not degassed a reduction peak appeared at the exact same position as the oxygen reduction (-1.37 V), this time with a peak reduction current of -0.11 nA. However this reduction process was irreversible, with no obvious oxidation peak appearing on the return scan.

The irreversible peak at -1.37 V (Figure 22, red line) was identified as oxygen reduction because it appeared at the same reduction potential as oxygen and was only seen when the solution was not degassed. The solutions prepared for NMR analysis in Chapter Three were also prepared with non-degassed MeCN and there was no evidence of any products formed from a reaction between oxygen and trifluoroacetylpyridinium. The irreversibility of the oxygen peak seen when oxygen was present in the trifluoroacetylpyridinium solution was caused by the oxygen acting as a redox mediator between the electrode and the trifluoroacetylpyridinium (illustrated in Figure 23). Thus, the oxygen was reduced by the electrode to form superoxide and re-oxidised by the trifluoroacetylpyridinium, with the concomitant reduction of the trifluoroacetylpyridinium in turn. The absence of the superoxide oxidation peak is due to the electron transfer occurring between superoxide and trifluoroacetylpyridinium and not the electrode surface.

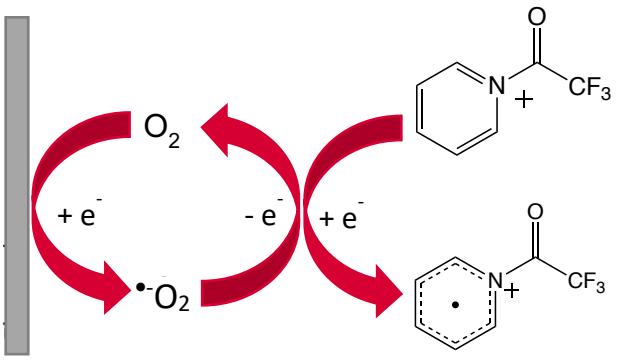

Figure 23: Illustration of $^{\bullet}$ oxygen acting as a redox mediator between the electrode and trifluoroacetylpyridinium in solution.

Another notable difference in behaviour is how the current changed after the reduction peak of trifluoroacetylpyridinium had passed, when compared between the degassed and non-degassed solutions (marked with an asterisk in Figure 22). In the degassed solution the current was diffusion limited, so the current gradually decreased as the concentration of fresh trifluoroacetylpyridinium at the electrode surface also decreased. When the solution was not degassed we see two processes happen after the reduction peak. Initially, the current decreased with a gradient expected for diffusion limited currents, then at approximately -2.1 V the current reached a 'shoulder' and decreased more gradually as compared to the degassed solution. This increase in current can be attributed to oxygen acting as a redox mediator. The current was no longer solely limited to the diffusion of trifluoroacetylpyridinium to the electrode surface, as the regeneration of oxygen at the electrode surface and provided a fresh supply of oxygen. This meant that the current was not dependent on just the diffusion of trifluoroacetylpyridinium, and oxygen provided a constant source of electron transfer, thus maintaining a higher current.

Chronoamperometry was used to calculate the amount of charge passed for different electrochemical conditions, the results of which are shown in Figure 24. The working electrode was held at the peak potential for oxygen reduction (-0.96 V, ref. Ag wire) and trifluoroacetylpyridinium (-1.52 V, ref. Ag wire) in degassed and non-degassed solutions of trifluoroacetylpyridinium. The electrode was also held at -0.96 V in a non-degassed solution of just the background electrolyte, to understand how oxygen

behaved when trifluoroacetylpyridinium was not present in solution. The starting current, end current and total amount of charge passed for each condition are summarised in the table below (Table 14).

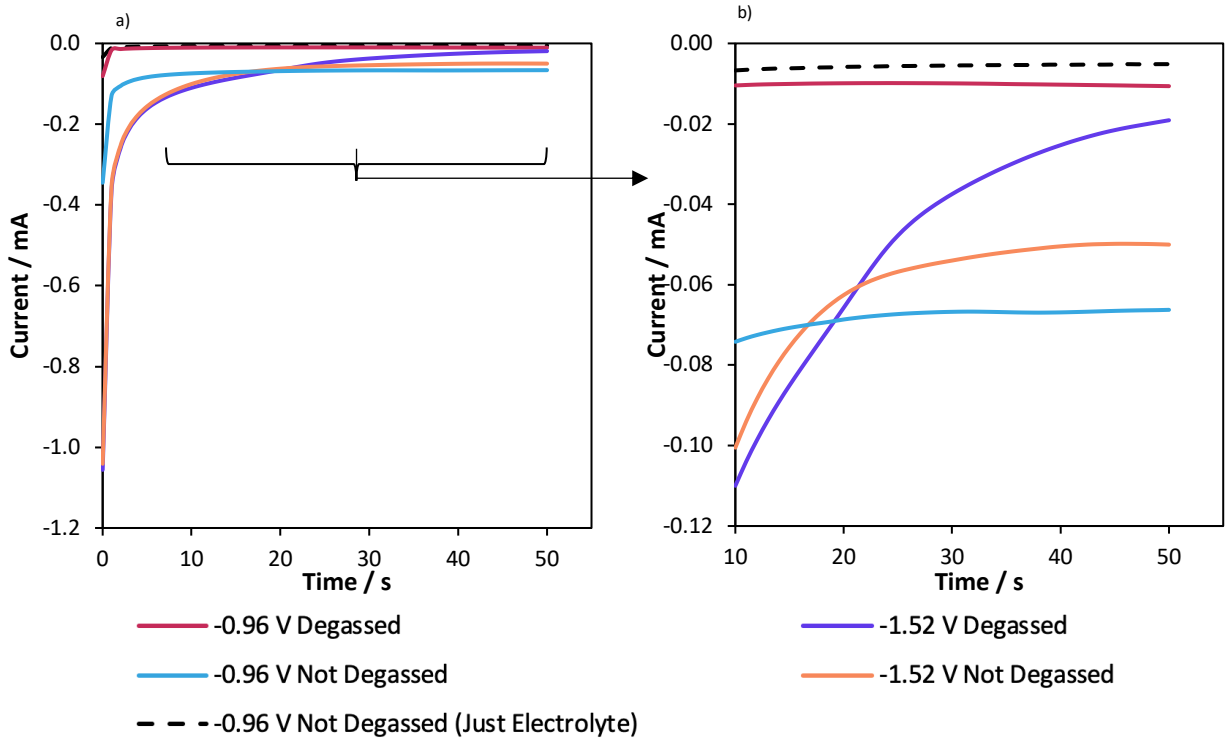

Figure 24a: Chronoamperometry curves showing how the current changes over a 50 s interval when the working electrode is held at different potentials in degassed and non-degassed solutions of 10 mM trifluoroacetylpyridinium. Red: -0.96 V degassed; purple: -1.52 V degassed; orange: -1.52 V not degassed; light blue: -0.96 V not degassed; black dotted line: -0.96 V not degassed, just electrolyte.

Figure 24b: A focus on the same curves as in Figure 24a, but only showing the range from 10 s to 50 s.

Condition	Starting Current / mA	End Current / mA	Total Charge Passed / mC
-0.96 V Degassed	-0.08	-0.01	-2.2
-0.96 V Not Degassed	-0.35	-0.07	-3.7
-1.52 V Degassed	-1.06	-0.02	-4.2
-1.52 V Not Degassed	-1.04	-0.05	-4.6
-0.96 V Not Degassed (Just Electrolyte)	-0.03	-0.005	-0.3

Table 14: The starting current, end current and total charge passed for the various conditions applied to the chronoamperometry experiments conducted in Figure 24.

Overall, comparing all five conditions, several observations can be made. Firstly, when the potential was held at -1.52 V, for both the degassed an non-degassed solutions, higher currents were seen. This is to be expected as the concentration of trifluoroacetylpyridinium in solution was much higher than oxygen. When the solution was degassed the current continuously falls, and was still decreasing at the end of the 50 s interval. This continuous decline in current was caused by the electrode surface being passivated due to electrode modification. Whereas, when the solution was not degassed the current reached a steady constant current of -0.05 mA from approximately 22 s onwards. This steady current was caused by the oxygen in solution being regenerated by the trifluoroacetylpyridinium near the electrode during and after electrode modification had taken place (see Figure 23). This indicates that the layer formed at the electrode surface is not a blocking layer and electrons can still be transferred to species in solution. This effect is covered in more detail in Chapter Five, but for now it is sufficient to say that the layer formed at the electrode, under these conditions, was passivating towards trifluoroacetylpyridinium but electron transfer with oxygen was still possible.

When comparing the chronoamperometry curves taken at -0.96 V it should be noted that there was not absolute control over the concentration of oxygen in the solution. When the solutions were degassed, as much oxygen as possible was removed but it cannot be assured that there was no oxygen in solution. However, a qualitative approach can be taken, so it can be said there was more oxygen in the non-degassed solutions compared to the degassed solutions.

The degassed solution of trifluoroacetylpyridinium (Figure 24, red line) and the non-degassed solution of just electrolyte (Figure 24, black dotted line) held at -0.96 V show low currents and small amounts of charge passed. Comparing the two curves, the degassed solution containing trifluoroacetylpyridinium showed higher currents than the non-degassed solution without any trifluoroacetylpyridinium. This is further evidence that oxygen was acting as a redox mediator. There was still a small amount of oxygen still present in the degassed solution, and if it was acting as a redox mediator, then a fresh supply of oxygen would always be present at the electrode surface. Thus, a higher current was maintained in the trifluoroacetylpyridinium solution compared to the solution where oxygen was not acting as a redox mediator because the supply of fresh oxygen continuously decreased, causing the current to also decrease.

This is also seen for the chronoamperogram taken when the non-degassed solution of trifluoroacetylpyridinium was held at -0.96 V (Figure 24, blue line). This solution had more oxygen in it than the degassed solution (Figure 24, red line), and again the oxygen acted as a redox mediator, which is why higher currents were seen and more charge is passed.

4.6.3 XPS Studies of Modified Electrodes When Oxygen is Present

XPS studies were performed in order to assess if oxygen was incorporated into the organic layer when the solutions were not degassed, or, if any layers formed at all when oxygen acts as a redox mediator. To do this, graphite rods were modified in various ways:

- Constant potential for 10 min at -1.52 V in both degassed and non-degassed solutions
- Constant potential for 10 min at -0.96 V in both degassed and non-degassed solutions

		C1s total at.%	N1s total at.%	O1s total at.%	F1s total at.%
1	-0.96 V Degassed	92	<1	6	1
2	-0.96V Not Degassed	93	<1	3	3
3	-1.52 V Degassed	77	5	11	7
4	-1.52 V Not Degassed	78	9	8	5

Table 15: Chemical composition of the modified electrodes modified under constant potential (1-4) or cyclic voltammetry (5-6) methods in degassed (1,3,5) or non-degassed (2,4,6) solutions of 10 mM trifluoroacetylpyridinium, determined from the XPS survey spectra.

		C1s Peak Centre / eV (Area %)						N1s Peak Centre / eV (Area %)	
	Binding Energy (eV)	284.8	285.5	286.4	287.0	288.5	292.1	399	402
1	-0.96 V Degassed	79	-	21	-	-	-	-	-
2	-0.96 V Not Degassed	76	-	24	-	-	-	-	-
3	-1.52 V Degassed	54	23	6	9	5	3	67	33
4	-1.52 V Not Degassed	55	23	6	8	5	3	67	33

Table 16: Peak centre and the associated area for peaks in the C1s and N1s region for the modified electrodes modified under constant potential (1-4) or cyclic voltammetry (5-6) methods in degassed (1,3,5) or non-degassed (2,4,6) solutions of 10 mM trifluoroacetylpyridinium.

From the XPS results shown here it is clear that when the potential of the electrode is held at -0.96 V no organic layer was formed at the electrode surface. This is evidenced by the absence of any nitrogen environments in the survey scan or when the N1s region was examined. The lack of C-N, N-C=O and $COCF_3$ environments when the C1s region was scanned also proved that there was no layer formed on the electrode surface.

When the electrode was held at -1.52 V the characteristic XPS peaks associated with the formation of the organic layer at the electrode surface were seen. The layers

formed when the solution was degassed and not degassed are very similar, indicating that the presence of oxygen did not affect the formation of the layer when the potential is held at -1.52 V. The C1s peaks for the layer formed via constant potential in non-degassed solution show similar area % to the peaks for the layer formed from 9 consecutive cyclic voltammograms, seen previously (Table 7, entry 2). However, the ratio of cationic nitrogen to neutral nitrogen is different. For the layers formed via cyclic voltammetry the N:N^+ ratio is roughly 50:50, whereas when it is formed via constant potential it is roughly 70:30. Similarly for the case of trifluoroacetyl-2-iodopyridinium this higher concentration of pyrN was caused by further reduction of the trifluoroacetylpyridinium film. This also shows that more reduction of the pyridinium layer occurred when constant potential was used rather than a sweeping potential. When the electrode was modified via cyclic voltammetry the potential was swept from 0 V to -2 V, and so there were times when the trifluoroacetylpyridinium film was not being reduced. Conversely, when the electrode was held at -1.52 V there was more opportunity for trifluoroacetylpyridinium film reduction, leading to a higher concentration of neutral pyrN.

4.6.4 Oxygen as a Redox Mediator

The results discussed here clearly point to oxygen acting as a redox mediator between the electrode and the trifluoroacetylpyridinium in solution. The oxygen was involved in a catalytic cycle, being reduced by the electrode and then oxidised by the trifluoroacetylpyridinium in solution. This constant regeneration of oxygen at the electrode surface negates the usual diffusion limited currents seen for species in solution. Instead, the constant supply of fresh oxygen re-oxidised by the trifluoroacetylpyridinium caused higher currents in both cyclic voltammograms (Figure 22) and chronoamperometry experiments (Figure 24). The role of oxygen as a redox mediator was also proven via XPS studies, where no layer was formed at the electrode surface when it was held at -0.96 V because electron transfer was only between oxygen and the electrode surface. The high currents are a result of electron transfer between the oxygen and the trifluoroacetylpyridinium, re-oxidising oxygen and reducing the trifluoroacetylpyridinium. The absence of layer formation at this potential

shows that the reduction of oxygen was the main process occurring at this potential at the electrode surface, and the direct reduction of trifluoroacetylpyridinium occurs further away from the electrode surface, preventing the formation of an organic layer on the electrode surface. In Chapter Six I will discuss a synthetic reaction in which the potential of the electrode will be held at -0.96 V and the formation of a product formed from the reduction of trifluoroacetylpyridinium will be produced, further proving the role of oxygen as a redox mediator.

4.7 Conclusions

The findings presented in this chapter have demonstrated a new way of attaching pyridine to the surface of carbon based electrodes, as compared to previous diazonium or acid based methods. The exploration of a wide variety of substituents on the pyridine ring allowed for many deductions to be made about the method in which the trifluoroacetylpyridinium salts attached to the electrode surface. It was established that trifluoroacetylpyridinium salts containing electron donating substituents did not form a film on the electrode surface (evidenced by the peak current maintaining a constant value over successive cyclic voltammograms). Whereas, trifluoroacetylpyridinium salts containing electron withdrawing substituents, or no substituents at all, did form a film at the electrode surface (evidenced by the passivation of the electrode surface and subsequent decreasing peak currents over successive cyclic voltammograms). The behaviour of all the salts tested is summarised below (Figure 25).

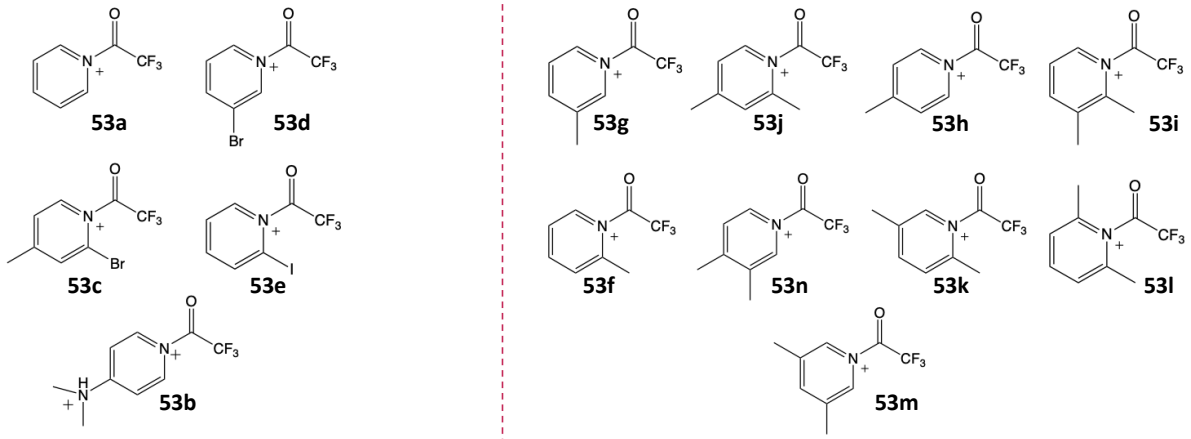

Forms films on electrode surface Doesn't form films on electrode surface

Figure 25: Representation of trifluoroacetylpyridinium salts that did coat the electrode (left) and those that did not coat the (right), upon reduction at the electrode surface.

For the salts that did form films on the electrode surface, the substituents on the pyridine ring also had an influence over the rate at which the film was formed. For the trifluoroacetyl-2-bromo-4-methylpyridinium and trifluoroacetyl-2-iodopyridinium the rate of film formation was fast, forming thin films. This was proven through relatively quick passivation of the electrode surface during cyclic voltammetry and chronoamperometry and a larger ratio of graphite-carbon:pyridine-carbon in the C1s region of the XPS studies conducted. The XPS data for trifluoroacetyl-3-bromopyridinium salt suggested that it also formed thin films, however the cyclic voltammograms of this salt showed slow passivation of the electrode surface. Alternatively, the trifluoroacetylpyridinium and trifluoroacetyl-4-dimethylamino pyridinium showed slow passivation of the electrode surface through cyclic voltammetry and chronoamperometry experiments, and they formed thick films as shown by a smaller ratio of graphite-carbon:pyridine-carbon in the XPS studies.

Overall, it appears that there could be evidence that fast passivation of the electrode surface correlates with thin films, whereas slow passivation of the electrode surface correlates with the formation of thick films. Before final conclusions are drawn on the

mechanism of the formation of the films, further analysis of the modified electrode surfaces using redox probes is discussed in the next chapter.

Chapter Five – Properties of the Modified Electrodes

This chapter will cover the experiments undertaken to explore the properties of the modified electrodes. This will mainly be done by exploring the interactions of redox probes with the modified electrode surfaces. The effect of pH on the film will also be discussed. The five pyridinium salts used to modify the electrodes in the previous chapter will be examined again in this chapter, however for some experiments only the trifluoroacetylpyridinium (unsubstituted) salt was used. This was partly because it showed the greatest interaction with the redox probes, which was useful for some experiments, but also because it was the cheapest and most abundant pyridinium salt to hand.

5.1 Redox Probes

Redox probes are species that undergo reversible redox processes at well-established potentials. The reliability of these redox processes means that the redox probes can be used to investigate electrode surfaces, as any changes in behaviour will be easily detected. Redox probes can undergo one of two electron transfer mechanisms with the electrode surface: an inner-sphere mechanism or an outer-sphere mechanism. In the case of inner-sphere mechanisms, electron transfer proceeds through a covalent bond via a ligand bridged between the electrode and the redox probe. For this reason, inner-sphere redox probes are usually surface sensitive. With outer-sphere mechanisms, the electron transfer proceeds through electron tunnelling between the electrode and the redox probe without physical or chemical interaction, and is usually surface insensitive.

In this chapter, an array of redox probes were used to investigate the blocking properties of the modified electrode surfaces. For these experiments redox probes with different charged electroactive species were chosen so that the behaviour of the

redox probes towards the positively charged electrode surfaces could be investigated. The glassy carbon electrodes used for these experiments were either clean, or had been modified via 9 consecutive cyclic voltammograms in a 10 mM solution of each salt.

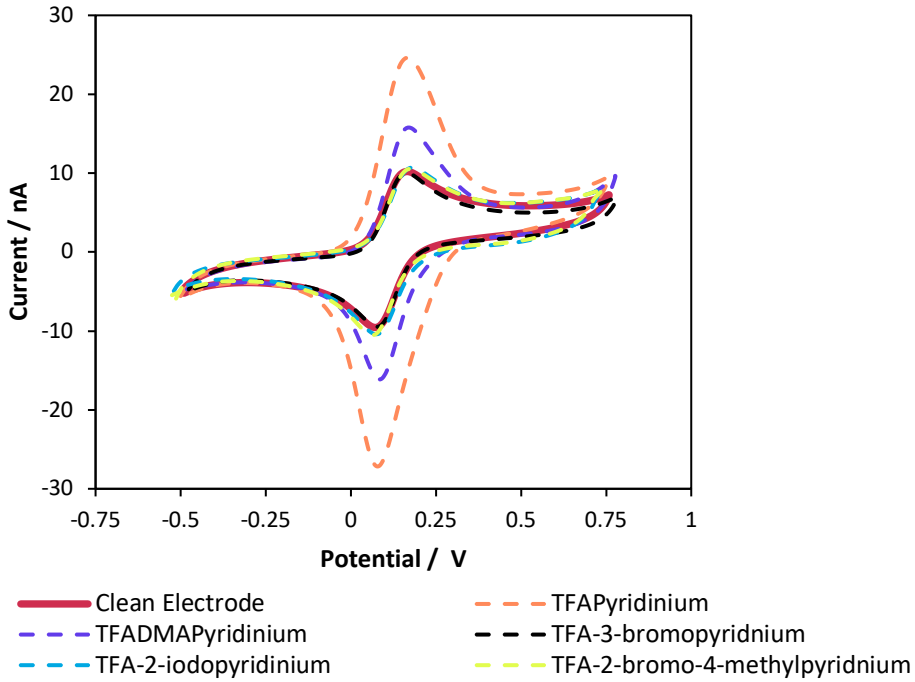

Figure 26: Cyclic voltammograms for a clean (solid line) and modified electrode (dashed lines) in 1 mM potassium ferrocyanide solution in NaCl/H_2O (0.1 M).

5.1.1 Potassium Ferrocyanide

The first redox probe to be tested was potassium ferrocyanide ($[Fe(CN)_6]K_4$), and the results using this probe are seen in Figure 26. The ferrocyanide ion was oxidised from $[Fe(CN)_6]^{4-}$ to $[Fe(CN)_6]^{3-}$ and then reduced back to the $[Fe(CN)_6]^{4-}$ ion. When cyclic voltammograms of potassium ferrocyanide were taken using a clean glassy carbon electrode (solid red line), clear reversible redox behaviour was seen. The electrode was swept in the positive direction first, and a peak oxidation current of 10.2 nA was seen at 0.16 V. The electrode was then swept in the negative direction and a peak reduction current of -9.6 nA was seen at 0.07 V. For the electrodes modified with trifluoroacetyl-2-iodopyridinium (light blue line), trifluoroacetyl-3-bromopyridinium (black line) and trifluoroacetyl-2-bromo-4-methylpyridinium (yellow line) the cyclic voltammograms of potassium ferrocyanide closely matched the cyclic voltammogram

taken with a clean glassy carbon electrode. When the electrode had been modified with trifluoroacetyl-4-dimethylaminopyridinium (purple line) the peak oxidation current increased to 15.8 nA at 0.17 V and the reduction peak also increased to -16.1 nA at 0.08 V. Finally, when the electrode had been modified with trifluoroacetylpyridinium (orange line) the currents increased further to 24.6 nA at 0.16 V for the oxidation peak, and -27.1 nA at 0.07 V for the reduction peak.

The increased currents seen here for the electrodes modified from trifluoroacetylpyridinium and trifluoroacetyl-4-dimethylaminopyridinium are due to the ferrocyanide adsorbing to the film on the modified electrode surface. We know from the XPS studies discussed in the previous chapter that the modified electrodes all contained cationic nitrogen. The negatively charged ferrocyanide ions were attracted to the positively charged film on the electrode surface, and this attraction led to the adsorption of the ferrocyanide ions to the film. This then increased the concentration of the ferrocyanide ions at the electrode surface, which in turn caused the higher redox currents seen in Figure 26. It is possible that after the initial attraction of the ferrocyanide to the electrode surface the ferrocyanide then absorbed into the pores in the film. However, to avoid confusion between using both terms (adsorption and absorption) only adsorption will be referred to from now on, but for thicker more porous films absorption is likely to contribute significantly.

We proposed that the adsorption of the ferrocyanide ions may be proportional to the thickness of the films on the modified electrode surfaces. Therefore, we wanted to theorise how many layers (i.e. pyridine linkages) were incorporated in the films on the modified electrodes. To do this, the total amount of charge passed during film formation was calculated via integration of the 9 consecutive cyclic voltammograms performed to modify the electrodes before they were used for the experiment in Figure 26. The total amount of charge passed for each pyridinium salt during the 9 consecutive cyclic voltammograms can be seen below in Table 17. The total amount of charge was then divided by the charge of an electron (1.60×10^{-19} C) to find the total number of electrons passed during the 9 consecutive cyclic voltammograms (seen in Table 17). The area of the glassy carbon electrode was calculated to be

50.27 mm^2. The area of a trifluoroacetylpyridinium molecule was estimated to be between 2.5-3.6 x 10^{-13} mm^2 (using values of radii for 2-ethylpyridine and 2-hexylpyridine).[136] Dividing the area of the electrode by the average area of a molecule of trifluoroacetylpyridinium (3.05 x 10^{-13} mm^2) it was estimated that 1.705 x 10^{14} molecules of trifluoroacetylpyridinium would make up one monolayer on the electrode surface. From the previous XPS studies it was assumed that the substituents on the pyridine ring were removed during the electrodeposition, therefore it was accurate to presume that the trifluoroacetylpyridinium radical would be roughly the same size for each pyridinium salt used. The total number of electrons passed was then divided by two, as we assumed the mechanism for the formation of the layer would be a two electron process; one to form the radical on the pyridine ring and one to form the bond with the pyridine radical (as seen below in Scheme 15). The halved total number of electrons was then divided by the theoretical number of trifluoroacetylpyridinium molecules in one layer, to calculate the number of layers at the electrode surface (assuming the ratio of electrons passed to number of trifluoroacetylpyridinium radicals grafted was 1:1).

	Pyridinium Salt	Charge / mC	Total Number of Electrons	Number of Layers
1	Trifluoroacetylpyridinium	-0.16	1.0E+15	3.0
2	Trifluoroacetyl-2-iodopyridinium	-0.03	1.9E+14	0.55
3	Trifluoroacetyl-2-bromo-4-methylpyridinium	-0.03	1.8E+14	0.55
4	Trifluoroacetyl-4-dimethylaminopyridinium	-0.08	4.7E+14	1.35
5	Trifluoroacetyl-3-bromopyridinium	-0.10	6.3E+14	1.85

Table 17: Total amount of charge passed over 9 consecutive cyclic voltammograms taken of each salt, and the number of electrons this equates to.

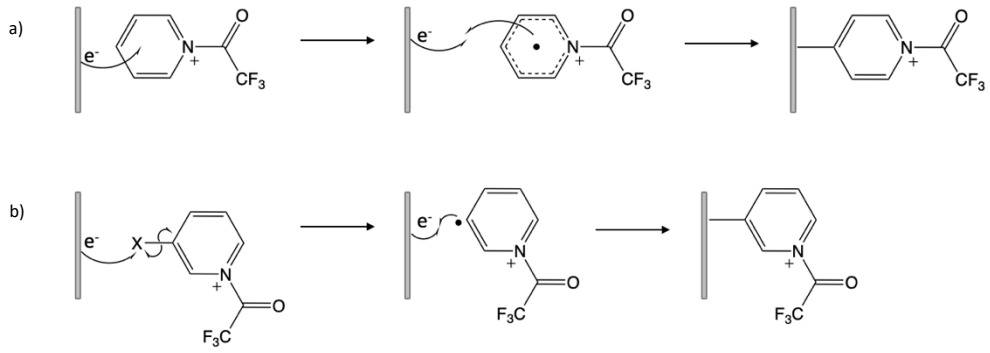

Scheme 15: Proposed mechanism for the formation of abond between the electrode surface and the trifluoroacetylpyridinium salt when it was a) unsubstituted and b) substituted

The theorised results seen in Table 17 largely correlate with the experimental results presented in Figure 26. The electrode modified from trifluoroacetylpyridinium contained the most amount of layers in the film (6) and also showed the most ferrocyanide adsorption. Then, the electrode modified from trifluoroacetyl-4-dimethylaminopyridinium contained fewer layers (2.7) than the electrode modified from trifluoroacetylpyridinium, and it also adsorbed less ferrocyanide. The electrodes modified from trifluoroacetyl-2-iodopyridinium and trifluoroacetyl-2-bromo-4-methylpyridinium contained the least amount of layers (1.1) and showed no ferrocyanide adsorption. The one anomaly of these results is the theorised number of layers for the electrode modified from trifluoroacetyl-3-bromopyridinium. For this modified electrode, it was thought that the film contained 3.7 layers. Hypothetically, this should mean that it would have displayed ferrocyanide adsorption somewhere between what was seen for the electrodes modified from trifluoroacetylpyridinium and trifluoroacetyl-4-dimethylaminopyrdinium. On the contrary, the electrode modified from trifluoroacetyl-3-bromopyridine showed no ferrocyanide adsorption. This difference in results is because it was assumed that all the electrons passed from the electrode to the solution, during the 9 cyclic voltammograms, would contribute directly to the electrodeposition of the salt. However, we know from the cyclic voltammograms taken in Chapter Four, that the trifluoroacetyl-3-bromopyridinium salt took the most amount of scans (7) until no reduction peaks were seen, compared to the other salts (1-3 scans). Therefore, it is likely that not all of the electrons passed during the cyclic

voltammograms of trifluoroacetyl-3-bromopyridinium were directly contributing to the formation of a film. Based on the fact that no ferrocyanide adsorbed to the electrode modified from trifluoroacetyl-3-bromopyridinium it is likely that there was only 1 layer formed on the electrode film, and the rest of the electrons passed contributed to the reduction of the pyridinium salt to form species that diffused away from the electrode surface, rather than graft to it.

5.1.2 Hexaaminеruthenium Chloride

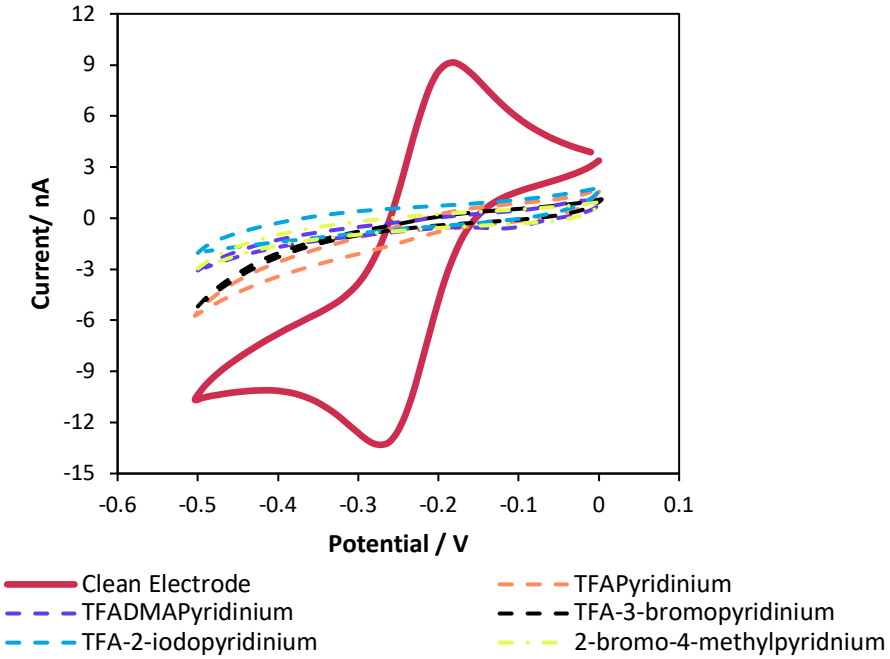

Figure 27: Cyclic voltammograms for a clean (solid line) and modified electrode (dashed lines) in 1 mM hexaaminеruthenium chloride solution in NaCl/H_2O (0.1 M). Scan rate 0.1 V s^{-1}.

The second redox probe to be used was hexaaminеruthenium chloride ($[Ru(NH_3)_6]Cl_3$), the hexaaminеruthenium ion was reduced from $[Ru(NH_3)_6]^{3+}$ to $[Ru(NH_3)_6]^{2+}$ and oxidised back to the $[Ru(NH_3)_6]^{3+}$ ion. Figure 27 shows the cyclic voltammograms of hexaaminеruthenium chloride, taken with a clean (solid line) and modified (dashed lines) electrodes. When the clean glassy carbon electrode was used reversible redox peaks were seen. The electrode was initially swept in the negative direction and a reduction peak was seen at -0.27 V with a peak current of -13.3 nA. Then the electrode was then swept in the positive direction and an oxidation peak was

seen at -0.18 V with a peak current of 9.1 nA. When the modified electrodes were used no redox peaks were seen at all.

The absence of any redox peaks when each modified electrode was used is further evidence that the modified electrodes all include a positively charged film on the surface. Here, the positively charged hexaammineruthenium ion was repelled from the modified electrode surface. This meant there were no electroactive species at the electrode surface, so no redox peaks were seen.

5.1.3 Ferrocenemethanol

Ferrocenemethanol (FcMeOH) was the final probe used to investigate the behaviour of the modified electrodes (Figure 28). Ferrocenemethanol was oxidised to form ferrocenium methanol ($FcMeOH^+$) and then reduced back to the original neutral species. When the clean electrode was used to take a cyclic voltammogram of ferrocenemethanol, the potential of the electrode was swept in the positive direction and an oxidation peak was seen at 0.18 V with a peak height of 9.4 nA. The potential of the electrode was then reversed and swept in the negative direction, where a peak current of -9.4 nA was seen at 0.10 V. When the electrode had been modified from trifluoroacetylpyridinium the oxidation peak was seen at 0.19 V with a peak current of 9.5 nA, and the reduction peak was seen at 0.11 V with a peak current of -7.5 nA.

The behaviour of ferrocenemethanol towards the modified electrode once again proves that the modified electrode surface was positively charged. When the modified electrode was swept in the positive direction, the ferrocenemethanol at the surface was neutral, and oxidised to a positive ion. At this point the peak oxidation current for the modified electrode matched that of the clean electrode. Then when the electrode was swept in the negative direction the ferrocenium methanol at the surface of the electrode was positively charged, and so the ferrocenium methanol ions were repelled from the electrode surface, hence why a smaller peak reduction current was seen as compared to the clean electrode.

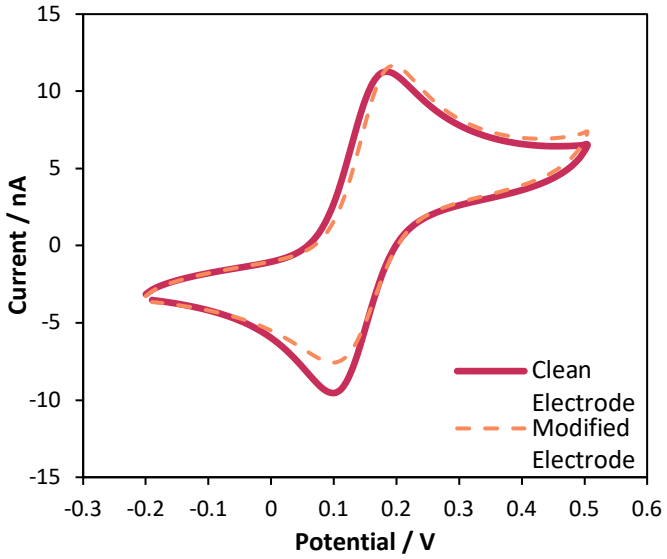

Figure 28: Cyclic voltammograms for a clean electrode (solid line) and an electrode modified from trifluoroacetylpyridinium (dashed lines) in 1 mM ferrocenemethanol solution in NaCl/H_2O (0.1 M). Scan rate 0.1 V s^{-1}.

It was noted that the decrease in current in the reverse scan was comparatively small as compared to when the positively charged hexaammineruthenium ions were used, where no redox peaks were seen at all. This may be due to the hydrophobic nature of the ferrocenium methanol which meant that it mostly still dissolved into the organic film, despite being positively charged, whereas the hexaammineruthenium ions are hydrophilic and so would not penetrate the film. Another thing to consider when comparing the behaviour of the hexaammineruthenium ions and the ferrocenium methanol is that when the modified electrode was placed in the solution of hexaammineruthenium chloride, there would have been a couple of minutes delay between the electrode entering the solution and the cyclic voltammogram being run. This would have allowed enough time for all of the hexaammineruthenium ions to be repelled. Whereas in the case of the ferrocenemethanol, there would have only been a couple of seconds passed between the formation of the ferrocenium methanol ions and the start of the reverse scan. This would not have allowed much time for the ferrocenium methanol ions to be repelled, which is another possible reason why only a small decrease in the reduction current was seen.

5.1.4 Comparison of all Redox Probes

The behaviour of all three redox probes tested confirms that the films on the modified electrode surface are positively charged. Hence why the hexaammineruthenium ion was repelled from all the modified electrodes, and the ferrocenemethanol was repelled once it had been oxidised to a cation, but not when it was neutral. The ferrocyanide ions also confirmed that the electrodes were positively charged, with the ferrocyanide ion being attracted to, and adsorbed into the film. It was thought that the amount of ferrocyanide adsorbed would be proportional to the thickness of the film on the modified electrode surface, and this was somewhat proved by the theoretical calculations of the number of layers in each film. The films formed from trifluoroacetyl-2-iodopyridinium, trifluoroacetyl-3-bromopyridinium and trifluoroacetyl-2-bromo-4-methylpyridinium were so thin than no ferrocyanide could adsorb to them, hence why they showed the same redox behaviour as the clean electrode. This would also confirm what was seen in the XPS studies, where electrodes modified from trifluoroacetylpyridinium and trifluoroacetyl-4-dimethylaminopyridinium showed thicker films than the electrodes modified from trifluoroacetyl-2-iodopyridinium, trifluoroacetyl-3-bromopyridinium and trifluoroacetyl-2-bromo-4-methylpyridinium. The theory of the dependence of the film thickness versus how much ferrocyanide was adsorbed is continued in the next sub-chapter.

5.2 Ferrocyanide Adsorption

To investigate the relationship between film thickness and the amount of ferrocyanide adsorbed to the modified electrode surface, a glassy carbon electrode was modified via constant potential, in a 10 mM solution of trifluoroacetylpyridinium, for different lengths of time. For this experiment, trifluoroacetylpyridinium was chosen to modify the electrode as films from this salt showed the most amount of ferrocyanide adsorption (Figure 26). The electrode was held at constant potential for increasing lengths of time as it was assumed that the longer the electrode was modified for, the thicker the film on the electrode surface would become. Once modified, the electrodes were cleaned via sonication in MeCN for 2 min and placed in a 1mM solution of

potassium ferrocyanide for 5 min, to allow for maximum adsorption. The modified electrodes were then rinsed with water and placed in a solution of 0.1 M NaCl/H_2O. Cyclic voltammograms were then taken in the solution of NaCl/H_2O, meaning that the only electroactive species present should have been the ferrocyanide that adsorbed to the modified electrode surface. The results of this experiment can be seen in Figure 29.

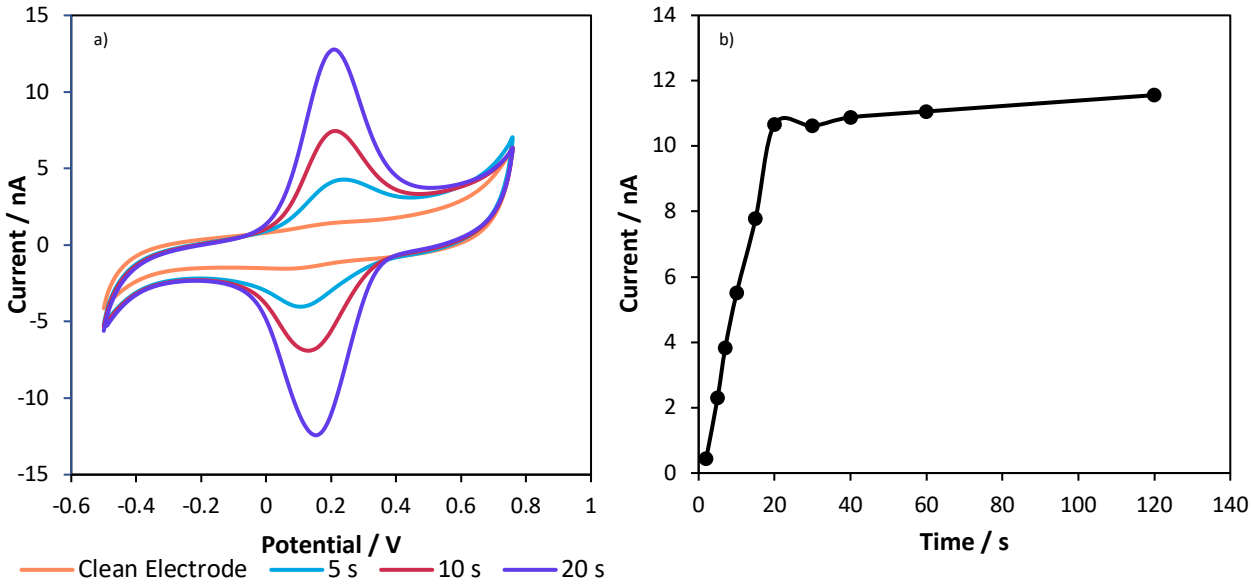

Figure 29a: Cyclic Voltammograms in 0.1 M NaCl/H_2O of a glassy carbon electrode that is clean (orange) and modified in 10 mM trifluoroacetylpyridinium for 5 s (blue), 10 s (red) and 20 s (purple).

Figure 29b: Plot of peak oxidation current (nA) vs length of time (s) for electrode modification via constant potential.

Figure 29a shows the cyclic voltammograms of the glassy carbon electrode that had been modified from trifluoroacetylpyridinium for increasing amounts of time. When the electrode was clean (orange line) no redox peaks were observed. This was to be expected as the ferrocyanide did not adsorb to the clean electrode, and so there were no electroactive species in the solution. The cyclic voltammogram for the electrode that had been modified for 5 s is shown in light blue. The potential of the electrode was swept in the positive direction and an oxidation peak was seen at 0.22 V with a corresponding peak current of 2.13 nA. The potential was then swept in the negative value, and a reduction peak was seen at 0.11 V with a corresponding peak current of

-2.63 nA. When the electrode had been modified for 10 s (red line) the oxidation peak occurred at 0.21 V with an increased peak current of 5.52 nA. The reduction peak also shifted, to 0.13 V with an increased peak current of -5.58 nA. Finally, when the electrode had been modified for 20 s (purple line) the oxidation peak occurred at 0.21 V with a peak current of 10.8 nA, and the reduction peak occurred at 0.16 V with a peak current of -11.2 nA.

Figure 29b shows the relationship of the peak oxidation current (taken from cyclic voltammograms, like those seen in Figure 29a) and the length of time the electrode was modified for. When the electrode had been modified for 2 s the peak oxidation current was 0.45 nA. When the electrode had been modified for 15s the peak oxidation current increased to 7.79 nA, and when it had been modified for 20 s it increased even further, to 10.8 nA. However, modification for any length of time greater than 20 s showed a minimal increase in the oxidation current (or reduction current, not shown). For example, after the electrode had been modified at constant potential for 120 s the peak observation current had only increased to 11.6 nA.

The results seen in Figure 29 show that the amount of ferrocyanide adsorbed to the modified electrode surface was proportional to the length of time the electrode was modified for. From this, it can be implied that the amount of ferrocyanide adsorbed is also proportional to the thickness of the film formed. Using this principle, we see that after 20s of constant potential, the amount of ferrocyanide adsorbed to the modified electrode reaches a plateau. Thus, it would appear that the film reached a maximum thickness, and at this point no further growth was seen. This was because when the film formed it was positively charged and the trifluoroacetylpyridinium salt needed to grow the film was also positively charged. Therefore, a point was reached in which the newly formed film repelled the trifluoroacetylpyridinium salt away from the electrode surface. When this happened there was no available trifluoroacetylpyridinium to be reduced, and so the film became self-limiting in growth.

5.3 pH Dependence of the Modified Electrode

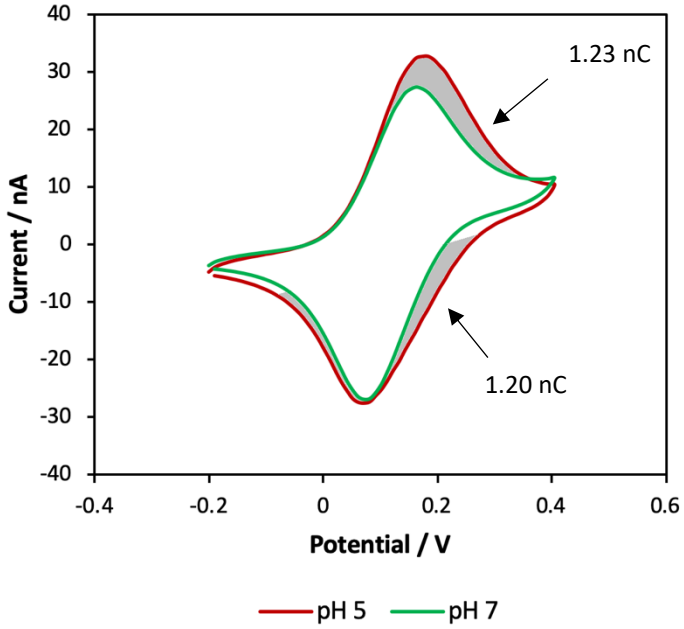

Figure 30: Cyclic voltammograms of 1 mM potassium ferrocyanide taken with a glassy carbon electrode modified from 10 mM trifluoroacetylpyridinium for 30 s at constant potential. The cyclic voltammograms were taken at different pH values: red line – pH 5 and green line – pH 7. The shaded grey area shows the difference in charge passed between the oxidation peaks (1.22 nC) and the reduction peaks (1.20 nC).

The behaviour of ferrocyanide at the electrode modified from trifluoroacetylpyridinium was then investigated at a range of different pH values, to provide information on how the charge on the modified electrode surface changed in acidic or basic environments. To do this, solutions of 1 mM ferrocyanide were prepared with different 1 M phosphate buffers (potassium dibasic and potassium monobasic) to create solutions of ferrocyanide at a range of pH values. Electrodes that had been modified from trifluoroacetylpyridinium, via constant potential for 30 s (to ensure maximum film growth) were then used to conduct cyclic voltammetry in the ferrocyanide solutions. The modified electrodes were placed in the ferrocyanide solutions for 5 min before the cyclic voltammograms were taken, to allow the films to be equilibrated to the pH of the solution. The effect of pH on the redox response of ferrocyanide at the modified electrodes is seen in Figures 30 and 31.

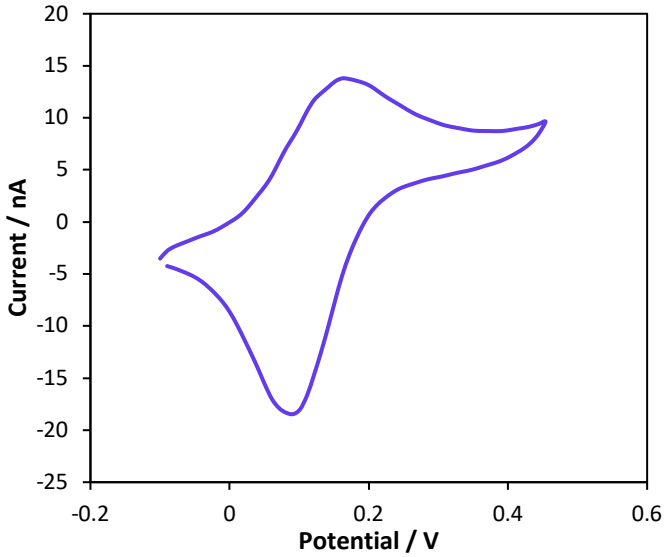

Figure 31: Cyclic voltammogram of 1 mM ferrocyanide in pH 9, taken with a glassy carbon electrode modified from 10 mM trifluoroacetylpyridinium for 30 seconds.

Figure 30 shows the cyclic voltammograms of potassium ferrocyanide taken at pH 5 and pH 7. When pH 5 was used (red line) the oxidation peak potential occurred at 0.18 V with a peak current of 32.8 nA, and the reduction peak potential occurred at 0.07 V with a peak current of -27.5 nA. When pH 7 was used (green line) the oxidation peak current decreased to 27.4 nA and the peak potential shifted to 0.16 V. The reduction peak current only decreased slightly, to -27.0 nA and the peak potential shifted to 0.07 V. Figure 31 shows the cyclic voltammogram of ferrocyanide taken at pH 9. Here, the ferrocyanide oxidation peak occurred at 0.16 V with a peak current of 13.8 nA. The reduction peak occurred at 0.09 V with a peak current of -18.5 nA.

The oxidation and reduction peaks for each cyclic voltammogram presented in Figure 30 and Figure 31 were integrated to find the amount of charge passed during the oxidation and reduction of ferrocyanide at each pH. The calculated results are shown in Table 18.

	pH	Peak / V	Charge Passed / nC
1	5	0.18 (ox)	4.65
2	5	0.07 (red)	5.84
3	7	0.16 (ox)	3.42
4	7	0.07 (red)	4.64
5	9	0.16 (ox)	1.54
6	9	0.09 (red)	2.47

Table 18: the amount of charge passed for each oxidation (ox) or reduction (red) peak of ferrocyanide calculated via integration of the cyclic voltammograms seen in Figure 30 and Figure 31.

The shaded grey area in Figure 30 shows the difference in charge passed between the voltammogram taken at pH 5 and the voltammogram at pH 7, the value of this area was calculated according to the values in Table 18. To find the difference in oxidation peaks, the total amount of charge passed at pH 7 (3.42 nC) was subtracted from the total amount of charge passed at pH 5 (4.65 nC), and the absolute value was found to be 1.23 nC. The same calculation was made for the difference in reduction peaks, where the total amount of charge passed at pH 7 (4.64 nC) was subtracted from the total amount of charge passed at pH 5 (5.84 nC) and the absolute value was found to be 1.20 nC.

Comparing the peak shapes of the two cyclic voltammograms shown in Figure 30, the oxidation peak current increased as the pH was changed from pH 5 to pH 7, but the reduction peak currents remained the same. Comparison of the peak height alone would suggest that increasing the acidity caused more ferrocyanide to be oxidised than reduced. However, comparison of the difference in charge passed for the oxidation and reduction peaks for pH 5 and pH 7 (grey area in Figure 30) showed that the oxidation and reduction of ferrocyanide increased equally, by roughly 1.20 nC. Consideration of the protonation state of the pyridine within the film on the modified electrode can help to explain this increase in charge passed.

We know from the XPS studies discussed in Chapter Four that the films on the modified electrode were comprised of neutral pyridine and cationic (trifluoroacylated) pyridinium species bound to the electrode surface. When the modified electrode was

placed in an acidic pH, some of the neutral pyridine would have been protonated to form additional cationic (protonated) pyridinium species. These three species will be referred to often in this chapter, so for clarity they are represented below:

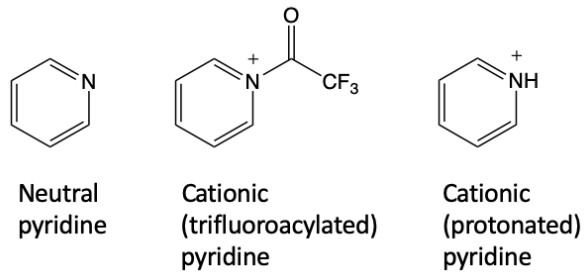

Figure 32: Representation of neutral, cationic (trifluoroacylated) pyridine and cationic (protonated) pyridine.

The concentration of protonated pyridinium species [pyrH$^+$] present at different pH values can be estimated using the Henderson-Hasslebach equation:

$$pH = pK_a + \log_{10}\left(\frac{[pyr]}{[pyrH^+]}\right) \qquad \textit{Eq. 21}$$

This equation can be rearranged, to show the relationship of [pyrH$^+$] and pH:

$$[pyrH^+] = \frac{1}{1 + 10^{pH-pK_a}} \qquad \textit{Eq. 22}$$

A plot of normalised [pyrH$^+$] versus pH is seen in Figure 33. For these graphs the combined concentration of neutral pyridine [pyr] and protonated pyridine [pyrH$^+$] was assumed to be 1.

$$[pyr] + [pyrH^+] = 1 \qquad \textit{Eq. 23}$$

Different pK_a values of substituted pyridines were used to calculate these curves as it was unknown how the pyridine would be grafted to the electrode surface, and so a range of different pK_a values would help to give us a window of estimation. It should also be noted that the pK_a of free pyridine to surface bound pyridine will differ, but these estimations should still help as a rough guide.

Therefore, using the graphs in Figure 33, it can be estimated that when the modified electrode was placed in a solution of pH 7, between 1-18% of the neutral pyridine would have been protonated, whereas when it was placed in a solution of pH 5,

between 60-97% of the neutral pyridine would have been protonated. Again, as these values are estimates they should not be taken as exact values, however, they do help to highlight that when the acidity of the solution was increased from pH 7 to pH 5 significantly more of the neutral pyridine would have been protonated to form pyridinium cations.

The increase in the concentration of pyridinium cations due to the protonation of neutral pyridine would have led to an increase in positively charged sites on the modified electrode surface. This increase in positive charge attracted more negative ferrocyanide ions to the surface of the modified electrode. We know from the ferrocyanide adsorption experiments discussed previously (Figures 29a and 29b) that the amount of ferrocyanide adsorption is proportional to the thickness of the film. As each of the electrodes used at pH 7 and pH 5 were modified for 30 s it can be assumed that they both had the maximum thickness of film. Thus increasing the acidity of the pH would not increase the amount of ferrocyanide that could adsorb into the film, as they were already saturated. Instead, it increased the amount of free ferrocyanide in solution near the electrode surface. As the amount of charge passed in the oxidation and reduction scans increased equally when the acidity was increased from pH 7 to pH 5, it can be assumed that this increase in charge was proportional to the amount of ferrocyanide that was attracted to the electrode surface. This process is illustrated below, in Figure 34.

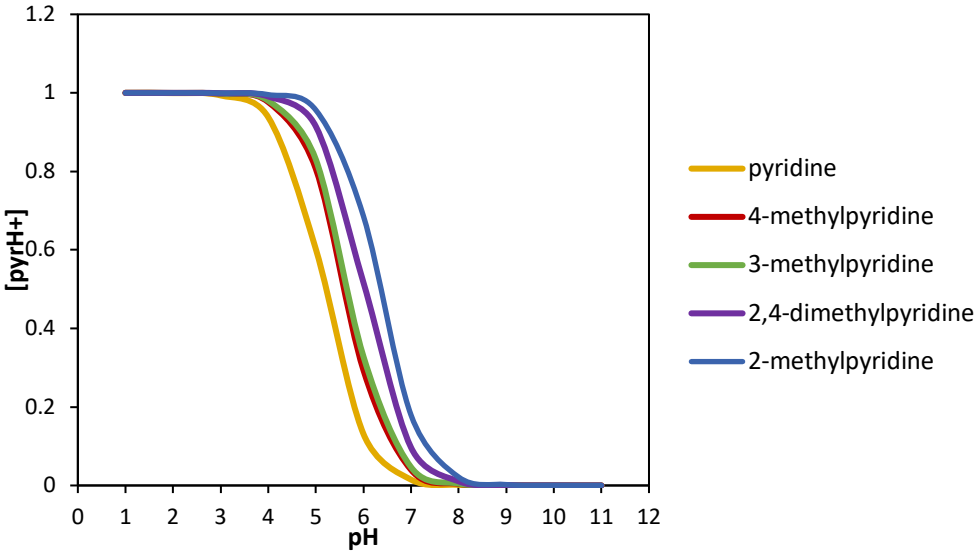

Figure 33: Plot of the calculated concentration of protonated pyridine ([pyrH⁺]) versus the pH of the theoretical solution. Values for [pyrH⁺] were calculated using the Henderson-Hasslebach equation. pK_a values of different substituted pyridines were used: yellow – pyridine; red – 4-methylpyridine; green – 3-methylpyridine; purple – 2,4-dimethylpyridine; blue – 2-methylpyridine.

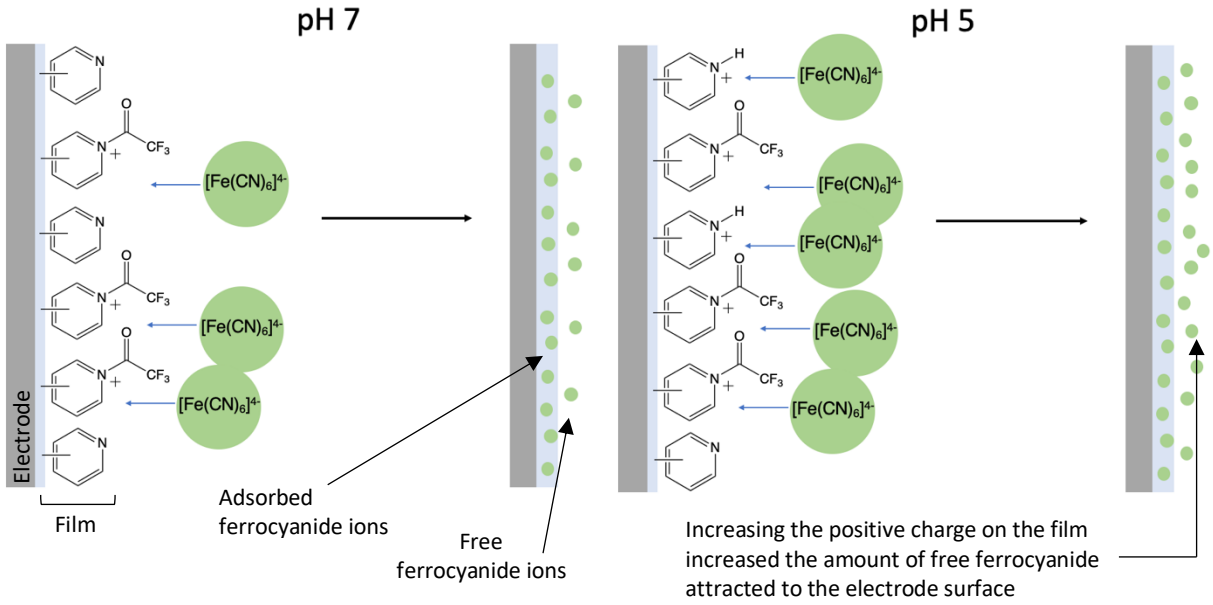

Figure 34: Illustration of what happens at the modified electrode surface when the acidity of the solution was increased from pH 7 to pH 5.

Returning to Table 18, overall it was seen that the amount of charge passed for the oxidation and reduction peaks decreased as the pH was increased. Thus it can be concluded that the concentration of ferrocyanide attracted to the electrode surface was proportional to the concentration of positively charged sites in the film, which increased as neutral pyridine was protonated in acidic solutions. Further comparison of the amount of charge passed for each oxidation and reduction peak showed that the amount of charge passed during the reverse (reduction) scan was always more than the forward (oxidation) scan, independent of what the pH was. When the cyclic voltammogram was taken in pH 5, 1.19 nC of extra charge was passed in the reduction peak than in the oxidation peak. When the cyclic voltammogram was taken in pH 7, 1.22 nC of extra charge was passed in the reduction peak compared to the oxidation peak. Lastly, when the cyclic voltammogram was taken in pH 9, 0.93 nC of extra charge was passed in the reduction peak compared to the oxidation peak.

The difference between the forward and reverse scan is seen most clearly in the voltammogram taken in Figure 31 (taken at pH 9). In the forward scan the peak shape shows that the current was diffusion controlled, whereas in the reverse scan the peak shape was symmetrical. This symmetrical shape indicated that a surface bound species was contributing to electron transfer. The difference in peak shape between the forward and reverse scans can be explained with the following rationale:
When the modified electrode was placed in the ferrocyanide solution, of pH 9, the surface concentration of pyridinium ions was low and so a small amount of ferrocyanide adsorbed to the surface. When the electrode potential was swept in the forward direction the majority of the ferrocyanide that was oxidised had to diffuse from the solution to the electrode surface, hence why diffusion controlled currents were seen. As the ferricyanide was generated at the electrode surface it adsorbed to the film, meaning that on the reverse scan a high concentration of ferricyanide was present at the electrode surface. This high concentration of adsorbed ferricyanide caused the increase in charge passed for the reduction scan as compared to the oxidation scan.

5.4 Oxidation of the Modified Electrode Surface

An experiment was undertaken to investigate any possible redox properties of the film on the modified electrode surface. Figure 35 shows the cyclic voltammograms of the film on the electrode surface taken with an electrode modified from 10 mM trifluoroacetylpyridinium via constant potential for 5 s (so a thin film was formed on the electrode surface), taken in 0.1 M NaCl/H_2O. The cyclic voltammograms were taken at pH 5 (red) and pH 9 (blue). At pH 5, an oxidation peak can be seen at 0.232 V and a corresponding oxidation current of 0.13 nA. When the cyclic voltammogram was taken at pH 9, the oxidation peak had shifted to a more negative potential, 0.001 V and the oxidation peak current was 0.62 nA.

The shift in potential with pH can be explained with consideration of the Nernst equation. Here we consider a reaction involving *m*-protons and *n*-electrons:

$$\mathrm{A} + m\mathrm{H}^+ + n\mathrm{e}^- \leftrightharpoons \mathrm{B} \qquad \textit{Eq. 24}$$

Thus the Nernst equation becomes:

$$E_{\mathrm{eq}} = E_0 - \frac{RT}{nF}\ln\frac{[\mathrm{B}]}{[\mathrm{A}][\mathrm{H}^+]^m} \qquad \textit{Eq. 25}$$

Which can be rearranged to:

$$E_{\mathrm{eq}} = E_0 + \frac{RT}{nF}\ln[\mathrm{H}^+]^m - \frac{RT}{nF}\ln\frac{[\mathrm{B}]}{[\mathrm{A}]} \qquad \textit{Eq. 26}$$

$$E_{\mathrm{eq}} = E_0 - 2.303\frac{mRT}{nF}pH - \frac{RT}{nF}\ln\frac{[\mathrm{B}]}{[\mathrm{A}]} \qquad \textit{Eq. 27}$$

$$E_{\mathrm{p}} = E_0 - 2.303\frac{mRT}{nF}pH \qquad \textit{Eq. 28}$$

Thus, the peak potential (E_p) varies by a value of $2.303\frac{mRT}{nF}$ per pH unit. Commonly, when *m* = *n* this corresponds to approximately 59 mV per pH unit, at 25 ^{0}C. In the cyclic voltammograms seen in Figure 35, the peak potential shifted 230 mV over a pH

range of 5-9, which corresponds to 57.5 mV per pH unit. Thus, this shift in oxidation potential corresponds to an electron transfer coupled to a proton transfer.

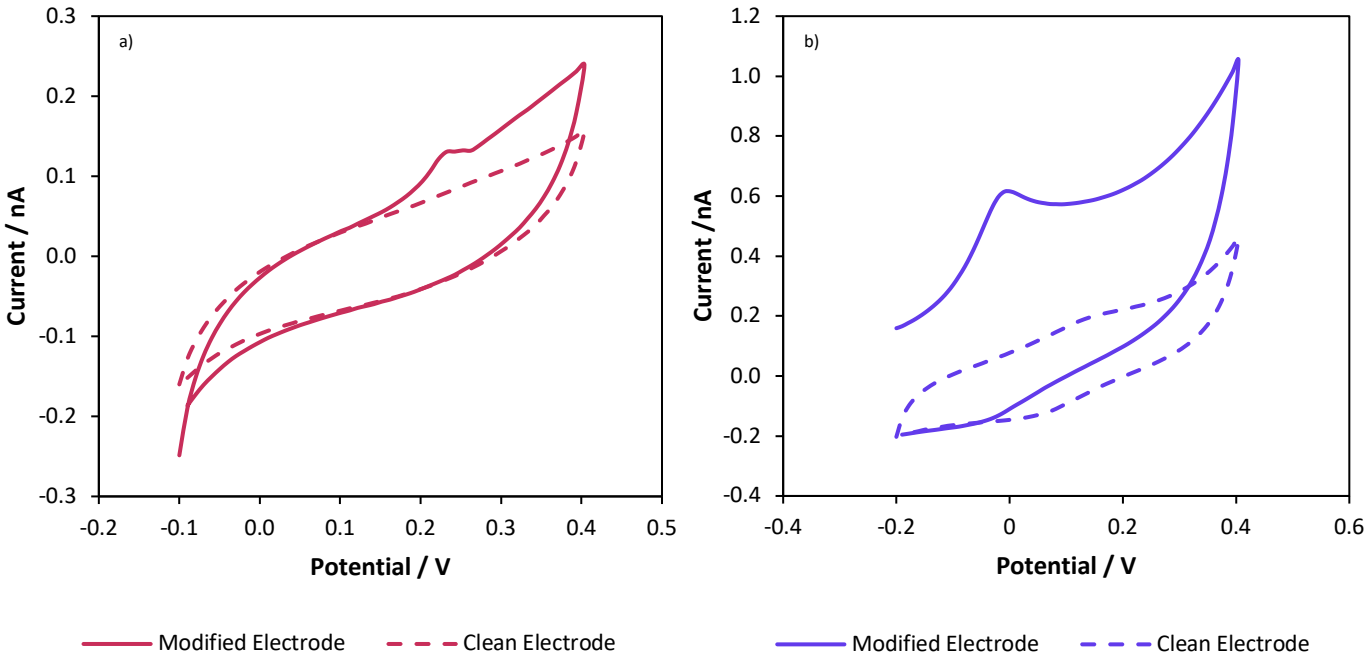

Figure 35: Cyclic voltammograms of the modified electrode surface in aqueous potassium phosphate buffer solutions (0.1 M) taken at a) pH 5 and b) pH 9. Solid lines represent the modified electrode, dashed lines represent the clean electrode.

It was previously mentioned that the increase in charge passed during the reduction of ferrocyanide as compared to oxidation, could be due to the adsorption of ferricyanide to the electrode surface during the forward scan. However, the oxidation of the film seen here in Figure 35 could be an alternative explanation for the increase in charge passed. The adsorption of the ferro/ferricyanide species may be linked to the protonation state of the film which is altered during cycling. Overall it is possible that both processes took place simultaneously, rather than one explanation being more plausible than the other.

5.5 Charge Control of the Modified Electrode

It is now well established that placing the modified electrode in acidic pH protonated the neutral pyridine in the film, whilst placing it in a basic pH neutralises the pyridinium species. We wanted to investigate whether we could control the surface charge, as this could be a useful quality of the films if they were to be used for sensing or other surface-sensitive techniques. To identify whether the charge on the surface of the modified electrodes could be manipulated, the electrodes were modified from a 10 mM trifluoroacetylpyridinium solution via constant potential for 30 seconds, to ensure a thick film was formed. The modified electrodes were then cleaned via sonication in MeCN for 2 min. After that the electrodes were pre-treated, before being used to conduct cyclic voltammograms of potassium ferrocyanide. Two forms of pre-treatment were carried out; base-treatment (placed in a solution of 1 M NaOH for 3 min) or base/acid-treatment (placed in a solution of 1 M NaOH for 3 min, rinsed, then placed in a solution of 1 M H_2SO_4 for 3 min). The results of this experiment can be seen in Figure 36.

When a clean glassy carbon electrode was used (blue dashed line) the ferrocyanide was oxidised at 0.16 V with a peak current of 10.70 nA, and it was reduced at 0.06 V with a peak current of -9.59 nA. When the glassy carbon electrode had been modified, but not pre-treated (black line), the ferrocyanide oxidation peak appeared at 0.17 V with a peak current of 22.6 nA, and the reduction peak occurred at 0.06 V with a peak current of -22.5 nA. For the base-treated modified electrode (blue solid line) the ferrocyanide oxidation occurred at 0.15 V with a peak current of 12.4 nA, and a reduction at 0.05 V with a peak current of -14.9 nA. For the base/acid treated modified (red line) the ferrocyanide oxidation occurred at 0.18 V with a peak current of 23.3 nA and the reduction peak occurred at 0.08 V with a peak current of -23 nA.

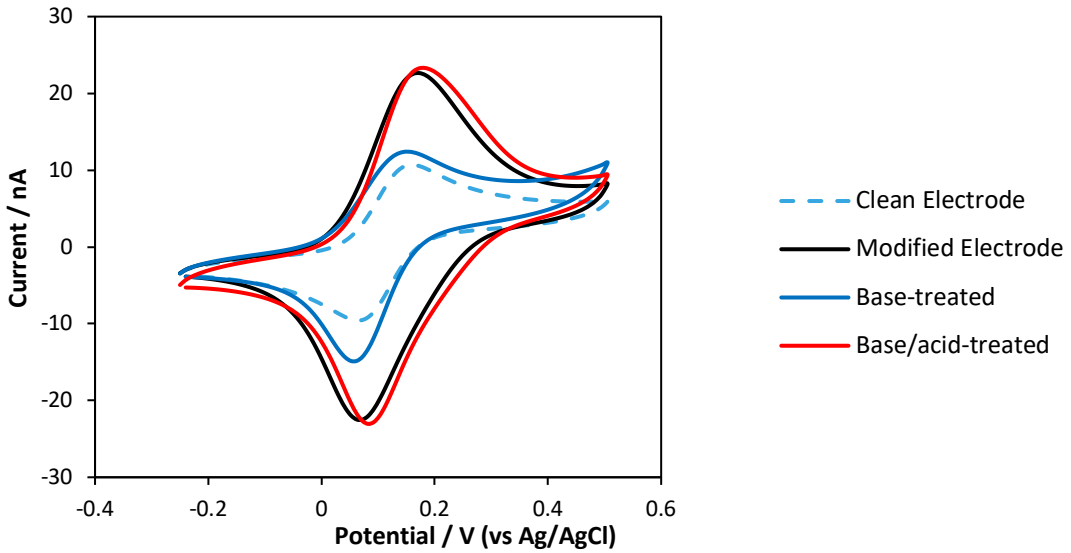

Figure 36: Cyclic voltammograms of glassy carbon electrodes when they were clean (dashed line) and modified from 10 mM trifluoroacetylpyridinium via constant current for 30 s (solid lines). The modified electrodes were pre-treated after modification and before the voltammograms were taken in various ways: black line – no pre-treatment; blue line – placed in a solution of NaOH for 5 min; red line – placed in a solution of NaOH for 2 min, then a solution of H_2SO_4 for 2 min.

The results shown in Figure 36 indicate that the positive charge, originating from the cationic nitrogen species on the modified electrode surface, can be removed with a base and then reinstalled with an acid. This is evidenced through the adsorption of the ferrocyanide. When the electrode was modified but not pre-treated, the ferrocyanide adsorbed into the film which increased the amount of ferrocyanide at the electrode surface and caused an increase in the redox currents, as compared to the clean electrode. Then when the electrode was base-treated (blue solid line), a reduction in the redox current was seen, indicating that less ferrocyanide had adsorbed to the electrode surface due to a decrease in positive pyridinium sites. These results were unsurprising as we had already witnessed such behaviour when taking cyclic voltammograms of ferrocyanide at in solutions of different pH (Figures 30 and 31). The most noteworthy part of this experiment was for the electrode that had been base/acid-treated (red line). For this electrode we saw redox peaks of a very similar potential and peak current as the modified electrode that had not received any pre-treatment (black line). Thus it can be assumed that when the electrode was base/acid-treated, a similar

concentration of cationic nitrogen was formed as compared to the originally modified electrode. No cyclic voltammogram was taken between the base and acid treatment, but it can be assumed that the positive charge was removed. Thus, treatment with the acid re-protonated the film. This process demonstrated that we can remove the positive charge on the film and then revert it back to the original state it was in before any pre-treatment.

To investigate the films after they were base-treated or base/acid-treated, XPS studies were carried out on the pre-treated modified graphite electrodes. The results of these experiments are seen below. The tabulated peak centres (eV) and the area of the peaks (%) include the electrode modified with trifluoroacetylpyridinium from Chapter Four, so that comparisons may be drawn between the pre-treated and non-treated electrodes. A few spectra of interest are included here, and full spectra can be seen in Appendix C.

Figure 37a shows the C1s region of the base-treated modified electrode. Here, peaks that had already been assigned to the trifluoroacetylpyridinium film in Chapter Four were seen again. These peaks are the ones at 284.8 eV (C-C graphite), 285.5 eV (C-C pyridine), 286.4 (C-O graphite), 287.0 (C-N pyridine) 288.5 (C=O trifluoroacetamide), 292.1 eV (CF_3 trifluoroacetamide). A new peak was also seen at 289.7 eV which corresponds to (O=C-O) bonding.[137, 138] Figure 37b shows the peaks assigned to the C1s region of the base/acid-treated modified electrode. These peaks are the same ones as seen in the non-treated modified electrode, except that the peak corresponding to CF_3 group was missing.

		C1s Peak Centre / eV (*Area %*)						
		284.8	285.5	286.4	287.0	288.5	289.7	292.1
1	Non-treated	*47*	*28*	*6*	*10*	*5*	-	*4*
2	Base-treated	*48*	*10*	*10*	*7*	*6*	*18*	*2*
3	Base/acid-treated	*55*	*21*	*9*	*9*	*6*	-	-

Table 19: Peak centre and the associated area for peaks in the C1s region of an electrode modified from trifluoroacetylpyridinium and treated with NaOH (2) and then further treated with sulphuric acid (3).

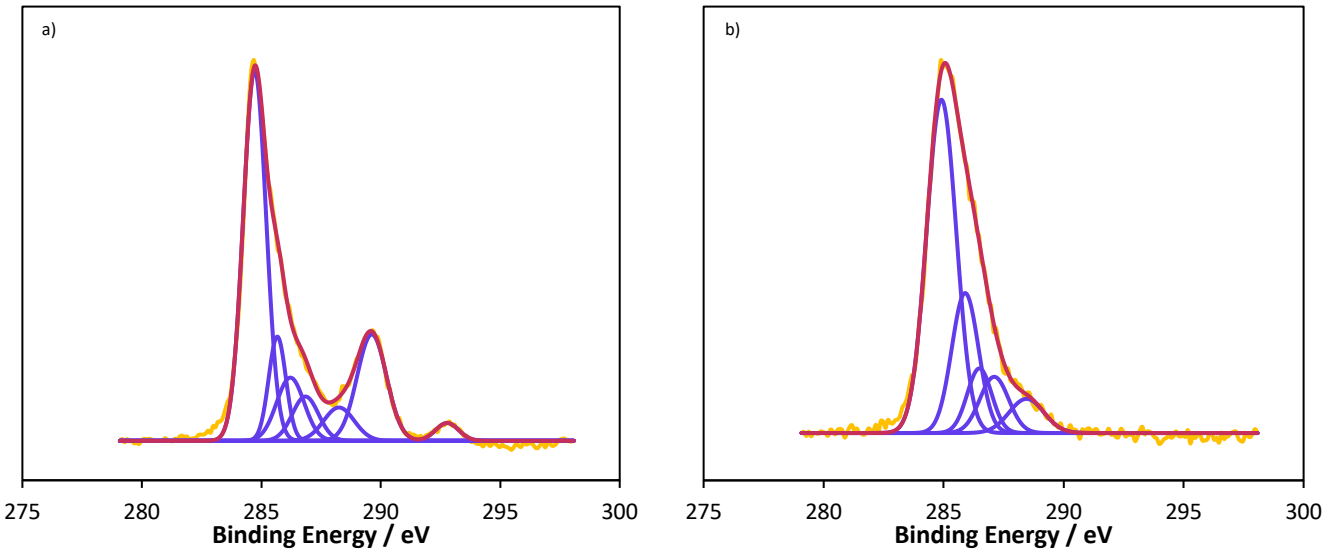

Figure 37: C1s region of electrodes modified from trifluoroacetylpyridinium and treated with NaOH (a) and then further treated with sulphuric acid (b). Red line – cumulative fitted peak; blue line – independent fitted peaks; yellow line – raw data.

		N1s Peak Centre / eV (Area %)		F1s Peak Centre / eV (Area%)	
		399	402	686	688
1	Non-treated	48	52	44	56
2	Base-treated	58	42	-	100
3	Base/acid-treated	43	57	100	-

Table 20: Peak centre and the associated area for peaks in the N1s and F1s regions of an electrode modified from trifluoroacetylpyridinium and treated with NaOH (2) and then further treated with sulphuric acid (3)

Table 20 shows the peaks found in the N1s and F1s regions for the base-treated (entry 2) and base/acid-treated (entry 3) modified electrodes. Analysis of the N1s region showed that when the modified electrode had been base-treated the concentration of cationic nitrogen (402 eV) decreased (42%) as compared to the non-treated modified electrode (52%), and when the modified electrode had been base/acid-treated the concentration of cationic nitrogen increased (57%). Analysis of the F1s region for the base-treated modified electrode showed that the only fluorine environment present in the film belonged to the CF_3 group (688 eV). Whereas, for the base/acid-treated modified electrode, the only fluorine environment belonged to the PF_6^- anion (686 eV).

		O1s Peak Centre / eV (*Area %*)			
		530	532	533	535
1	Non-treated	-	*88*	*12*	-
2	Base-treated	*3*	*57*	*31*	*9*
3	Base/acid-treated	-	*74*	*26*	-

Table 21: Peak centre and the associated area for peaks in the N1s and F1s regions of an electrode modified from trifluoroacetylpyridinium and treated with NaOH (2) and then further treated with sulphuric acid (3).

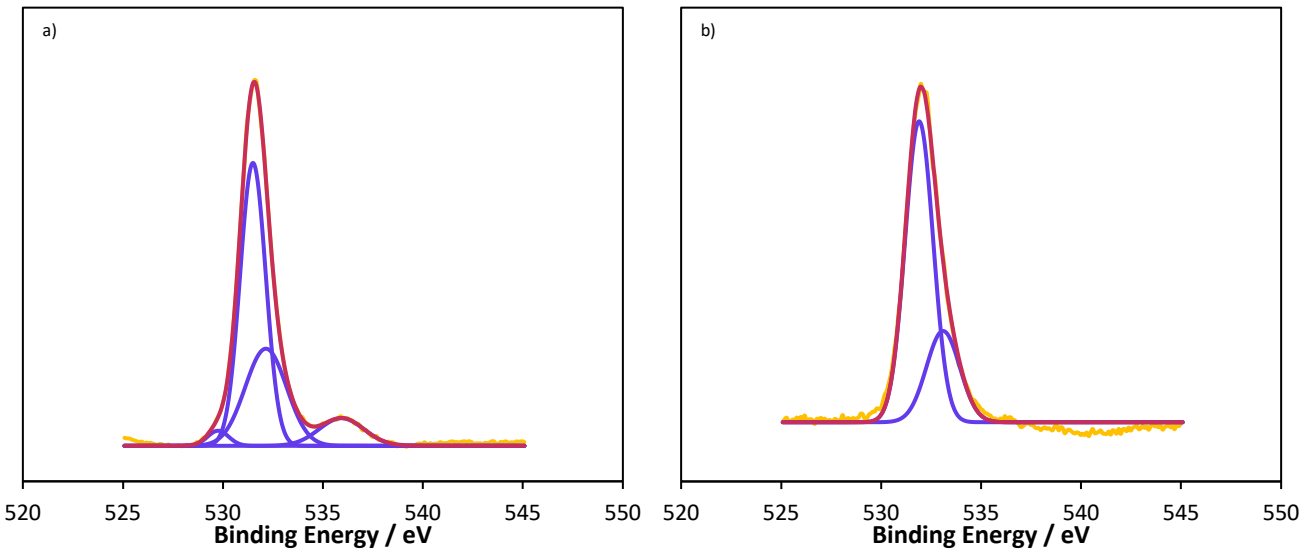

Figure 38: O1s region of electrodes modified from trifluoroacetylpyridinium and treated with NaOH (a) and then further treated with sulphuric acid (b). Red line – cumulative fitted peak; blue line – independent fitted peaks; yellow line – raw data.

Analysis of the O1s region for the base-treated modified electrode (Figure 38a) showed two new peaks, as compared to the non-treated electrode seen previously which only showed peaks at 532 eV (C-O graphite oxide) and 533 eV (C=O carbonyl). The new peaks in the base-treated electrode appeared at 530 eV and 535 eV which corresponds to OH hydroxide and Na Auger peaks respectively.[139] The O1s region for the base/acid-treated electrode showed the same C-O graphite oxide and C=O carbonyl peaks as the non-treated modified electrode. Both the base-treated and the acid/base-treated modified electrodes showed higher concentrations of C=O carbonyl peaks as compared to the non-treated modified electrode.

Previous analysis of the N1s region of the non-treated electrode modified from trifluoroacetylpyridinium showed that the ratio between pryN:pyrN$^+$ was roughly 50:50 (Table 20, entry 1). From the results seen for the pre-treated modified electrodes, when the electrode was base-treated the ratio of pryN:pyrN$^+$ was roughly 60:40 (Table 20, entry 2) and when it was base/acid-treated it was 40:60 (Table 20, entry 3). This is evidence that the NaOH removed the trifluoroacetyl group from the pyridinium species in the film (Scheme 16), creating surface-bound neutral pyridine and trifluoroacetic acid. Further treatment with H_2SO_4 then protonated the neutral pyridine in the film and washed away the trifluoroacetic acid.

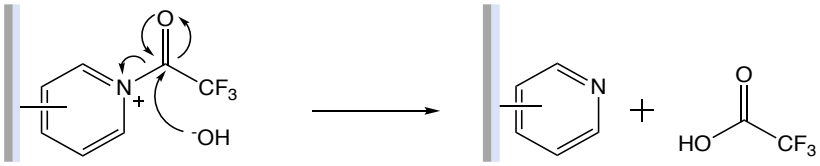

Scheme 16: Reaction of sodium hydroxide with the surface bound trifluoroacetylpyridinium to form surface-bound neutral pyridine.

We had expected to see the base- and base/acid-treatment to have more of an effect in removing the trifluoroacetyl group and protonating the modified electrode respectively. For instance, looking back at the graphs of [pyrH$^+$] vs pH (Figure 33) using a very strong base it would be expected that all of the pyridinium species would have been converted to pyridine. Similarly, using a very strong acid it would be

expected that almost all neutral pyridine would have been protonated. One explanation for this difference in the predicted results versus the experimental results could be due to the rinsing of the electrodes with ultrapure water after they were pre-treated, which would have altered the pH of the electrode surface. Thus the base-treated electrode would have been partially re-protonated and the base/acid-treated electrode would have been partially de-protonated, when they were both were rinsed with water. Hence why the pryN:pyrN$^+$ ratio was not altered as much we had expected.

The presence or absence of the PF_6^- anion is indicative of what the charge on the pre-treated electrode would have been before it was rinsed with water. We saw that when the electrode was base-treated the only fluorine species present was the CF_3 environment. Thus, when the electrode had been treated with the base the concentration of cationic pyridine was decreased which lessened the positive charge on the film. Simultaneously, the PF_6^- anion (that had been incorporated in the film during modification) was no longer attracted to, or, adsorbed into the film, hence the absence of a peak at 686 eV. Similarly, when the electrode was base/acid-treated the O=C-CF_3 group was displaced by the acid proton, to form a pyrH$^+$ cation. The surface was still positively charged and so the PF_6^- anion was still adsorbed into the surface and this was shown by the peak at 686 eV in the F1s spectrum.

5.6 Theory of Electrode Modification Mechanism

Chapters Four and Five have presented all the data known about the process of electrode modification and the properties of the modified electrodes. In this section, this information shall be summarised and used to theorise a mechanism for the formation of the film on the electrode surface. We believed that the mechanism of film formation could be inferred from the thickness of the films and the rate at which they were formed.

As previously discussed, according to the literature the diazonium salt method of electrode modification relies on the addition of an electron to remove the dinitrogen group and form a radical in the position of the leaving group. It was also previously

mentioned that the position of the leaving group impacted the thickness of the layers formed from diazonium salts, with layers formed from 3-aminopyridine being compact and thick, whilst layers formed from 2-aminopyridine were sparse and thick, and layers formed from 4-aminopyridine were thin but compact. Hartig *et al.* reported on the effect of diazonium surface dipole effects during electrodeposition onto silicon surfaces.[140] In their work, Hartig *et al.* described how the orientation and strength of the dipole moment was correlated to the grafting rate of the radicals. Largely, radicals with stronger dipole moments (such that the dangling bond of the radical is less negatively charged) grafted more quickly to the electrode surface.

Table 22, below, summarises the main characteristics of the electrodes modified from trifluoroacetylpyridinium, trifluoroacetyl-2-iodopyridinium, trifluoroacetyl-2-bromo-4-methylpyridinium, trifluoroacetyl-4-dimethylaminopyridinium and trifluoroacetyl-3-bromopyridinium, in terms of rate of passivation and thickness of the layers. Entry 1 documents how many cyclic voltammograms were conducted before no reduction peaks were seen for the pyridinium salts (taken from Chapter Four). Entry 2 lists the theoretical number of layers formed from the calculations made previously (taken from Chapter Five, Table 17). Entry 3 documents the ratio of $C_{graphite}$:$C_{pyridine}$ taken from XPS data (taken from Chapter Four, Table 7).

		TFA-pyridinium	TFA-2-iodopyridinium	TFA-2-bromo-4methyl-pyridinium	TFA-4-DMAP	TFA-3-bromopyrdinium
1	Passivation	3 CV	1 CV	1 CV	3 CV	7 CV
2	Theoretical number of layers (CV)	6.0	1.1	1.1	2.7	3.7
3	$C_{graphite}$:$C_{pyridine}$	50:30	60:20	60:20	50:20	60:20

Table 22: Summary of the main characteristics of the films formed from the five trifluoroacetylpyridinium salts discussed in Chapters Four and Five.

Reviewing the results in Table 22, we see that films formed from trifluoroacetyl-2-iodopyridinium and trifluoroacetyl-2-bromo-4-methylpyridinium form the thinnest films at the fastest rate. The films formed from trifluoroacetylpyridinium and trifluoroacetyl-4-dimethylaminopyridinium form thicker films at a slower rate. Films formed from trifluoroacetyl-3-bromopyridinium form thin films at a slow rate. It is proposed here that the rate and thickness of film formation are influenced by the position of the leaving group on the pyridinium ring. There are two reasons why the position of the leaving group could affect the rate or the thickness of the film. Firstly, the rate at which the film was formed will be influenced by the rate at which the pyridinium radical was produced. Thus, if some substituted positions are easier to cleave then radical formation, and film formation, would be faster for those pyridinium salts.

Secondly, the thickness of the films would have been influenced by the charge density of the films on the modified electrodes, as formation of the film stopped once the free pyridinium ions in solution were repelled from the surface. Therefore, if a densely packed film was formed, the charge density of the pyridinium cations per layer would have been high and film formation would stop after a few layers were formed. If a loosely packed film was formed, the charge density of the pyridinium cations per layer would be low, and so, multiple layers would form before the free pyridinium ions were repelled from the modified electrode surface. The density of the layers would depend on the steric hindrance and surface area of the bound trifluoroacetylpyridinium. This would also have been influenced by the substituent position, as the radical would have formed where the substituent was cleaved, and subsequently bound to the electrode at this position. On this basis, we propose the following:

- For the pyridinium salts with substituents on the 2-position (trifluoroacetyl-2-iodopyridinium and trifluoroacetyl-2-bromo-4-methylpyridinium) the substituent was easily cleaved to form a radical at the 2-position at a fast rate. This radical then bonded to the electrode surface to form a densely packed (near) monolayer film. The reasoning behind this is that the cyclic voltammograms (Chapter Four, Figures 10 and 11) and chronoamperograms (Chapter Four, Figure 15) showed rapid passivation of the electrode surface, evidencing that the modified electrode

surface became positively charged very quickly. The XPS (Chapter Four, Table 7) and ferrocyanide experiments (Chapter Five, Figure 26) evidence that a thin, non-porous film was formed, due to the high amount of graphite-carbon shown and the fact that no ferrocyanide adsorption was seen.

- For the pyridinium salts with substituents on the 4-position (trifluoroacetyl-4-dimethylaminopyridinium) the substituent was cleaved at a slower rate to form a radical at the 4-position. The radical then bonded with the electrode surface, and gradually a porous multilayer film was formed on the electrode surface. The reasoning for this is that the cyclic voltammograms (Chapter Four, Figure 12) showed that it took 3 scans for the electrode surface to be fully passivated. The chronoamperogram (Chapter Four, Figure 15) also showed that the passivation of the electrode was not as rapid as with the pyridinium salts substituted at the 2-position, and a diffusion controlled current was maintained. The XPS results showed that less of the graphite-carbon and more of the pyridine-carbon was discovered on the modified electrode surface, and a relatively moderate amount of ferrocyanide adsorption was seen (Chapter Five, Figure 26). Altogether, this shows that a thick porous film was formed somewhat slowly.

- For the pyridinium salts with substituents on the 3-position (trifluoroacetyl-3-bromopyridinium) the substituent was cleaved to form a radical at the 3-position at a very slow rate. The radical bonded with the electrode to gradually form a densely packed (near) monolayer film at the electrode surface. This was evidenced through the many cyclic voltammograms it took to passivate the electrode surface (Chapter Four, Figure 13), and the thin layer evidenced through XPS (Chapter Four, Table 7) and the ferrocyanide adsorption experiments (Chapter Five, Figure 26).

The bonding of the substituted pyridinium salts is illustrated below, in Figure 39.

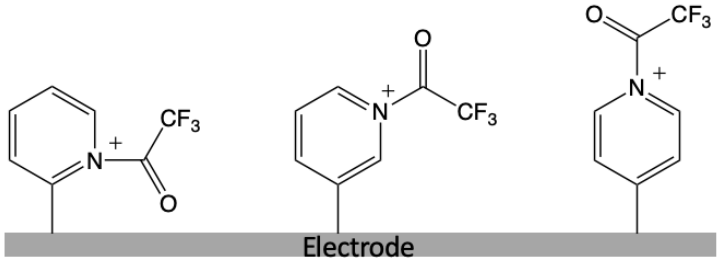

Trifluoroacetylpyridinium salts substituted at the 2-positon form thin layers at a fast rate.

Trifluoroacetylpyridinium salts substituted at the 3-positon form thin layers at a very slow rate.

Trifluoroacetylpyridinium salts substituted at the 4-positon form thick layers at a moderate rate.

Figure 39: Illustration of how the substituted trifluoroacetylpyridinium salts bond to the electrode surface.

For the substituted pyridinium salts there is a lot of evidence in the literature to help inform us when considering the mechanism for the formation of the pyridinium radical. For the unsubstituted trifluoroacetylpyridinium salt, there is far less support from the literature when it comes to considering a mechanism. From the experimental results gathered, it was seen that electrodes modified from trifluoroacetylpyridinium formed thick, porous layers moderately quickly. This is not dissimilar to the characteristics of the electrodes modified from trifluoroacetyl-4-dimethylaminopyridinium, which means that the radical may have been formed at the 4-position.

5.7 Theory for the Formation of Multilayer Films

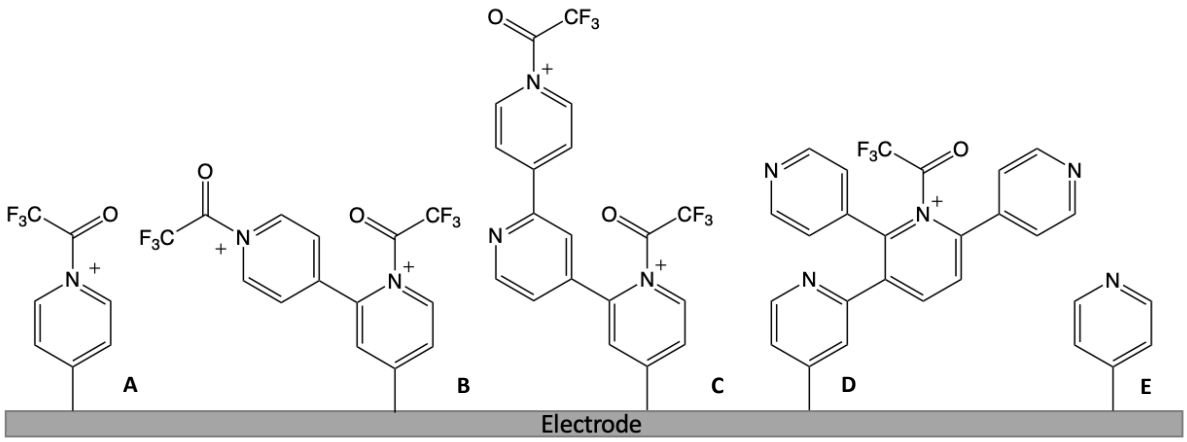

Figure 40: Illustration which shows a proposed idea of how multilayers could form on the electrode surface from the reduction of trifluoroacetylpyridinium or trifluoroacetyl-4-dimethylaminopyridinium.

From the calculations discussed earlier (Table 17) we know that the trifluoroacetylpyridinium and trifluoroacetyl-4-dimethylaminopyridinium salts were the only ones to form multilayers (calculated to be 3 and 1.25 layers, respectively). This was also confirmed from our investigations with ferrocyanide, where the films formed from trifluoroacetylpyridinium and trifluoroacetyl-4-dimethylaminopyridinium were the only ones thick enough to absorb the ferrocyanide into the film. We have therefore only considered these salts when proposing what a multilayer film may look like, which can be seen in Figure 40.

We also know that the electrodes modified from trifluoroacetylpyridinium and trifluoroacetyl-4-dimethylaminopyridinium contained films made up of a roughly 50:50 ratio of N^+:N (XPS results, Table 8, Chapter 4). It was concluded that the neutral pyridine was likely caused by further electron transfer which reduced the N^+-$COCF_3$ bond, forming grafted, neutral pyridine and a trifluoroacetyl radical (Scheme 14, Chapter 4).

With all this in mind, we propose the following theory for the formation of a multilayer film. First, the pyridinium salt would graft to the electrode at the 4-position as seen in Figure 40 A. The trifluoroacetyl-4-dimethylaminopyridinium salt would graft at this position as cleaving the dimethylamino group would create a radical at the 4-position that could form a bond with the electrode surface. As discussed previously, it was thought that the trifluoroacetylpyridinium salt would also form a radical at the 4-position, as we know films formed from this salt are thick and porous - like those formed from trifluoroacetyl-4-dimethylaminopyridinium and unlike the thin dense films formed from trifluoroacetyl-2-iodopyridinium, trifluoroacetyl-2-bromo-4-methylpyridinium or trifluoroacetyl-3-bromopyridinium.

Once the trifluoroacetylpyridinium had grafted it could either be reduced to form a single grafted pyridine molecule (Figure 40 E) or it could be subject to further attack from another trifluoroacetylpyridinium radical (Figure 40 B), creating the second layer to the film. The neutral pyridine could also be subject to attack from the trifluoroacetylpyridinium radical, forming a bond such as that seen in Figure 40 D. As

the formation of the film was fast and most likely random due to the nature of radical reactions it is difficult to say with accuracy, precisely how the multilayer was formed. However, we believe it was probably made up of clusters of chains such as those in Figure 40 C and D and that overall these clusters would average out to give a total surface coverage with a 50:50 ratio of $N^{+}N$ and an average number of layers of 3 or 1.25 layers for the films formed from trifluoroacetylpyridinium and trifluoroacetyl-4-dimethylaminopyridinium

5.8 Conclusions

The findings presented in this chapter have demonstrated the different characteristics of the electrodes modified from trifluoroacetylpyridinium salts. The redox probes used demonstrated that the positively charged films on the modified electrode surfaces repel positively charged ions and adsorb negatively charged ions, if the films are thick/porous. It was established that films formed from trifluoroacetyl-2-iodopyridinium, trifluoroacetyl-3-bromopyridinium and trifluoroacetyl-2-bromo-4-methylpyridinium formed thin and densely packed films. Whereas films formed from trifluoroacetylpyridinium and trifluoroacetyl-4-dimethylaminopyridinium form thicker, porous films.

The positive charge on the surface of the pyridine films was due to the surface-bound trifluoroacetylpyridinium or neutral pyridine that had been protonated. This positive charge caused the strong adsorption of ferrocyanide into the films formed from trifluoroacetylpyridinium. It was observed that the adsorption of ferrocyanide was proportional to the thickness of the film on the electrode surface. The redox response of ferrocyanide was also used to investigate the effect of pH on the modified electrodes. Through this, it was seen that acidic pH protonated the surface-bound neutral pyridine present in the films which increased the amount of ferrocyanide attracted to the surface. Basic pH removed the trifluoroacetylpyridinium group from the surface-bound trifluoroacetylpyridinium and de-protonated the protonated pyridinium which decreased the amount of ferrocyanide adsorbed into the film. This effect of removing the positive charge on the film and then reinstalling it via protonation

could be controlled which may be a beneficial characteristic if the films were to be used for sensing of certain ions.

Chapter Six – Electrosynthetic Oxytrifluoromethylation of Styrene

6.1 Motivation for this work

The work discussed in this chapter covers the main goal of this PhD thesis, to develop an electrosynthetic trifluoromethylation reaction. We knew from the start of this project that we wanted to use a new, cheaper $CF_3^\bullet$ radical source than those previously reported. This led us to attempt to synthesise trifluoroacetylpyridinium salts, as discussed in Chapter Three. The use of these pyridinium salts provided an opportunity to explore the cathodic (reductive) generation of $CF_3^\bullet$ radicals which is far less reported than anodic (oxidative) generation. Both of these methods were discussed in detail in the introduction to this thesis, and a summary of the electrosynthetic trifluoromethylation reactions reported by other groups is given in Tables 23a and 23b. Here, the reagents, substrates, products, yield and electrosynthesis conditions used in each reaction are listed. These reactions were studied to help inform our decisions when designing our own electrosynthetic trifluoromethylation reaction.

Looking at the summarised reactions in Tables 23a and 23b it is obvious that the oxidation of Langlois Reagent under constant current methods in a single cell is the most popular electrosynthetic trifluoromethylation method. This is probably because it is much easier to perform oxidation reactions, as a proton donor can be reduced (to produce H_2) to balance the reaction at the cathode, whereas there is not an equivalent 'go to' reaction to balance the anode for reduction reactions. Constant current is often employed as it is an easier setup (doesn't require a reference electrode) and higher yields are often observed as any reaction will take place to maintain the set current. Using a single cell is also an easier setup as specialist glassware (H-cell) is not required. Even when Langlois Reagent wasn't employed, all of the reactions reported relied on cleaving the CF_3-S bond to produce a $CF_3^\bullet$ radical. This further demonstrates the novelty of using trifluoroacetylpyridinium salts for electrochemical trifluoromethylation. The cathodic reduction of a triflyltriethylammonium complex, reported by Cantillo *et al.* (entry 11, Table 23b), is the electrosynthetic reaction most closely related to our idea, which came out during our studies. However, in their work

they report how the triflyltriethylammonium complex is incredibly unstable and so they were unable to study the electrochemical behaviour of the complex and had to use incredibly high currents (-40 mA) to reduce it quickly before it decomposed. Therefore, we hope by using a cheaper, more stable $CF_3^{\bullet}$ radical source we will improve upon their method.

In this chapter, all of the reactions discussed were monitored via ^{19}F NMR (and occasionally ^{1}H NMR) to determine the progress of each reaction. When it appeared that all of the pyridinium salt had been reduced (due to the peak corresponding to the salt decreasing/disappearing) or no further reduction had taken place for more than an hour, the electrochemical cell was turned off. For all reactions, TFAA was used in excess to the pyridine (or other nucleophile) in a 1.5:1 ratio. This was to ensure all of the pyridine was converted to the pyridinium salt. All yields reported were calculated by ^{1}H integration of the crude mixture, using a NMR standard, unless stated otherwise.

	CF_3 Source and Molar Equivalents	Additional Reagents	Substrate	Product	Yield (%)	Electro-synthesis	Electron Equiv. (F mol^{-1})	Length of reaction (h)	Ref.
1	$Zn(SO_2CF_3)_2$ 1.4 eqv.	-	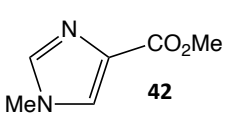 **42**	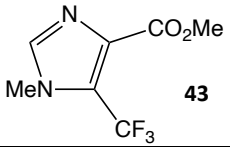 **43**	53%	Oxidation (25 mA) single cell	1.62	8	[51]
2	$Zn(SO_2CF_3)_2$ 2 eqv.	-	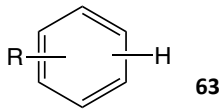 **63**	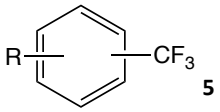 **5**	18-65	Oxidation (5 mA cm^{-2}) single cell	-	5-8	[141]
3	CF_3SO_2Na 2-3 eqv.	-	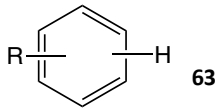 **63**	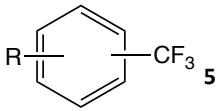 **5**	50-90	Oxidation (10 mA) single cell	-	5	[142]
4	CF_3SO_2Na 2 eqv.	-	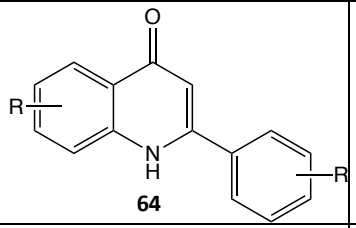 **64**	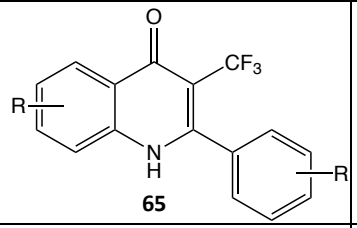 **65**	50-76	Oxidation (10 mA) single cell	-	6	[143]
5	CF_3SO_2Na 2 eqv.	$MgCl_2$	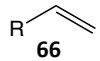 **66**	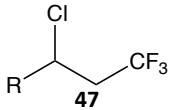 **47**	46-83	Oxidation (15 mA) single cell	-	4	[144]
6	CF_3SO_2Na 2 eqv.	MeOH	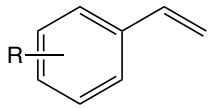 **67**	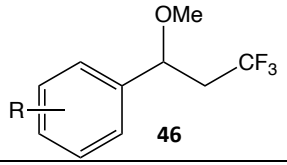 **46**	54-89	Oxidation (15 mA) single cell	-	3	[145]

Table 23a: Summary of electrochemical trifluoromethylation reactions reported by other groups.

	CF_3 Source and Molar Equivalents	Additional Reagents	Substrate	Product	Yield (%)	Electro-synthesis	Electron Equiv. (F mol^{-1})	Length of reaction (h)	Ref.
7	CF_3SO_2Na 1.6 eqv.	H_2O	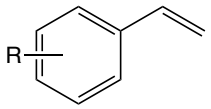 67	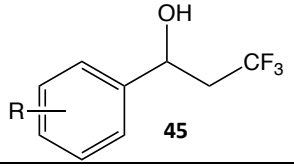 45	27-96	Oxidation (60 mA) single cell	2.5-3.2	-	52
8	CF_3SO_2Na 2 eqv.	AcOH	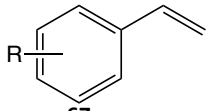 67	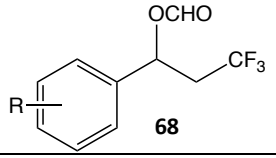 68	47-85	Oxidation (3 mA) single cell	9-17.9	24-28	146
9	CF_3SO_2Na 2 eqv.	-	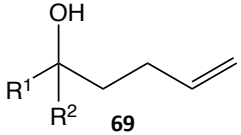 69	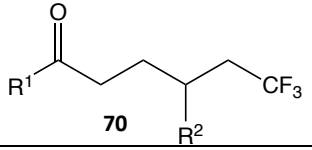 70	38-90	Oxidation (3 V) single cell	-	12	147
10	CF_3SO_2Na 1.2 eqv.	H_2O	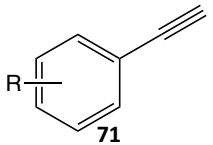 71	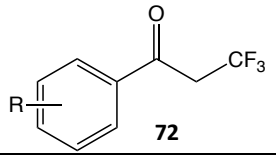 72	12-40	Oxidation (25 mA) single cell	2.2	-	148
11	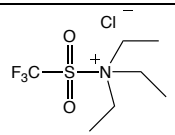 2.5 eqv.	-	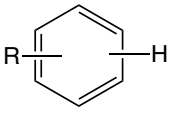 63	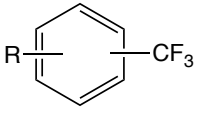 5	1-89	Reduction (10-40 mA) single cell	2-8	24	56

Table 23b: Summary of electrochemical trifluoromethylation reactions reported by other groups.

6.2 Cell Set-up

6.2.1 Divided Cell

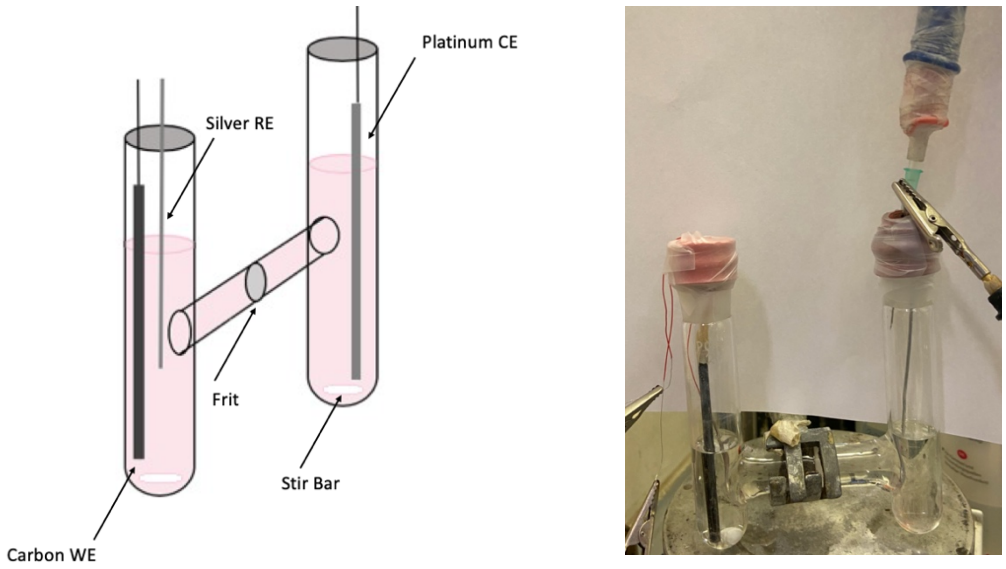

Figure 41: Left- illustration of a divided cell set up, with the carbon working electrode, silver reference electrode, platinum counter electrode, frit and stir bar annotated. Right – image of set-up in the lab.

A divided cell set up was initially chosen to perform the electrochemical synthesis reaction, despite how little it is used in the literature. This was selected because, at the beginning of the project, it was unknown what type of reaction would occur and what, if any, intermediates would be involved. It was therefore unknown how the intermediates or products may interact with the working electrode (WE) or the counter electrode (CE). For example, a species could be produced via reduction at the WE and then be converted into something else at the CE, and vice versa. Thus, to avoid confusion when there were so many unknowns, a divided cell was used so that the WE and CE were in separate compartments joined by a frit. The reference electrode (RE) was placed in the same compartment as the WE so that the potential of the WE could be controlled. Stir bars were also included in both compartments, to ensure fresh reactant was delivered to the electrodes. Dried, degassed MeCN was used and an inert argon atmosphere was maintained by attaching an argon balloon to the cell. These steps were taken because it was thought that if the pyridinium salt was exposed

to water it would decompose to pyridinium ($C_5H_5NH^+$) and trifluoroacetic acid (CF_3CO_2H).

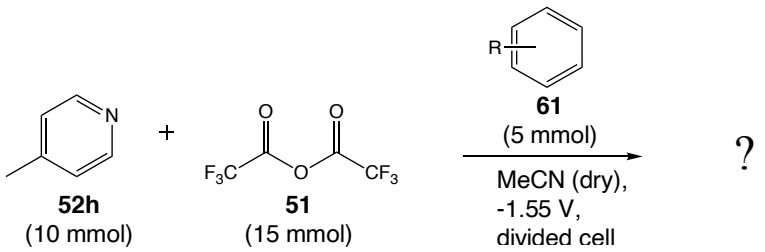

Scheme 17: Reaction of trifluoroacetyl-4-methylpyridinium with different aromatic substrates.

	Electrolyte	Substrate	**Yield (%)**
1	$LiClO_4$	Benzene	**0**
2	$LiClO_4$	Naphthalene	**0**
3	$LiClO_4$	Styrene	**0**
4	$TBAPF_6$	Benzene	**0**
5	$TBAPF_6$	Naphthalene	**0**
6	$TBAPF_6$	Styrene	**0**

Table 24: Yield of reaction when varying synthesis conditions were used along with: trifluoroacetyl-4-methylpyridinium (10 mmol), platinum CE, carbon WE, silver RE, in dry degassed MeCN and an inert atmosphere and constant potential electrosynthesis (-1.55 V).

Table 24 details the initial results when using a divided cell. For these reactions 4-methylpyridine was chosen as the nucleophile to react with TFAA, to avoid using a pyridinium salt that would form a film on the electrode surface upon reduction (as detailed in Chapter Four). The electrosynthesis was carried out using constant potential, despite this method being used so little in the literature. The choice to carry out the reaction using constant potential was again influenced by how many unknowns there were at the time. It was therefore thought best to carry out the reaction at a potential where only the trifluoroacetyl-4-methylpyridinium salt would be reduced, rather than allow the electrode to be held at a potential where unknown reactions could occur. Aromatic substrates were chosen in the hope that the $CF_3^\bullet$ radical would attack the π-system to eliminate a hydrogen atom and reform the double bond, or to form a new di-substituted product, as seen in the literature examples in Tables 23a and 23b.

From the results reported in Table 24 it is obvious that this set of reactions were not successful. There are many possible reasons why this might be. Very low currents were observed for all the syntheses performed, which suggests that the resistance in the cell was very high and the rate of reaction was slow. After 24 hr of constant potential, only a small amount of the trifluoroacetyl-4-methylpyridinium salt appeared to have been consumed (from ^{19}F NMR analysis) and no obvious fluorine-containing products had formed. This supports the theory that the rate of electron transfer between the WE and the trifluoroacetyl-4-methylpyridinium salt was very slow. After 36 hr of constant potential, there was no evidence that a new product had formed according to the ^{19}F and ^{1}H NMR and a large amount of unreacted pyridinium salt remained in solution.

Two types of electrolytes were used, lithium perchlorate ($LiClO_4$) and tetrabutylammonium hexafluorophosphate ($TBAPF_6$). At first, $LiClO_4$ was chosen as this allowed for small amounts of the reaction solution to be sampled and used for NMR analysis, to observe the reaction progression. As $LiClO_4$ has no carbon/hydrogen/fluorine environments the NMR spectrum could be analysed without dominating peaks from the electrolyte, which was in much higher concentration than the substrate. Baran *et al.* recently reported the influence of $LiClO_4$ on an electrosynthetic oxidation reaction, whereby the yield was diminished when $LiClO_4$ was used due to the chelation of the lithium ion to quinuclidine which was used as a mediator.[149] Therefore, the electrolyte was changed from $LiClO_4$ to $TBAPF_6$ to determine if this change in electrolyte would promote the formation of a fluorinated product, however this was not the case. After this change in electrolyte bore no success, attention was then turned to the solvent. It was found that when the solvent was not dried, nor degassed the oxytrifluoromethylation of styrene occurred to produce 3,3,3-trifluoro-1-phenylpropan-1-one (**70a**), at a 6% yield. Characterisation of **70a** was obtained through NMR, IR and mass spectrometry (see Appendix D) which matched the reported data for 3,3,3-trifluoro-1-phenylpropan-1-one.[150]

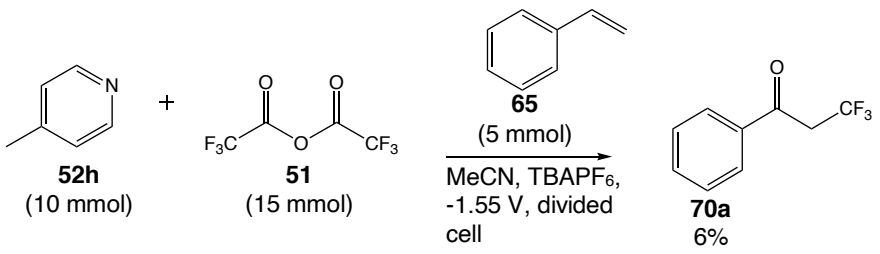

Scheme 18: Reaction of trifluoroacetyl-4-methylpyridinium with styrene at constant potential (-1.5 V) to form 3,3,3-trifluoro-1-phenylpropan-1-one.

At this point, it was extremely promising to have made a trifluoromethylated product via electrochemical synthesis. The effect of including water and oxygen is explored in more detail further on in this chapter, for now we will discuss the efforts undertaken to improve the yield. Although a divided cell had initially been chosen as the preferred electrochemical cell, some impracticalities had come to light after implementing it. The frit separating the two compartments did not successfully contain the reactants as hoped. When styrene was only added to the WE compartment, small amounts of it leaked into the CE compartment by the end of the reaction. It was thought that the styrene diffused into the CE compartment to balance the concentration gradient between the two sides, so styrene was added to both compartments. However, this seemed wasteful as half the styrene was not used to make the desired product (no CF_3 products were observed in the CE compartment) and it was not clear if styrene would diffuse out of the CE compartment as the concentration of styrene decreased in the WE compartment. This made it difficult to calculate a precise yield of **70a** as it was unclear how much of the styrene had been available for reaction. Therefore, to make such calculations simpler a single cell was considered.

6.2.2 Single Cell

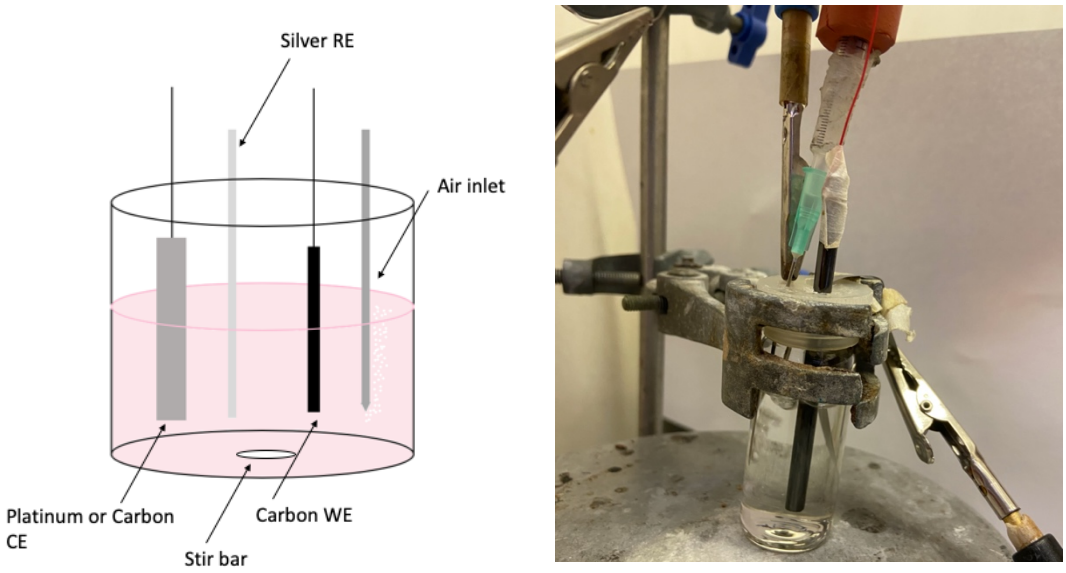

Figure 42: Left - illustration of a single cell set up, with the carbon working electrode, silver reference electrode, platinum counter electrode and stir bar annotated. Right – image of the set-up used in the lab.

	Electrolyte	CE	**Yield 70a (%)**
1	$LiClO_4$	Platinum	**0**
2	$LiClO_4$	Carbon	**0**
3	$TBAPF_6$	Platinum	**0**
4	$TBAPF_6$	Carbon	**0**

Table 25: Yield of reaction when varying synthesis conditions were used along with: trifluoroacetylpyridinium-4-methylpyridine (10 mmol), styrene (5 mmol), carbon WE, silver RE, in dry degassed MeCN and an inert atmosphere, with constant potential electrosynthesis.

Figure 42 illustrates the single cell set-up used, whilst Table 25 documents the results from these reactions. Despite exactly replicating the conditions (solvent, electrolyte, ratio of pyridinium salt to styrene etc.) used previously for the divided cell, changing to the single cell completely diminished the yield of **70a**, and no other trifluoromethylated products were seen. The electrolyte and material of the counter electrode were altered to see if this would affect the success of the reaction, but to no avail. Cyclic voltammetry was used to investigate the reaction solutions to see if there were any oxidation or reduction processes taking place that had previously been overlooked

(Figure 43). Carbon and platinum were each used as the WE to investigate if any oxidation processes were happening when they were used as the CE. The cyclic voltammograms show the reduction of the pyridinium salt when a carbon WE was used (-1.98 V) and when a platinum WE was used (-1.20 V). The difference in current between the two peaks was due to differing electrode areas of the carbon and platinum WE. When the platinum WE was used slight oxidation of the MeCN occurred at 1.30 V. However, it was unlikely that the oxidation of the solvent occurred during synthesis as there was no evidence of an MeCN-oxidation product in the crude reaction mixture. Despite not seeing an obvious oxidation process that would take place at the counter electrode in the cyclic voltammograms, it was acknowledged that one must have taken place to balance the cell. We therefore decided to use a sacrificial anode as the CE, which would provide a known oxidation reaction to balance the electrochemical cell.

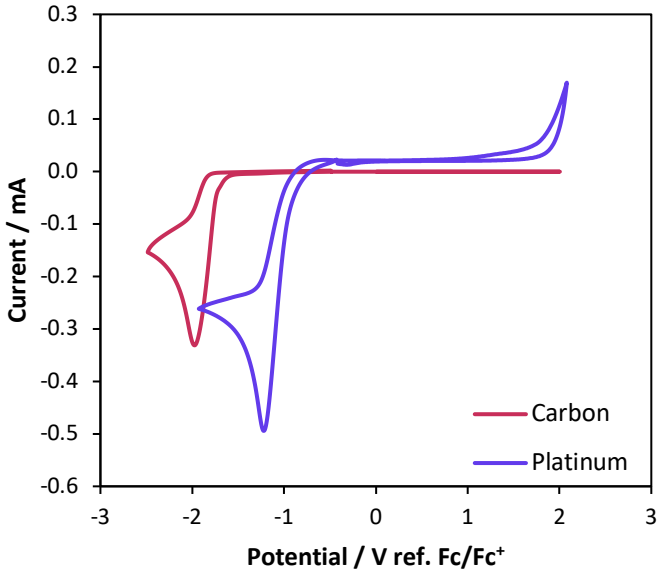

Figure 43: Cyclic voltammograms of the reaction solution using trifluoroacetylpyridinium salt (10 mM), styrene (5 mM), $TBAPF_6$ (0.1 M) in dry MeCN with platinum CE, silver RE. Two working electrodes were used: carbon (red) and platinum (blue). Reported potentials were referenced to ferrocene.

6.2.3 Sacrificial Anode

A sacrificial anode is a positively charged electrode which is partially consumed during electrosynthesis.[151] Typically, sacrificial anodes are made of metal, such as aluminium,[152] zinc,[153] or silver.[154] When a sacrificial metal anode is used as the counter electrode in a cathodic reaction, it is oxidised to liberate a metal cation and this reaction balances the electrochemical cell.[50] Thus, electron transfer between the anode and a species in solution can largely be avoided.

	Sacrificial Anode	Standard Electrode Potential / V	**Yield 70a (%)**
1	Aluminium	-1.66	**4**
2	Zinc	-0.76	**6**
3	Nickel	-0.25	**12**

Table 26: Yield of reaction when varying synthesis conditions were used along with: trifluroroacetyl-4-methylpyridinium (10 mmol), styrene (5 mmol), $TBAPF_6$ (0.1 M), carbon WE, silver RE, in dry degassed MeCN and an inert atmosphere, with constant potential electrosynthesis. The standard electrode potentials listed are in refence to the standard hydrogen electrode.[155]

A summary of the yields of **70a** when using sacrificial anodes is seen in Table 26. It is clear from these results that using a sacrificial anode increased the yield of **70a** as compared to when non-sacrificial anodes were used (Table 25). It was also apparent that the yield was significantly higher when a nickel (Ni) electrode was used instead of aluminium (Al) or zinc (Zn). This could possibly be due to the standard electrode potential of the metals, which are also listed in Table 26. It's seen here that nickel has the lowest standard electrode potential, meaning that it was more easily oxidised. Thus, if Ni^{2+} ions were liberated more easily than Zn^{2+}or Al^{3+} ions, it is possible that that the oxidation of the nickel anode was the dominant reaction taking place. Whereas, with the electrodes that were less easily oxidised, species in solution may have also been oxidised to balance the cell instead.

The reactions were monitored via ^{19}F NMR and it was observed that the rate of consumption of the trifluoroacetyl-4-methylpyridinium salt was still very slow. At this point, a new pyridinium salt was considered. Originally pyridinium salts that coated the WE were avoided; however, it was thought that the presence of a stir bar would provide a sufficient movement of reactants in the solution such that the pyridinium radicals formed would not stay at the electrode surface long enough to coat the electrode. Therefore, trifluoroacetylpyridinium was chosen to replace the trifluoroacetyl-4-methylpyridinium salt. This proved to have a great effect on the yield of **70a**, increasing it to 45%. All further reactions discussed will use this trifluoroacetylpyridinium salt.

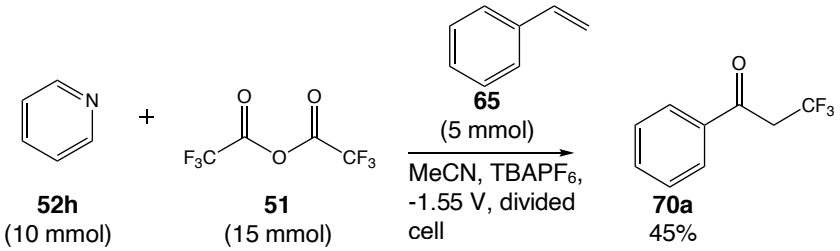

Scheme 19: Reaction of trifluoroacetylpyridinium with styrene at constant potential (-1.5 V) to form 3,3,3-trifluoro-1-phenylpropan-1-one.

6.2.4 IKA Electrasyn

One of the main barriers stopping organic chemists from adopting electrochemistry as an everyday technique is the expensive equipment needed as well as the (commonly perceived) difficult set-up required. Therefore, Baran *et al.* (one of the main research groups promoting the widespread uptake of electrosynthesis) in conjunction with IKA have designed an easy-to-use electrochemical cell called the IKA Electrasyn. The Electrasyn is roughly the same cost as a heating/stir plate and takes up a similar amount of space, which makes it easy to store in an organic lab as compared to bulky potentiostats. The single cell can be screwed into a holder in which the electrodes are placed. The electrodes used are also bought from IKA and are always the same shape and size, independent of the material used. This helps to ensure continuity of reaction conditions as the electrode area and the distance they are held apart are always the same. Replicating this with 'homemade' electrochemical cells can be difficult, as even

though great care can be taken to keep reaction conditions the same in one lab, if another group in a different laboratory tried to replicate your reaction conditions they may struggle to reproduce the exact same cell shape/size and electrodes used. However, this simplification of the set-up means some aspects of the traditional electrochemical cell have been lost. For example, no reference electrode is supplied – this must be bought separately and constant potential electrosynthesis, and cyclic voltammograms can be run without one. This calls into question the accuracy of any potentials reported using the IKA Electrasyn. The electrosynthetic reactions are pre-programmed so you can enter the potential, current, length of reaction and amount of charge passed but that is all. With a potentiostat built for electrochemical analysis far more features can be controlled for example, a maximum current can be set for a constant potential reaction. Despite these limitations, the IKA Electrasyn has proved popular and successful among organic chemists who are interested in using electrosynthesis.

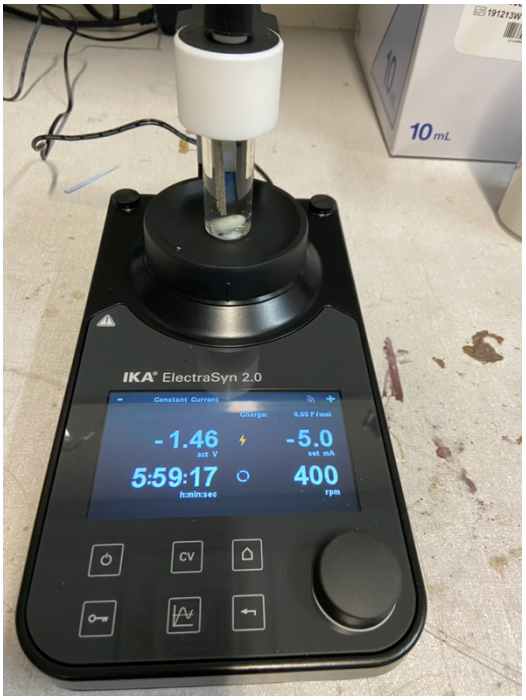

Figure 44: Image of an IKA Electrasyn set up for a constant current electrosynthetic oxytrifluoromethylation reaction of styrene using trifluoroacetylpyridinium.

Towards the end of this project, the Chemistry Department at UCL purchased an IKA Electrasyn, which we used to perform the oxytrifluoromethylation of styrene with the hope that this 'professional' cell might improve the yield. Unfortunately, the yields of **70a** produced with the Electrasyn were similar to what had previously been obtained with the homemade cell (Table 27). The current observed and the amount of charge passed overall was also in line with what had been seen in the homemade cell. Although it was disappointing that the yield had not improved, it also showed that the cell we had designed was working efficiently. For clarity, only the yield in entry 2 of Table 27 was from a reaction using the Electrasyn, all other yields reported in this thesis are from 'homemade' cells.

	Cell	**Yield 70a (%)**
1	Homemade	**45**
2	Electrasyn	**41**

Table 27: Yield of reaction when a homemade electrochemical cell was used, and when the IKA Electrasyn was used. Both constant current and constant potential electrosynthetic methods were used. All reactions were performed in 15 ml dry MeCN, with 0.1 M $TBAPF_6$, 10 mmol trifluoroacetylpyridinium salt, 1 mmol styrene, carbon WE, nickel CE. Reactions in the homemade cell were performed with a silver RE.

6.3 Effect of Water and Oxygen

The breakthrough of discovering that the formation of **70a** was possible came when the MeCN was neither dried nor degassed, however it was not clear if the formation of **70a** was due to the presence of water or oxygen, or even a combination of both of them. Specifically, we were unsure where the oxygen in the ketone bond of **70a** originated from. Therefore, a series of reactions were conducted to observe the effects of including water and oxygen in the solvent and what influence this had on the formation of **70a**.

		Yield (%)			
		Air Atmosphere		Argon Atmosphere	
		-0.96 V	-1.55 V	-0.96 V	-1.55 V
1	Wet MeCN	**19**	**37**	**12**	**15**
2	Dry MeCN	**43**	**44**	**24**	**35**

Table 28: Yield of reaction when varying synthesis conditions (wet solvent/dry solvent/air atmosphere/argon atmosphere) were used along with: pyridine and TFAA (15 equivalents), with styrene (1 equivalent), $TBAPF_6$ electrolyte, carbon WE, nickel CE, silver RE with constant potential electrosynthesis.

To determine the effect of oxygen and water (together and separately) on the yield of **70a** the reaction was performed under air or argon atmospheres with dry or wet MeCN, the results of which can be seen in Table 28. Here, 'wet' refers to when the solvent was used straight from the bottle without being dried (i.e. no added water). It is clear that when the MeCN was wet (entry 1) the yields of **70a** were diminished as compared to when it was dried (entry 2). The presence of water causing a lower yield could be evidence that the oxygen in the ketone bond of **70a** did not originate from water, as it would be expected that the presence of water would increase the yield if it was involved in the synthesis. However, this is not conclusive as it could also be possible that a very small amount of water is needed to produce the product but too much water would hydrolyse the salt. A more precise experiment would be to include an exact amount (equal to the mmol of styrene used) of water-^{18}O ($H_2{}^{18}O$) in the reaction solution. Then, if the oxygen in the ketone bond did originate from water this could be identified via ^{18}O NMR and mass spectrometry.

The potential of the WE was held at two different values, -0.96 V (ref Ag wire) which corresponded to the reduction potential of oxygen and -1.55 V (ref Ag wire) which corresponded to the reduction of trifluoroacetylpyridinium. It was discussed in Chapter Four that oxygen acted as a redox mediator between the carbon WE and trifluoroacetylpyridinium. Thus, it was thought that if the potential was held at -0.96 V oxygen would act as a redox mediator again and we could observe what effect this

had on the yield. From the yields reported, it would appear that the reaction was more successful when the potential was held at -1.55 V rather than -0.96 V. This was probably because the concentration of pyridinium salt in the solution was far higher than the concentration of oxygen dissolved in the solution. Consequently, electron transfer from the electrode to the trifluoroacetylpyridinium was more efficient than electron transfer between the oxygen and trifluoroacetylpyridinium.

If the ketone oxygen in **70a** did not originate from water, the next logical explanation would be that it came from atmospheric oxygen dissolved in the solvent. It was therefore surprising that the yield of **70a** only decreased slightly when the reaction was run in dry, degassed MeCN, at -1.55 V in an argon atmosphere (35%, Table 28); as compared to the same conditions in an air atmosphere with air bubbling through the solution (44%, Table 28) . The only other source of oxygen in the reaction solution was the trifluoroacetate ion. Therefore, excess trifluoroacetate was added to the reaction solution to see if this increased the yield, however this was not the case and the excess trifluoroacetate did not appear to have any effect on the yield. This was not surprising as it was difficult to conceive exactly how the trifluoroacetate ion would donate an oxygen molecule to the styrene substrate. On this basis, it is most likely that atmospheric oxygen was the source of the ketone oxygen and still managed to dissolve into the solution when an argon atmosphere was present, (at a decreased concentration) leading to a slightly smaller yield of **70a**. Again, a more certain way to determine if atmospheric oxygen was involved in the synthesis of **70a** would be to dissolve $^{18}O_2$ into the reaction solution and see if it is detected in the product via ^{18}O NMR and mass spectrometry. However, a cylinder of $^{18}O_2$ is also extremely expensive and had delivery times of over a year when we looked into ordering it, which meant it was not a viable option.

6.4 Optimising the Reaction Conditions

6.4.1 Varying the Concentrations of the Reaction Solution

Looking at the ratio of $CF_3^\bullet$ radical source to substrate in the literature examples (Tables 23a and 23b) we saw that for most reactions, twice as much $CF_3^\bullet$ radical source to substrate was used. In this section, the concentrations of TFAA, pyridine and styrene were altered to investigate what effect this had on the yield.

	TFAA (mmol)	Pyridine (mmol)	Styrene (mmol)	Length of Reaction (h)	Charge Passed (C)	Equivalent Electrons (mmol)	**Yield (%)**
1	4.5	3	1.5	8	545	5.6	**18**
2	7.5	5	3	6	572	5.9	**7**
3	7.5	5	1.5	6	250	2.6	**24**
4	7.5	5	0.5	6	268	2.8	**25**
5	15	10	1	2.5	185	1.9	**39**
6	30	20	1	5.5	1409	14.6	**51**

Table 29: Yield of reaction when different concentrations of trifluoroacetylpyridinium salt and styrene were used. Reactions were carried out in a single cell, 15 ml MeCN, 0.1 M $TBAPF_6$, carbon WE, nickel CE, silver RE, with air bubbled through the reaction, constant potential (-1.55 V).

For two of the reactions 1.5 mmol of styrene was used (entries 1 and 3). When the amount of the trifluoroacetylpyridinium salt was increased from 3 mmol to 5 mmol the yield of **70a** also increased from 18% to 24%. Similarly, when 1 mmol of styrene was used (entries 5 and 6) and the concentration of trifluoroacetylpyridinium was increased from 10 mmol to 20 mmol the yield increased from 39% to 51%. Thus, it can be concluded that increasing the concentration of the trifluoroacetylpyridinium salt also increased the yield of reaction. This was most likely due to the increase in concentration of $CF_3^\bullet$ radicals formed in solution, which increased the likelihood of the radical being trapped by the styrene. However, if 20 mmol of trifluoroacetylpyridinium salt was reduced to form 0.5 mmol of **70a** that meant a large number of radicals were reacting to form something else. It was speculated that the $CF_3^\bullet$ radicals that weren't

reacting with styrene may be extracting a hydrogen from the solution (from the MeCN solvent) to form CF_3H that was then leaving the solution as a gas, which is why no other CF_3 products were seen in the NMR.

Increasing the concentration of styrene did not have the same effect on the yield. Entries 2, 3 and 4 of Table 29 show the results of the reactions when 5 mmol of salt was used. For these reactions, when 0.5 mmol of styrene was used the yield was 25 % (entry 4). When the concentration of styrene was increased to 1.5 mmol the yield decreased ever so slightly to 24% (entry 3). When the concentration of styrene was increased further to 3 mmol the yield decreased even more to 7% (entry 2). A significant amount of unreacted styrene was recovered after all three reactions, evidencing that the majority of the styrene had not been involved in any side reactions. This was also proven by the fact that there were no detectable amounts of side products seen in the NMR spectra of the crude reaction mixture, or after workup.

Returning to the yields presented in Table 29, it seemed very wasteful that doubling the amount of trifluoroacetylpyridinium salt only led to a 12% increase in yield, especially when it was assumed that any $CF_3^\bullet$ radicals that weren't reacting with styrene were forming a toxic greenhouse gas, CF_3H. It was thought that having all of the $CF_3^\bullet$ radical source in the solution at the start of the reaction meant that we lost control over the rate at which the radicals were produced. That is, the $CF_3^\bullet$ radicals were being produced at the electrode faster than they were reacting with styrene, thus forming CF_3H instead. Therefore, it was thought that using the same overall amount of trifluoroacetylpyridinium spread out over multiple additions would slow down the rate of $CF_3^\bullet$ radical production so that more of the radicals would react with styrene to form **70a** rather than producing CF_3H. Table 30 shows the results of the reactions undertaken in which the trifluoroacetylpyridinium salt was added over multiple additions. For these reactions, TFAA and pyridine were pre-mixed immediately before being added to the reaction solution. The reactions were monitored via ^{19}F NMR every hour and an addition of the trifluoroacetylpyridinium salt would be added when it was apparent that the previous addition of trifluoroacetylpyridinium in the solution had been consumed.

The yields of **70a** presented in Table 30 show that adding smaller quantities of the trifluoroacetylpyridinium salt over multiple additions hindered the yield as compared to having all of the salt in the reaction solution from the start. For instance, when 25 mmol of the trifluoroacetylpyridinium salt was used over five 5 mmol additions, the yield was 45% (Table 30, entry 4). When 20 mmol of the salt was used in one addition at the start of the reaction the yield was 51% (Table 29, entry 6). Comparing the reactions presented in entries 1 and 2 of Table 30, the same amount of trifluoroacetylpyridinium salt was used overall, however, when three 5 mmol additions were made the yield was 30% and when six additions of 2.5 mmol were made the yield was 20%. It would appear that in our attempt to control the rate of $CF_3^{\bullet}$ radical production we actually made the rate of production too slow such that the concentration of $CF_3^{\bullet}$ radicals was too low and therefore fewer radicals were trapped by the styrene, which decreased the yield of **70a**.

	Total TFAA (mmol)	TFAA additions	Total Pyridine (mmol)	Pyridine additions	Length of Reaction (h)	Charge Passed (C)	Equivalent Electrons (mmol)	**Yield 70a (%)**
1	22.5	3 x 7.5 mmol	15	3 x 5 mmol	7	655	6.8	**30**
2	22.5	6 x 3.75 mmol	15	6 x 2.5 mmol	8	633	6.6	**20**
3	22.5	3 x 7.5 mmol	5	1 x 5 mmol	5	216	2.2	**2**
4	37.5	5 x 7.5 mmol	25	5 x 5 mmol	8	864	9.0	**45**

Table 30: Yield of reaction when multiple additions of TFAA and pyridine were made over the course of the reaction. Reactions were carried out in a single cell, 15 ml MeCN, 0.1 M $TBAPF_6$, 1 mmol styrene, carbon WE, nickel CE, silver RE, with air bubbled through the reaction, constant potential (-1.55 V).

Another way to reduce the excess amount of trifluoroacetylpyridinium salt used was to recycle the pyridine in solution. That is, if the trifluoroacetylpyridinium salt was

reduced to form the $CF_3^{\bullet}$ radical and carbon monoxide, then this would regenerate pyridine. Thus, if more TFAA was added to the reaction solution the trifluoroacetylpyridinium salt would be re-formed and available to act as a $CF_3^{\bullet}$ radical source. This would mean that a smaller amount of pyridine could be used in the reaction solution, reducing the amount of waste produced and make the reaction costs even cheaper. Entry 3 of Table 30 shows the results of the reaction when 5 mmol of the trifluoroacetylpyridinium salt was added at the beginning of the reaction, and then two further additions of TFAA were made, one by one. Unfortunately, this led to a very low yield of 2%. It was unclear exactly why such a small yield was achieved when trying to recycle the pyridine, but it could be because the extra additions of TFAA did not react with the pyridine under those reaction conditions and so the trifluoroacetylpyridinium salt was not formed.

6.4.2 Using Different Nucleophiles

Moving forward, other nucleophiles instead of pyridine were investigated to establish if other N^+-$COCF_3$ type motifs would act as a better $CF_3^{\bullet}$ radical source which would improve the yield of reaction. The cyclic voltammograms of each TFAA-nucleophile species can either be seen in Chapter Four or Appendix B.

	Nucleophile	Reduction Potential (V)	Length of Reaction (h)	Charge Passed (C)	Equivalent Electrons (mmol)	**Yield (%)**
1	Pyridine	-1.98	2.5	-185	1.9	**39**
2	4-methylpyridine	-2.02	6	-243	2.5	**14**
3	2,6-lutidine	-2.00	7	-234	2.4	**18**
4	DMAP	-2.29	6	-264	2.7	**19**
5	1-methylimidazole	-2.24	4	-277	2.9	**30**
6	1-methylpyrazole	-2.29	5	-293	3.0	**26**

Table 31: Yield of reaction when different nucleophiles (10 mmol) were used with TFAA (15 mmol). Reactions were carried out in a single cell, 15 ml MeCN, 0.1 M $TBAPF_6$, styrene (1 mmol), carbon WE, nickel CE, silver RE, with air bubbled through the reaction, constant potential. The potential of the WE was set at the reduction potential of each salt.

The different yields of **70a** when using various nucleophiles with TFAA can be seen in Table 31. Successful synthesis of **70a** was still achievable when using other nucleophiles, although the yields were not as high as compared to when pyridine was used. One possible explanation for this could be that the trifluoroacetylpyridinium salt was more reactive than the other N^+-$COCF_3$ species, which is evidenced through the shorter reaction time (2.5 h). Due to this shorter reaction time, the rate of $CF_3^\bullet$ radical production would have been faster, thus a higher concentration of $CF_3^\bullet$ radicals would have been available to be trapped by the styrene, hence the higher yield.

6.5 Substrate Scope and Mechanism

Finally, after analysis of the cell type, electrolyte, solvent, starting materials and electrode materials it was concluded, given the time constraints of the project, the optimal reaction conditions had been met. These were: single cell, $TBAPF_6$ electrolyte, dry MeCN, pyridine and TFAA (1:1.5 ratio) with carbon WE, nickel CE, silver RE. With these conditions, electrosynthetic oxytrifluoromethylation of a range of substituted styrenes was undertaken, the results of which can be seen below:

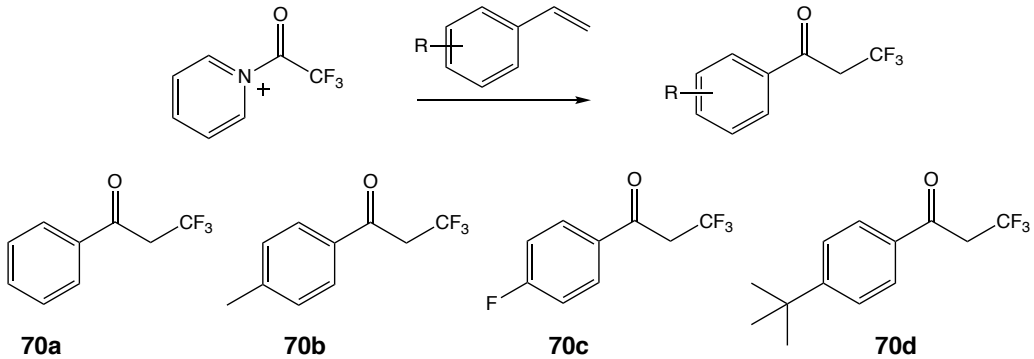

70a **45%** **70b** **20%** **70c** **37%** **70d** **30%**

Scheme 20: Synthesis of 3,3,3-trifluoro-1-phenylpropan-1-one, 3,3,3-trifluoro-1-(4-methylphenyl)propan-1-one*, 1-(4-fluorophenyl)-3,3,3-trifluoropropan-1-one, 1-(4-(tert-butyl)phenyl)-3,3,3-trifluoropropan-1-one.*

The identities of these products were confirmed via NMR, IR and mass spectrometry data that matched with those found in the literature.[150, 156, 157, 158] The yields reported here were from the isolated products, not from ^{1}H NMR integration. To help inform us of the mechanistic details of the oxytrifluoromethylation reaction the electrosynthesis was performed using TFAA alone, without pyridine. Using these reaction conditions resulted in no formation of **70a**, proving that the trifluoroacetylpyridinium salt is necessary for the reaction to proceed. A speculative mechanism of the electrosynthetic oxytrifluoromethylation is included below, which is similar to that reported by others when synthesising trifluorophenylpropanes.[157, 159, 160, 161]

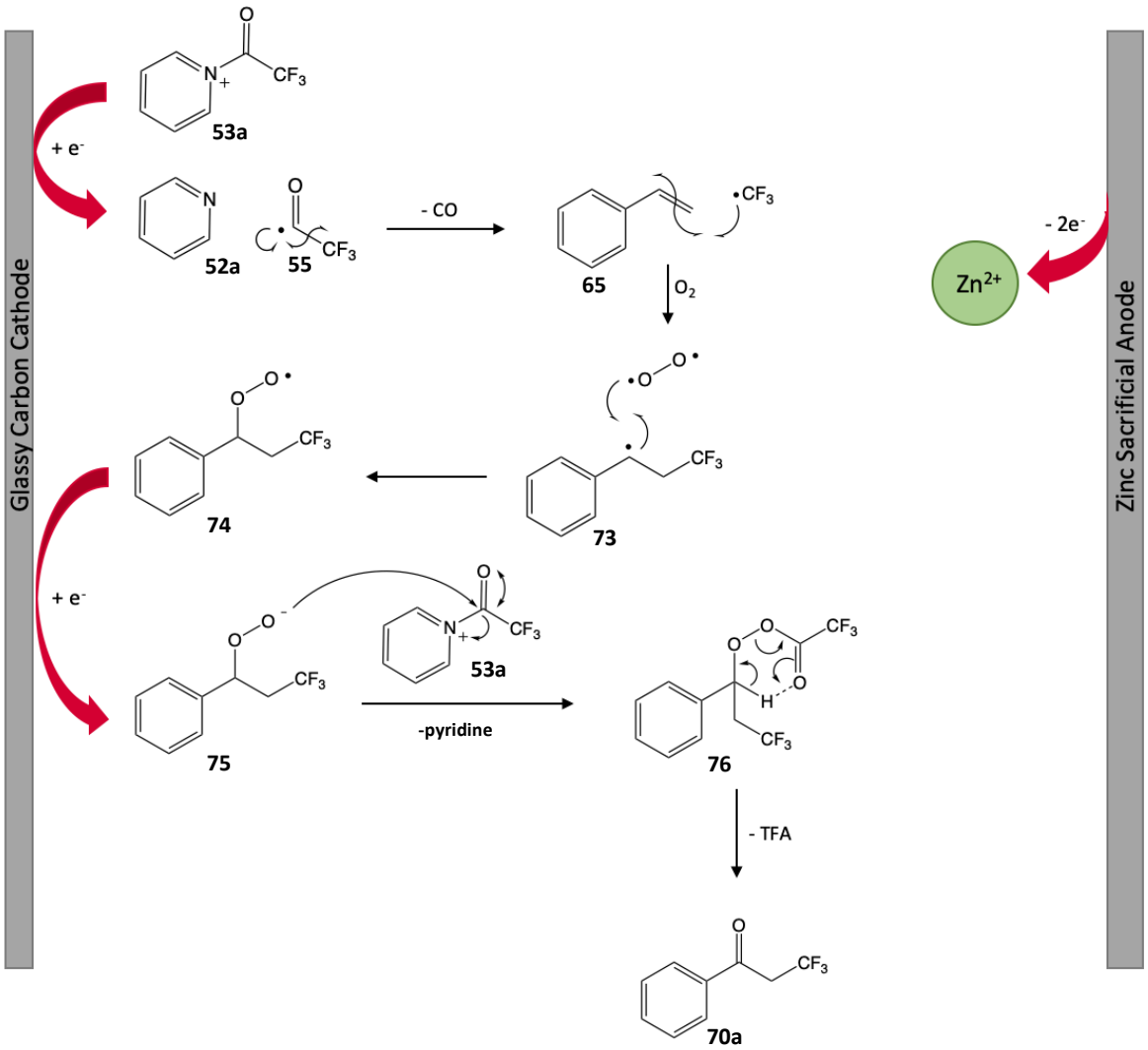

Scheme 21: Proposed mechanism for the electrosynthetic oxytrifluoromethylation of styrene.

It was believed that reduction of the trifluoroacetylpyridinium salt would result in the production of an acyl radical (**55**). As oxygen was present it is probable that it was also acting as a redox mediator (as discussed in Chapter Four) to reduce the trifluoroacetylpyridinium salt. However, as the potential was set to the reduction of the pyridinium salt and given the high concentration of the salt in solution it is likely that the majority of the electron transfer occurred between the electrode and the trifluoroacetylpyridinium salt, and so this part of the mechanism is not included. Once the acyl radical was formed it quickly decarbonylated to form carbon monoxide (which left as a gas) and a CF_3• radical. The CF_3• radical then went on to react with the terminal end of the styrene double bond, to form a new C-C bond and a β-radical (**73**). This radical then reacted with oxygen present in solution to form a peroxide group

(**74**), which underwent further reduction at the electrode surface to form an anion (**75**). This anion then reacted with trifluoroacetylpyridinium salt (**53a**) that remained in solution to form the peroxytrifluoroacetic acid **76**, which underwent a concerted elimination mechanism to form 3,3,3-trifluoro-1-phenylpropan-1-one (**70a**) and trifluoroacetic acid (TFA).[162]

6.6 Conclusions

The results presented in this chapter prove that trifluoroacetylpyridinium salts can be used for electrosynthetic reactions, making it one of the cheapest $CF_3^\bullet$ sources currently available. However, whilst the formation of a novel electrosynthetic reaction was promising there are a few areas that still need improvement. Although using trifluoroacetylpyridinium salts is an improvement on the use of traditional toxic metal reagents, the possible formation of CF_3H during the reaction somewhat negates the use of these cleaner conditions. Therefore, future work should focus on determining if CF_3H is produced during the reaction, and if so, making the reaction more efficient so the $CF_3^\bullet$ radicals only react with the substrate.

One possible way of doing this could be to reduce the volume of the electrochemical cell, as this would mean that a higher concentration of the reaction solution would be in contact with the WE. This may also mean that fewer equivalents of the trifluoroacetylpyridinium salt could be used. These efforts should also help to improve the yield of the oxytrifluoromethylated products, which is currently the main feature preventing this reaction from being a viable alternative to other radical trifluoromethylation reactions.

Chapter Seven – Conclusions and Future Work

7.1 Trifluoroacetylpyridinium Salts

We set out to create a cheap and simple electrosynthetic trifluoromethylation reaction that would improve upon current electrosynthetic and traditional methods. To do this, we wanted to use a cheaper and less toxic $CF_3^\bullet$ radical source than those previously used. In doing so, it was hoped that not only would we provide a superior method for trifluoromethylation, but also showcase the benefits of electrosynthesis to a hesitant organic chemistry community.

We predicted that trifluoroacetylpyridinium salts could be a prospective $CF_3^\bullet$ radical source that would fit our criteria, as they are synthesised from cheap and readily available starting materials (pyridine and TFAA). It was also hypothesised that the salts should be easily reduced, so that a simple electrosynthetic reaction should be achievable. NMR was used to characterise the products formed upon reaction of TFAA with different pyridines. From this it was clear that the TFAA and pyridine reacted to form a cationic pyridinium species, although a definitive structure could not be assigned. However, it was thought that the predicted pyridinium structure was the most likely product of the reaction of pyridine and TFAA given the data available. Future work should focus on assigning a conclusive structure of these salts. This could be achieved by using more characterisation techniques such as IR and Raman spectroscopy and variable temperature NMR.

7.2 Electrode Modification

The trifluoroacetylpyridinium salts were screened for their viability to perform in electrosynthetic reactions. Here, we were looking to see if the salts would undergo a single reduction process isolated from any other electron transfer processes. It was also important to try and understand the electrochemical behaviour of the salts to help eliminate the suggestion that electrosynthetic processes are a ‘black box’. Initial investigations showed that the trifluoroacetylpyridinium salts were promising

candidates for electrosynthesis as they underwent a single electron transfer process within the solvent window. Further investigations found that the substituents on the pyridine ring had a great effect over the electrochemical behaviour of the salts. Those trifluoroacetylpyridinium salts with electron withdrawing substituents formed a layer on the electrode surface upon reduction, whereas the salts that contained electron donating substituents did not. The formation of a layer on the electrode surface was initially identified via the passivation of the electrode (decreasing peak currents over consecutive cyclic voltammograms). XPS was then used to confirm the presence of these layers. It was proposed that the electrodes were passivated due to the fact that the layers formed were positively charged, due to the binding of the cationic trifluoroacetylpyridinium species to the electrode surface. Thus, as the film formed the positive charge at the electrode surface increased, which repelled the free trifluoroacetylpyridinium species in solution until none remained, meaning there were no redox active species present at the electrode.

The modified electrodes were then characterised using XPS, cyclic voltammetry, chronoamperometry and redox probes. It was found that layers formed from trifluoroacetyl-2-bromo-4-methylpyridinium and trifluoroacetyl-2-iodopyridinium formed thin, densely packed films that quickly passivated the electrode surfaces. Films formed from trifluoroacetyl-3-bromopyridinium formed thin, densely packed films that slowly passivated the electrode. Films formed from trifluoroacetylpyridinium and trifluoroacetyl-4-dimethyaminopyidinium formed thick, porous films that passivated the electrode surface at a ‘medium’ rate compared to the other salts.

The XPS studies revealed that the heteroatom substituents on the pyridine ring of these trifluoroacetylpyridinium salts were removed during the electrode modification process. It was therefore presumed that the substituents acted as leaving groups and the pyridinium species bound to the electrode at the ring position where the substituent had previously been, i.e. the trifluoroacetyl-2-iodopyridinium species bound to the electrode at the 2-position after the iodine had been cleaved. It was also shown that the difference in rate of passivation, thickness and porosity of the layers was influenced by the position of the substituents on the pyridine ring. The rate of

passivation of the electrode was controlled by how easily the radical was produced and how closely packed the trifluoroacetylpyridinium radicals could attach to the electrode surface. Thus, when the leaving groups were on the 2-position of the ring they were easily cleaved and the resulting trifluoroacetylpyridinium radicals could graft closely together. Hence why films formed from trifluoroacetyl-2-bromo-4-methylpyridinium and trifluoroacetyl-2-iodopyridinium formed densely packed layers quickly. When the leaving groups were at the 3-position they were less easily cleaved, but the resulting radicals could graft closely together. This was why films formed from trifluoroacetyl-3-bromopyridinium formed densely packed films slowly. When the leaving groups at the 4-position they were less easily cleaved than those at the 2-position but more easily cleaved than those at the 3-position. The resulting radicals could not graft closely together, thus films formed from trifluoroacetyl-4-dimethyaminopyidinium formed porous films at a 'medium' rate. The thickness of the films was determined by their porosity. Densely packed films would have a high concentration of positive charge meaning the electrode would be quickly passivated and film formation was stopped quickly, forming thin layers. Porous films would slowly build up a positive charge, meaning thick layers could gradually be formed.

The control of the amount of positive charge on the films was also investigated. The films were made up of neutral and positively charged pyridine, whereby the cationic nature of the pyridine could be attributed to being protonated (N^+-H) or trifluoroacylated (N^+-$COCF_3$). When the modified electrodes were treated with a base this either deprotonated the N^+-H bond or cleaved the N^+-$COCF_3$ bond to produce neutral pyridine and decrease the positive charge on the electrode. This positive charge could be reintroduced by treating the electrode with an acid, which re-protonated the neutral pyridine.

Future work could focus on further characterising the films using techniques such as atomic force microscopy (AFM) to determine the exact thickness of the different films. Once the films are fully characterised, investigations could be carried out to determine how effective the modified electrodes are as sensors. For instance, they could be used

to detect traces of negatively charged contaminants in drinking water samples, such as perfluoroalkyl and polyfluoroalkyl substances (PFAS).[163,164]

7.3 Oxytrifluoromethylation of Styrene

Alongside the investigations into the electrochemical behaviour of the trifluoroacetylpyridinium salts, their use in electrosynthetic trifluoromethylation reactions was also explored. This was something that had not been reported in the literature before, and so our electrosynthetic reaction had to be designed from scratch. We originally started with a divided cell approach as we were unsure of what product would be formed and if any intermediates would be involved. Therefore, we wanted to separate the reduction and oxidation reactions to avoid the oxidation of any reduction products and vice versa. Through this we discovered that the oxytrifluoromethylation of styrene had occurred in the reduction compartment of the cell. However, possibly due to the high resistance in the cell the yield of the oxytrifluoromethylation product was very low. The reaction cell was changed to a single cell set-up, however having both electrodes in the same compartment led to no yield of reaction. The reason for this was unclear but could have been due to an electron transfer process occurring at the counter electrode (anode). A sacrificial anode was introduced, and this allowed for a successful reaction to take place. Our attention was focused on optimising the reaction to achieve the highest yield possible. This was important to us as we wanted our electrosynthetic reaction to be comparable to (or better) than the current reported methods. To improve the yield, different nucleophiles, solvents, stoichiometry and electrode materials were tested. The highest yield we recorded of the oxytrifluoromethylation product was 51%. This was achieved using trifluoroacetylpyridinium as the starting material, single cell, carbon cathode, nickel anode, silver reference electrode, $TBAPF_6$ electrolyte, MeCN as the solvent, constant potential (-1.5 V) and 20 molar equivalents of the salt compared to 1 molar equivalent of styrene. Other styrenes were used for synthesis and successful oxytrifluoromethylation was achieved with 4-methylstyrene, 4-fluorostyrene and 4-*tert*-butylstyrene.

Future work should focus on improving the yield of reaction, which could be achieved using a syringe pump to control the amount of trifluoroacetylpyridinium in solution, so that a steady rate of radicals is produced. Other works could focus on using the oxytrifluoromethylation reaction on other substrates such as alkenes, or as part of a multistep synthesis. These steps are suggested to further prove the benefits of electrosynthesis to the organic chemistry community.

7.4 Final Thoughts

Overall, the main objectives set out at the start of this project have been achieved. A successful electrosynthetic trifluoromethylation reaction was carried out using cheap and readily available starting materials. Although the current yield of reaction is not as high as we would have hoped, future work will hopefully achieve this. Once this has been achieved we hope to publish this work and demonstrate to the organic community the simplicity and utility of our reaction. In an effort to understand the electrochemical behaviour of these salts we were able to modify carbon-based electrodes in way that has not been previously reported. This work offers a new way to graft pyridine to electrode surfaces and gives an insight into the effect substituents have on the electrografting of such a material.

References

1. Koch, A., Aro, R., Wang, T. & Yeung, L. W. Y. Towards a comprehensive analytical workflow for the chemical characterisation of organofluorine in consumer products and environmental samples. *TrAC - Trends Anal. Chem.* **123**, 115423 (2020).
2. Mei, H., Han, J., Fustero, S., Medio-Simon, M., Sedgwick, D. M., Santi, C., Ruzziconi, R. & Soloshonok, V. A. Fluorine-Containing Drugs Approved by the FDA in 2018. *Chem. - A Eur. J.* **25**, 11797–11819 (2019).
3. Szpera, R., Moseley, D. F. J., Smith, L. B., Sterling, A. J. & Gouverneur, V. The Fluorination of C–H Bonds: Developments and Perspectives. *Angew. Chemie - Int. Ed.* **58**, 14824–14848 (2019).
4. Purser, S., Moore, P. R., Swallow, S. & Gouverneur, V. Fluorine in medicinal chemistry. *Chem. Soc. Rev.* **37**, 320–330 (2008).
5. Hagmann, W. K. The many roles for fluorine in medicinal chemistry. *J. Med. Chem.* **51**, 4359–4369 (2008).
6. Barnes-Seeman, D., Jain, M., Bell, L., Ferreira, S., Cohen, S., Chen, X-H., Amin, J., Snodgrass, B., Hatsis, P. Metabolically stable *tert*-butyl replacement. *ACS Med. Chem. Lett.* **4**, 514–516 (2013).
7. Leroux, F. R., Manteau, B., Vors, J. P. & Pazenok, S. Trifluoromethyl ethers - Synthesis and properties of an unusual substituent. *Beilstein J. Org. Chem.* **4**, (2008).
8. Wang, J., Sánchez-Rolselló, M., Aceña, J. L., del Pozo, C., Sorochinsky, A. E., Fusteri, S., Soloshonok V. A., Liu, H.Fluorine in pharmaceutical industry: Fluorine-containing drugs introduced to the market in the last decade (2001-2011). *Chem. Rev.* **114**, 2432–2506 (2014).
9. Filler, R. & Saha, R. Fluorine in medicinal chemistry: A century of progress and a 60-year retrospective of selected highlights. *Future Med. Chem.* **1**, 777–791 (2009).
10. Zhu, W., Wang, J., Wang, S., Gu, Z., Aceña, J. L., Izawa, K., Liu, H.,Soloshonok, V. A.,Recent advances in the trifluoromethylation methodology and new CF3-containing drugs. *J. Fluor. Chem.* **167**, 37–54 (2014).

11. Fujiwara, T. & O'Hagan, D. Successful fluorine-containing herbicide agrochemicals. *J. Fluor. Chem.* **167**, 16–29 (2014).
12. United Nations. Population Division of the Department of Economic and Social Affairs of the United Nations Secretariat. World Population Prospects: The 2012 Revision. 2013 (2012).
13. Ma, J.-A. & Cahard, D. Strategies for nucleophilic, electrophilic, and radical trifluoromethylations. *J. Fluor. Chem.* **128**, 975-996 (2007).
14. Prakash, G. K. S., Jog, P. V, Batamack, P. T. D. & Olah, G. A. Taming of Fluoroform : Direct Nucleophilic Trifluoromethylation of Si, B, S, and C Centers. *Science.* **338**, 1324–1327 (2012).
15. Zanardi, A., Novikov, M. A., Martin, E., Benet-Buchholz, J. & Grushin, V. V. Direct cupration of fluoroform. *J. Am. Chem. Soc.* **133**, 20901–20913 (2011).
16. Han, W., Li, Y., Tang, H. & Liu, H. Treatment of the potent greenhouse gas , CHF_3 — An overview. *J. Fluor. Chem.* **140**, 7–16 (2012).
17. Folléas, B., Marek, I., Normant, J. F. & Saint-Jalmes, L. Fluoroform: An efficient precursor for the trifluoromethylation of aldehydes. *Tetrahedron* **56**, 275–283 (2000).
18. Novák, P., Lishchynskyi, A. & Grushin, V. V. Fluoroform-derived CuCF 3 for low- cost, simple, efficient, and safe trifluoromethylation of aryl boronic acids in air. *Angew. Chemie - Int. Ed.* **51**, 7767–7770 (2012).
19. Ruppert, I., Schlich, K., Volbach, W., Die ersten CF_3-substituierten organyl(chlor)silane. *Tetrahedron* **25**, 2195–2198 (1984).
20. Prakash, G. K. S., Krishnamurti, R. & Olah, G. A. Fluoride-Induced Trifluoromethylation of Carbonyl Compounds with Trifluoromethyltrimethylsilane (TMS-CF_3). A Trifluoromethide Equivalent. *J. Am. Chem. Soc.* **111**, 393–395 (1989).
21. Liu, X., Xu, C., Wang, M. & Liu, Q. Trifluoromethyltrimethylsilane: Nucleophilic trifluoromethylation and beyond. *Chem. Rev.* **115**, 683–730 (2015).
22. Tworowska, I., Dbkowski, W. & Michalski, J. Synthesis of tri- and tetracoordinate phosphorus compounds containing a PCF_3 group by nucleophilic trifluoromethylation of the corresponding PF compounds. *Angew. Chemie - Int. Ed.* **40**, 2898–2900 (2001).

23. Singh, R. P., Cao, G., Kirchmeier, R. L. & Shreeve, J. M. Cesium fluoride catalyzed trifluoromethylation of esters, aldehydes, and ketones with (trifluoromethyl)trimethylsilane. *J. Org. Chem.* **64**, 2873–2876 (1999).
24. Shevchenko, N. E., Vlasov, K., Nenajdenko, V. G. & Röschenthaler, G. V. The reaction of cyclic imines with the Ruppert-Prakash reagent. Facile approach to α-trifluoromethylated nornicotine, anabazine, and homoanabazine. *Tetrahedron* **67**, 69–74 (2011).
25. Radchenko, D. S., Michurin, O. M., Chernykh, A. V., Lukin, O. & Mykhailiuk, P. K. An easy synthesis of α-trifluoromethyl-amines from aldehydes or ketones using the Ruppert-Prakash reagent. *Tetrahedron Lett.* **54**, 1897–1898 (2013).
26. Levin, V. V., Dilman, A. D., Belyakov, P. A., Struchkova, M. I. & Tartakovsky, V. A. Nucleophilic trifluoromethylation of imines under acidic conditions. *European J. Org. Chem.* 5226–5230 (2008).
27. Large-Radix, S., Billard, T. & Langlois, B. R. Fluoride-assisted trifluoromethylation of aromatic thiones with (trifluoromethyl)trimethylsilane. *J. Fluor. Chem.* **124**, 147–149 (2003).
28. Eisenberger, P ., Gischig, S. & T ogni, A. Novel 10-I-3 hypervalent iodine-based compounds for electrophilic trifluoromethylation. *Chem. - A Eur. J.* **12**, 2579–2586 (2006).
29. Santschi, N., Geissbühler, P. & Togni, A. Reactivity of an electrophilic hypervalent iodine trifluoromethylation reagent with hydrogen phosphates - A mechanistic study. *J. Fluor. Chem.* **135**, 83–86 (2012).
30. Santschi, N. & Togni, A. Electrophilic trifluoromethylation of S-hydrogen phosphorothioates. *J. Org. Chem.* **76**, 4189–4193 (2011).
31. Allen, A. E. & MacMillan, D. W. C. The productive merger of iodonium salts and organocatalysis: A non-photolytic approach to the enantioselective α-trifluoromethylation of aldehydes. *J. Am. Chem. Soc.* **132**, 4986–4987 (2010).
32. Koller, R, Stanek, K., Stolz, D., Aardoom, R., Niedermann, K. & Togni, A. Zinc-mediated formation of trifluoromethyl ethers from alcohols and hypervalent iodine trifluoromethylation reagents. *Angew. Chemie - Int. Ed.* **48**, 4332–4336 (2009).

33. Umemoto, T. & Ishihara, S. Power-Variable Electrophilic Trifluoromethylating Agents. S-, Se-, and Te-(Trifluoromethyl)dibenzothio-, -seleno-, and -tellurophenium Salt System. *J. Am. Chem. Soc.* **115**, 2156–2164 (1993).
34. Umemoto, T. Recent Advances in Perfluoroalkylation Methodology. *ChemInform*, **37**, 2–15 (2006).
35. Umemoto, T., Adachi, K. & Ishihara, S. CF_3 oxonium salts, O-(trifluoromethyl)dibenzofuranium salts: In situ synthesis, properties, and application as a real CF_3^+ species reagent. *J. Org. Chem.* **72**, 6905–6917 (2007).
36. Siegemund, G., Schertfeger, W., Feiring, A., Smart, B., Behr, F., Vogel, H., McKusick, B. & Kirsch P. Fluorine compounds, organic: Ullmann's encyclopedia of industral chemistry, Wiley-VCH Verlag GmbH & Co., Hoboken, (2016).
37. Tomita, R., Yasu, Y., Koike, T. & Akita, M. Direct C-H trifluoromethylation of di- and trisubstituted alkenes by photoredox catalysis. *Beilstein J. Org. Chem.* **10**, 1099–1106 (2014).
38. Yasu, Y., Arai, Y., Tomita, R., Koike, T. & Akita, M. Highly regio- and diastereoselective synthesis of CF_3- substituted lactones via photoredox-catalyzed carbolactonization of alkenoic acids. *Org. Lett.* **16**, 780–783 (2014).
39. Yasu, Y., Koike, T. & Akita, M. Intermolecular aminotrifluoromethylation of alkenes by visible-light-driven photoredox catalysis. *Org. Lett.* **15**, 2136–2139 (2013).
40. Yasu, Y., Koike, T. & Akita, M. Three-component oxytrifluoromethylation of alkenes: Highly efficient and regioselective difunctionalization of C=C bonds mediated by photoredox catalysts. *Angew. Chemie - Int. Ed.* **51**, 9567–9571 (2012).
41. Takechi, N., Ait-Mohand, S., Medebielle, M. & Dolbier, W. R. Novel Nucleophilic Trifluoromethylation of Vicinal Diol Cyclic Sulfates. *Org. Lett.* **4**, 4671–4672 (2002).
42. Takechi, N., Aiït-Mohand, S., Médebielle, M. & Dolbier, W. R. Nucleophilic trifluoromethylation of acyl chlorides using the trifluoromethyl iodide/TDAE reagent. *Tetrahedron Lett.* **43**, 4317–4319 (2002).

43. Xu, W. & Dolbier, W. R. Nucleophilic trifluoromethylation of imines using the CF_3I/TDAE reagent. *J. Org. Chem.* **70**, 4741–4745 (2005).
44. Iqbal, N., Choi, S., Kim, E. & Cho, E. J. Trifluoromethylation of Alkenes by Visible Light Photoredox Catalysis. *J. Org. Chem.* **77**, 11383–11387 (2012).
45. Iqbal, N., Choi, S., Ko, E. & Cho, E. J. Trifluoromethylation of heterocycles via visible light photoredox catalysis. *Tetrahedron Lett.* **53**, 2005–2008 (2012).
46. Wang, J., Sánchez-Roselló, M., Aceña, J. L., del Pozo, C., Soronchinsky, A.E., Fustero, S., Soloshonok, V. A., Liu, H., Fluorine in pharmaceutical industry: Fluorine-containing drugs introduced to the market in the last decade (2001-2011). *Chem. Rev*. **114**, 2432- 2506 (2014).
47. Yan, M., Kawamata, Y. & Baran, P. S. Electrochemical Synthesis Synthetic Organic Electrochemistry:Calling All Engineers. *Angew. Chem. Int. Ed.* **57**, 4149-4155 (2018).
48. Raju, T. & Basha, C. A. Electrochemical cell design and development for mediated electrochemical oxidation-Ce(III)/Ce(IV)system. *Chem. Eng. J.* **114**, 55–65 (2005).
49. Horn, E. J., Rosen, B. R. & Baran, P. S. Synthetic Organic Electrochemistry: An Enabling and Innately Sustainable Method. *ACS Cent. Sci*. **2**, 302-308 (2016).
50. Kingston, C., Palkowitz, M. D., Takahira, Y., Vantourout, J. C., Petes, B. K., Kawamata, Y. & Baran, P.S. A Survival Guide for the 'electro-curious'. *Acc. Chem. Res.* **53**, 72-83 (2019).
51. O-Brien, A. G., Maruyama, A., Inokuma, Y., Fujita, M., Baran, P. S. & Blackmond, D. G. Radical C-H functionalization of heteroarenes under electrochemical control. *Angew. Chemie - Int. Ed.* **53**, 11868-11871 (2014).
52. Jud, W., Kappe, C. O. & Cantillo, D. Catalyst-Free Oxytrifluoromethylation of Alkenes through Paired Electrolysis in Organic-Aqueous Media. *Chem. - A Eur. J.* **24**, 17234–17238 (2018).
53. Zhang, L., Zhang, G., Wang, P., Li, Y. & Lei, A. Electrochemical Oxidation with Lewis-Acid Catalysis Leads to Trifluoromethylative Difunctionalization of Alkenes Using CF_3SO_2Na. *Org. Lett.* **20**, 7396-7399 (2018).

54. Sauer, G. S. & Lin, S. An Electrocatalytic Approach to the Radical Difunctionalization of Alkenes. *ACS Catal*. **8**, 5175-5187 (2018).
55. Jiang, Y.-Y., Dou, G.-Y., Xu, K. & Zeng, C.-C. Bromide-catalyzed electrochemical trifluoromethylation/cyclization of N-arylacrylamides with low catalyst loading. *Org. Chem. Front.* **5**, 2573 (2018).
56. Jud, W., Maljuric, S., Kappe, C. O. & Cantillo, D. Cathodic C-H Trifluoromethylation of Arenes and Heteroarenes Enabled by an in Situ-Generated Triflyltriethylammonium Complex. *Org. Lett.* **21**, 7970–7975 (2019).
57. Keyes, T. E. & Forster, R. J. *Spectroelectrochemistry*. *Handbook of Electrochemistry* (2007).
58. Bard, A. J. & Faulkner, L. L. *Electrochemical Methods: Fundamentals and Applications, 2nd Edition*. (2000).
59. Elgrishi, N., Rountree, K. J., McCarthy, B. D., Rountree, E. S., Eisenhart, T. T. & Dempsey, J. L. A Practical Beginner's Guide to Cyclic Voltammetry. *J. Chem. Educ.* **95** 197-206 (2018).
60. Laville, R., Genta-Jouve, G., Urda, C., Fernández, R., Thomas, O. P., Reyes, F. & Amade, P. Njaoaminiums A, B, and C: Cyclic 3-alkylpyridinium salts from the marine sponge Reniera sp. *Molecules* **14**, 4716–4724 (2009).
61. Luisetti, M., Ma, S., Iadarola, P., Stone, P. J., Viglio, S., Casado, B., Lin, Y. Y., Snider, G. L. & Turino, G. M. Desmosine as a biomarker of elastin degradation in COPD: Current status and future directions. *Eur. Respir. J.* **32**, 1146–1157 (2008).
62. Laville, R., Thomas, O. P., Berrue, F., Reyes, F. & Amade, P. Pachychalines A- C: Novel 3-alkylpyridinium salts from the marine sponge Pachychalina sp. *European J. Org. Chem.* 121–125 (2008).
63. Hosseini-Bab-Anari, E., Navarro-Suárez, A. M., Moth-Poulsen, K. & Johansson, P. Ionic liquid based battery electrolytes using lithium and sodium pseudo- delocalized pyridinium anion salts. *Phys. Chem. Chem. Phys.* **21**, 18393–18399 (2019).
64. Lim, C., Kim, S. H., Yoh, S. D., Fujio, M. & Tsuno, Y. The menschutkin reaction of 1-arylethyl bromides with pyridine: Evidence for the duality of clean S(N)1 and S(N)2 mechanisms. *Tetrahedron Lett.* **38**, 3243–3246 (1997).

65. Klauck, F. J. R., James, M. J. & Glorius, F. Deaminative Strategy for the Visible-Light-Mediated Generation of Alkyl Radicals. *Angew. Chemie - Int. Ed.* **56**, 12336–12339 (2017).
66. Basch, C. H., Liao, J., Xu, J., Piane, J. J. & Watson, M. P. Harnessing Alkyl Amines as Electrophiles for Nickel-Catalyzed Cross Couplings via C-N Bond Activation. *J. Am. Chem. Soc.* **139**, 5313–5316 (2017).
67. Ociepa, M., Turkowska, J. & Gryko, D. Redox-Activated Amines in C(sp^3)–C(sp) and C(sp^3)–C(sp^2) Bond Formation Enabled by Metal-Free Photoredox Catalysis. *ACS Catal.* **8**, 11362–11367 (2018).
68. Zhao, S., Xu, X., Zheng, L. & Liu, H. An efficient ultrasonic-assisted synthesis of imidazolium and pyridinium salts based on the Zincke reaction. *Ultrason. Sonochem.* **17**, 685–689 (2010).
69. Viana, G. H. R., Santos, I. C., Alves, R. B., Gil, L., Marazano, C. & Gil, R. P. F. Microwave-promoted synthesis of chiral pyridinium salts. *Tetrahedron Lett.* **46**, 7773–7776 (2005).
70. Petit, S., Azzouz, R., Fruit, C., Bischoff, L. & Marsais, F. An efficient protocol for the preparation of pyridinium and imidazolium salts based on the Mitsunobu reaction. *Tetrahedron Lett.* **49**, 3663–3665 (2008).
71. Liu, W. D., Xu, G. Q., Hu, X. Q. & Xu, P. F. Visible-Light-Induced Aza-Pinacol Rearrangement: Ring Expansion of Alkylidenecyclopropanes. *Org. Lett.* **19**, 6288–6291 (2017).
72. Jelier, B. J., Tripet, P. F., Pietrasiak, E., Franzoni, I., Jeschke, G. & Togni, A. Radical Trifluoromethoxylation of Arenes Triggered by a Visible-Light-Mediated N–O Bond Redox Fragmentation. *Angew. Chemie - Int. Ed.* **57**, 13784–13789 (2018).
73. Miyazawa, K., Ochi, R., Koike, T. & Akita, M. Photoredox radical C-H oxygenation of aromatics with aroyloxylutidinium salts. *Org. Chem. Front.* **5**, 1406–1410 (2018).
74. Barthelemy, A. L., Tuccio, B., Magnier, E. & Dagousset, G. Alkoxyl Radicals Generated under Photoredox Catalysis: A Strategy for anti-Markovnikov Alkoxylation Reactions. *Angew. Chemie - Int. Ed.* **57**, 13790–13794 (2018).

75. Bao, X., Wang, Q. & Zhu, J. Dual Photoredox/Copper Catalysis for the Remote C(sp^3)–H Functionalization of Alcohols and Alkyl Halides by N-Alkoxypyridinium Salts. *Angew. Chemie - Int. Ed.* **58**, 2139–2143 (2019).
76. Yuan, F., Yan, D-M., Gao, P-P., Shi, D-Q., Xiao, W-J. & Chen, J-R. Photoredox-Catalyzed Multicomponent Cyclization of 2-Vinyl Phenols, N-Alkoxypyridinium Salts, and Sulfur Ylides for Synthesis of Dihydrobenzofurans. *ChemCatChem* **13**, 543–547 (2021).
77. Jeon, J., He, Y. T., Shin, S. & Hong, S. Visible-Light-Induced ortho-Selective Migration on Pyridyl Ring: Trifluoromethylative Pyridylation of Unactivated Alkenes. *Angew. Chemie - Int. Ed.* **59**, 281–285 (2020).
78. Buquoi, J. Q., Lear, J. M., Gu, X. & Nagib, D. A. Heteroarene Phosphinylalkylation via a Catalytic, Polarity-Reversing Radical Cascade. *ACS Catal.* **9**, 5330–5335 (2019).
79. Kim, N., Lee, C., Kim, T. & Hong, S. Visible-Light-Induced Remote C(sp3)-H Pyridylation of Sulfonamides and Carboxamides. *Org. Lett.* **21**, 9719–9723 (2019).
80. Yamaguchi, R., Nakazono, Y., Matsuki, E. H. & Kawanisi, M. Highly Regioselective α-Addition of Alkynyl and Alkenyl Grignard Reagents to 1-Alkoxycarbonylpyridinium Salts and Its Application to Synthesis of 1-Azabicycloalkanes and (±)-Solenopsin A. *Bull. Chem. Soc. Jpn.* **60**, 215–222 (1987).
81. Lyle, R. E. & Comins, D. L. Regioselective nucleophilic addition to 3,4-lutidine. *J. Org. Chem.* **41**, 3250–3252 (1976).
82. Lyle, R. E., Marshall, J. L. & Comins, D. L. The reaction of 1-acylpyridinium salts with grignard and organocadmium reagents. *Tetrahedron Lett.* **18**, 1015–1018 (1977).
83. Gupta, N., Garg, R., Shah, K. K., Tanwar, A. & Pal, S. Deprotonation of 1,2-dialkylpyridinium ions: A DFT study of reactivity and site selectivity. *J. Phys. Chem. A* **111**, 8823–8828 (2007).
84. Maricq, M. M., Szente, J. J., Khitrov, G. A., Dibble, T. S. & Francisco, J. S. CF_3CO dissociation kinetics. *J. Phys. Chem.* **99**, 11875–11882 (1995).

85. Wallington, T. J., Hurley, M. D., Nielsen, O. J. & Sehested, J. Atmospheric chemistry of CF_3CO_x radicals: Fate of CF_3CO radicals, the UV absorption spectrum of $CF_3C(O)O_2$ radicals, and kinetics of the reaction $CF_3C(O)O_2 + NO \rightarrow CF_3C(O)O + NO_2$. *J. Phys. Chem.* **98**, 5686–5694 (1994).
86. Francisco, J. S. The role of $CF_3C(O)O_x$ radicals in atmospheric chemical processes. *Chem. Phys. Lett.* **191**, 7–12 (1992).
87. Ouyang, Y., Xu, X. H. & Qing, F. L. Trifluoromethanesulfonic Anhydride as a Low-Cost and Versatile Trifluoromethylation Reagent. *Angew. Chemie - Int. Ed.* **57**, 6926–6929 (2018).
88. Ames, J. R. Electrochemical reduction of arylethenylpyridinium salts: Relation to structure and anthelmintic activity. *J. Pharm. Sci.* **80**, 293–295 (1991).
89. King, J. A. An unusually facile formation of substituted 1,2-dihydropyridine derivatives: the reversible condensation of pyridines with reactive carbonyl groups. *J. Am. Chem. Soc.* **110**, 5764–5767 (1988).
90. Anthoni, U., Christensen, D., Christophersen, C., Nielsen, P. H., An NMR and Raman Study of Trifluoroacetic Anhydride in Pyridine. *Acta Chem. Scand.* **49**, 203–206 (1995).
91. Okada, E., Sakaemura, T. & Shimomura, N. A simple synthetic method for 3-trifluoroacetylated 4-aminoquinolines from 4-dimethylaminoquinoline by novel trifluoroacetylation and N-N exchange reactions. *Chem. Lett.* 50–51 (2000).
92. G. Simchen and A. Schmidt. Eine einfache Methode zur Darstellung von Aryl-trifluoromethylketonen. *Synth.* 1093–1094 (1996).
93. Occhialini, D., Daasbjerg, K. & Lund, H. Estimation of Reduction and Standard Potentials of Acyl Radicals. *Acta Chemica Scandinavica* **47**, 1100–1106 (1993).
94. Zhou, J., Khodakov, D. A., Ellis, A. V. & Voelcker, N. H. Surface modification for PDMS-based microfluidic devices. *Electrophoresis* **33**, 89–104 (2012).
95. Liu, W., Liu, S. & Wang, L. Surface Modification of Biomedical Titanium Alloy: Micromorphology, Microstructure Evolution and Biomedical Applications. *Coatings* **9**, 249 (2019).
96. Ramos Chagas, G., Cruz, G. M., Giraudon-Colas, G., Savina, F., Méallet-Renault, R., Amigoni, S., Guittard, F. & Darmanin, T. Anti-bacterial and

fluorescent properties of hydrophobic electrodeposited non-fluorinated polypyrenes. *Appl. Surf. Sci.* **452**, 352–363 (2018).

97. Fang, C., Bhattarai, N., Sun, C. & Zhang, M. Functionalized nanoparticles with long-term stability in biological media. *Small* **5**, 1637–1641 (2009).
98. Krivetskiy, V., Ponzoni, A., Comini, E., Badalyan, S., Rumyantseva, M. & Gaskov, A. Selectivity modification of SnO2-Based materials for gas sensor arrays. *Electroanalysis* **22**, 2809–2816 (2010).
99. Chen, N., Kim, D. H., Kovacik, P., Sojoudi, H., Wang, M. & Gleason, K. K. Polymer Thin Films and Surface Modification by Chemical Vapor Deposition: Recent Progress. *Annu. Rev. Chem. Biomol. Eng.* **7**, 373–393 (2016).
100. Zhang, J., Li, R., Wang, X. & Li, Q. Enhanced visible light adsorption of heavily nitrogen doped TiO2 thin film via ion beam assisted deposition. *J. Mater. Sci. Mater. Electron.* **27**, 2968–2973 (2016).
101. Banerjee, S., Adhikari, E., Sapkota, P., Sebastian, A. & Ptasinska, S. Atmospheric pressure plasma deposition of TiO2: A review. *Materials (Basel).* **13**, 1–36 (2020).
102. Mackiewicz, M., Marcisz, K., Strawski, M., Romanski, J. & Stojek, Z. Modification of gold electrode with a monolayer of self-assembled microgels. *Electrochim. Acta* **268**, 531–538 (2018).
103. Xu, K., Zhang, X., Hou, K., Geng, M. & Zhao, L. The Effects of Antimony Thin Film Thickness on Antimony pH Electrode Coated with Nafion Membrane. *J. Electrochem. Soc.* **163**, B417–B421 (2016).
104. Bélanger, D. & Pinson, J. Electrografting: A powerful method for surface modification. *Chem. Soc. Rev.* **40**, 3995–4048 (2011).
105. Combellas, C., Kanoufi, F., Pinson, J. & Podvorica, F. I. Indirect electrografting of aryl iodides. *Electrochem. commun.* **98**, 119–123 (2019).
106. Sommerfeldt, A., Pedersen, S. U. & Daasbjerg, K. Electrochemical grafting of heterocyclic molecules on glassy carbon and platinum using heteroaromatic iodonium salts or iodo-substituted heteroaromatics. *Electrochim. Acta* **261**, 356– 364 (2018).

107. Wang, T., Qi, S., Ren, B. & Tong, Z. Preparation and surface characteristics of low-temperature curing fluorinated cathodic electrodeposition coating. *Prog. Org. Coatings* **60**, 132–139 (2007).

108. Subrata, A., Veksha, A., Pong, Z. Y., Lisak, G. & Webster, R. D. Electrografting of Sterically Bulky Tetramethylaniline Groups on Glassy Carbon Electrodes through Aryldiazonium Chemistry: Reasons for the Formation of Multilayers. *ChemElectroChem* **7**, 3368–3380 (2020).

109. Louault, C., D'Amours, M. & Bélanger, D. The electrochemical grafting of a mixture of substituted phenyl groups at a glassy carbon electrode surface. *ChemPhysChem* **9**, 1164–1170 (2008).

110. Brooksby, P. A. & Downard, A. J. Electrochemical and Atomic Force Microscopy Study of Carbon Surface Modification via Diazonium Reduction in Aqueous and Acetonitrile Solutions. *Langmuir*, **20**, 5038-5045 (2004).

111. Laforgue, A., Addou, T. & Bélanger, D. Characterization of the Deposition of Organic Molecules at the Surface of Gold by the Electrochemical Reduction of Aryldiazonium Cations. *Langmuir*, **21**, 6855-6865 (2005).

112. Greenwood, J., Phan, T. H., Fujita, Y., Li, Z., Ivasenko, O., Vandrlinden, W., Van Gorp, H., Frederickx, W., Lu, G., Tahara, K., Tobe, Y., Uji-i, H., Mertens, S. F. L. & De Feyter, S. Covalent Modification of Graphene and Graphite Using Diazonium Chemistry: Tunable Grafting and Nanomanipulation. *ACS Nano*, **9**, 5520-5535 (2015).

113. Agullo, J., Canesi, S., Schaper, F., Morin, M. & Beíanger, D. Formation and Reactivity of 3-Diazopyridinium Cations and Influence on Their Reductive Electrografting on Glassy Carbon. *Langmuir*, **28**, 4889-4895 (2012).

114. Agullo, J., Morin, M. & Belanger, D. Modification of Glassy Carbon Electrode by Electrografting of In Situ Generated 3-diazopyridinium Cations. *J. Electrochem. Soc.* **159**, H758–H764 (2012).

115. Smida, H., Lebègue, E., Bergamini, J.-F. & Lagrost, C. Reductive electrografting of in situ produced diazopyridinium cations: Tailoring the interface between carbon electrodes and electroactive bacterial films. *Bioelectrochemistry,***120**, 157-165 (2018).

116. Yeşildağ, A. & Ekinci, D. Covalent attachment of pyridine-type molecules to glassy carbon surfaces by electrochemical reduction of in situ generated diazonium salts. Formation of ruthenium complexes on ligand-modified surfaces. *Electrochim. Acta* **55**, 7000–7009 (2010).

117. Nazeeruddin, M. K., Zakeeruddin, S. M., Lagref, J.-J., Liska, P., Comte, P., Barolo, C., Viscardi, G., Schenk, K. & Gratzel, M. Stepwise assembly of amphiphilic ruthenium sensitizers and their applications in dye-sensitized solar cell. *Coord. Chem. Rev.* **248**, 1317–1328 (2004).

118. Vergeer, F. W., Chen, X., Lafolet,F., De Cola, L., Fuchs, H. & Chi, L. Ultrathin Luminescent Films of Rigid Dinuclear Ruthenium(II) Trisbipyridine Complexes. *Adv. Funct. Mater.* **16**, 625-632 (2006).

119. Li, Q., Schönleber, K., Zeller, P., Höhlein, I., Rieger, B., Winntterlin, J. & Krischer, K. Activation of silicon surfaces for H_2 evolution by electrografting of pyridine molecules. *Surf. Sci.* **631**, 185–189 (2015).

120. Shockley, W. & Queisser, H. J. Detailed Balance Limit of Efficiency of p-n Junction Solar Cells. *J. Appl. Phys.* **32**, 510 (1961).

121. Strümpel, C., McCann, M., Beaucarne, G., Arkhipov, V., Slaoui, A., Svrček, V., del Cañizo, C. & Tobias, I. Modifying the solar spectrum to enhance silicon solar cell efficiency-An overview of available materials. *Sol. Energy Mater. Sol. Cells* **91**, 238–249 (2007).

122. Han, T., Privitera, S., Milazzo, R. G., Bongiorno, C., Di Franco, S., La Via, F., Song, X., Shi, Y., Lanza, M. & Lombardo, S. Photo-electrochemical water splitting in silicon based photocathodes enhanced by plasmonic/catalytic nanostructures. *Mater. Sci. Eng. B Solid-State Mater. Adv. Technol.* **225**, 128–133 (2017).

123. Xiao, H., Wang, W., Pi, S., Cheng, Y. & Xie, Q. Pyridine-2-sulfonic (or carboxylic) acid modified glassy carbon electrode for anodic stripping voltammetry analysis of Cd^{2+} and Pb^{2+}. *Anal. Chim. Acta.* **1135**, 20-28 (2020).

124. Xiao, H., Wang, W., Pi, S., Cheng, Y. & Xie, Q. Anodic stripping voltammetry analysis of mercury(II) on a pyridine-Au/pyridine/glassy carbon electrode. *Sensors Actuators, B Chem.* **317**, 128202 (2020).

125. Pippig, F., Sarghini, S., Holländer, A., Paulussen, S. & Terrvn, H. TFAA chemical derivatization and XPS. Analysis of OH and NH_x polymers. *Surf. Interface Anal.* **41**, 421–429 (2009).

126. Kehrer, M., Duchoslav, J., Hinterreiter, A., Cobet, M., Mehic, A., Stehrer, T. & Stifter, D. XPS investigation on the reactivity of surface imine groups with TFAA. *Plasma Process. Polym.* **16**, 1–8 (2019).

127. Agullo, J., Morin, M. & Bélanger, D. Modification of Glassy Carbon Electrode by Electrografting of In Situ Generated 3-diazopyridinium Cations. *J. Electrochem. Soc.* **159**, H758–H764 (2012).

128. Pchelintsev, N. A., Vakurov, A., Hays, H. H. & Millner, P. A. Thiols deposition onto the surface of glassy carbon electrodes mediated by electrical potential.

129. Ispas, A., Adolphi, B., Bind, A., & Endres, F., On the electrodeposition of tantalum from three different ionic liquids with the bis(trifluoromethyl sulfonyl) amide anion. *Phys. Chem. Chem. Phys* (2010).

130. Snelgrove, M., Zehe, C., Lundy, R., Yadav, P., Rueff, J-P., O'Connor, R., Bogan, J., Hughes, G., McGlynn, E., Morris, M. & Mani-Gonzalez, P. G. Surface characterization of poly-2-vinylpyridine—A polymer for area selective deposition techniques. *J. Vac. Sci. Technol. A* **37**, 050601 (2019).

131. Beshkov, G., Dimitrov, D. B., Georgiev, St., Juan-Cheng,J., Petrov,P., Velchev, N. & Krastev, V. XPS spectra of thin CN_x films prepared by chemical vapor deposition. *Diam. Relat. Mater.* **8**, 591–594 (1999).

132. Lyskawa, J. & Bélanger, D. Direct modification of a gold electrode with aminophenyl groups by electrochemical reduction of in situ generated aminophenyl monodiazonium cations. *Chem. Mater.* **18**, 4755–4763 (2006).

133. Al-Gaashani, R., Najjar, A., Zakaria, Y., Mansour, S. & Atieh, M. A. XPS and structural studies of high quality graphene oxide and reduced graphene oxide prepared by different chemical oxidation methods. *Ceram. Int.* **45**, 14439–14448 (2019).

134. Nelson, A. J., Glenis, S. & Frank, A. J. XPS and UPS investigation of PF6 doped and undoped poly 3-methyl thiophene. *J. Chem. Phys.* **87**, 5002–5006 (1987).

135. Vasudevan, D. & Wendt, H. Electroreduction of oxygen in aprotic media. *J. Electroanal. Chem.* **392**, 69–74 (1995).

136. Rowe, R. C., Wren, S. A. C. & McKillop, A. G. Molecular size/shape effects in the separation of the monosubstituted alkyl pyridines using capillary electrophoresis. *Electrophoresis* **15**, 635–639 (1994).

137. Wang, D. H., Hu, Y., Zhao, J. J., Zeng, L. L., Tao, X. M.& Chen, W. Holey reduced graphene oxide nanosheets for high performance room temperature gas sensing. *J. Mater. Chem. A* **2**, 17415–17420 (2014).

138. Flitsch, R. & Shih, D.-Y. An XPS study of argon ion beam and oxygen RIE modified BPDA-PDA polyimide as related to adhesion. *J. Adhesion Sci. Technol.,* **10**, 1241-1253 (1996).

139. Mekki, A., Holland, D., McConville, C. F. & Salim, M. An XPS study of iron sodium silicate glass surfaces. *J. Non. Cryst. Solids* **208**, 267–276 (1996).

140. Hartig, P., Dittrich, T. H. & Rappich, J. Surface dipole formation and non-radiative recombination at p-Si(111) surfaces during electrochemical deposition of organic layers. *J. Electroanal. Chem.* **524**–**525**, 120–126 (2002).

141. Dou, G.-Y., Jiang, Y.-Y., Xu, K. & Zeng, C.-C. Electrochemical Minisci-type trifluoromethylation of electron-deficient heterocycles mediated by bromide ions. *Org. Chem. Front.* **6**, 2392 (2019).

142. Deng, Y., Lu, F., You, S., Xia, T., Zheng, Y., Lu, C., Yang, G., Chen, Z., Gao, M. & Lei, A., External-Oxidant-Free Electrochemical Oxidative Trifluoromethylation of Arenes Using CF_3SO_2Na as the CF_3 Source. *Chinese J. Chem.* **37**, 817–820 (2019).

143. Xu, C., Liu, Y., Liu, H., Ma, J., He, X., Wu, H., Li, Y., Sun, Z. & Chu, W. Metal- free electrochemical oxidative trifluoromethylation/C(sp^2)–H functionalization of quinolinones. *Tetrahedron Lett.* **61**, 152226 (2020).

144. Ye, K. Y., Pombar, G., Fu, N., Sauer, G. S., Kereszetes, I. & Lin, S. Anodically Coupled Electrolysis for the Heterodifunctionalization of Alkenes. *J. Am. Chem. Soc.* **140**, 2438–2441 (2018).

145. Zhang, L., Zhang, G., Wang, P., Li, Y. & Lei, A. Electrochemical Oxidation with Lewis-Acid Catalysis Lead to Trifluoromethylative

Difunctionalization of Alkenes Using CF_3SO_2Na. *Org. Lett.* **20**, 7396-7399 (2018).

146. Sun, X., Ma, H. X., Mei, T. S., Fang, P. & Hu, Y. Electrochemical Radical Formyloxylation-Bromination, -Chlorination, and -Trifluoromethylation of Alkenes. *Org. Lett.* **21**, 3167–3171 (2019).

147. Zou, Z., Zhang, W., Wang, Y., Kong, L., Karotsis, G., Wang, Y. & Pan, Y. Electrochemically Promoted Fluoroalkylation-Distal Functionalization of Unactivated Alkenes. *Org. Lett.* **21**, 1857–1862 (2019).

148. Jud, W., Kappe, C. O. & Cantillo, D. On the reactivity of anodically generated trifluoromethyl radicals toward aryl alkynes in organic/aqueous media. *Org. Biomol. Chem.* **17**, 3529–3537 (2019).

149. Kawamata, Y., Yan, M., Liu, Z., Bao, D-H., Chen, J. & Starr, J. T. Scalable, Electrochemical Oxidation of Unactivated C-H Bonds. *J. Am. Chem. Soc.* **139**, 7448–7451 (2017).

150. Gan, L., Yu, Q., Liu, Y. & Wan, J. P. Scissoring Enaminone C=C Double Bond by Free Radical Process for the Synthesis of α-Trifluoromethyl Ketones with CF3SO2Na. *J. Org. Chem.* **86**, 1231–1237 (2021).

151. Chaussard, J., Folest, J-C., Nedelec, J-Y., Perichon, J., Sibille, S. & Troupel, M. Use of Sacrificial Anodes in Electrochemical Functionalization of Organic Halides. *Synthesis* **1990**, 369–381 (1990).

152. Scialdone, O., Sabatino, M. A., Galia, A., Filardo, G. & Silvestri, G. Synthesis of cyanoacetic acid by carbon dioxide and electrogenerated acetonitrile anion in undivided cells equipped with sacrificial anodes. *J. Electroanal. Chem.* **614**, 175–178 (2008).

153. Brevet, D., Mugnier, Y., Samreth, S. & Dellisc, P. New efficient electrochemical synthesis of 1,5-dithioxylopyranosides in the presence of a sacrificial anode. *Carbohydr. Res.* **338**, 1543–1552 (2003).

154. Kuntyi, O. I., Kytsya, A. R., Bondarenko, A. B., Mazur, A. S., Mertsalo & Bazylyak, L. I., Microplasma synthesis of silver nanoparticles in PVP solutions using sacrificial silver anodes. *Colloid Polym. Sci.* **299**, 855–863 (2021).

155. Lide, D. R. *CRC Handbook of Chemistry and Physics*.

156. Maji, A., Hazra, A. & Maiti, D. Direct synthesis of α-trifluoromethyl ketone from (hetero)arylacetylene: Design, intermediate trapping, and mechanistic investigations. *Org. Lett.* **16**, 4524–4527 (2014).

157. Yang, Y., Liu, Y., Jiang, Y., Zhang, Y. & Vicic, D. A. Manganese-Catalyzed Aerobic Oxytrifluoromethylation of Styrene Derivatives Using CF3SO2Na as the Trifluoromethyl Source. *J. Org. Chem.* **80**, 6639–6648 (2015).

158. Vil', V. A., Merkulova, V. M., Ilovaisky, A. I., Paveliev, S. A., Nikishin, G. I. & Terent'ev, A. O. Electrochemical Synthesis of Fluorinated Ketones from Enol Acetates and Sodium Perfluoroalkyl Sulfinates. *Org. Lett.* **23**, 5107–5112 (2021).

159. Yamaguchi, E., Kamito, Y., Matsuo, K., Ishihara, J. & Itoh, A. Photooxidative Keto-Trifluoromethylation of Styrenes by Means of an Anthraquinone-Based Organocatalyst. *Synth.* **50**, 3161–3168 (2018).

160. Zhang, C. P., Wang, Z. L., Chen, Q. Y., Zhang, C. T., Gu, Y. C. & Xiao, J. C. Generation of the CF_3 radical from trifluoromethylsulfonium triflate and its trifluoromethylation of styrenes. *Chem. Commun.* **47**, 6632–6634 (2011).

161. Wu, Y. B., Lu, G. P., Yuan, T., Xu, Z. B., Wan, L. & Cai, C. Oxidative trifluoromethylation and fluoroolefination of unactivated olefins. *Chem. Commun.* **52**, 13668–13670 (2016).

162. Moody, C. J. & O'Connell, J. L. Observations on the transition-metal catalysed oxidation of alkanes in trifluoroacetic acid: Urea-hydrogen peroxide/TFA as a convenient method for the oxidation of unactivated C-H bonds. *Chem. Commun.* 1311–1312 (2000).

163. Scher, D. P., Kelly, J. E., Huset, C. A., Barry, K. M., Hoffbeck, R. W., Yingling, V. L. & Messing, R. B. Occurrence of perfluoroalkyl substances (PFAS) in garden produce at homes with a history of PFAS-contaminated drinking water. *Chemosphere* **196**, 548–555 (2018).

164. Panikkar, B., Lemmond, B., Allen, L., Dipirro, C. & Kasper, S. Making the invisible visible: Results of a community-led health survey following PFAS contamination of drinking water in Merrimack, New Hampshire. *Environ. Heal. A Glob. Access Sci. Source* **18**, 1–16 (2019).

Appendix A

NMR Data of Pyridines and Pyridine/TFAA Mixtures

The ^{1}H and ^{13}C NMR spectra of the unreacted pyridines and pyridine with TFAA mixtures were discussed in Chapter Three. Within this chapter the peaks from each spectra were summarised in Table 2 and Table 3. The spectra from which these peaks were taken are seen below in Figures A1-A60.

TFAA

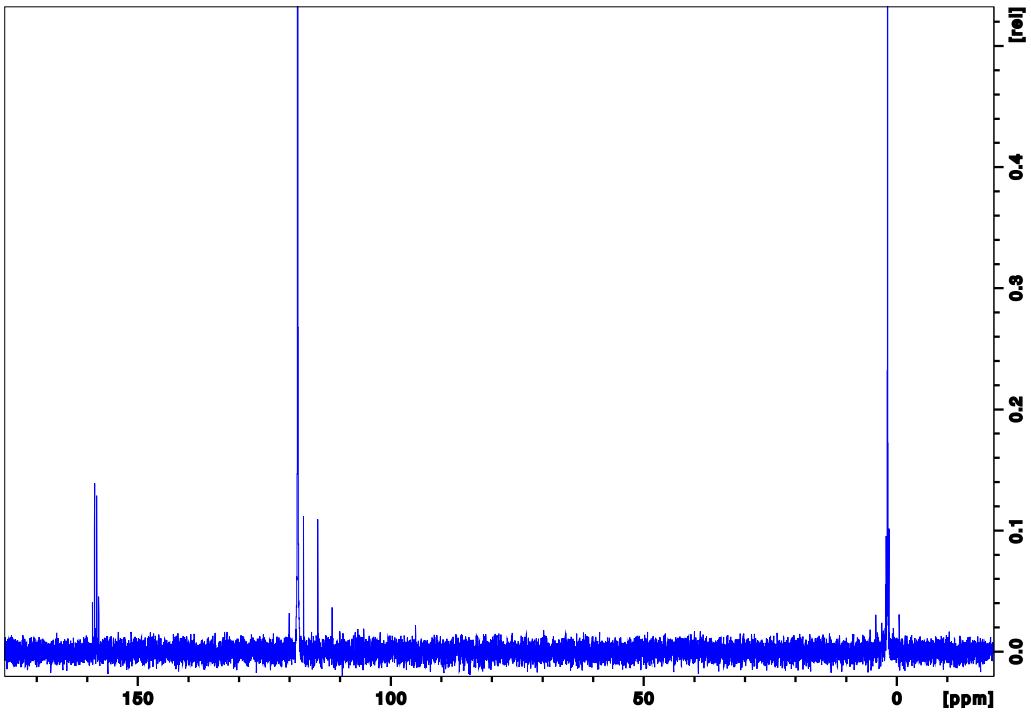

A1: ^{1}H NMR spectrum of TFAA

Pyridine

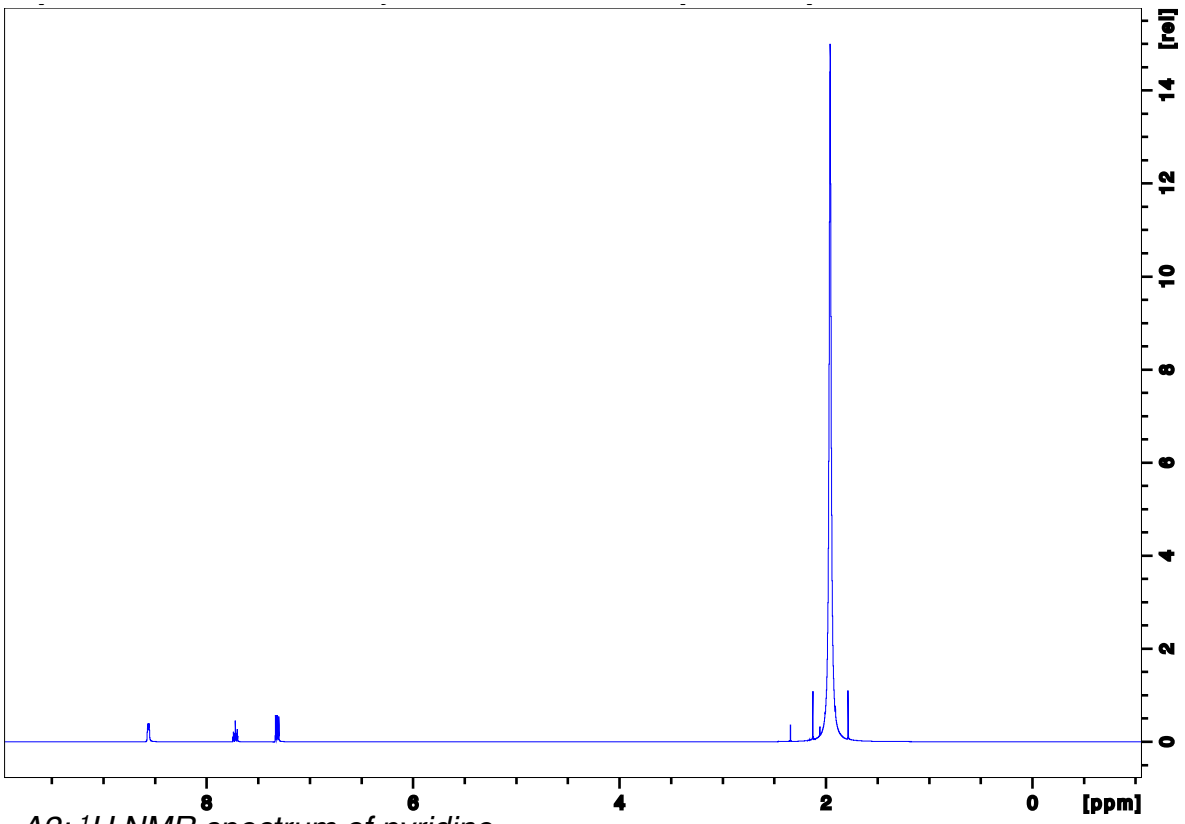

A2: ^{1}H NMR spectrum of pyridine

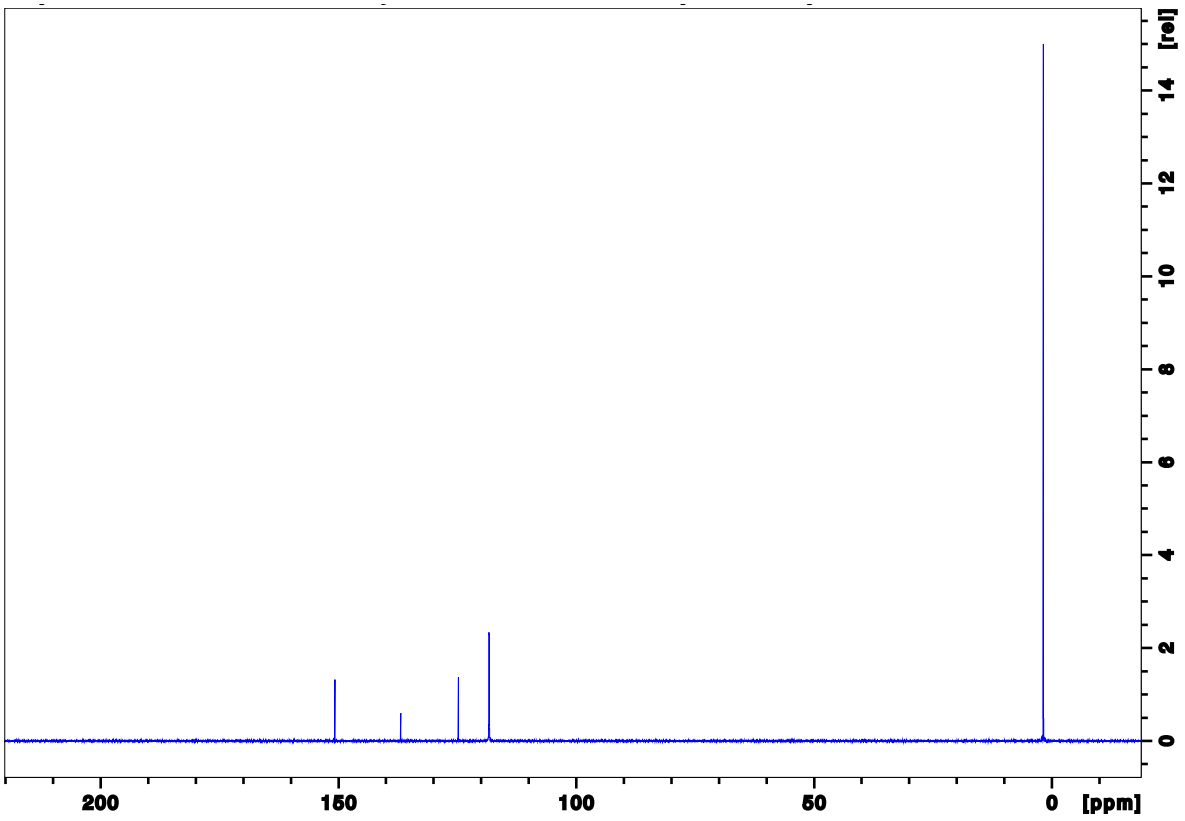

A3: ^{13}C NMR spectrum of pyridine

TFAA+Pyridine

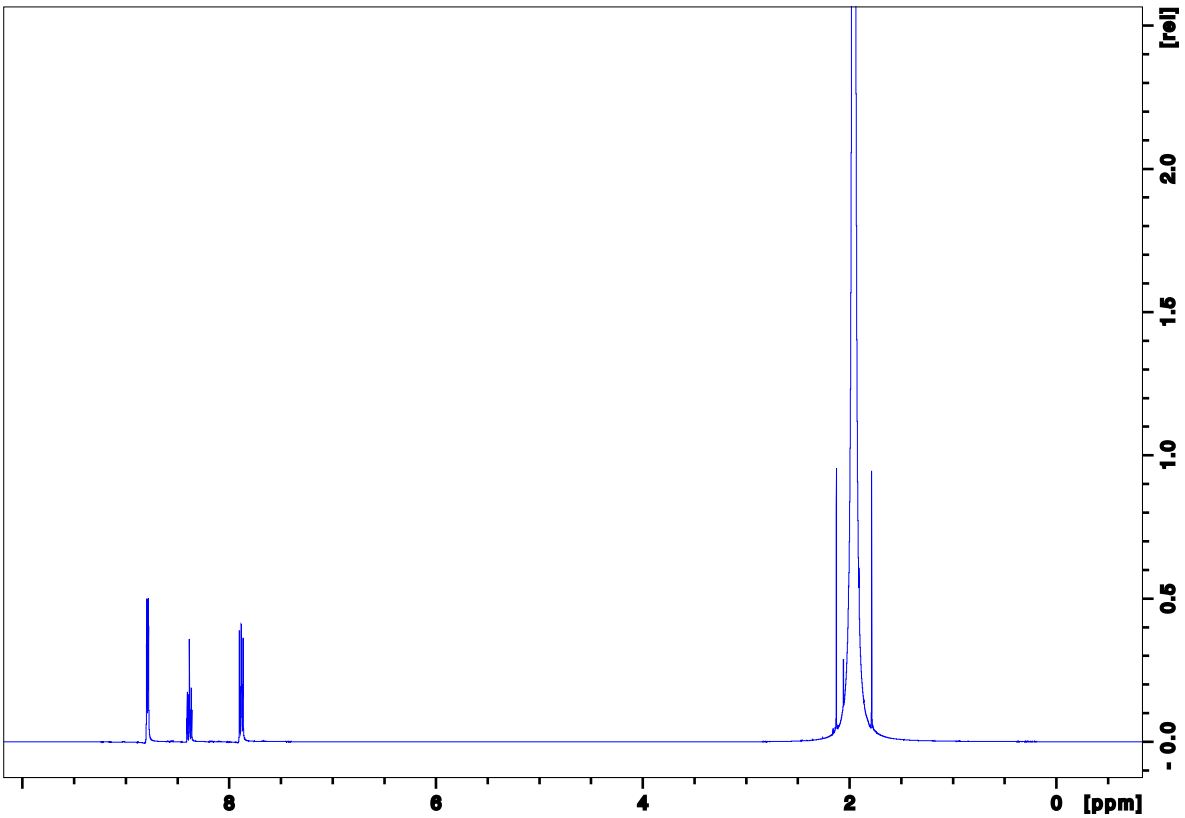

A4: ^{1}H NMR spectrum of TFAA+pyridine

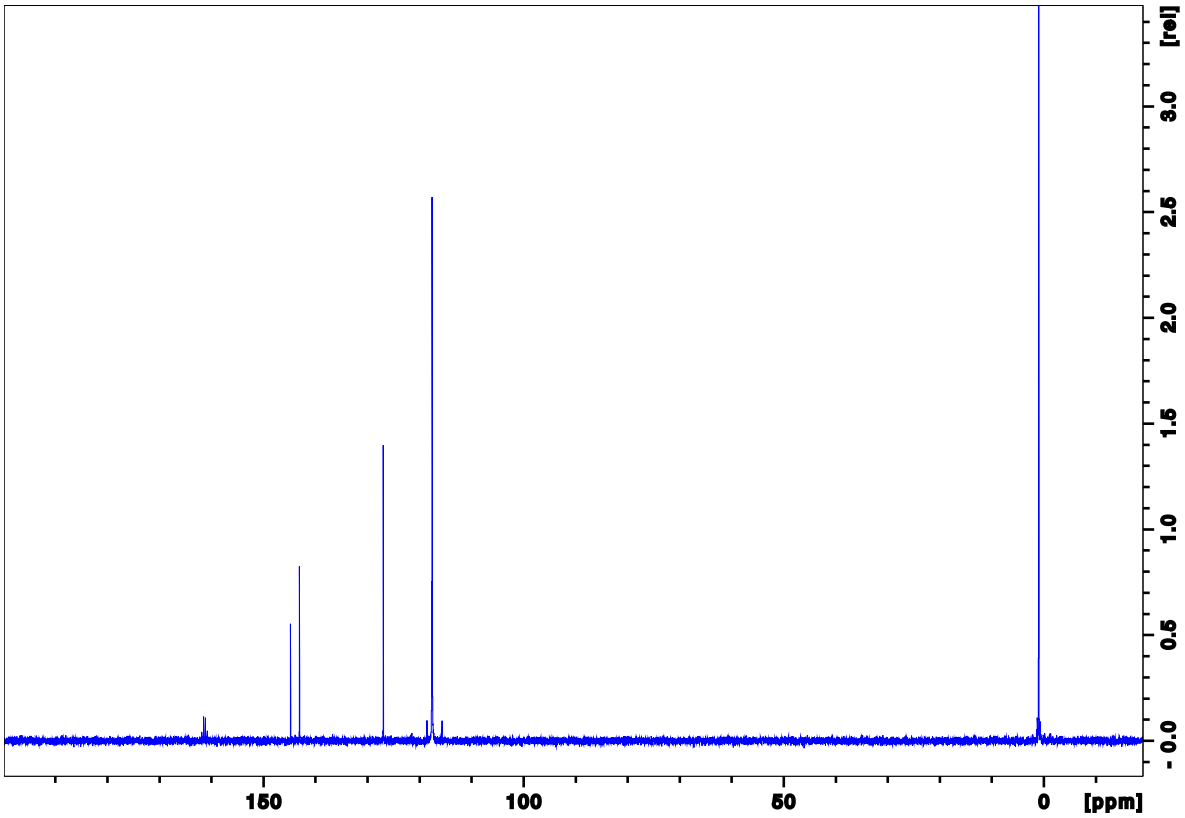

A5: ^{13}C NMR spectrum of TFAA+pyridine

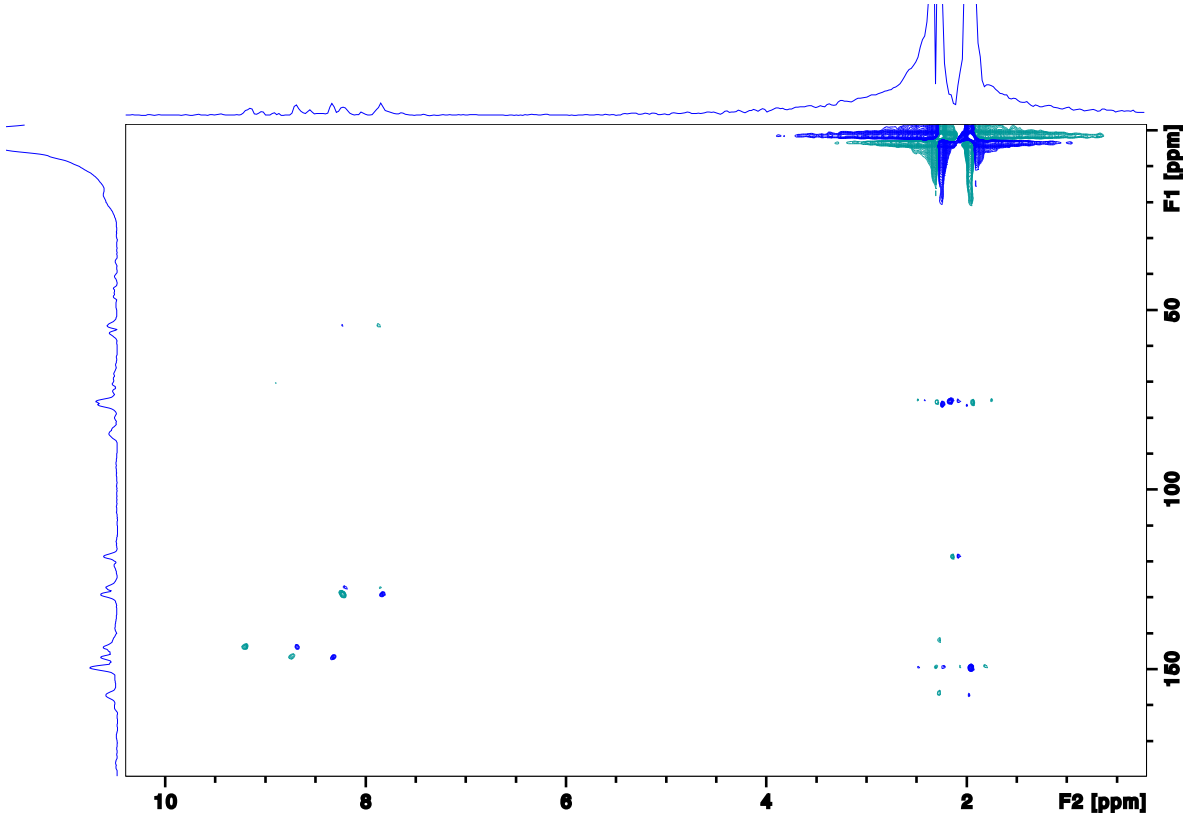

A6: HSQC NMR spectrum of TFAA+pyridine

DMAP

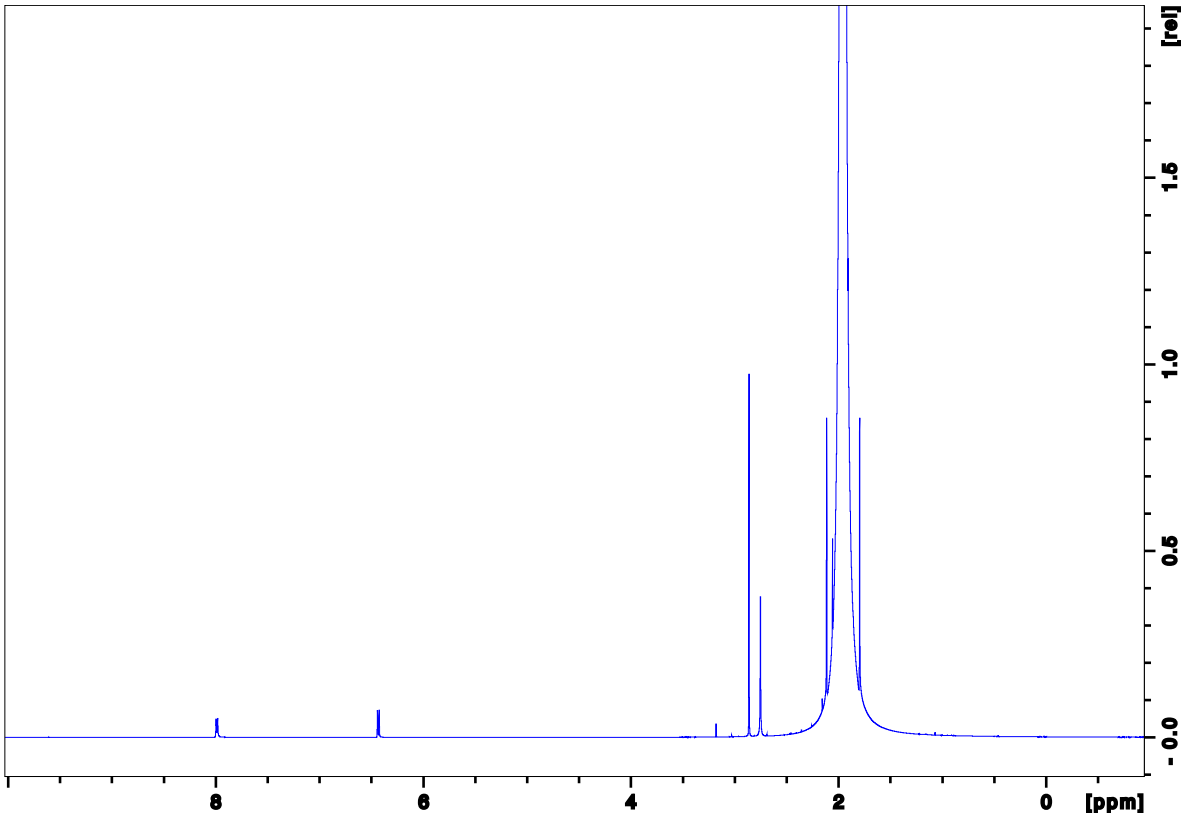

A7: ^{1}H NMR spectrum of DMAP

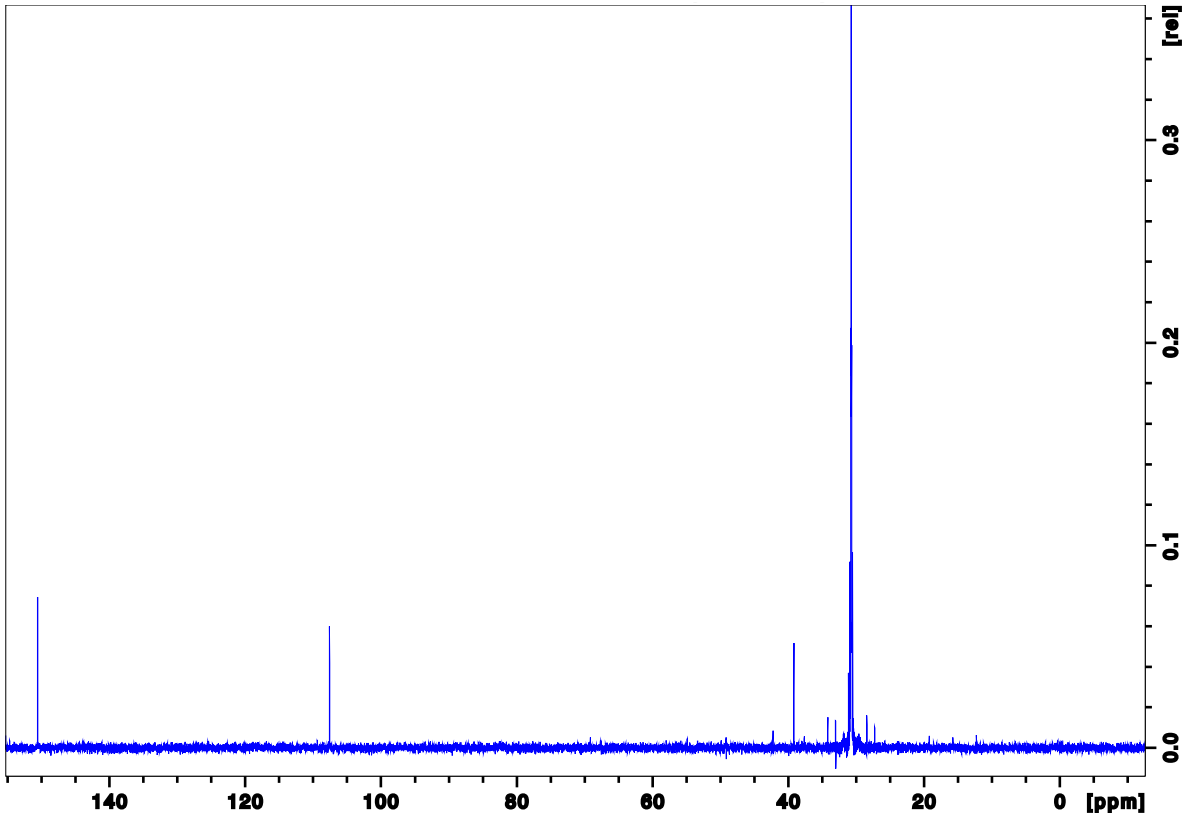

A8: ^{13}C NMR spectrum of DMAP

TFAA+DMAP

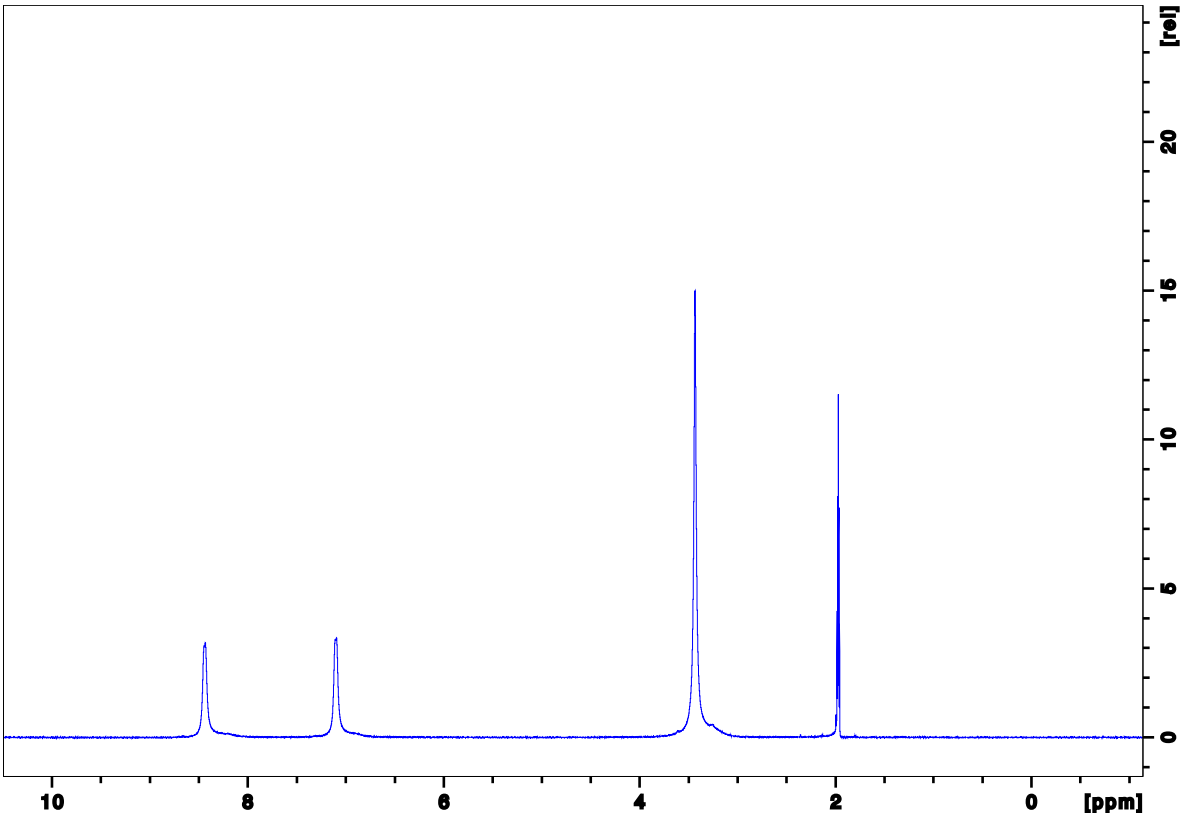

A9: ^{1}H NMR spectrum of TFAA+DMAP

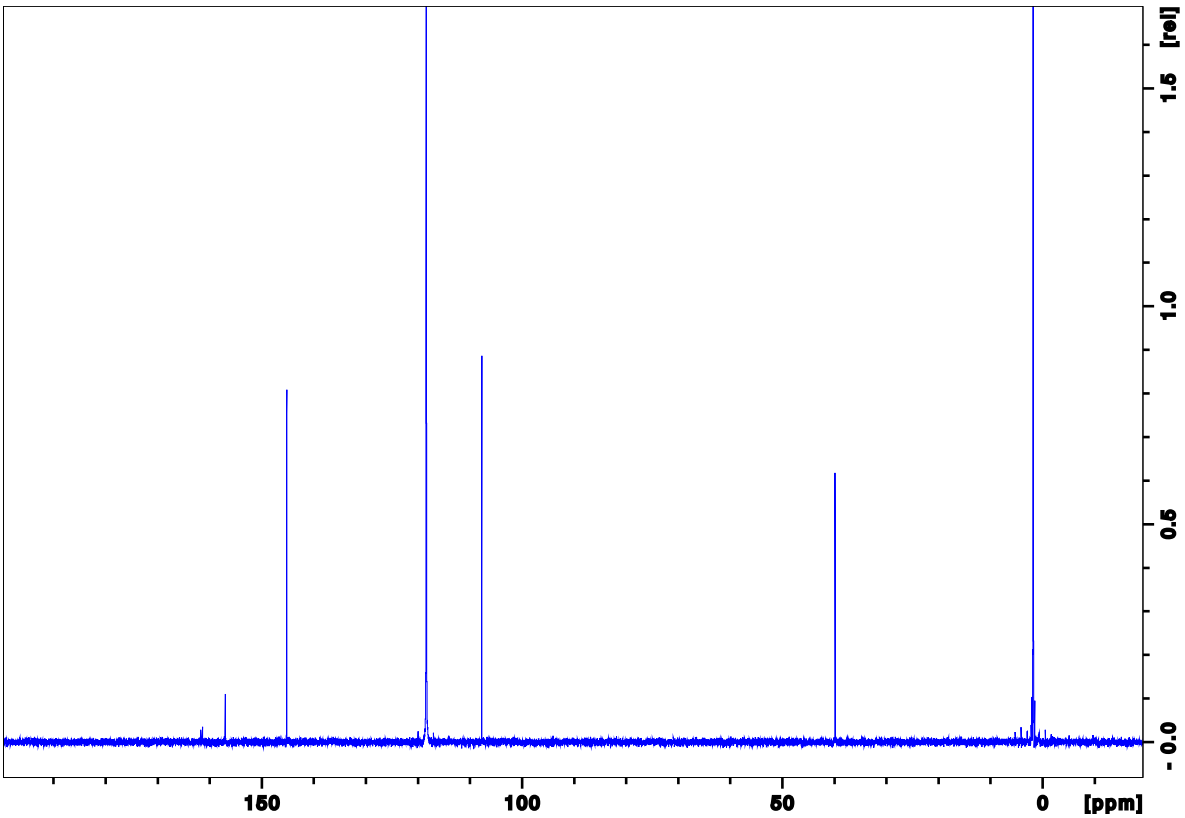

A10: ^{13}C NMR spectrum of TFAA+DMAP

2-bromo-4-methylpyridine

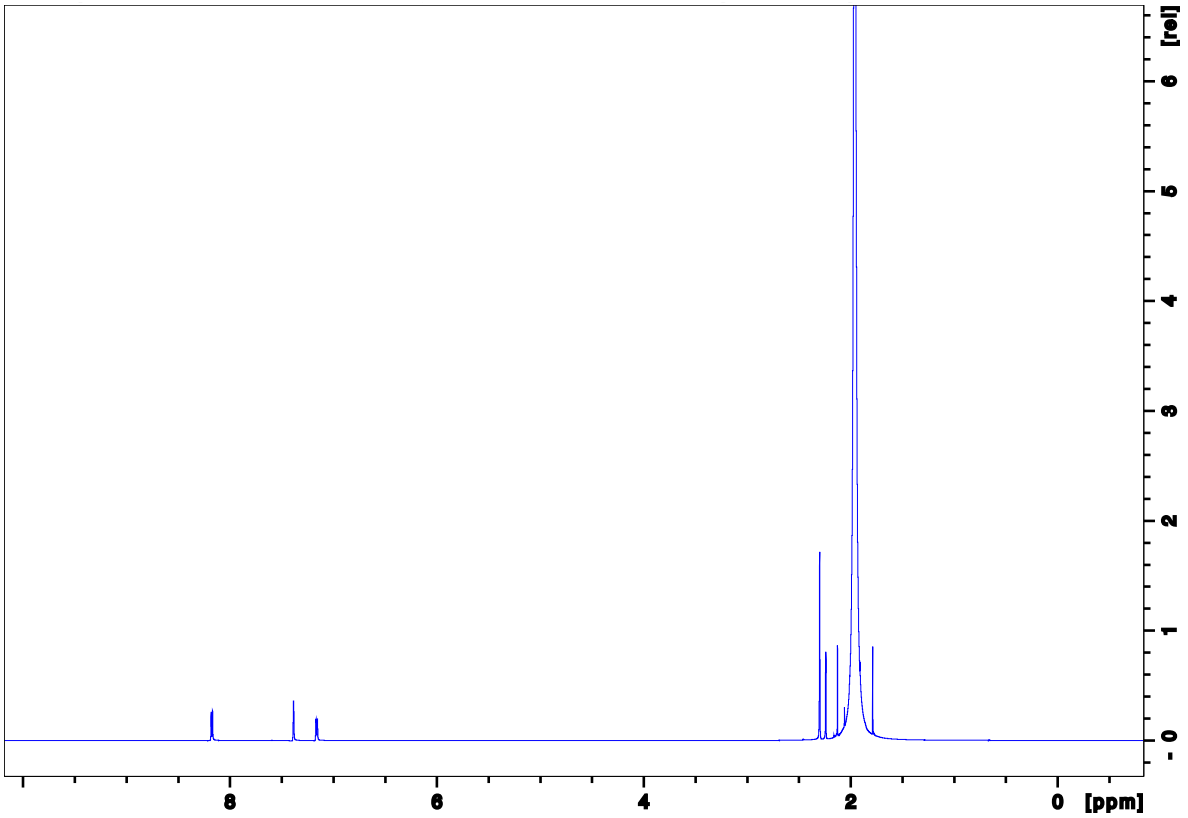

A11: ^{1}H NMR spectrum of 2-bromo-4-methylpyridine

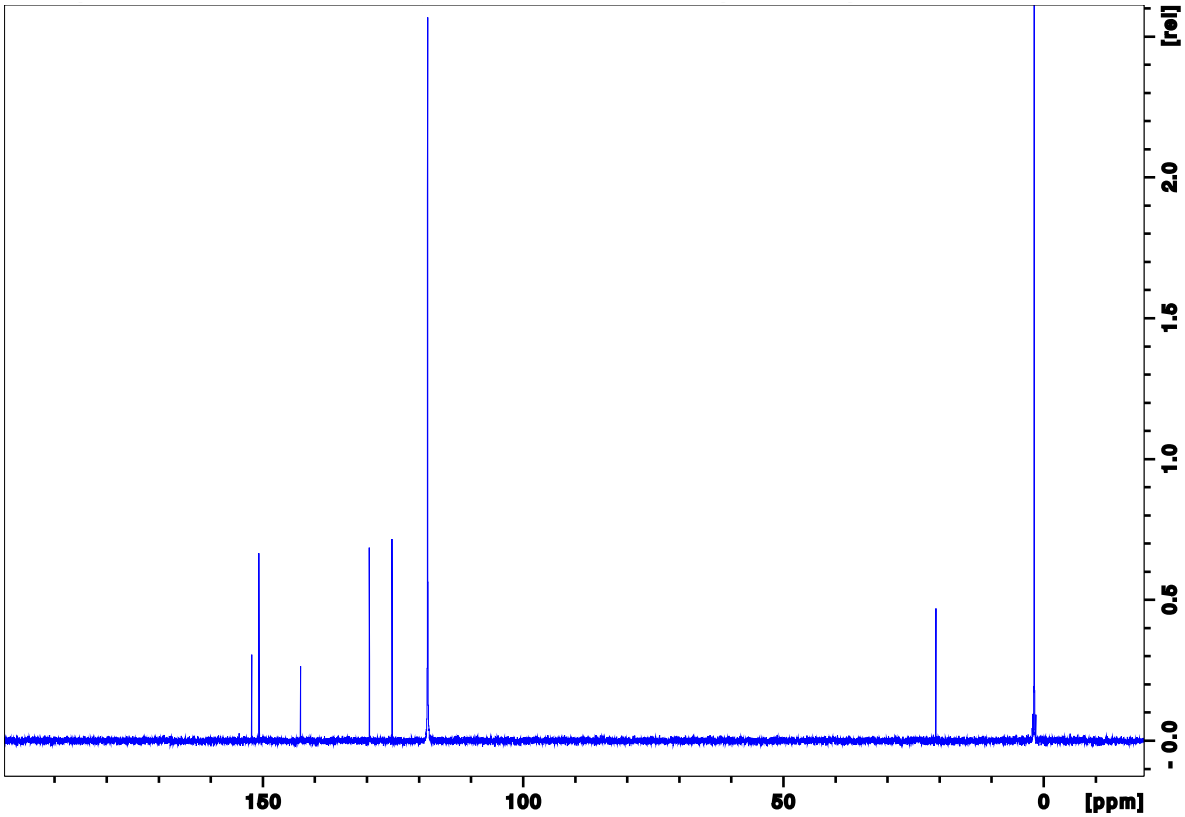

A12: ^{13}C NMR spectrum of 2-bromo-4-methylpyridine

TFAA+2-bromo-4-methylpyridine

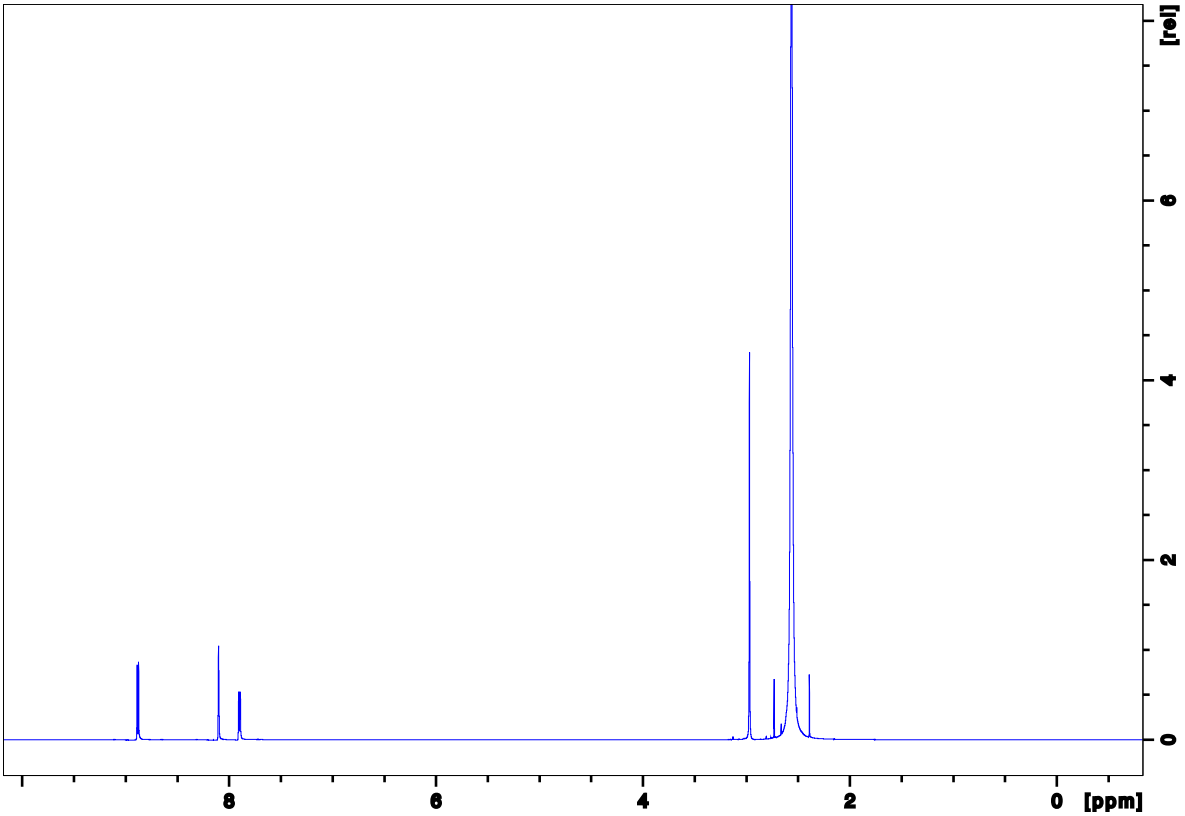

A13: ^{1}H NMR spectrum of TFAA+2-bromo-4-methylpyridine

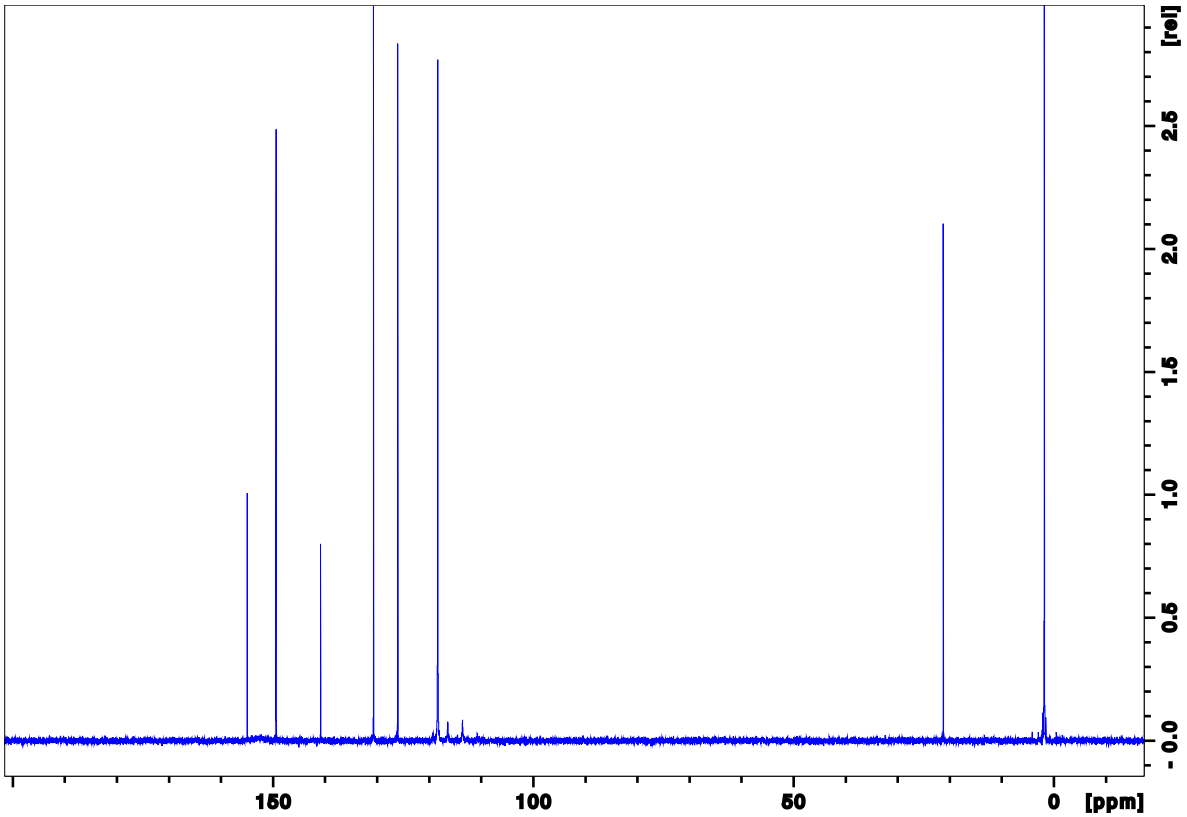

A14: ^{13}C NMR spectrum of TFAA+2-bromo-4-methylpyridine

3-bromopyridine

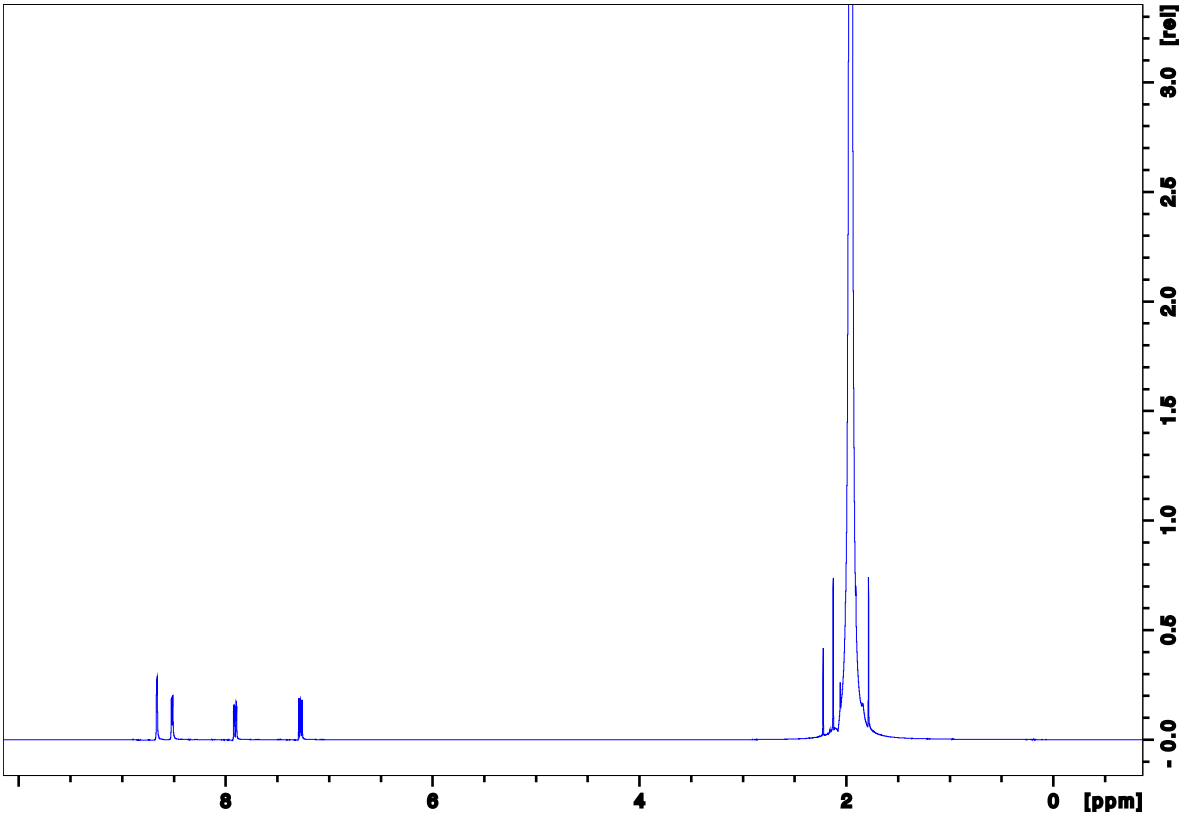

A14: ^{1}H NMR spectrum of 3-bromopyridine

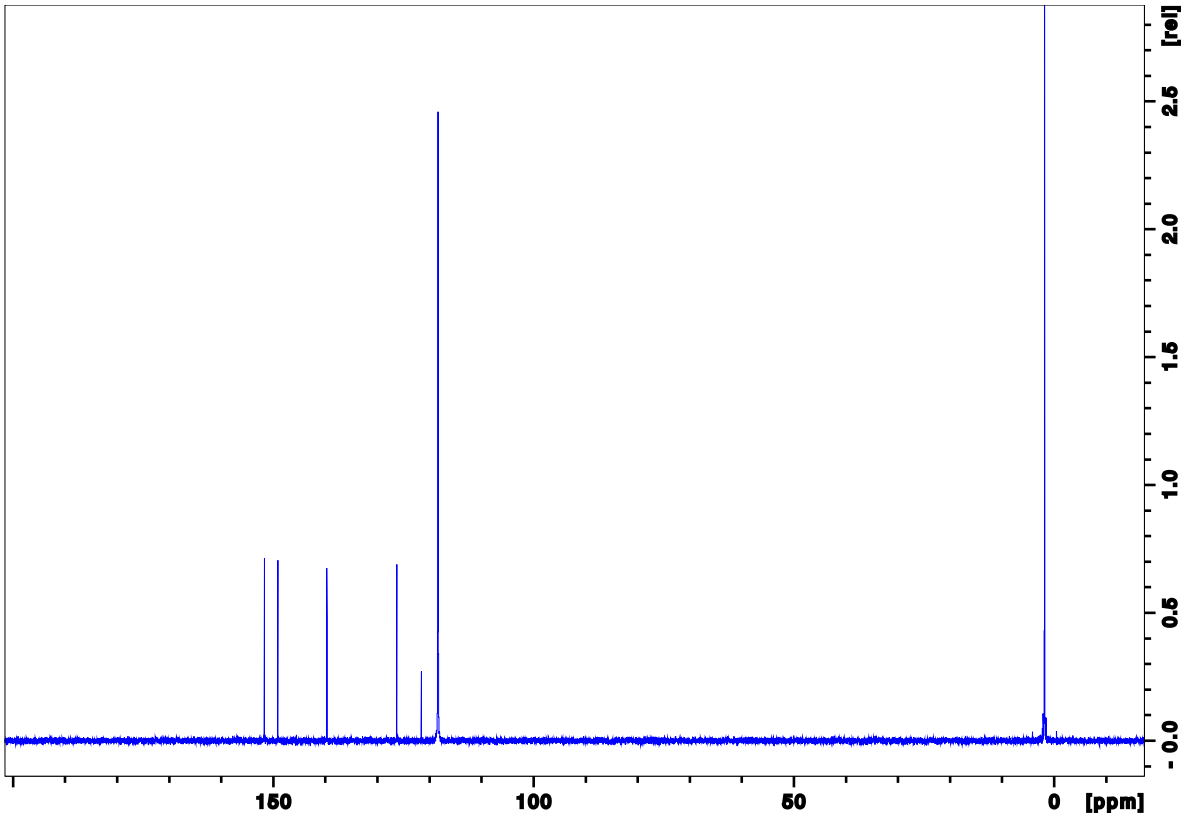

A15: ^{13}C NMR spectrum of 3-bromopyridine

TFAA+3-bromopyridine

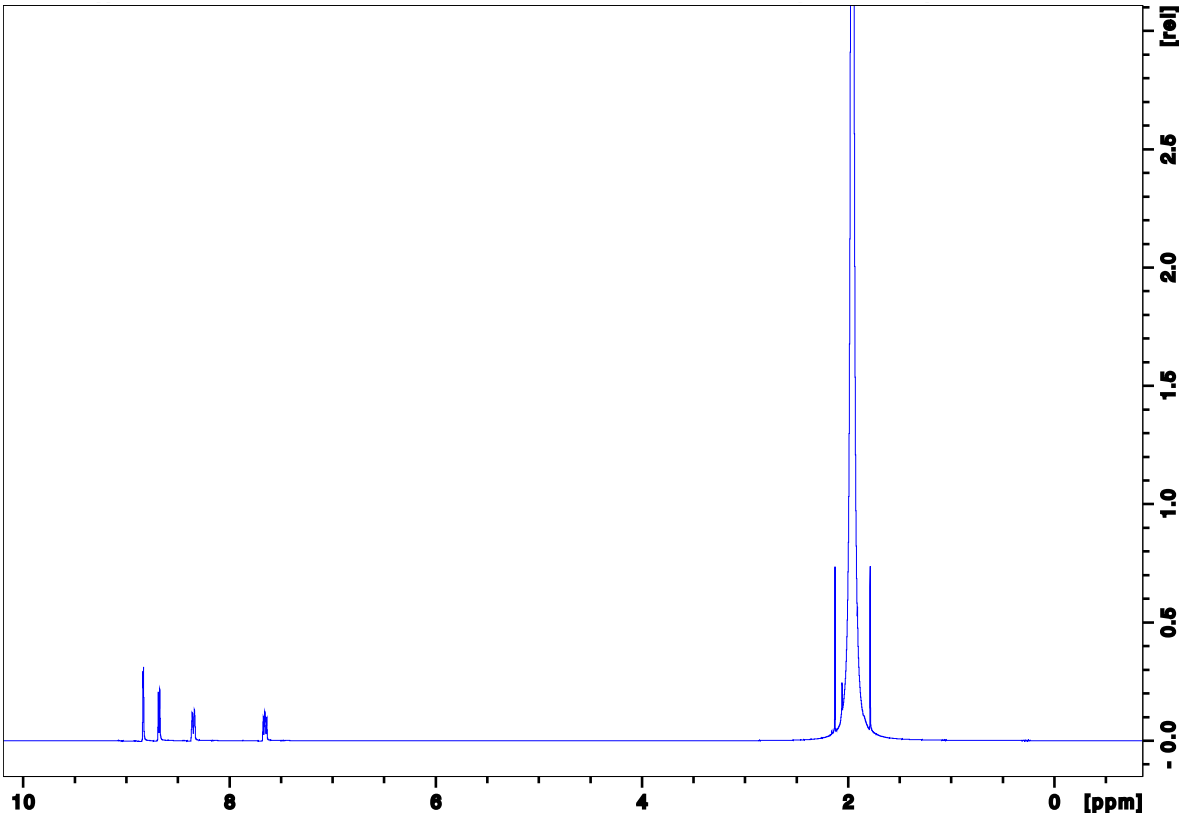

A16: ^{1}H NMR spectrum of TFAA_3-bromopyridine

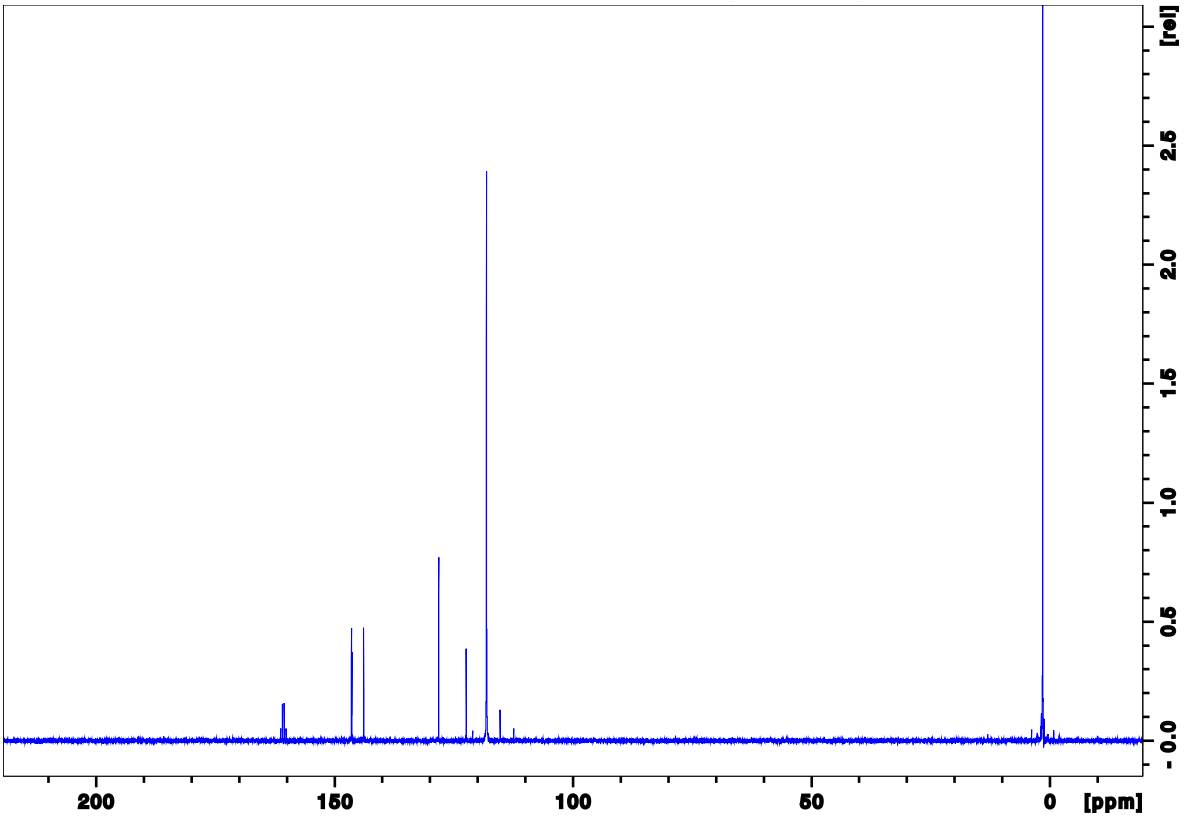

A17: ^{13}C NMR spectrum of TFAA+3-bromopyridine

2-iodopyridine

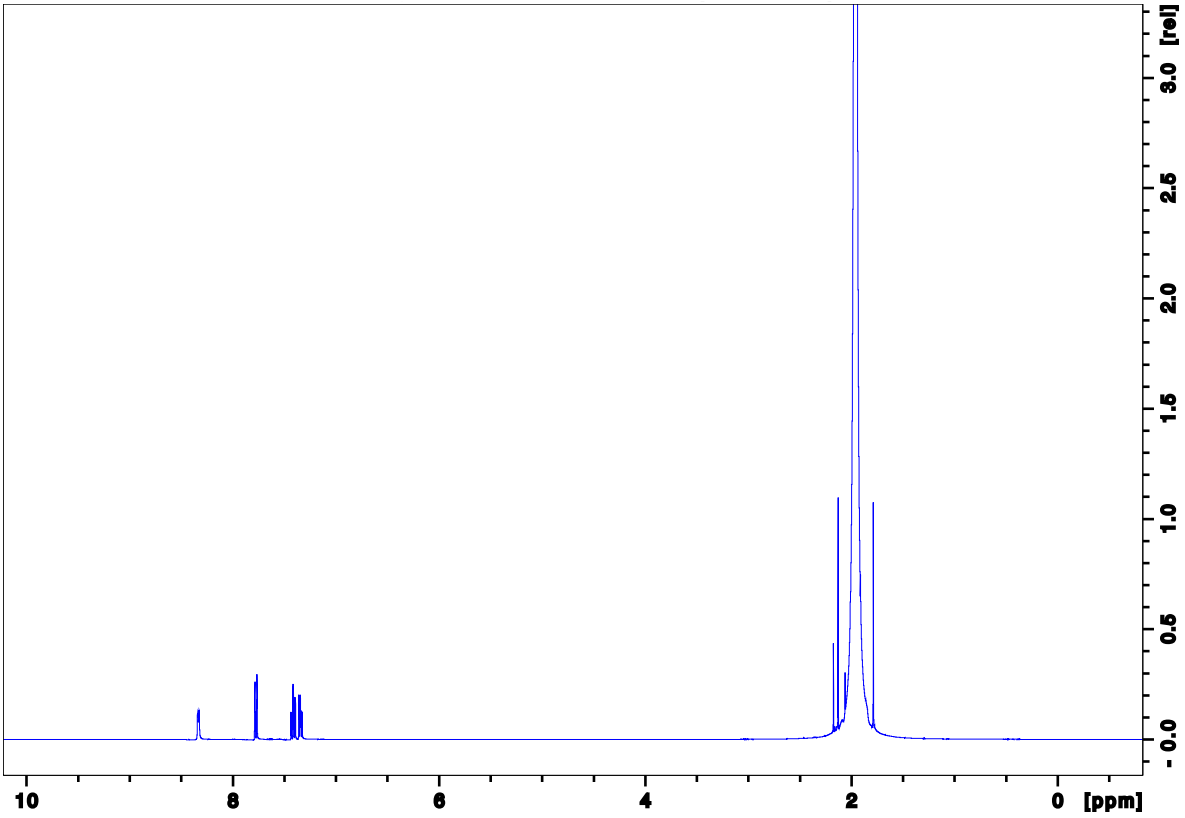

A18: ^{1}H NMR spectrum of 2-iodopyridine

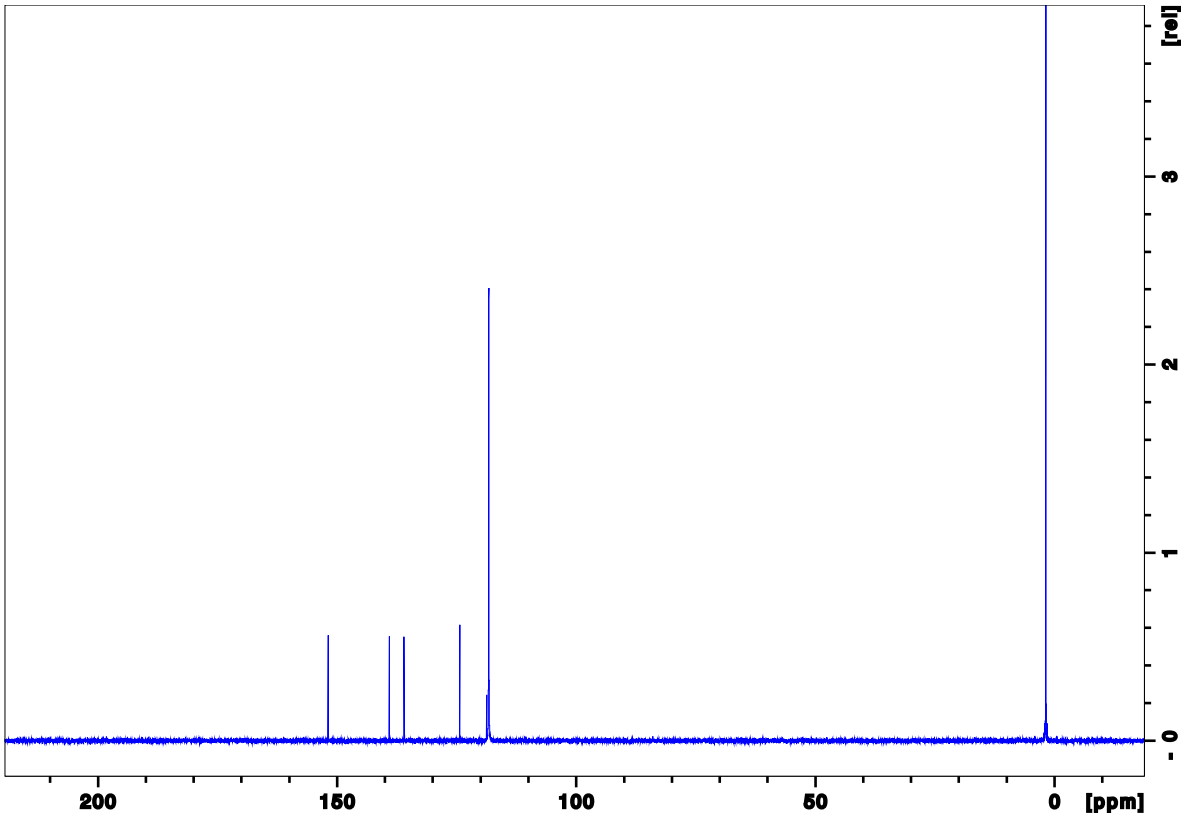

A19: ^{13}C NMR spectrum of 2-iodopyridine

TFAA+2-iodopyridine

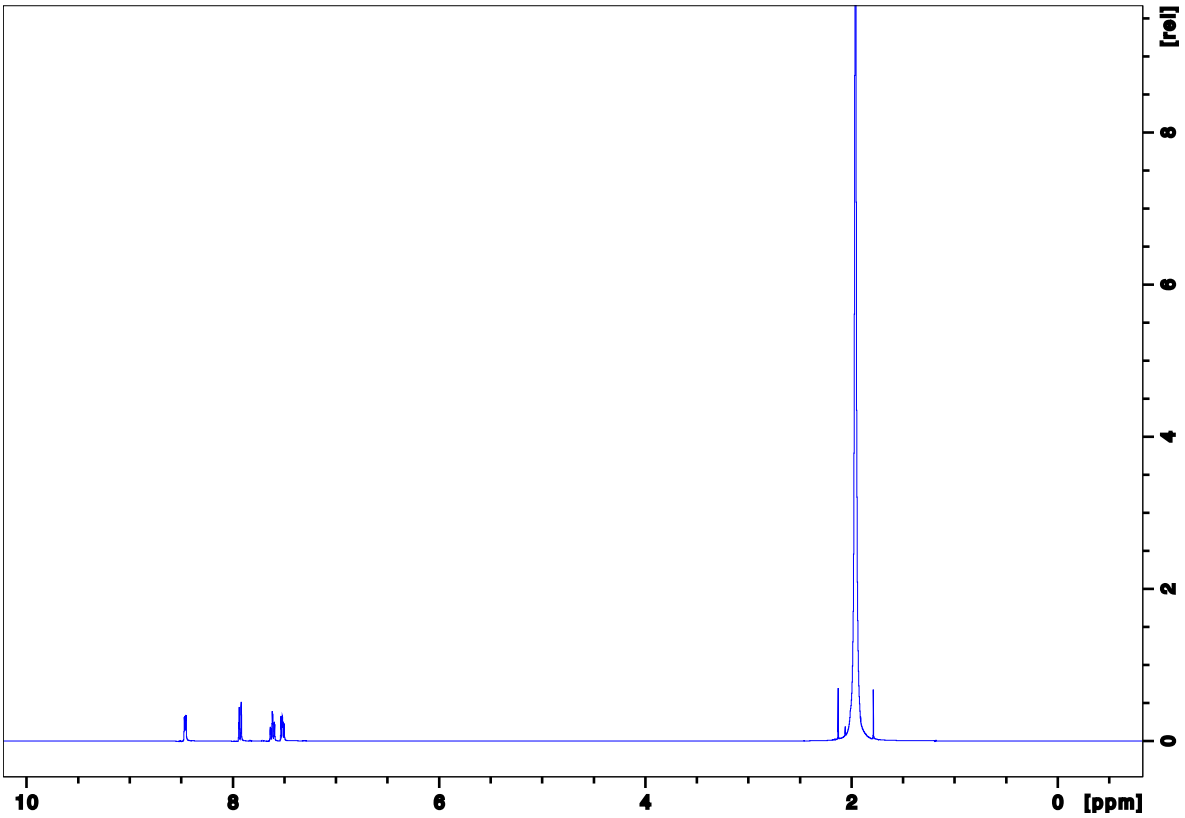

A20: ^{1}H NMR spectrum of TFAA+2-iodopyridine

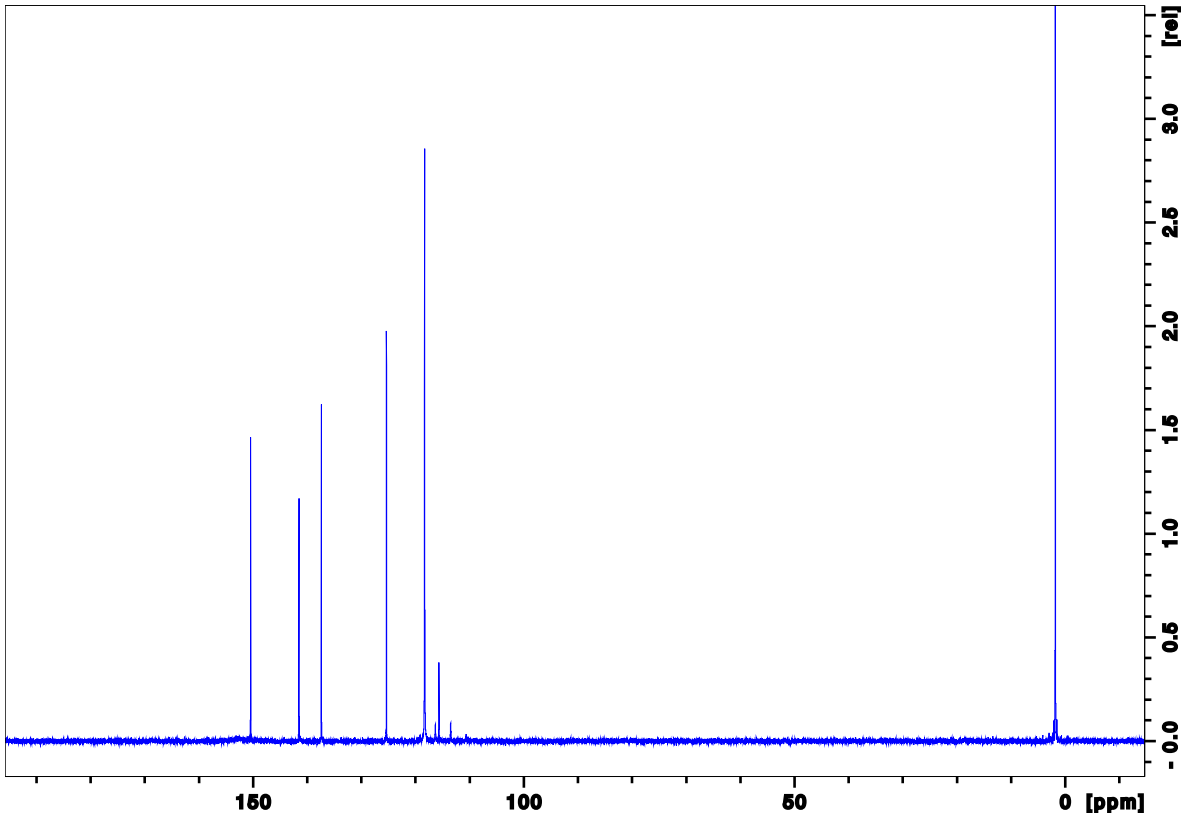

A21: ^{1}H NMR spectrum of TFAA+2-iodopyridine

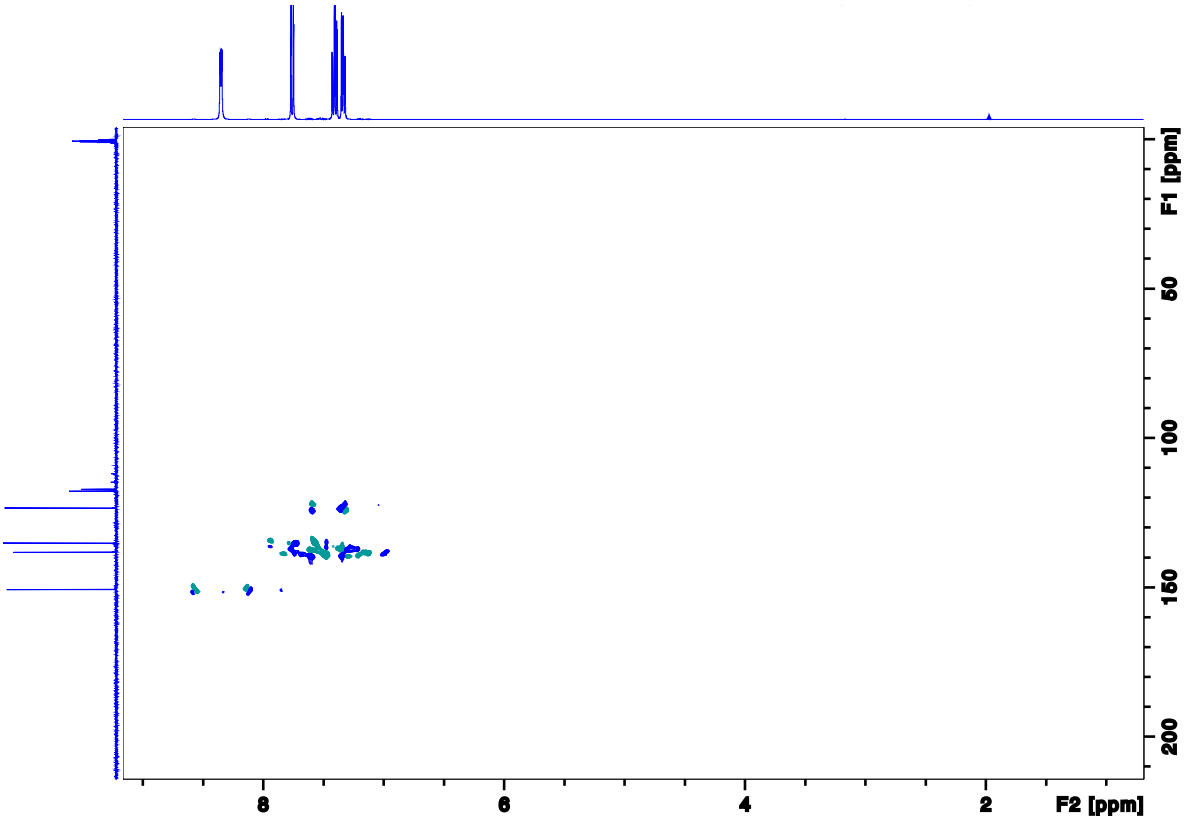

A22: HSQC NMR spectrum of TFAA+2-iodopyridine

2-methylpyridine

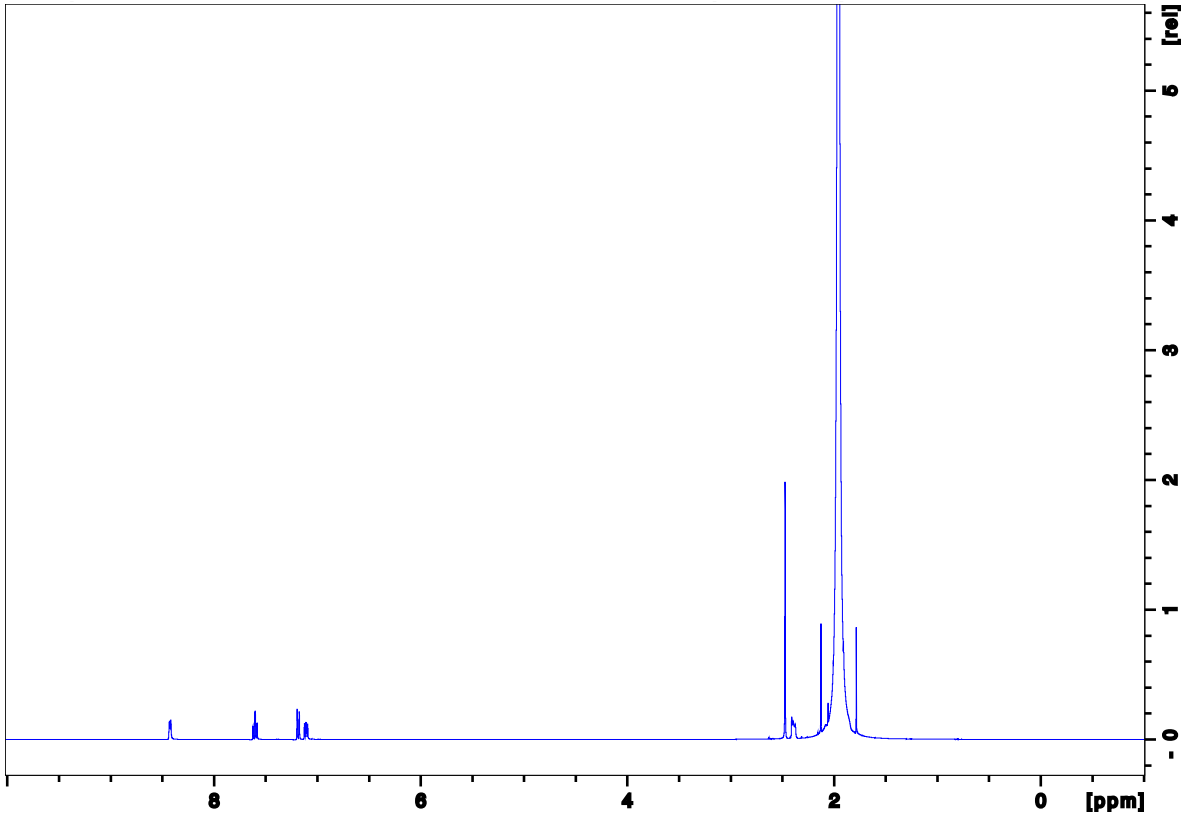

A23: ^{1}H NMR spectrum of 2-methylpyridine

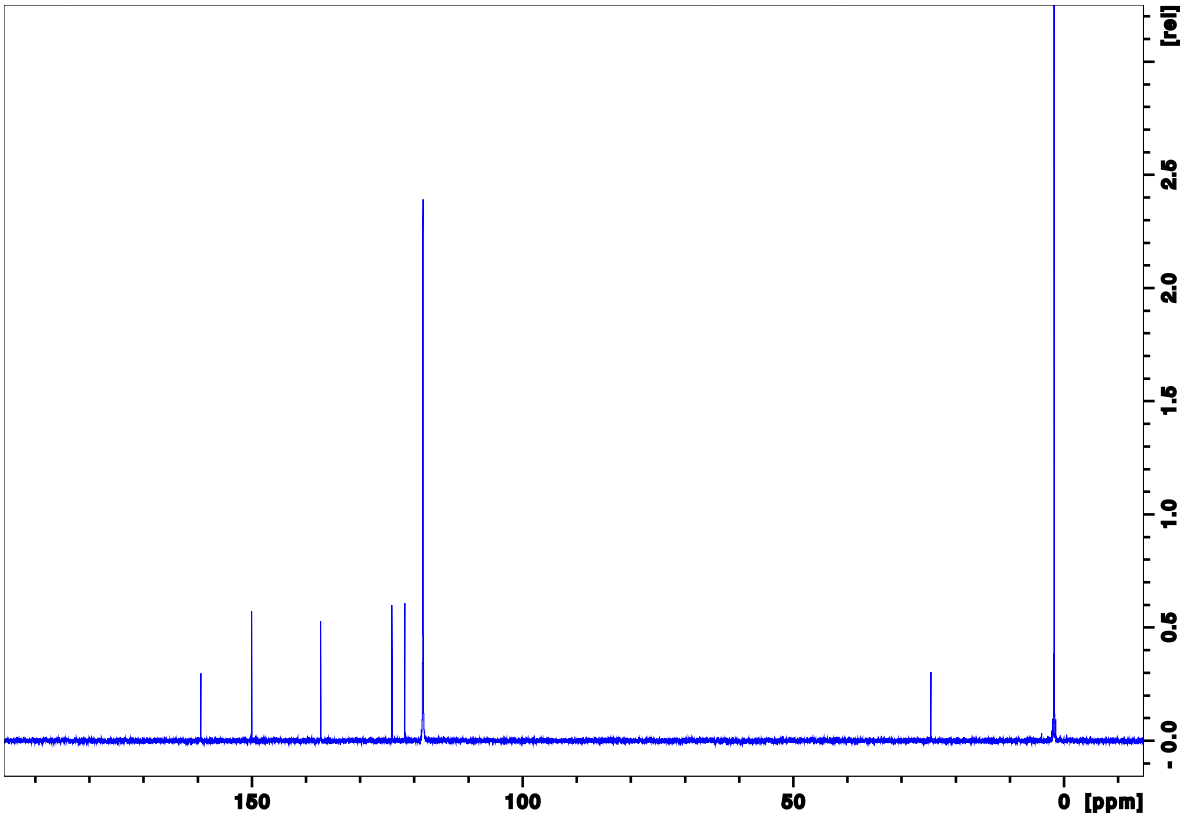

A24: ^{13}C NMR spectrum of 2-methylpyridine

TFAA+2-methylpyridine

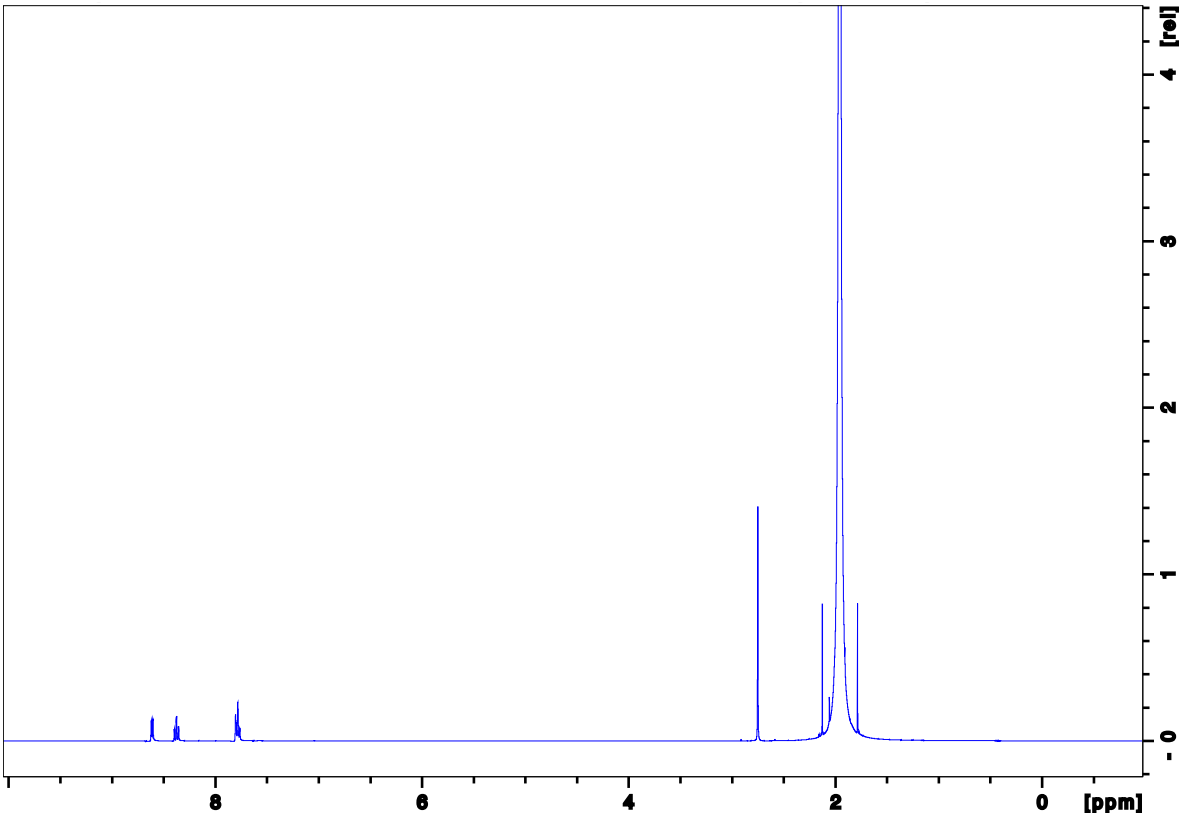

A25: ^{1}H NMR spectrum of TFAA+2-methylpyridine

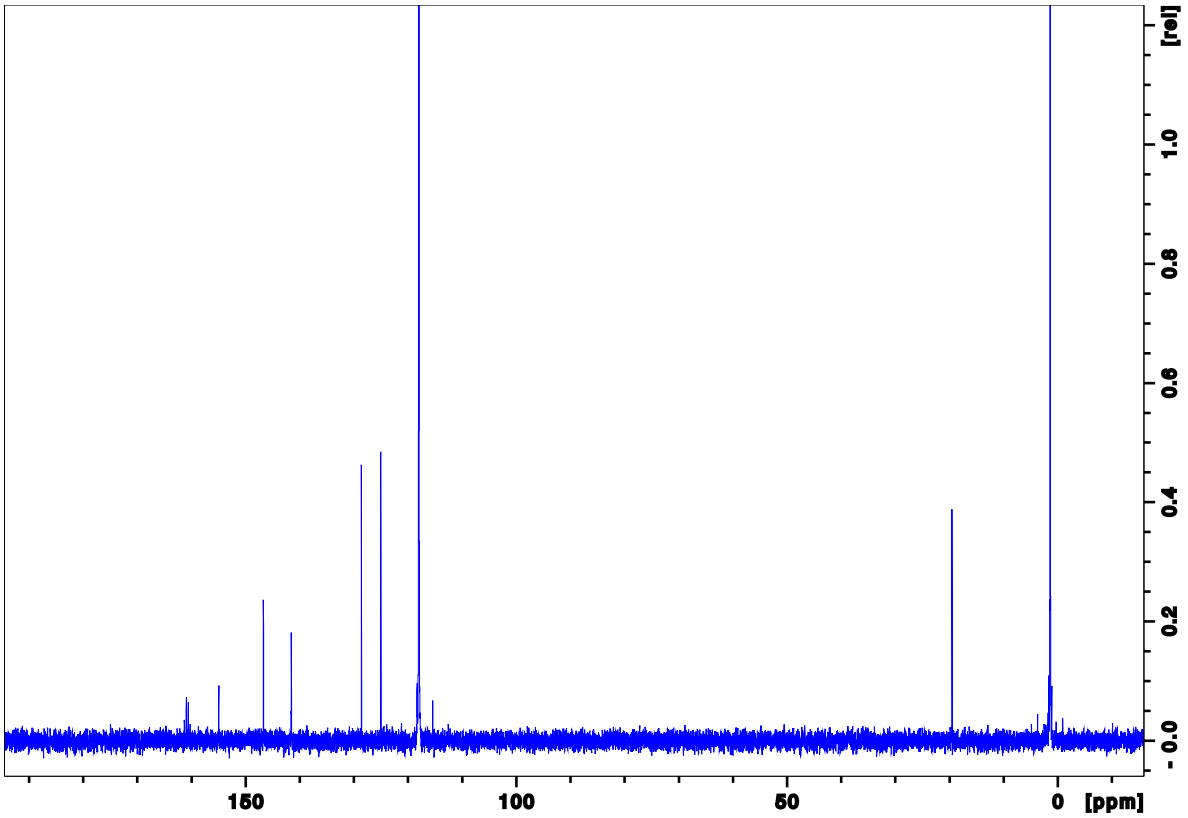

A26: ^{13}C NMR spectrum of TFAA+2-methylpyridine

3-methylpyridine

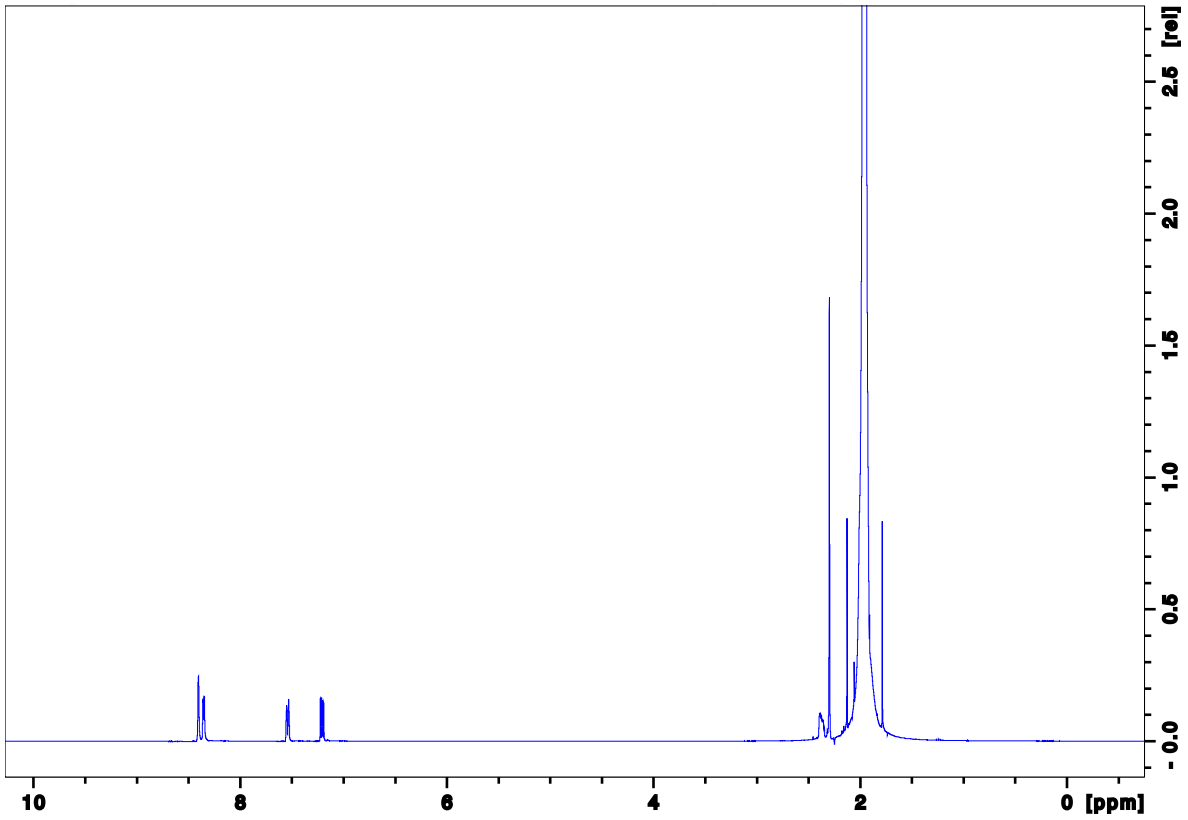

A27: ^{1}H NMR spectrum of 3-methylpyridine

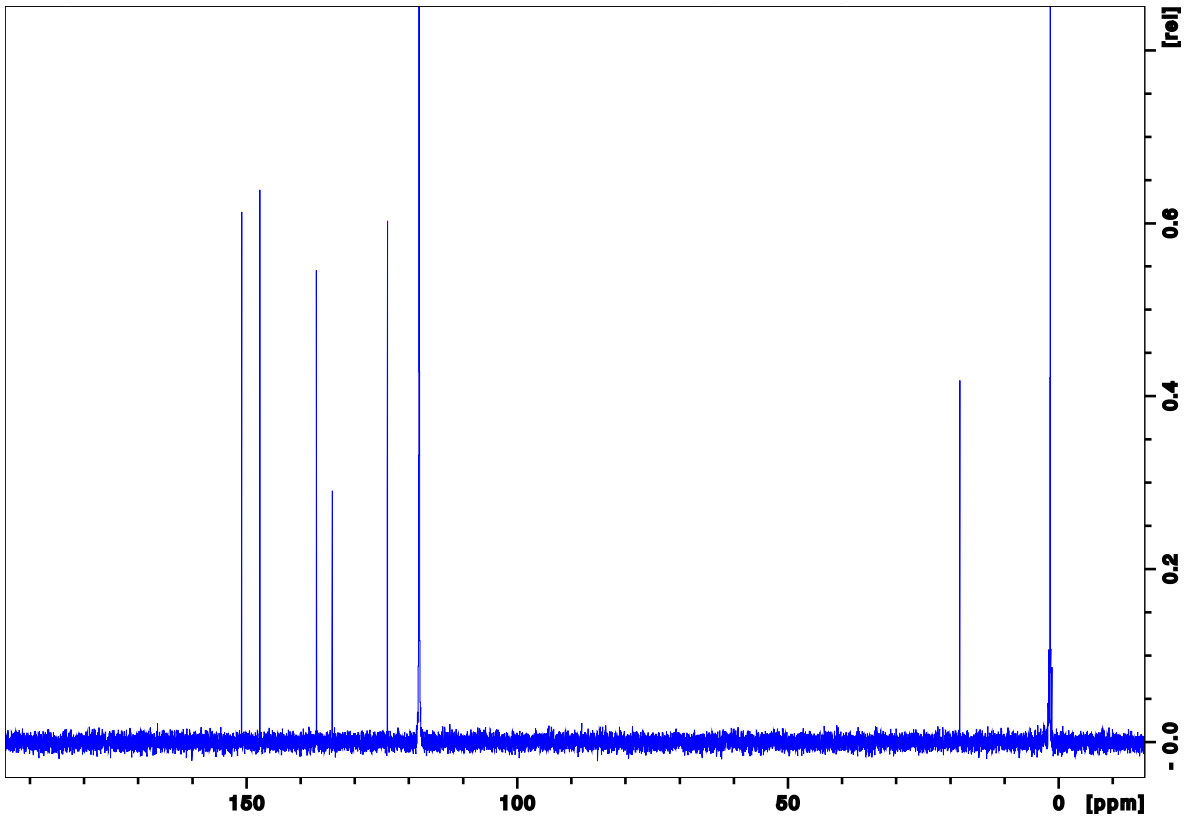

A28: ^{13}C NMR spectrum of 3-methylpyridine

TFAA+3-methylpyridine

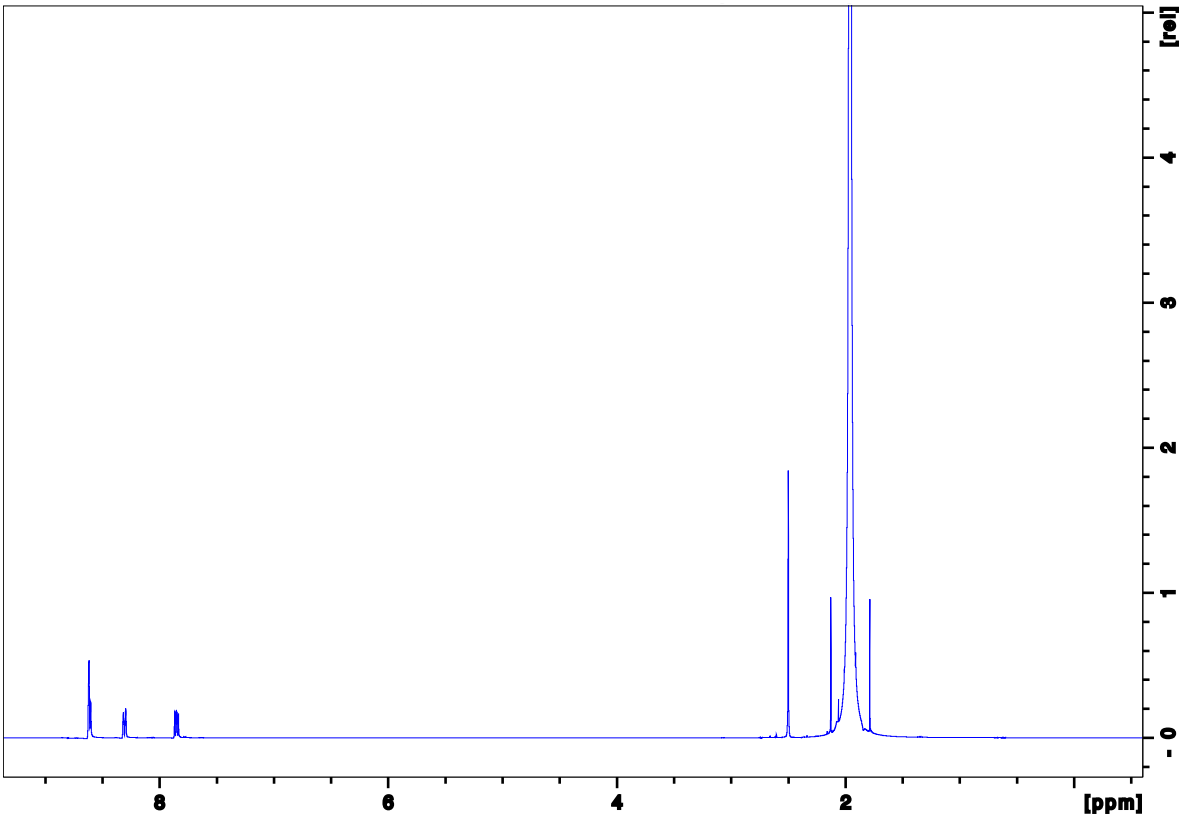

A29: ^{1}H NMR spectrum of TFAA+3-methylpyridine

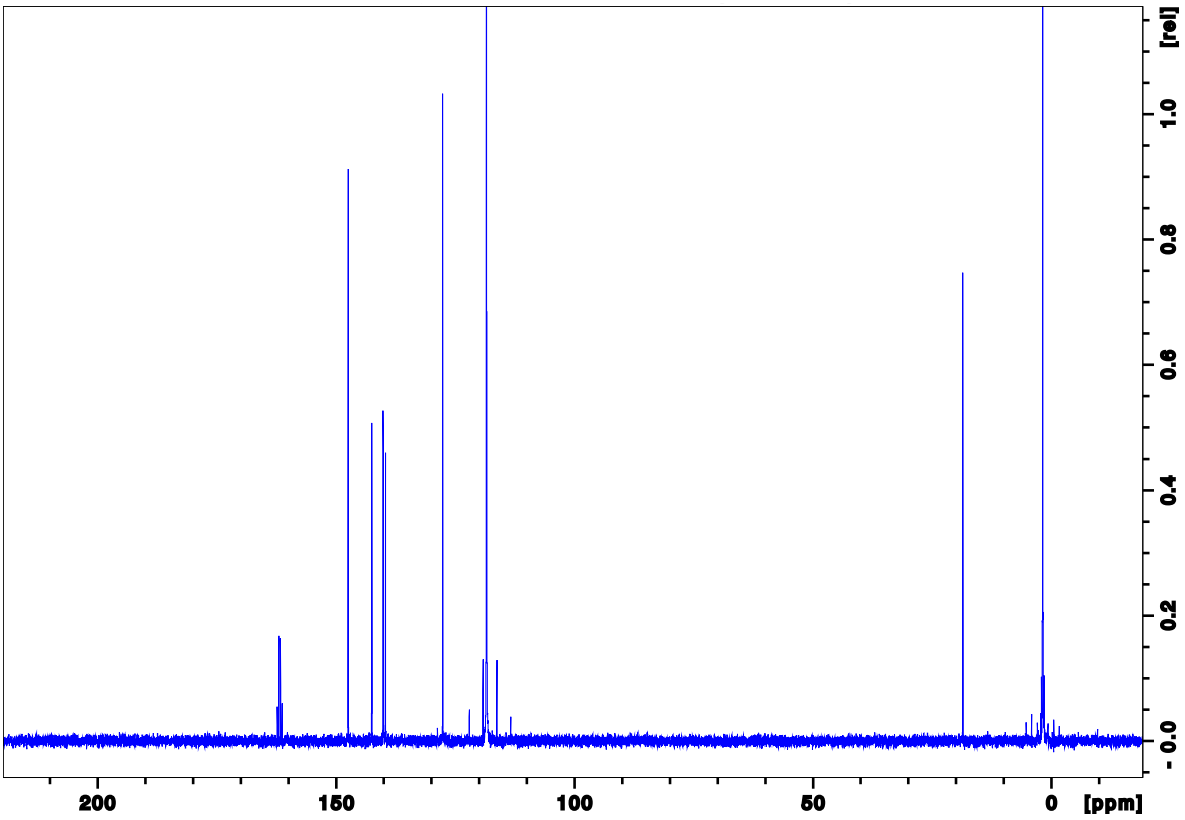

A30: ^{13}C NMR spectrum of TFAA+3methylpyridine

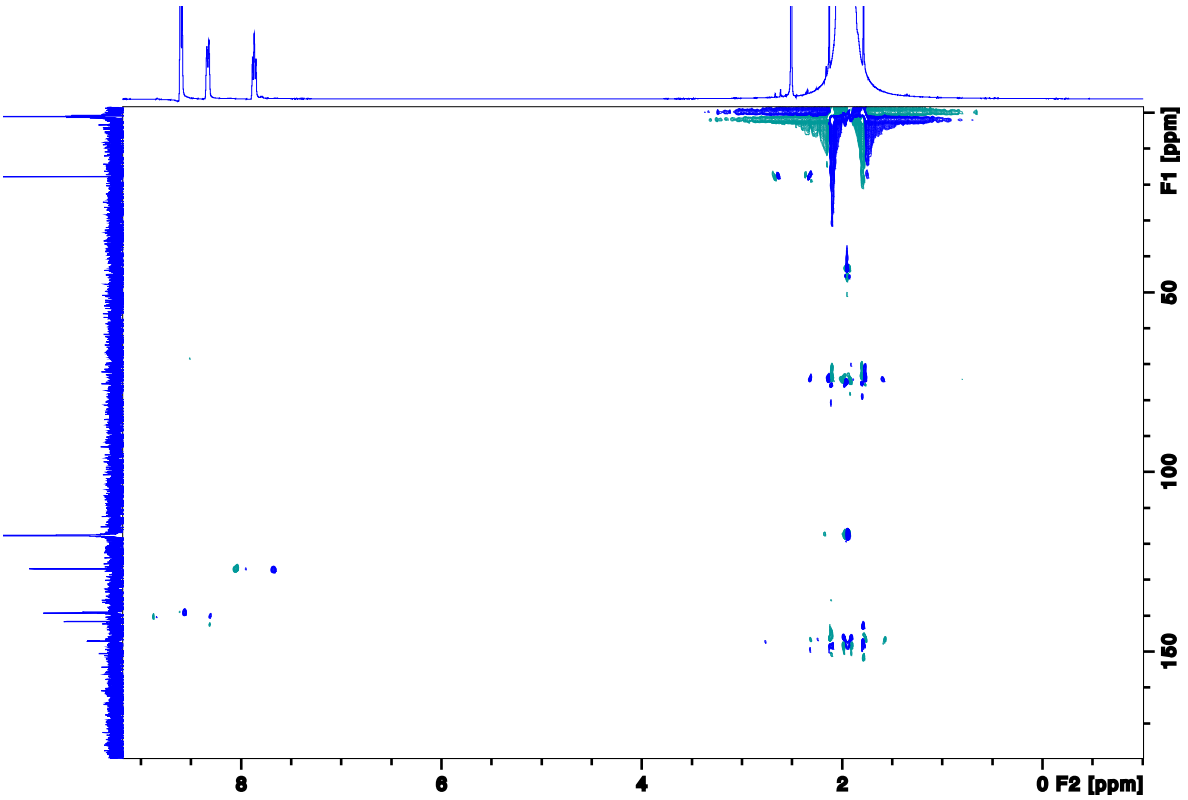

A31: HSQC NMR spectrum of TFAA

4-methylpyridine

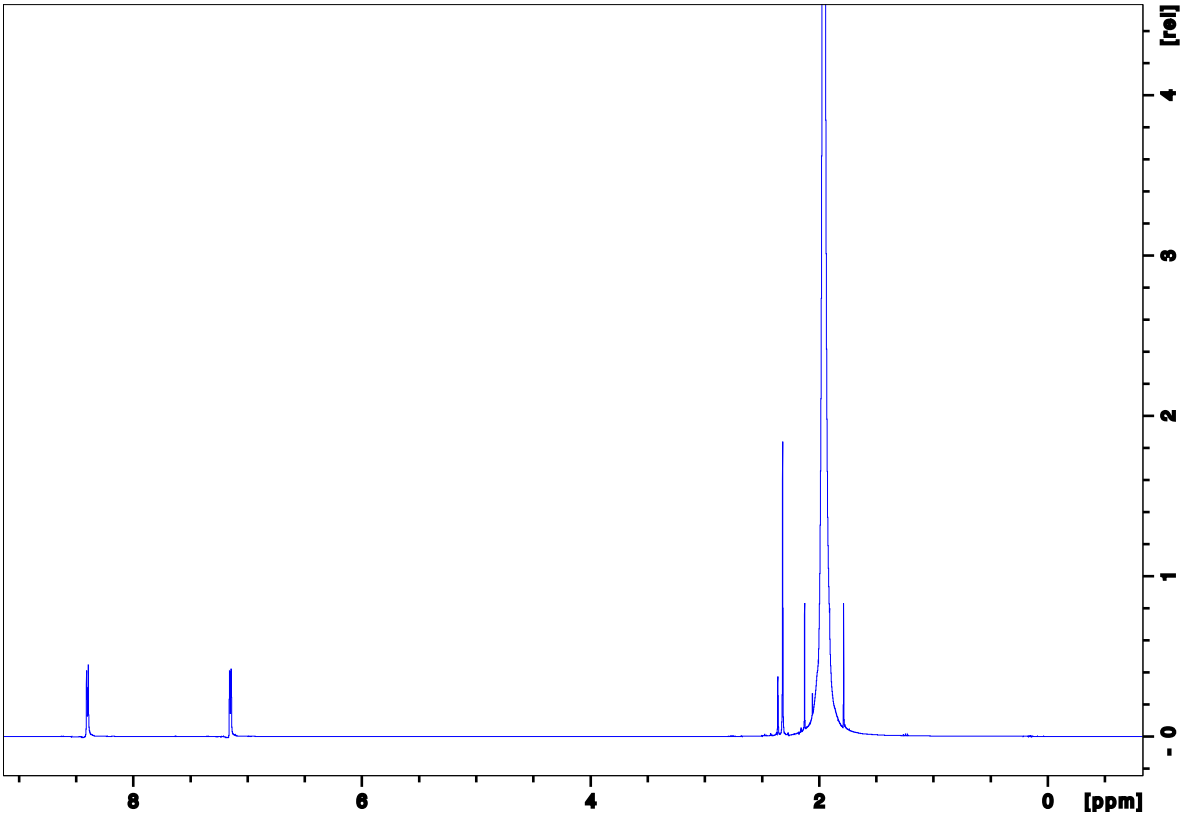

A32: ^{1}H NMR spectrum of 4-methylpyridine

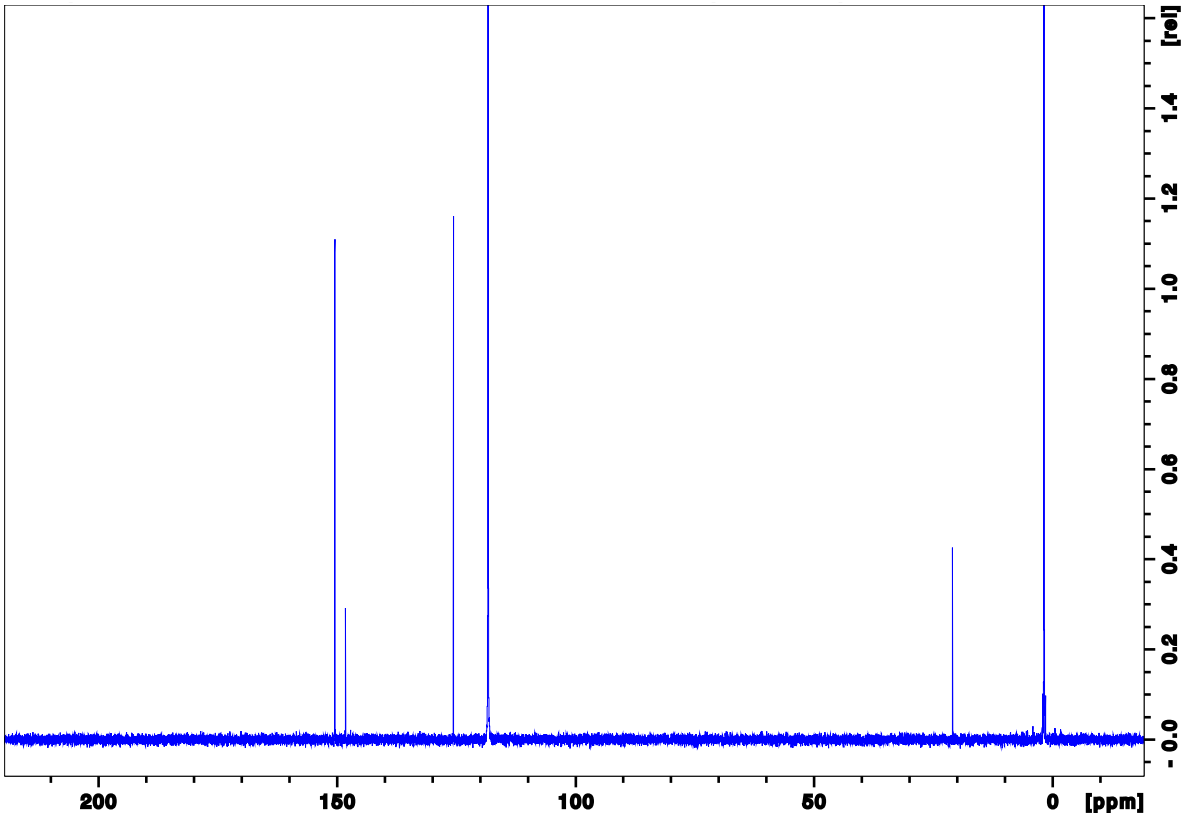

A33: ^{13}C NMR spectrum of 4-methylpyridine

TFAA+4-methylpyridine

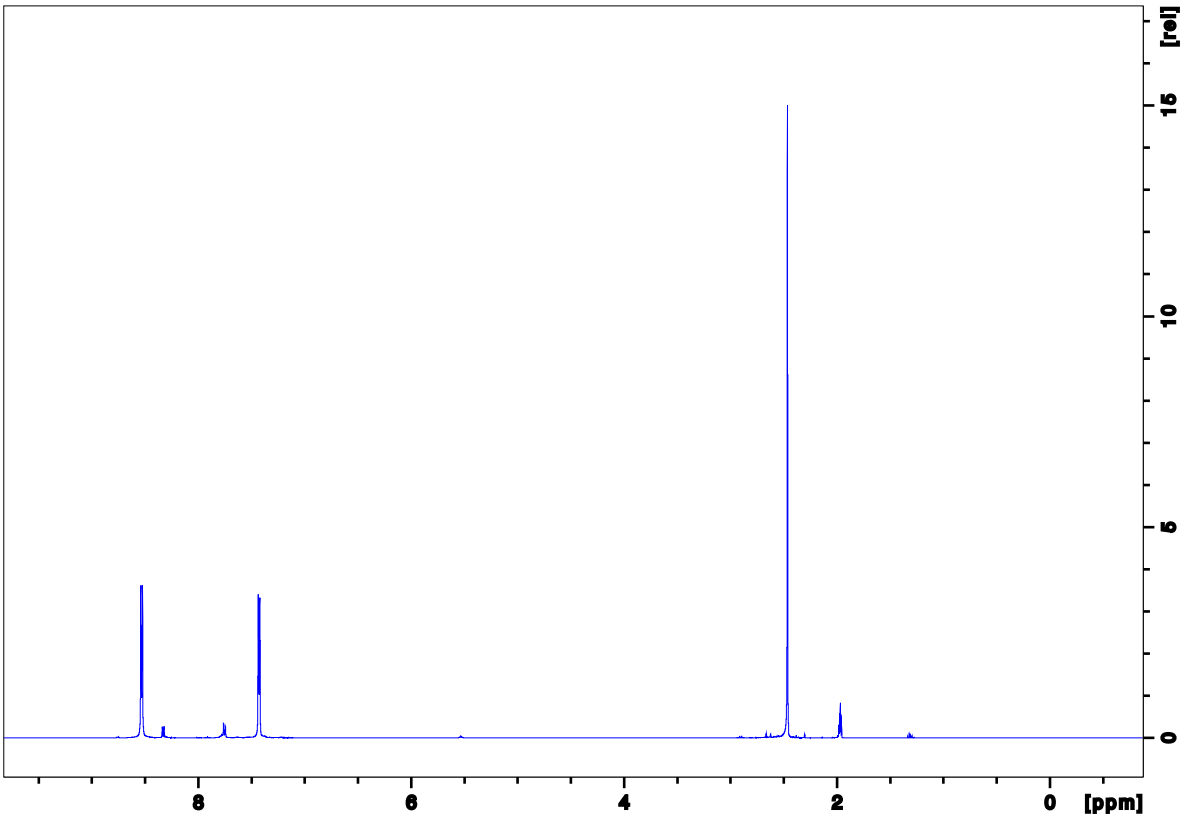

A34: ^{1}H NMR spectrum of TFAA+4-methylpyridine

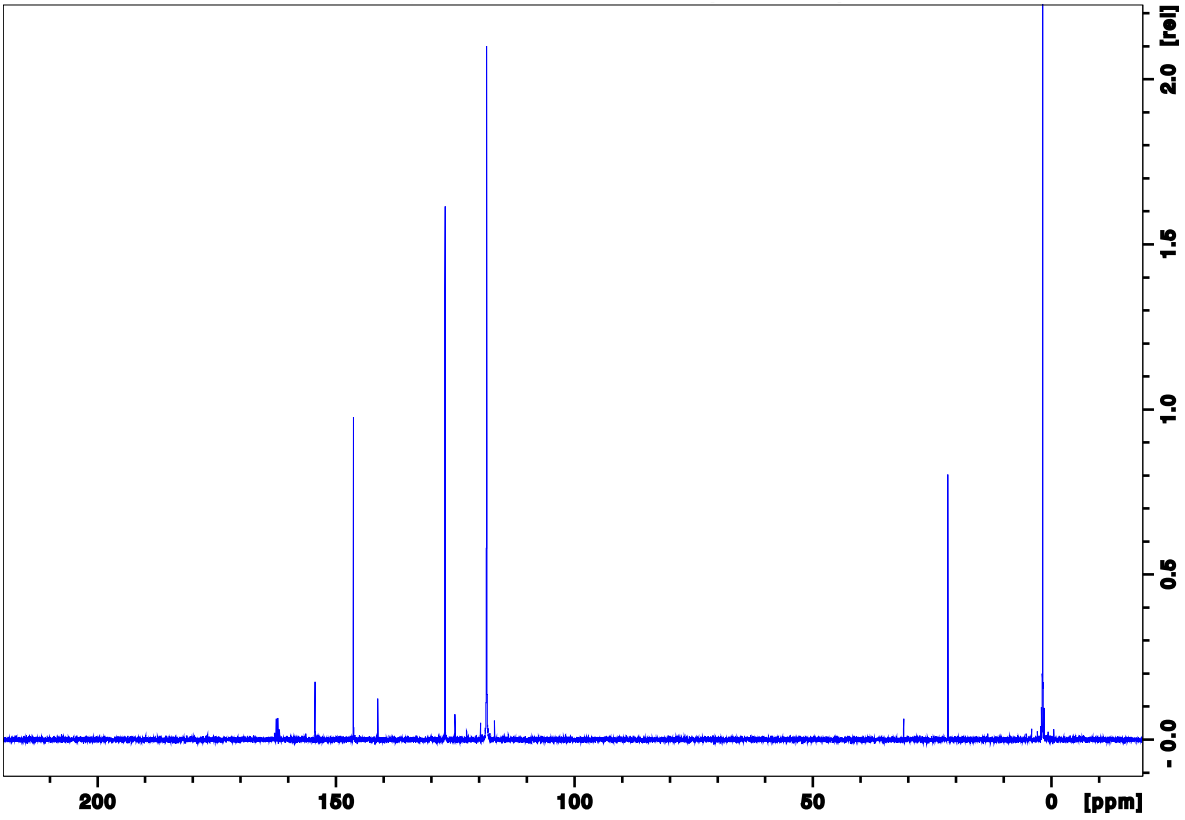

A35: ^{13}C NMR spectrum of TFAA+4-methylpyridine

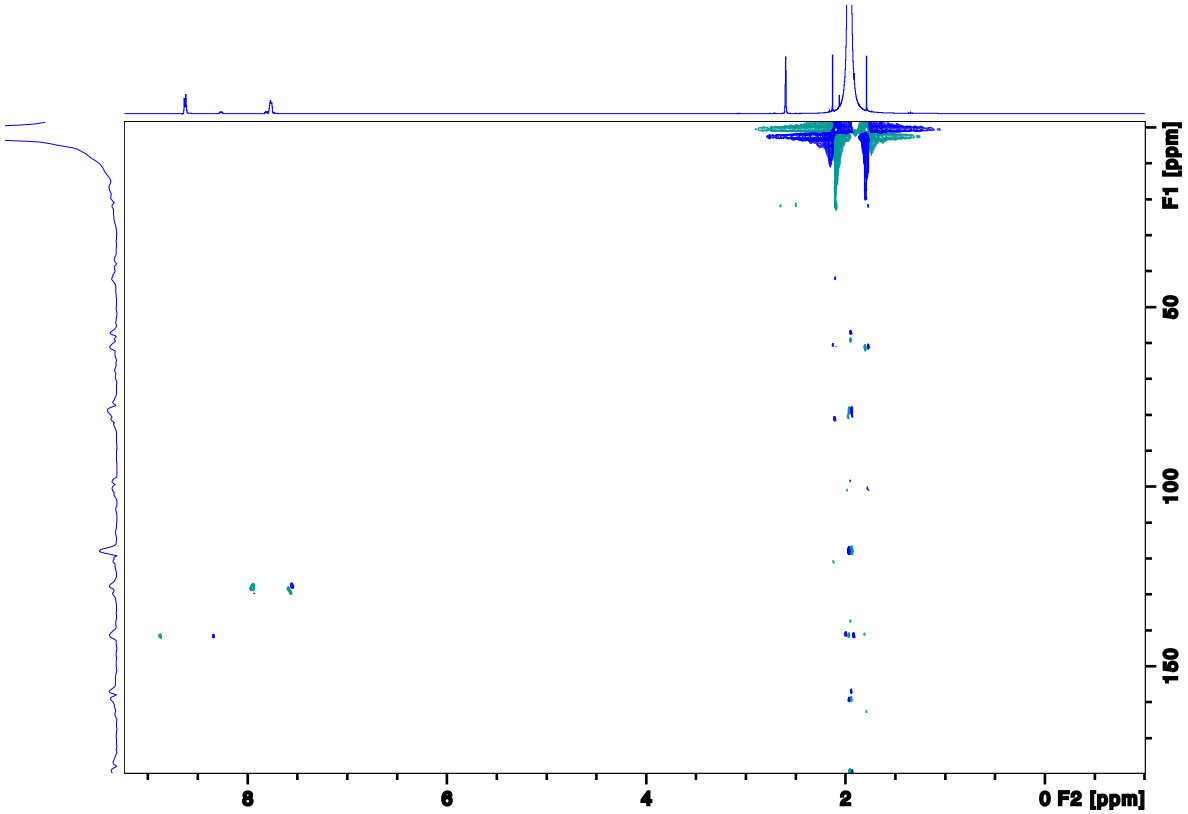

A36: HSQC NMR spectrum of TFAA+4-methylpyridine

2,3-dimethylpyridine

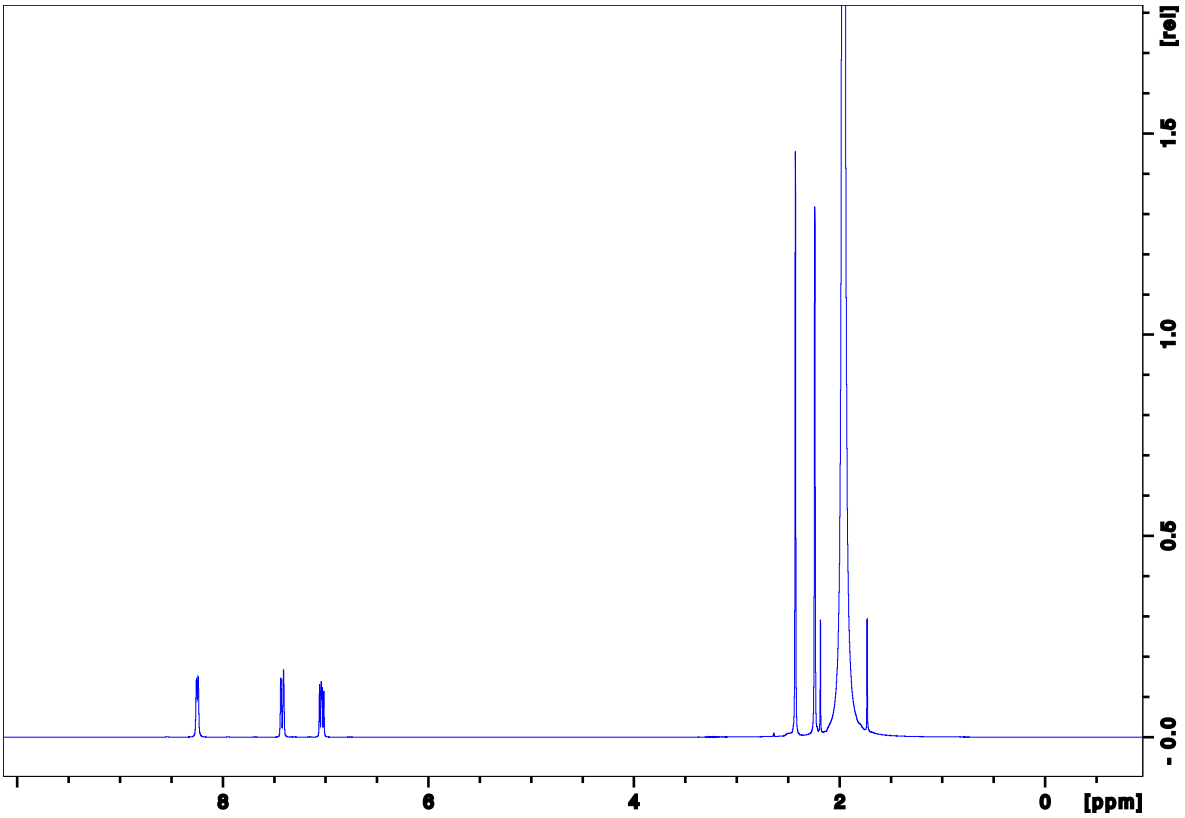

A37: ^{1}H NMR spectrum of 2,3-dimethylpyridine

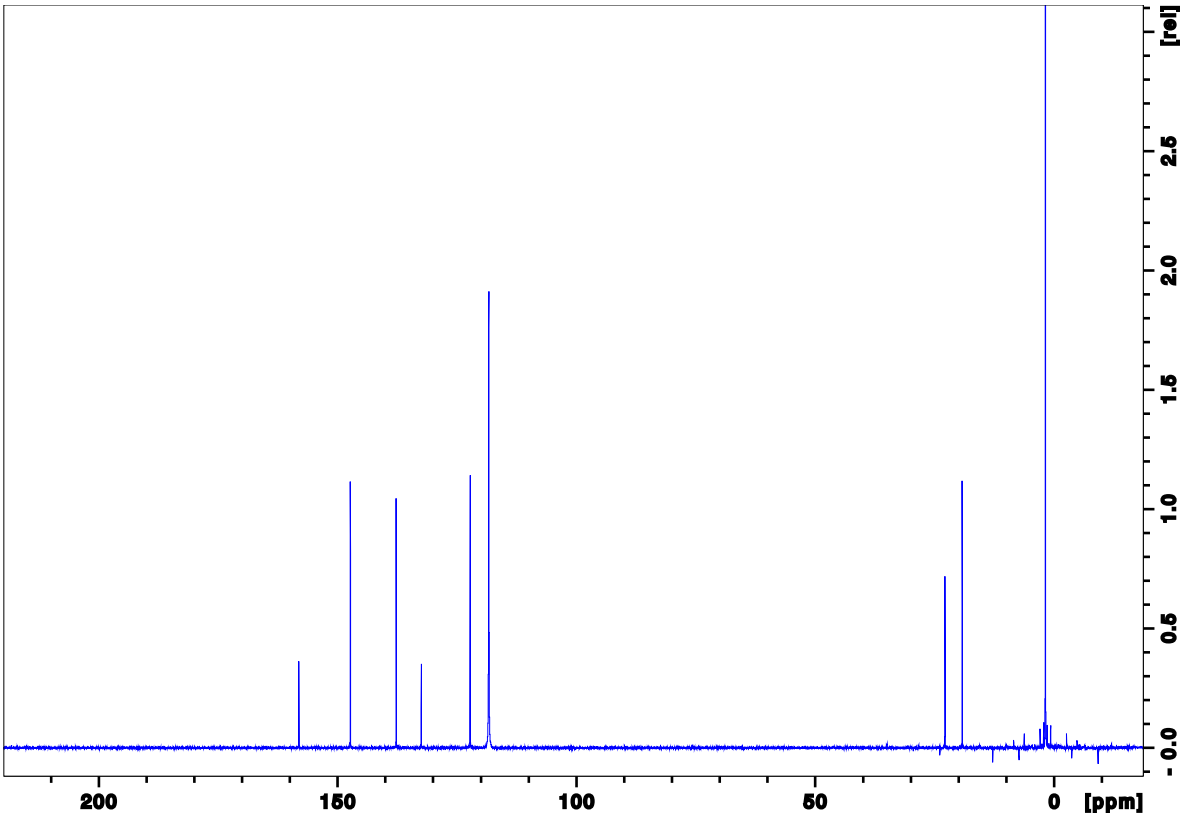

A38: ^{13}C NMR spectrum of 2,3-dimethylpyridine

TFAA+2,3-dimethylpyridine

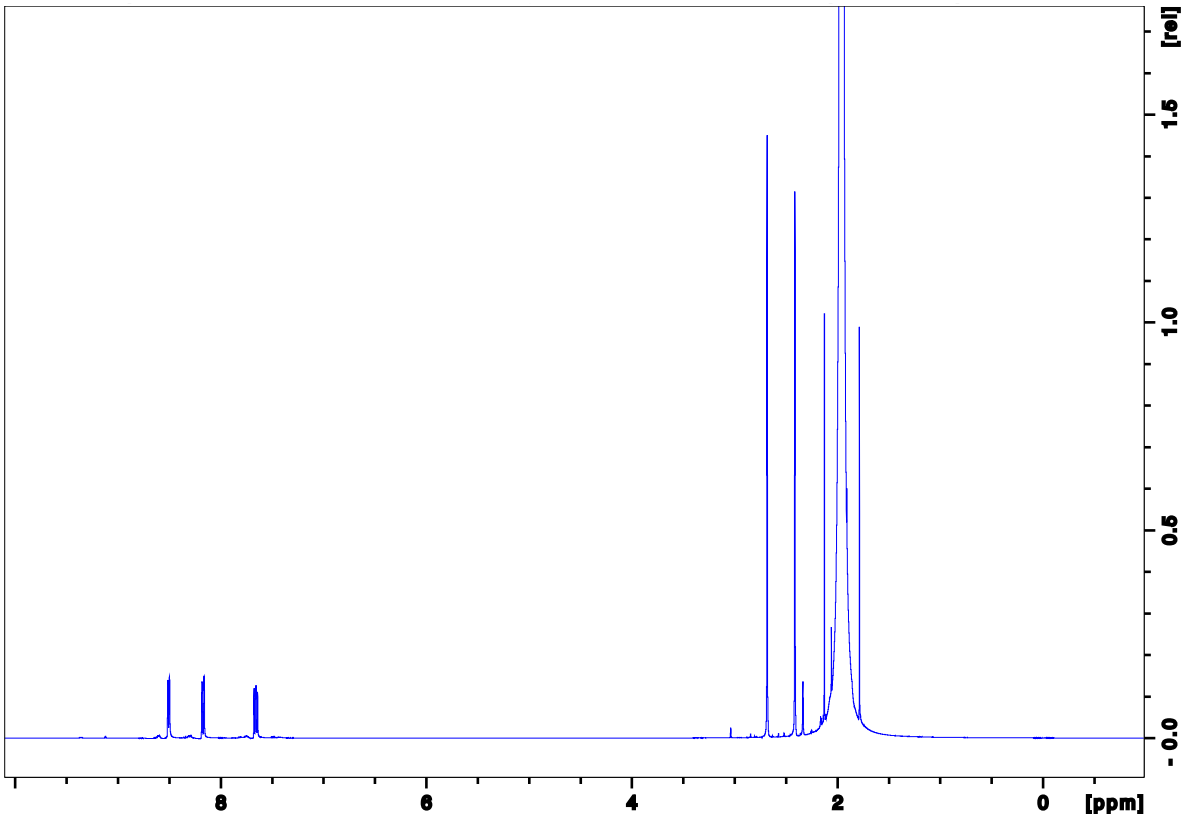

A39: ^{1}H NMR spectrum of TFAA+2,3-dimethylpyridine

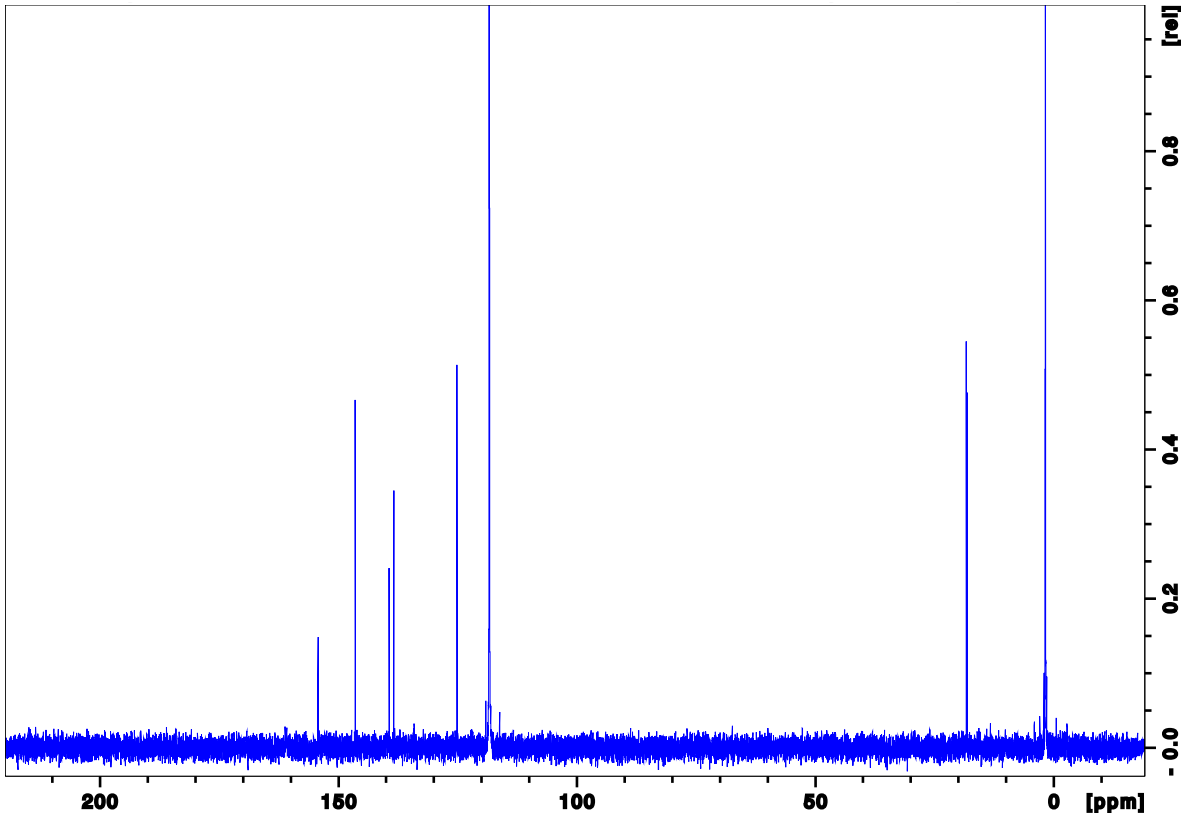

A40: ^{13}C NMR spectrum of TFAA+2,3-dimethylpyridine

2,4-dimethylpyridine

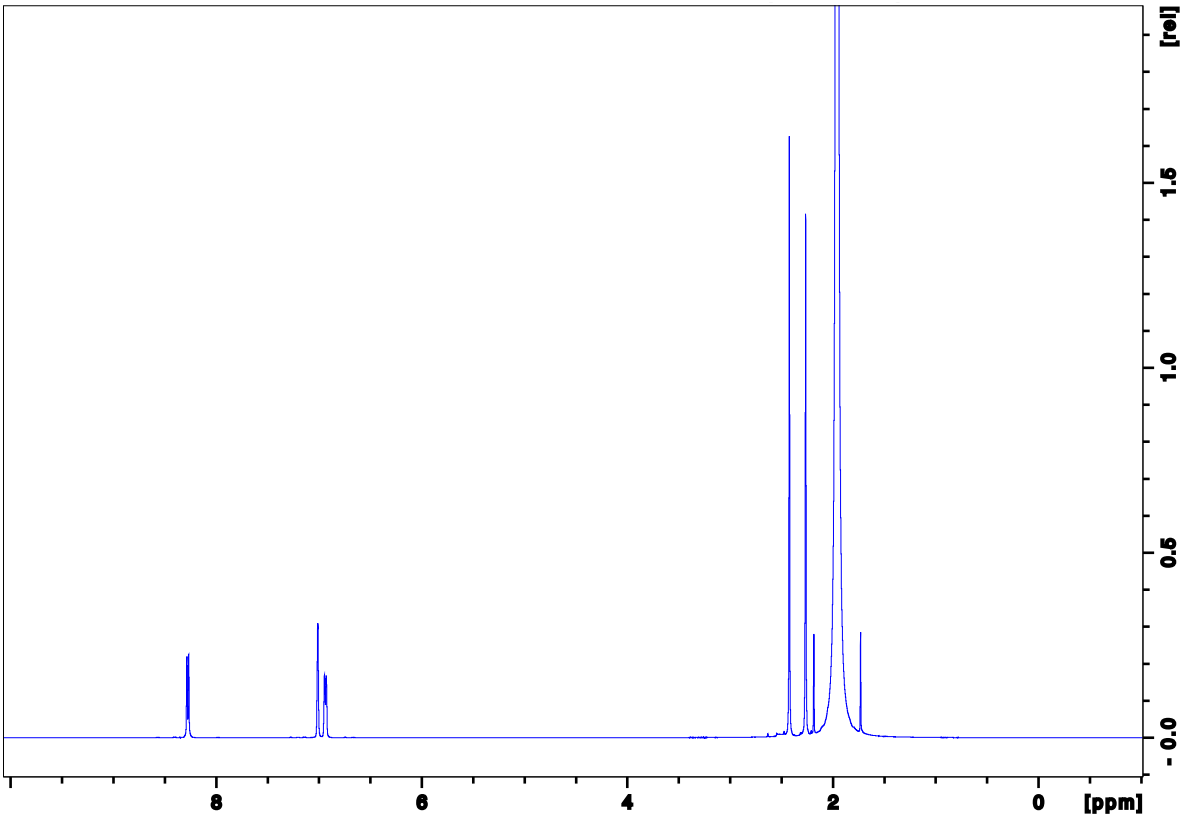

A41: ^{1}H NMR spectrum of 2,4-dimethylpyridine

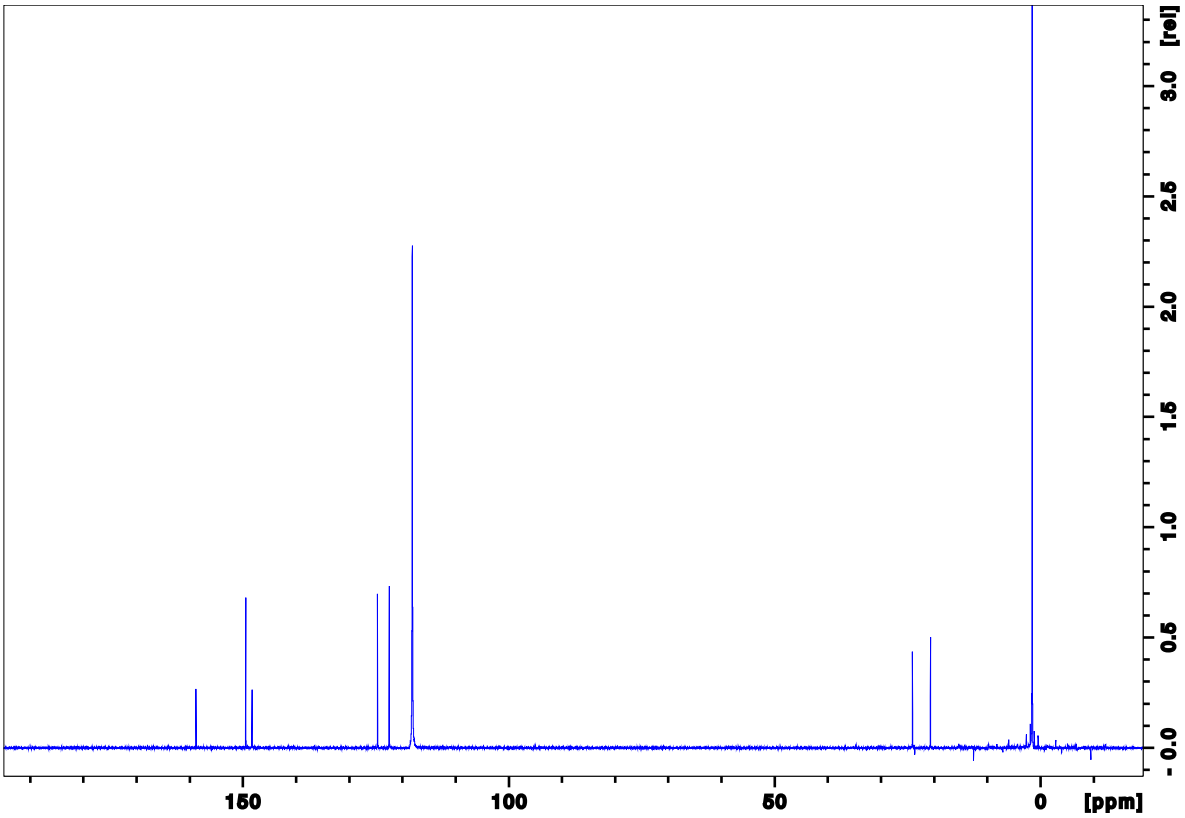

A42: ^{13}C NMR spectrum of 2,4-dimethylpyridine

TFAA+2,4-dimethylpyridine

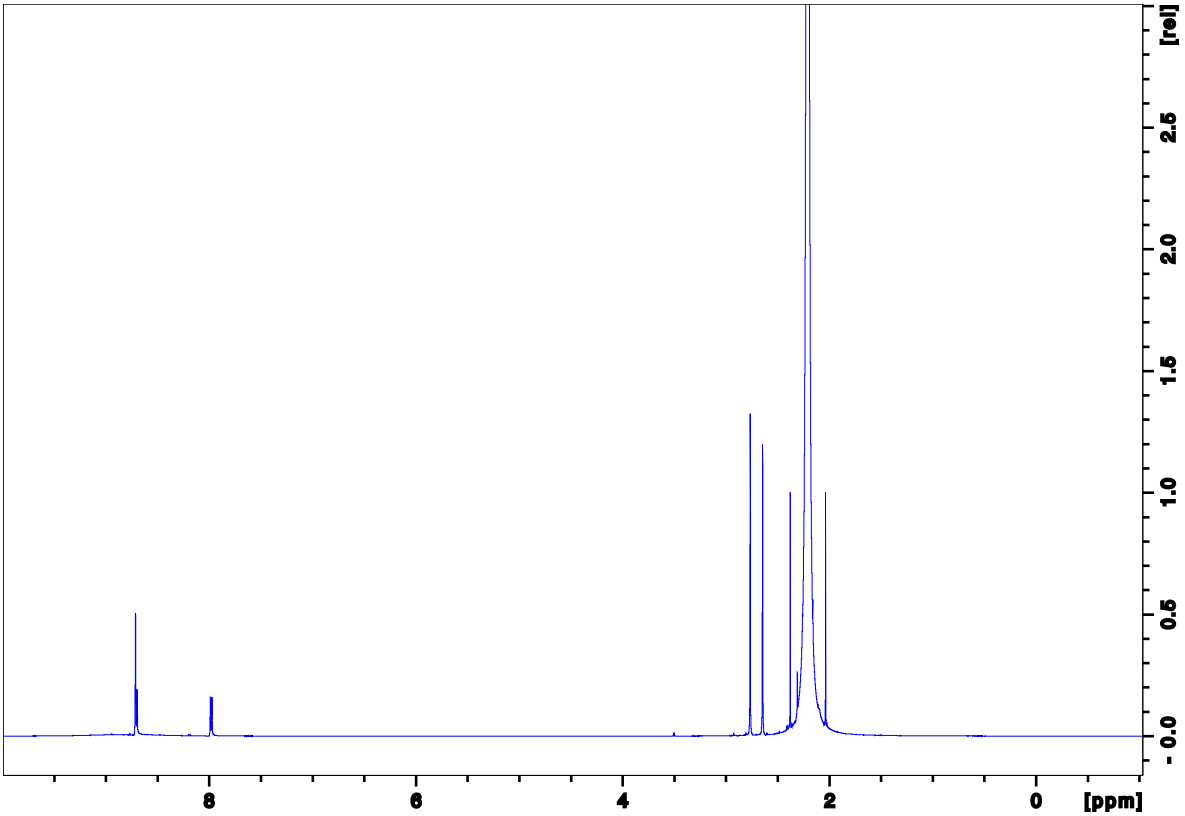

A43: ^{1}H NMR spectrum of TFAA+2,4-dimethylpyridine

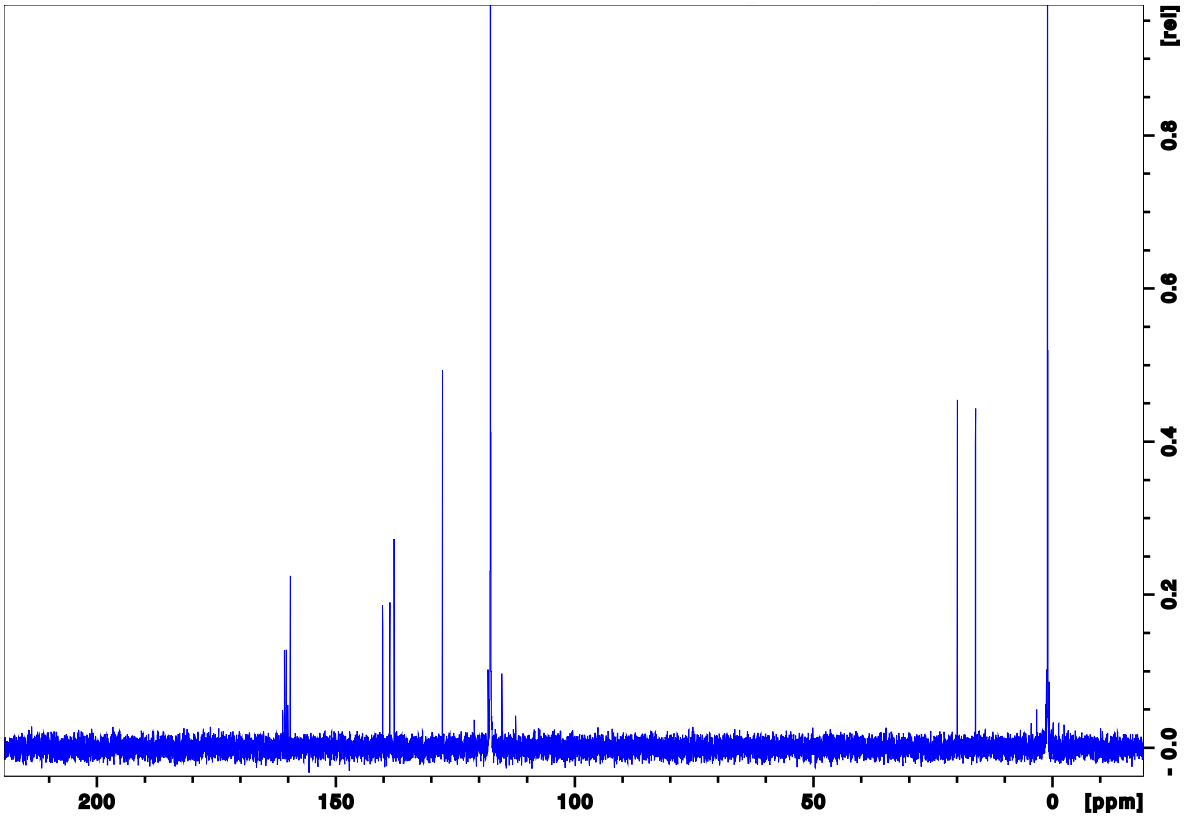

A44: ^{13}C NMR spectrum of TFAA+2,4-dimethylpyridine

2,5-dimethylpyridine

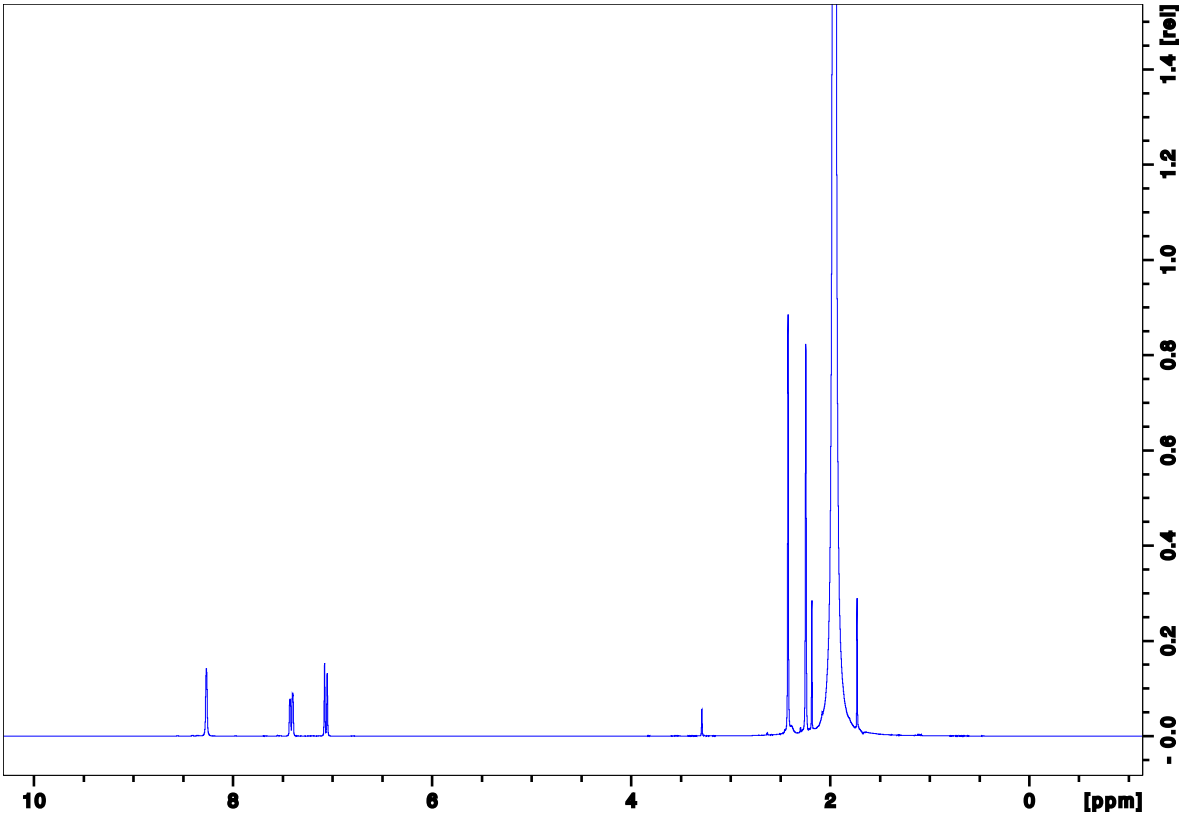

A45: ^{1}H NMR spectrum of 2,5-dimethylpyridine

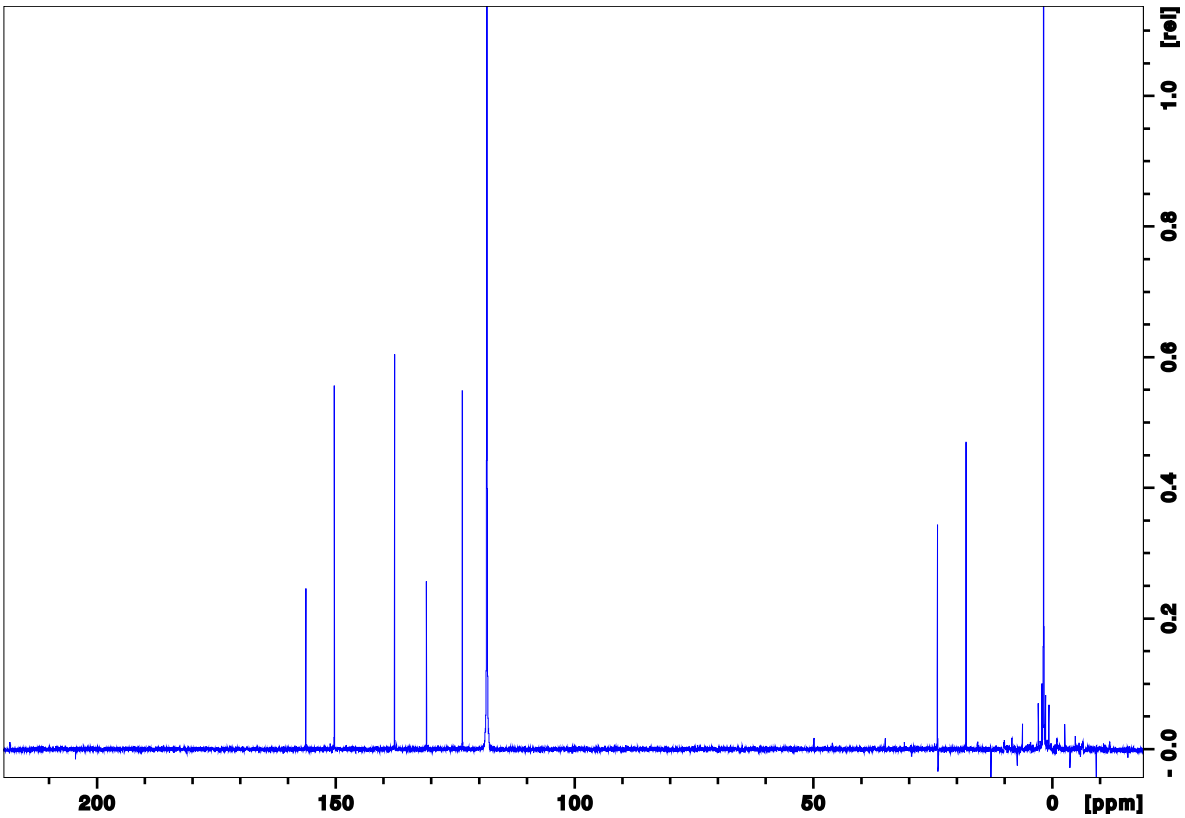

A46: ^{1}H NMR spectrum of 2,5-dimethylpyridine

TFAA+2,5-dimethylpyridine

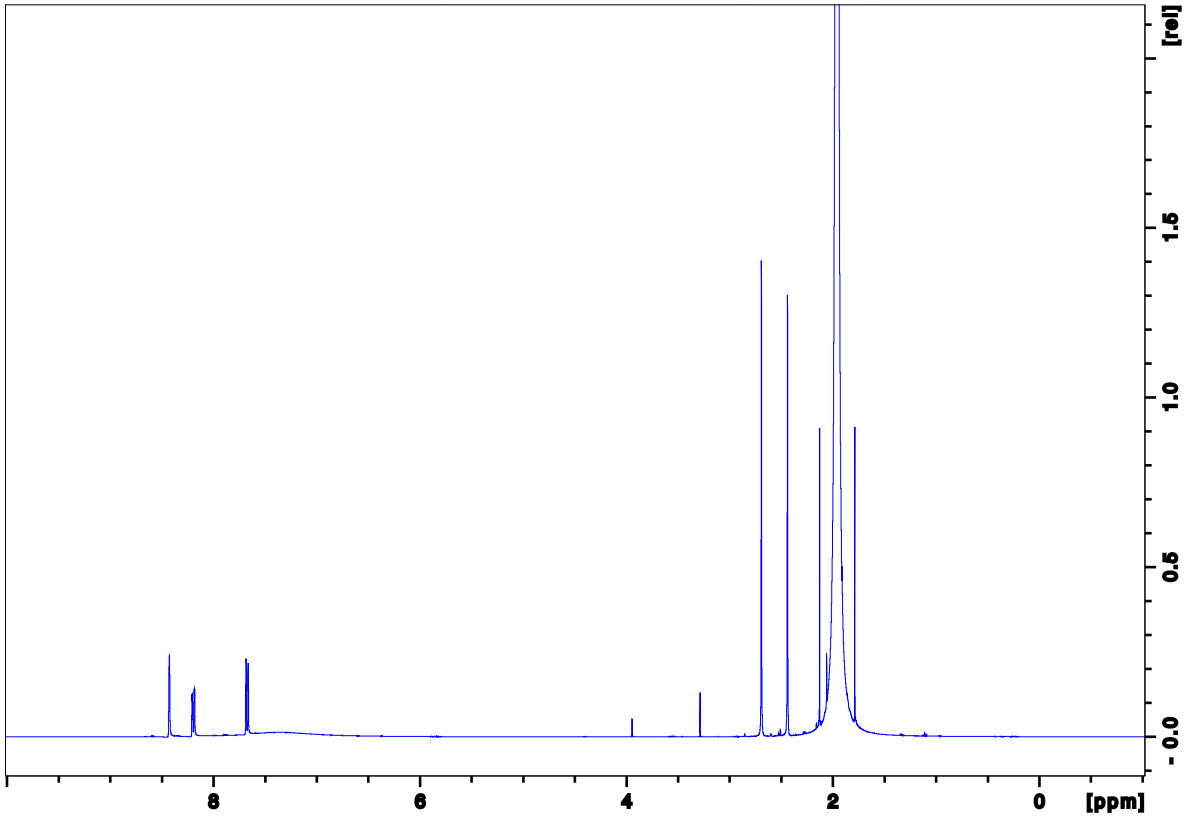

A47: ^{1}H NMR spectrum of TFAA+2,5-dimethylpyridine

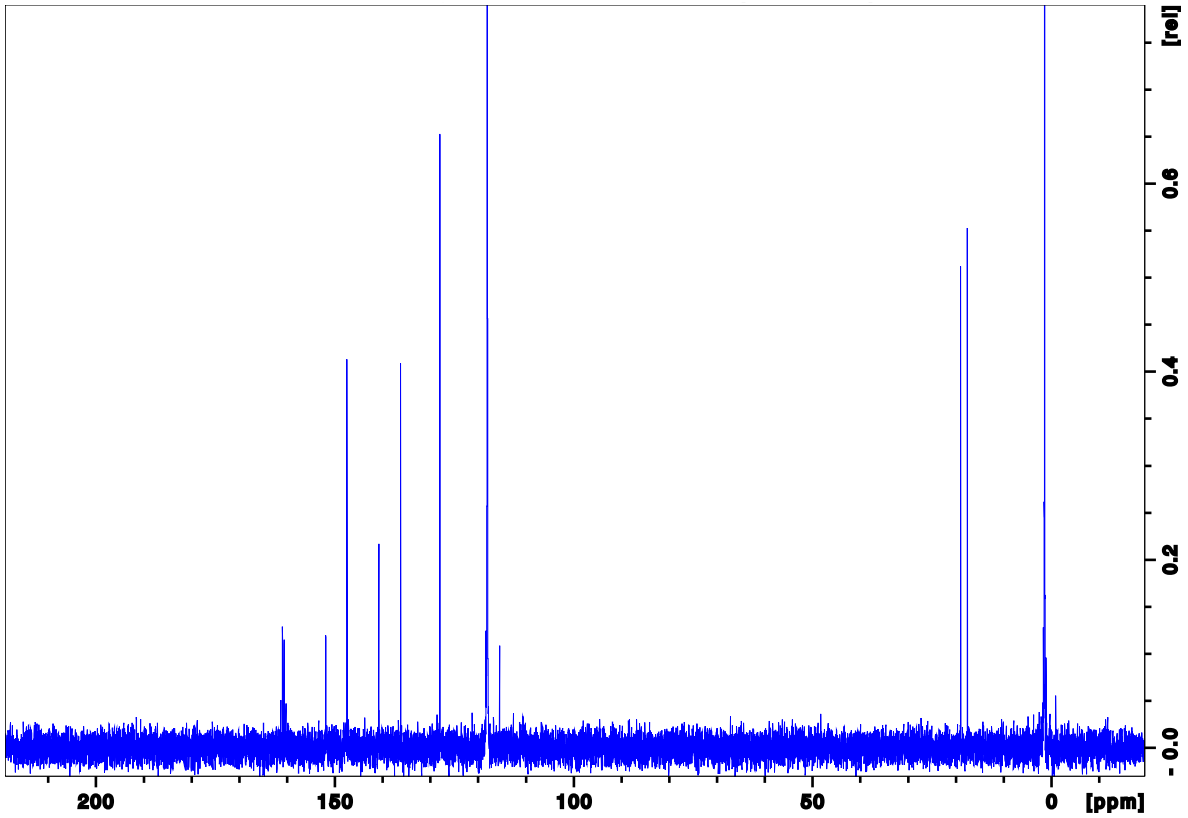

A48: ^{1}H NMR spectrum of TFAA+2,5-dimethylpyridine

2,6-dimethylpyridine

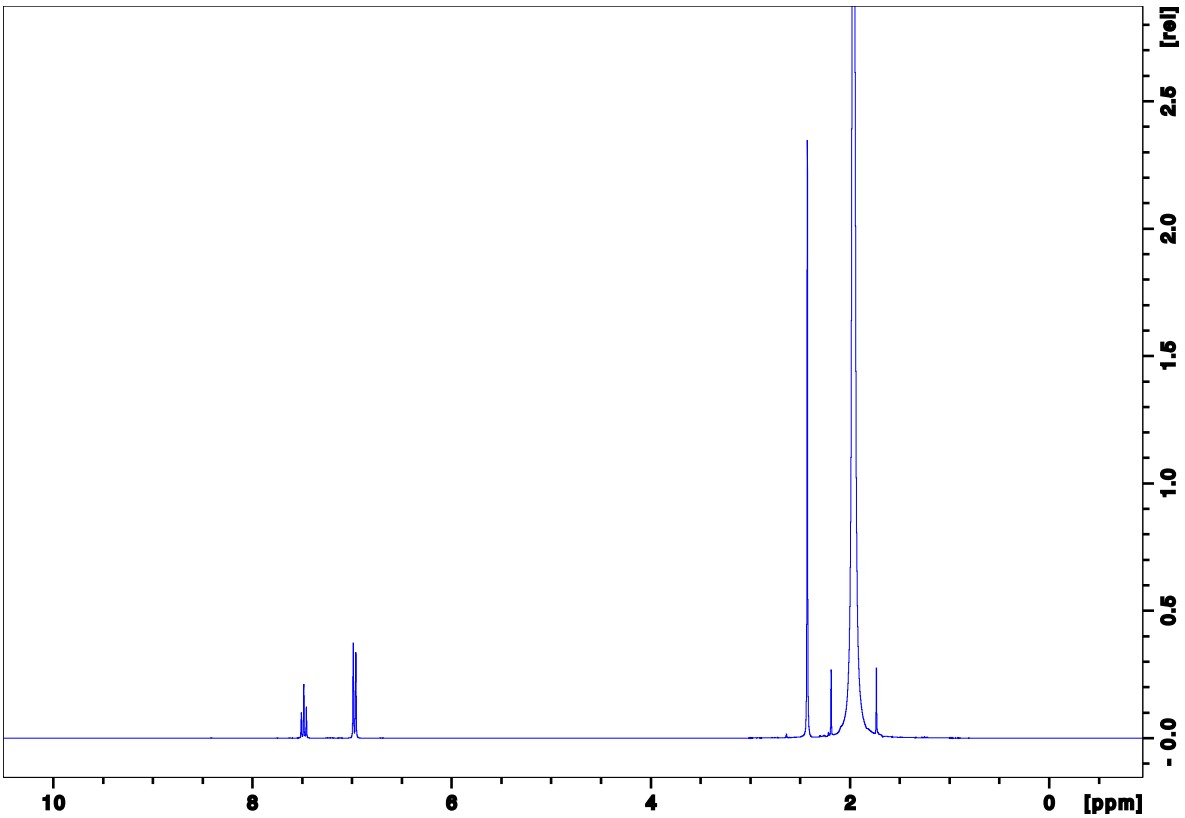

A49: ^{1}H NMR spectrum of 2,6-dimethylpyridine

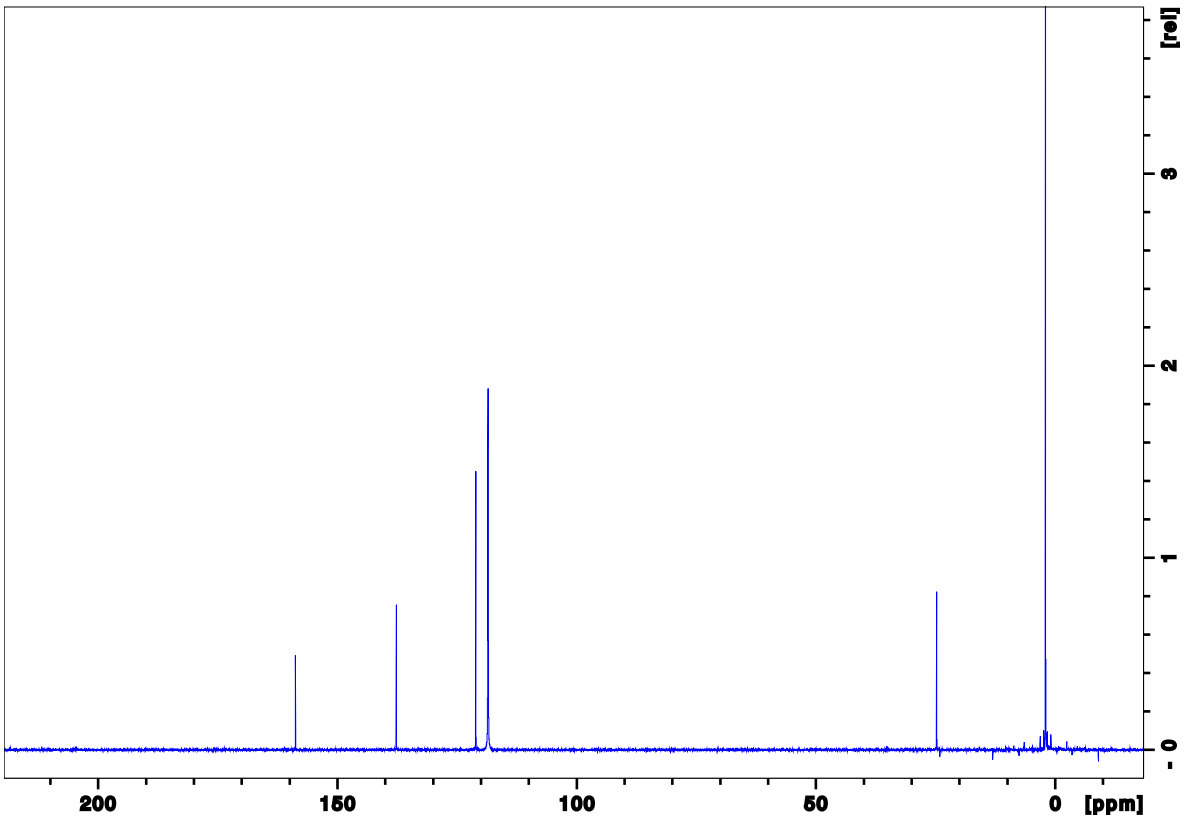

A50: ^{13}C NMR spectrum of 2,6-dimethylpyridine

TFAA+2,6-dimethylpyridine

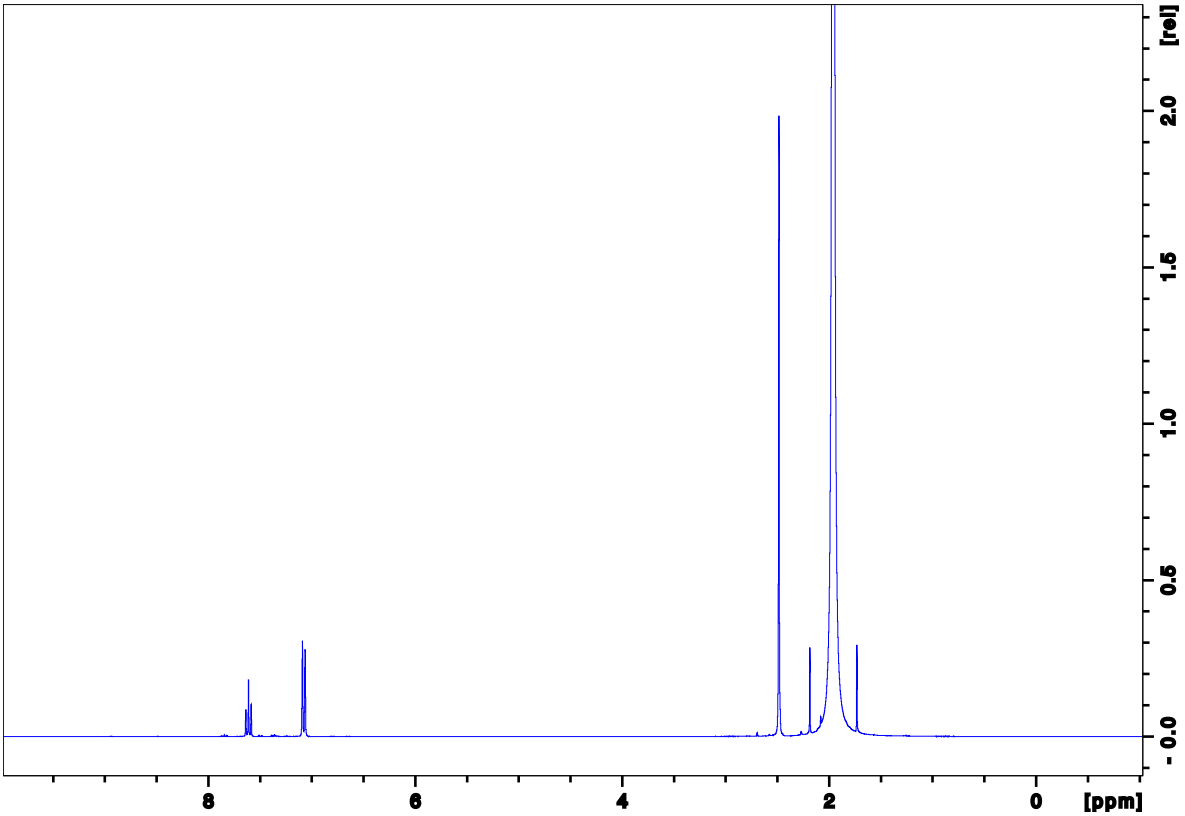

A51: ^{1}H NMR spectrum of TFAA+2,6-dimethylpyridine

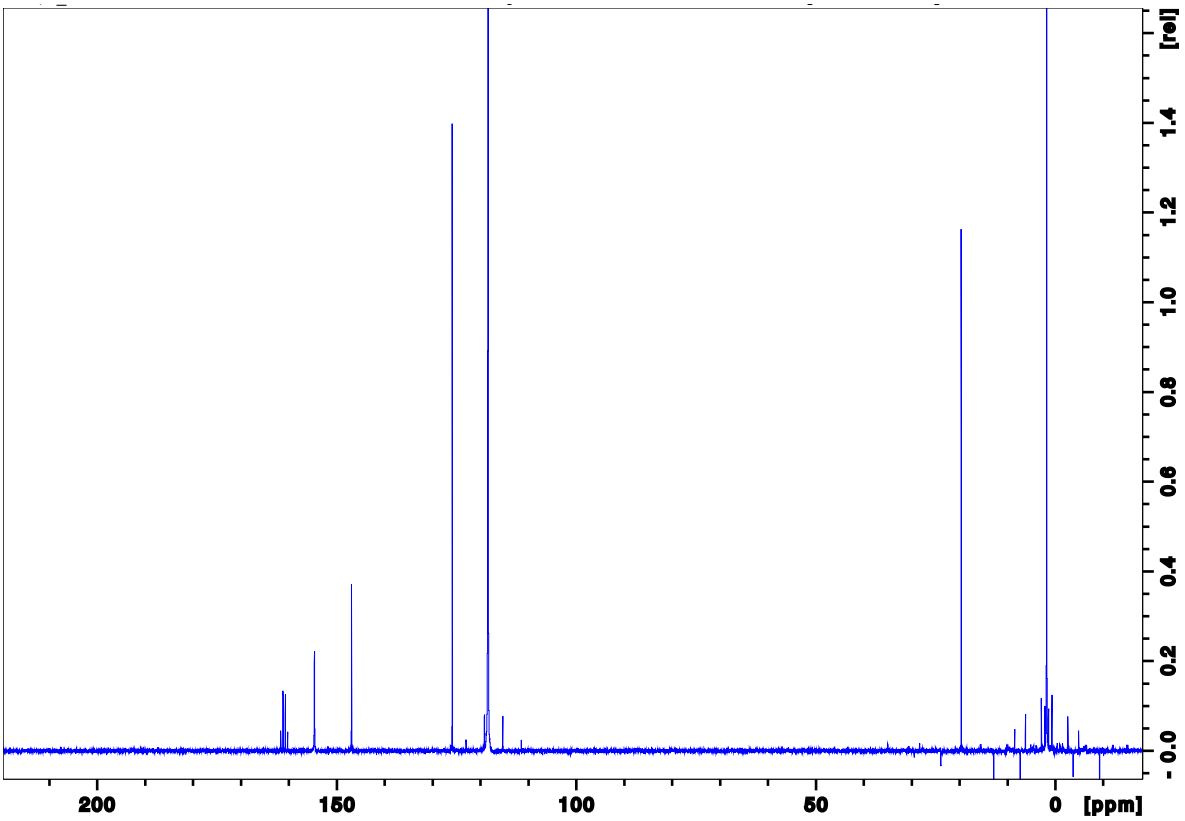

A52: ^{13}C NMR spectrum of TFAA+2,6-dimethylpyridine

3,4-dimethylpyridine

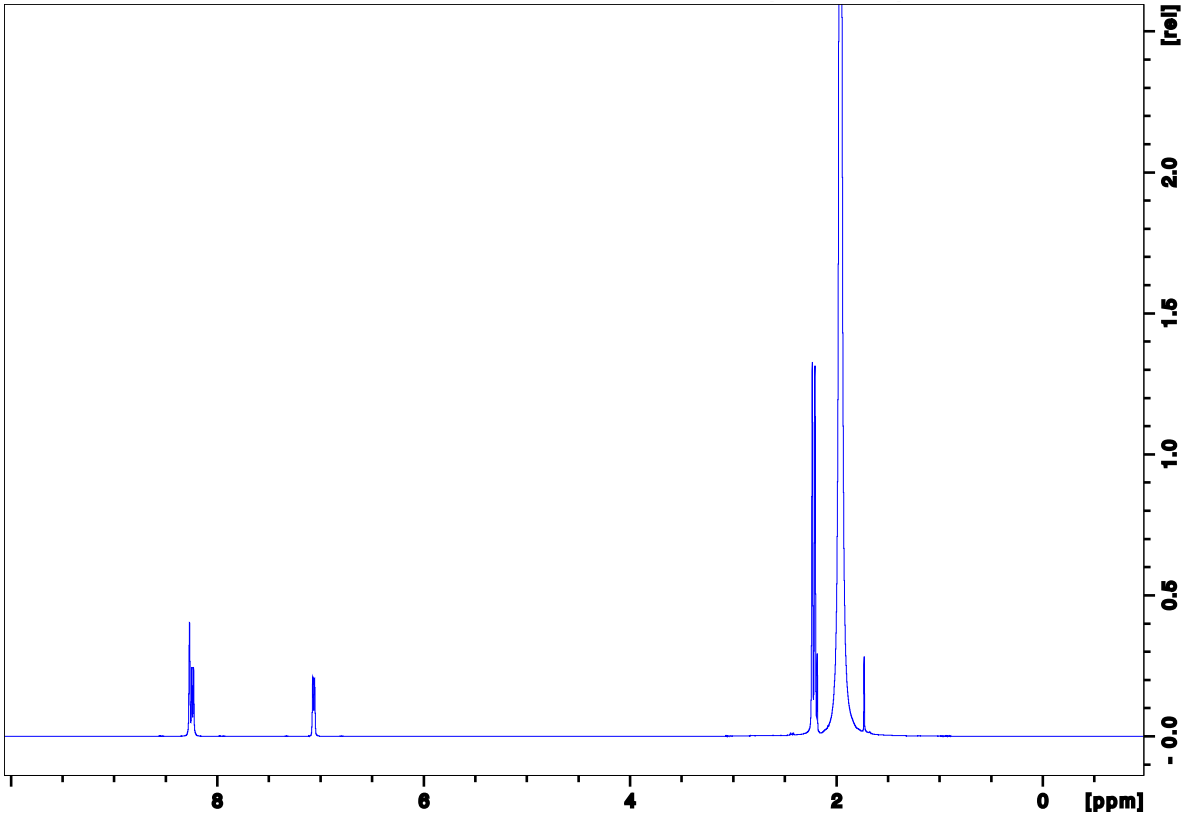

A53: ^{1}H NMR spectrum of 3,4-dimethylpyridine

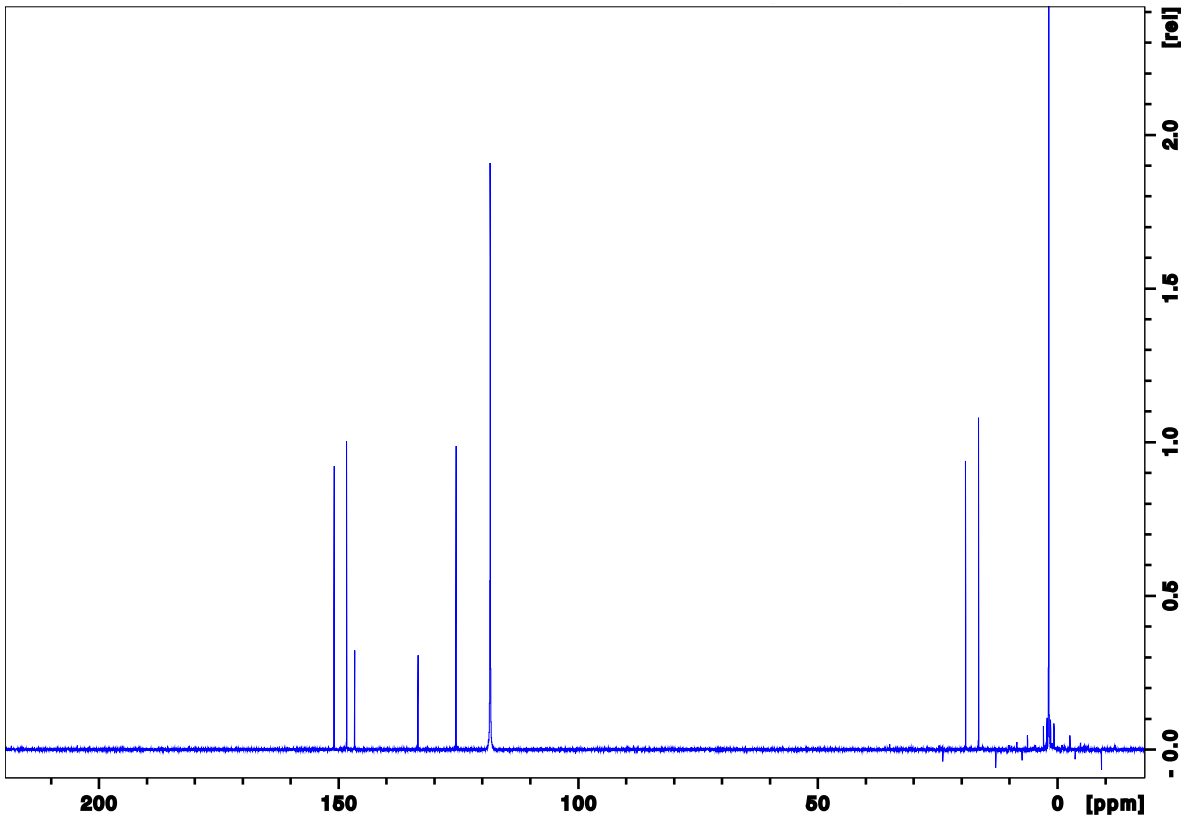

A54: ^{13}C NMR spectrum of 3,4-dimethylpyridine

TFAA+3,4-dimethylpyridine

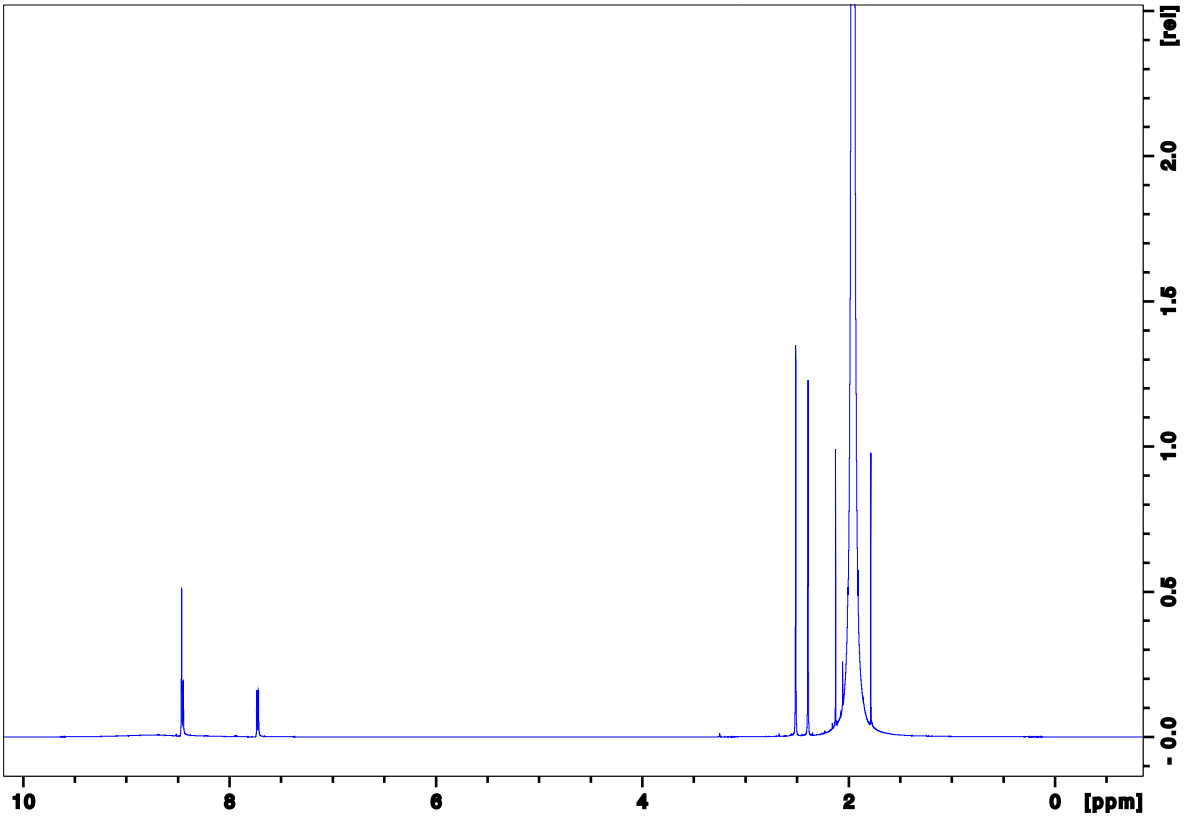

A55: ^{1}H NMR spectrum of TFAA+3,4-dimethylpyridine

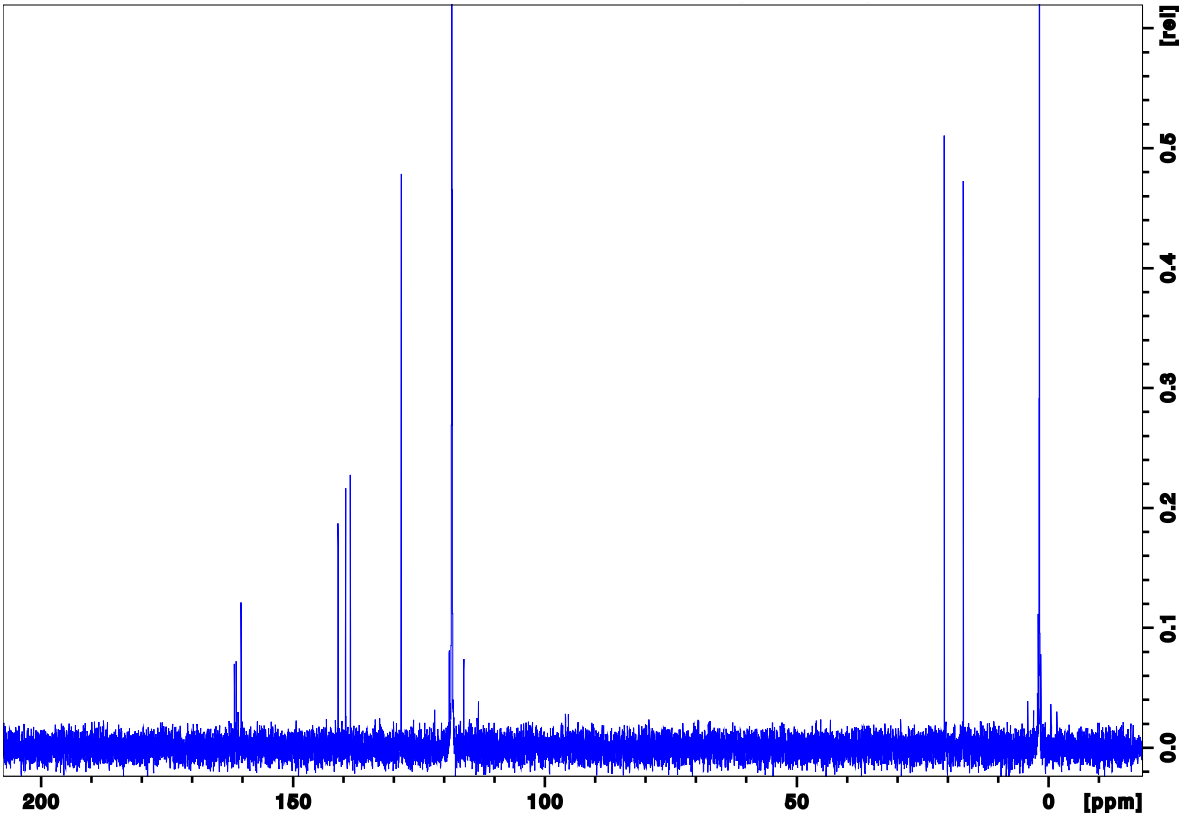

A56: ^{13}C NMR spectrum of TFAA+3,4-dimethylpyridine

3,5-dimethylpyridine

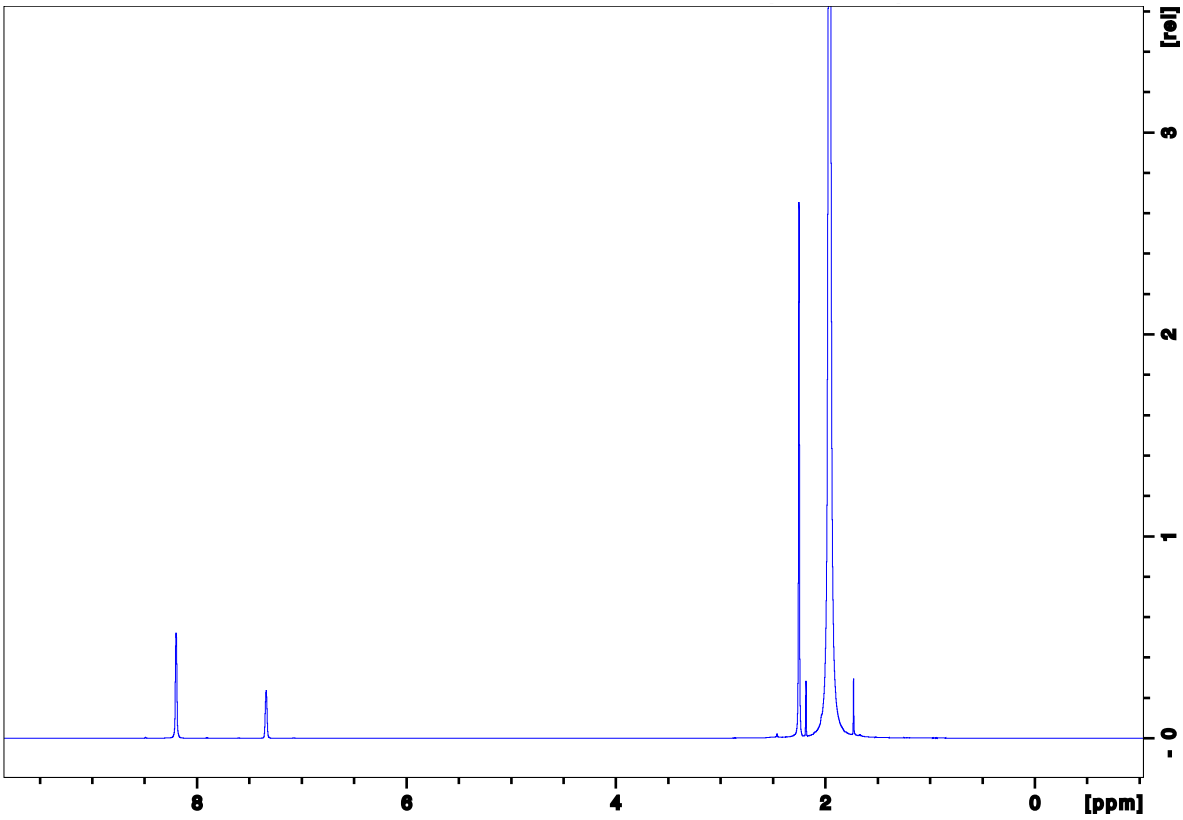

A57: ^{1}H NMR spectrum of 3,5-dimethylpyridine

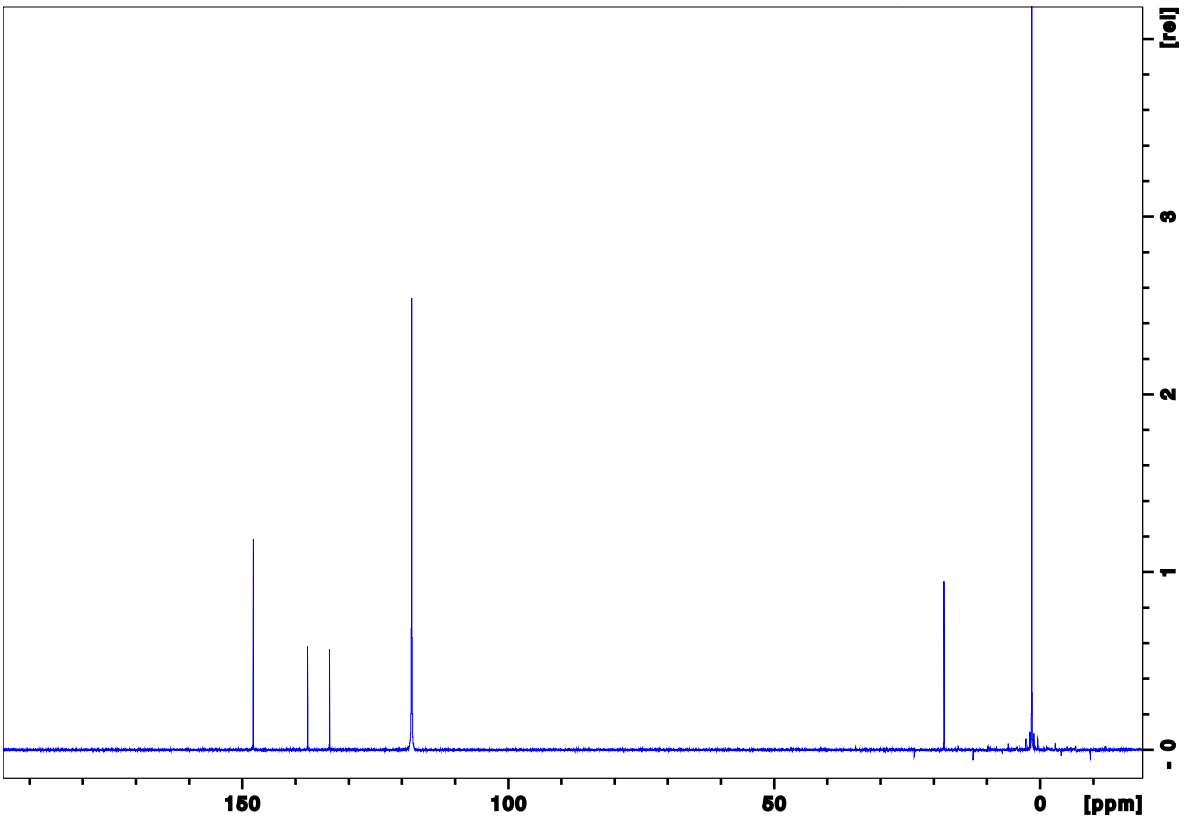

A58: ^{13}C NMR spectrum of 3,5-dimethylpyridine

TFAA+3,5-dimethylpyridine

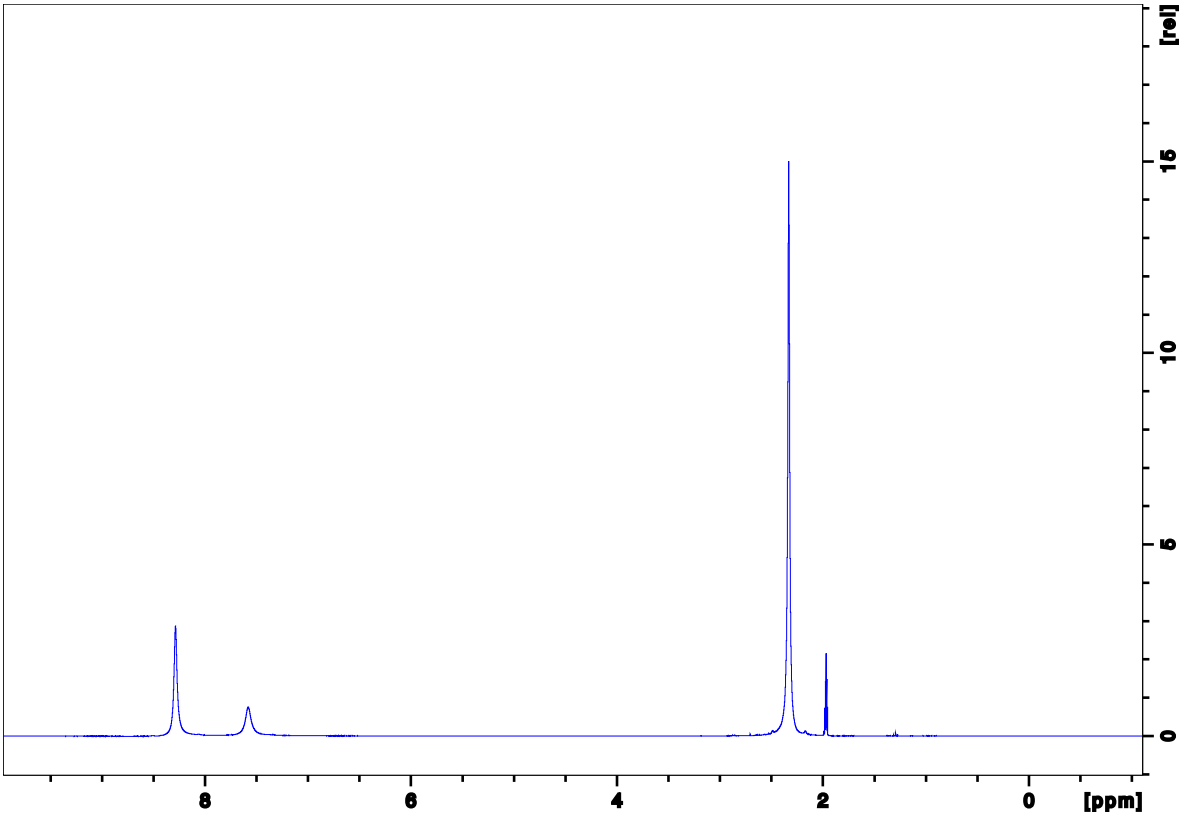

A59: ^{1}H NMR spectrum of TFAA+3,5-dimethylpyridine

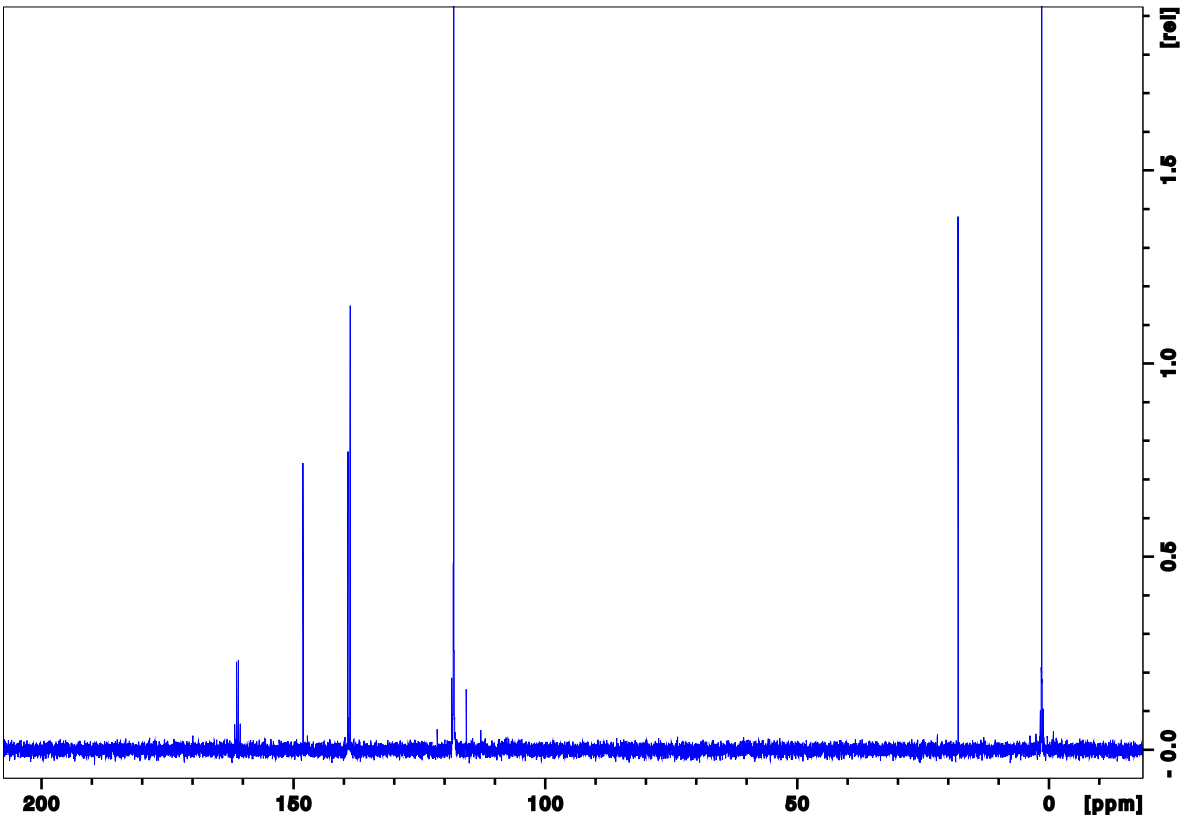

A60: ^{13}C NMR spectrum of TFAA+3,5-dimethylpyridine

Appendix B

Cyclic Voltammetry Data

In Chapter Four it was discussed that the trifluoroacetylpyridinium salts with methyl group substituents do not passivate the electrode surface upon reduction. The cyclic voltammograms evidencing this can be seen below in Figures B1-B9. In Chapter Six, other nucleophiles other than pyridine were used for synthesis, this included 1-methylimidazole and 1-methylpyrazole. The cyclic voltammograms of these nucleophiles with TFAA can be seen in Figures B10 and B11.

B1 Trifluoroacetyl-2-methylpyridinium

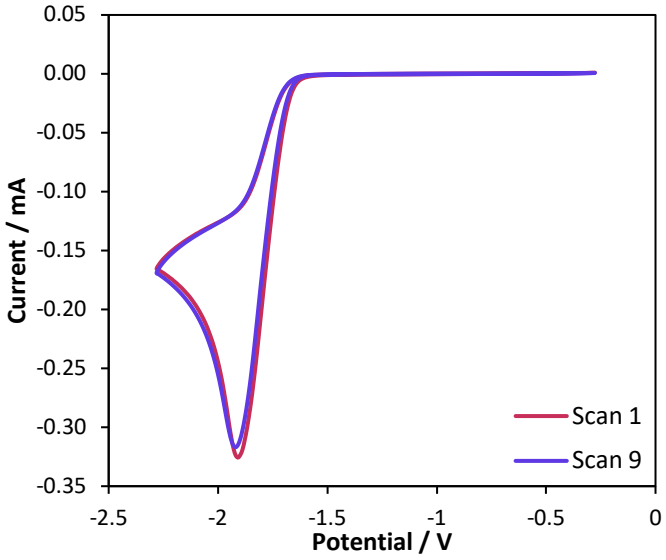

B2 Trifluoroacetyl-3-methylpyridnium

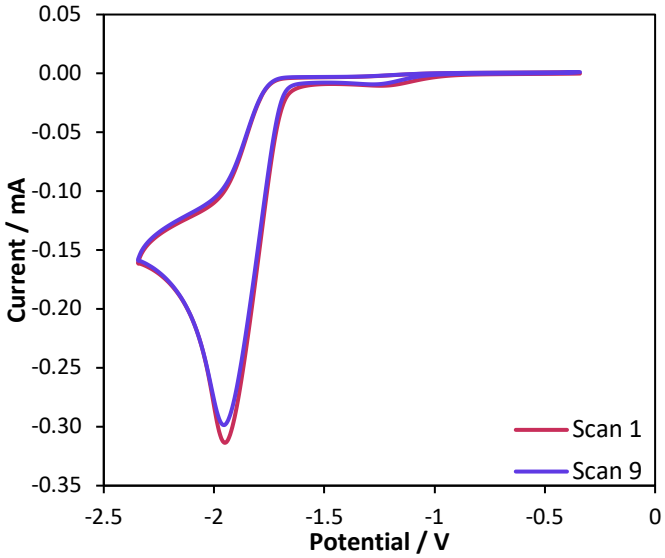

B3 Trifluoroacetyl-4-methylpyridinium

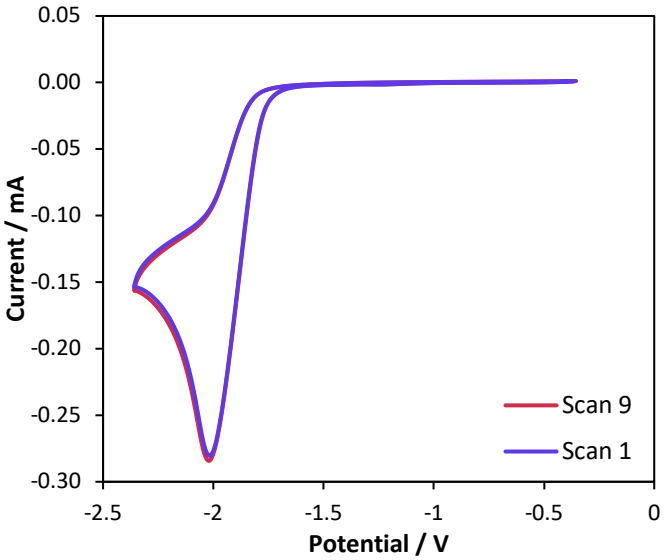

B4 Trifluoroacetyl-2,3-dimethylpyridinium

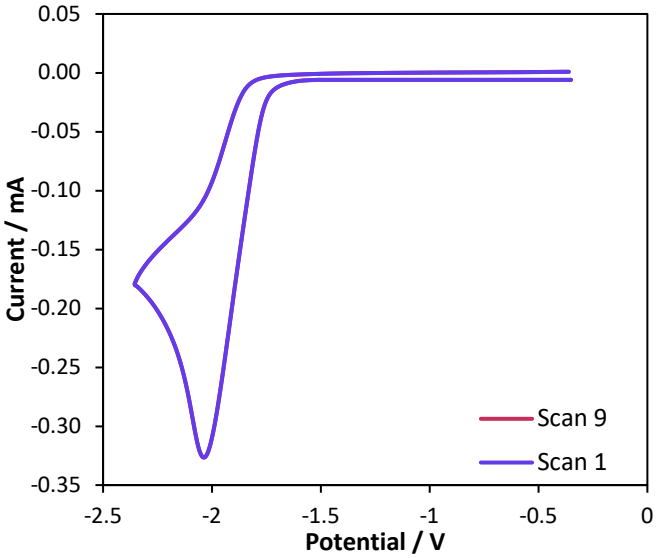

B5 Trifluoroacetyl-2,4-dimethylpyridnium

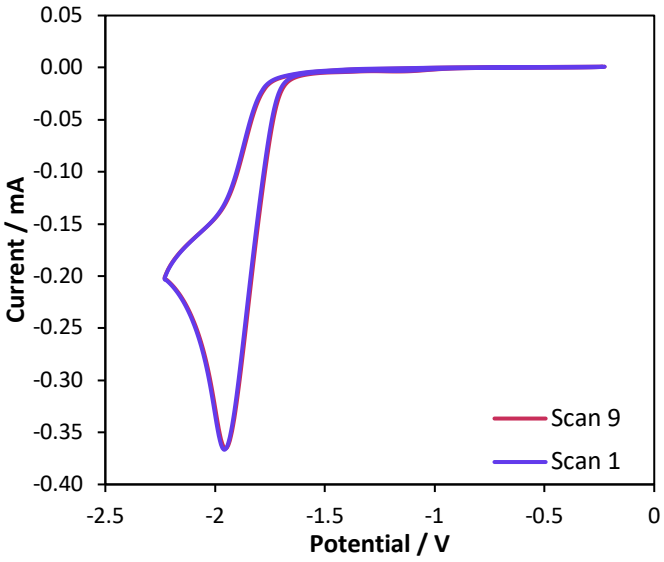

B6 Trifluoroacetyl-2,5-dimethylpyridinium

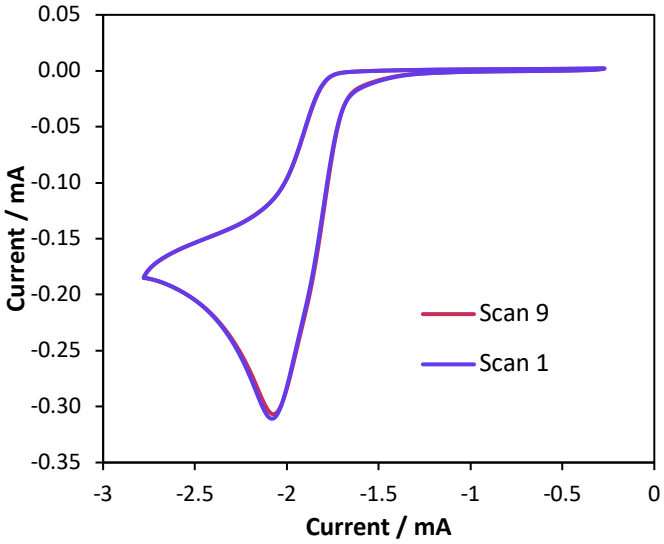

B7 Trifluoroacetyl-2,6-dimethylaminopyridinium

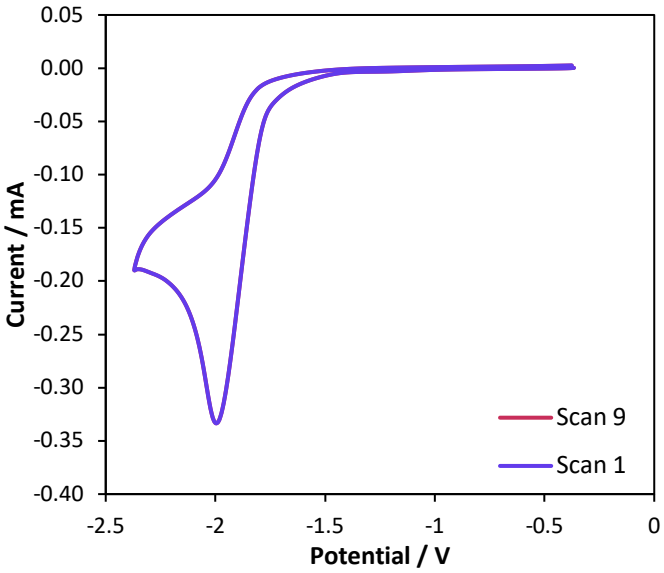

B8 Trifluoroacetyl-3,4-dimethylpyridinium

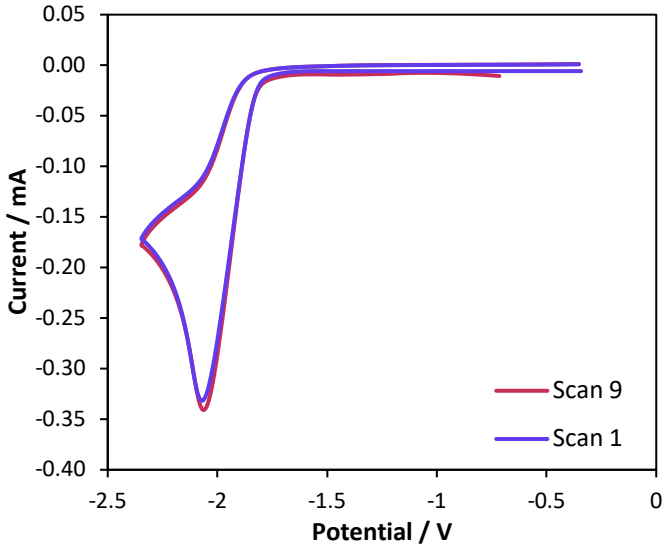

B9 Trifluoroacetyl-3,5-dimethylpyridinium

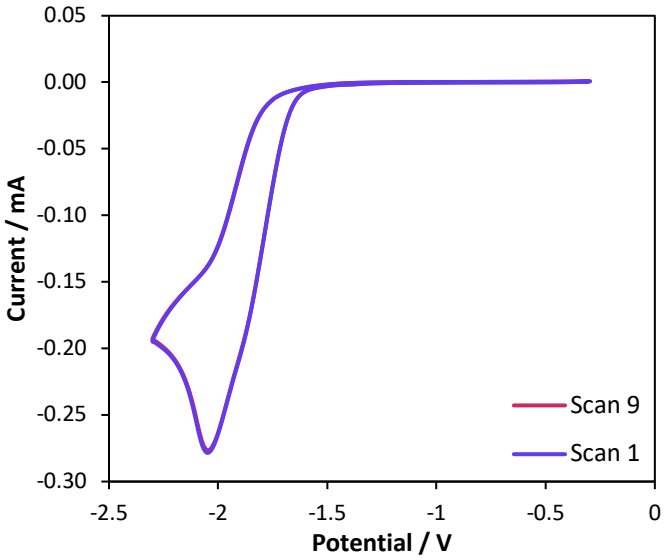

B10 Trifluoroacetyl-1-methylimidazole

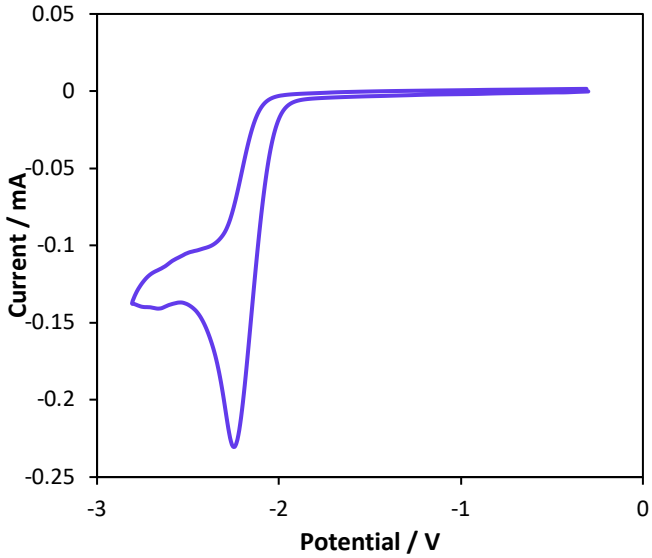

B11 Trifluoroacetyl-1-methylpyrazole

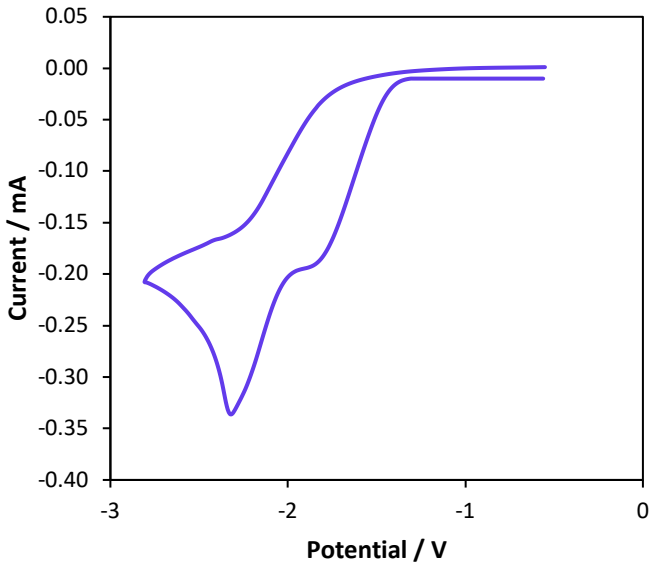

Appendix C

XPS Data

XPS data was discussed heavily throughout Chapters Four and Five, mostly summarised as tabulated data. The full spectra for each modified electrode discussed in this thesis can be seen below in Figures C1-C14.

Clean Carbon Electrode

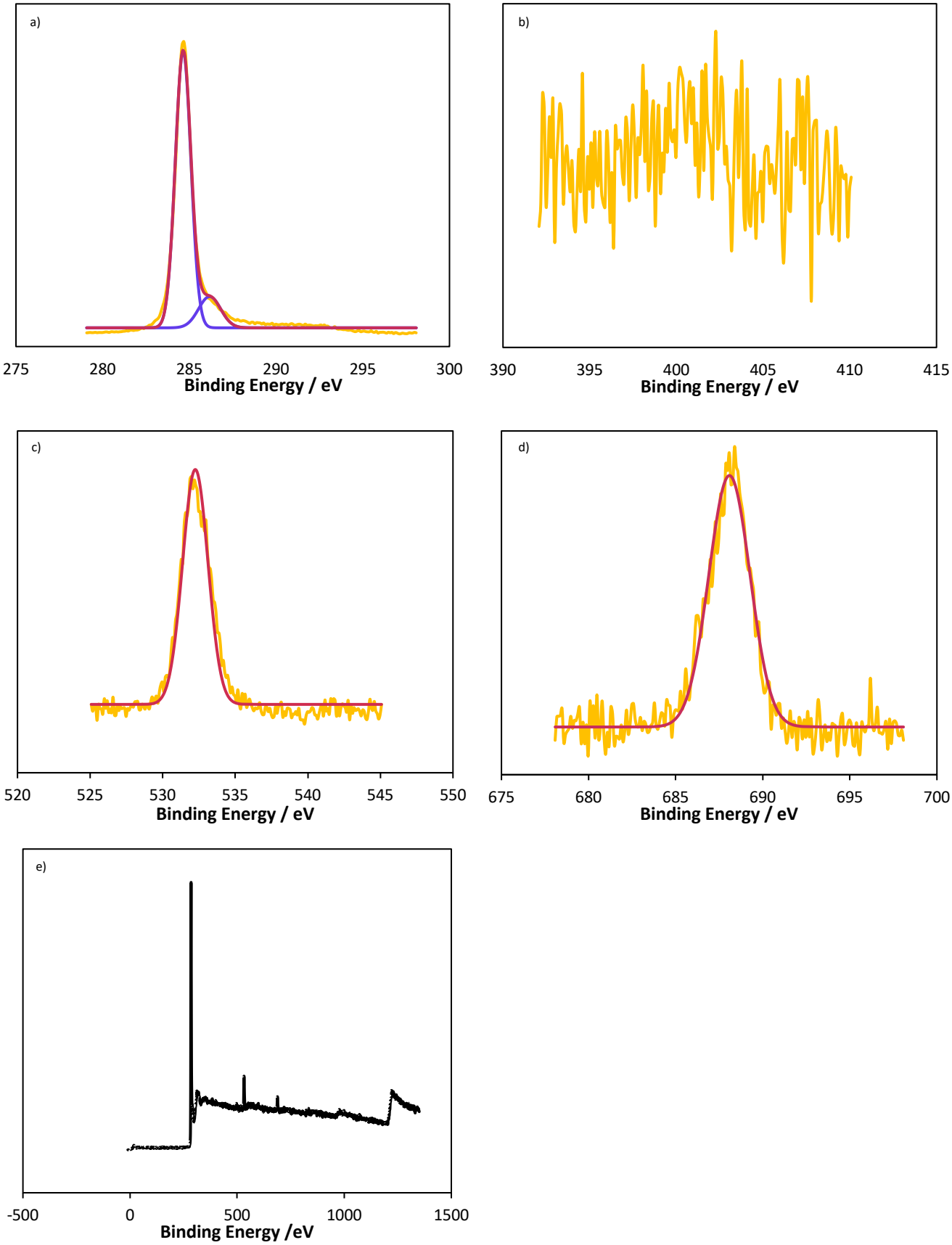

C1: XPS data of a clean carbon electrode showing the a) C1s region; b) N1s region; c) O1s region; d) F1s region; e) survey spectrum. Red line – cumulative fit; blue line – individual peaks; yellow line – raw data.

Carbon Electrode Modified from Trifluoroacetylpyridinium

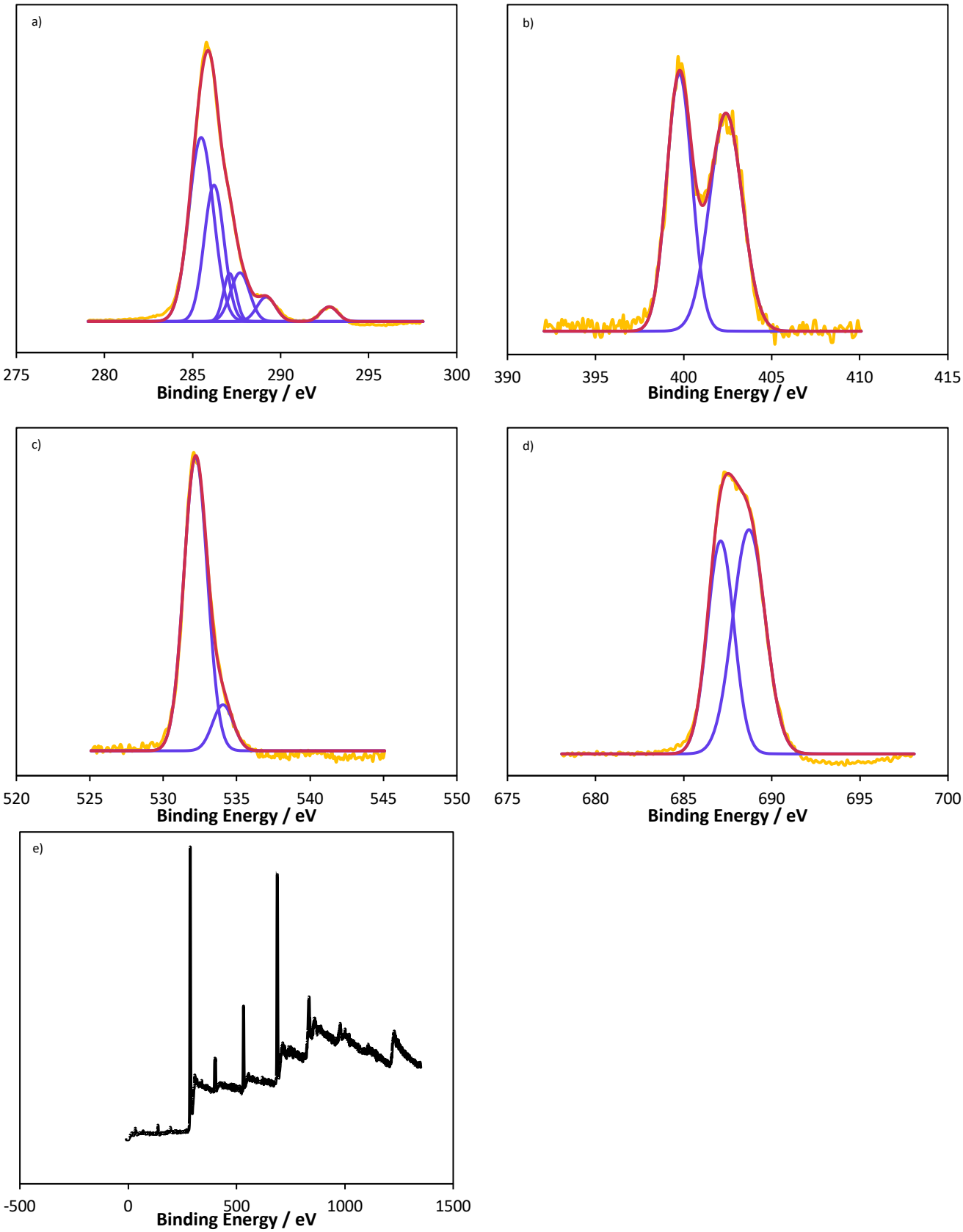

C2: XPS data of a carbon electrode modified from trifluoroacetylpyridinium showing the a) C1s region; b) N1s region; c) O1s region; d) F1s region; survey spectrum. Red line – cumulative fit; blue line – individual peaks; yellow line – raw data.

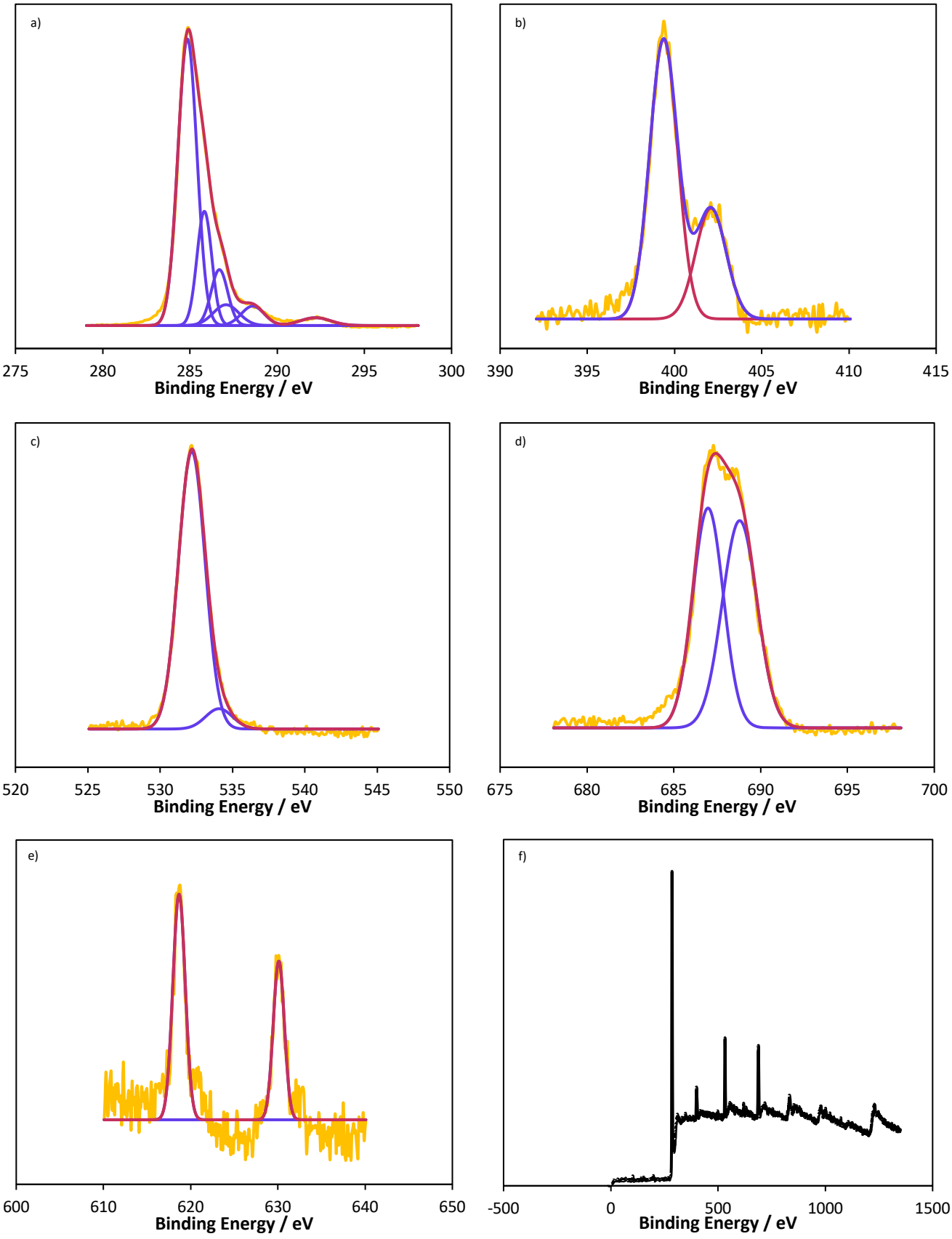

C3: XPS data of a carbon electrode modified from trifluoroacetyl-2-iodopyridinium showing the a) C1s region; b) N1s region; c) O1s region; d) F1s region; e) I3d region; f) survey spectrum. Red line – cumulative fit; blue line – individual peaks; yellow line – raw

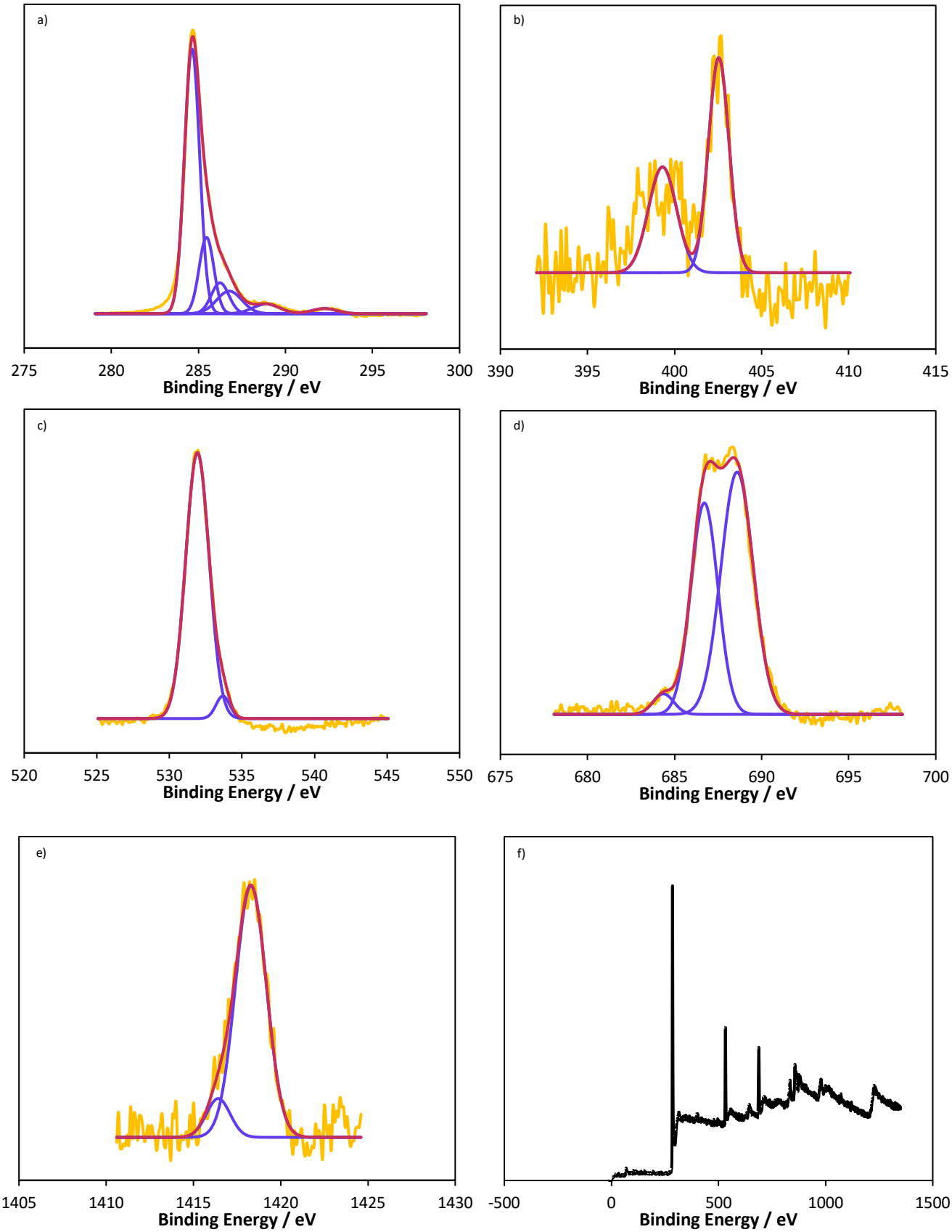

C4: XPS data of a carbon electrode modified from trifluoroacetyl-2-bromo-4-methylpyridinium showing the a) C1s region; b) N1s region; c) O1s region; d) F1s region; e) Br3d region; f) survey spectrum. Red line – cumulative fit; blue line – individual peaks; yellow line – raw data

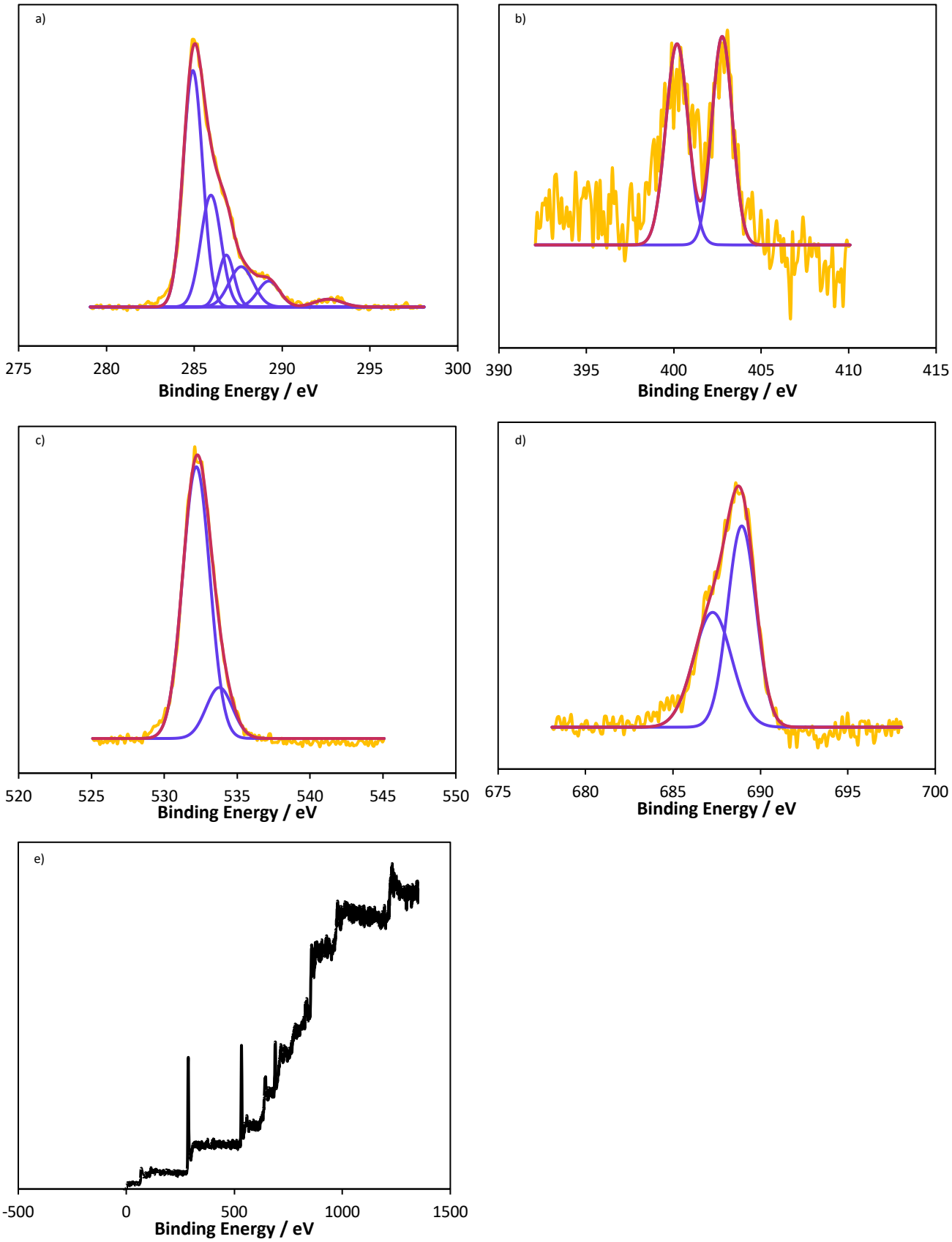

C5: XPS data of a carbon electrode modified from trifluoroacetyl-4-dimethylaminopyridinium showing the a) C1s region; b) N1s region; c) O1s region; d) F1s region; e) survey spectrum. Red line – cumulative fit; blue line – individual peaks; yellow line – raw data.

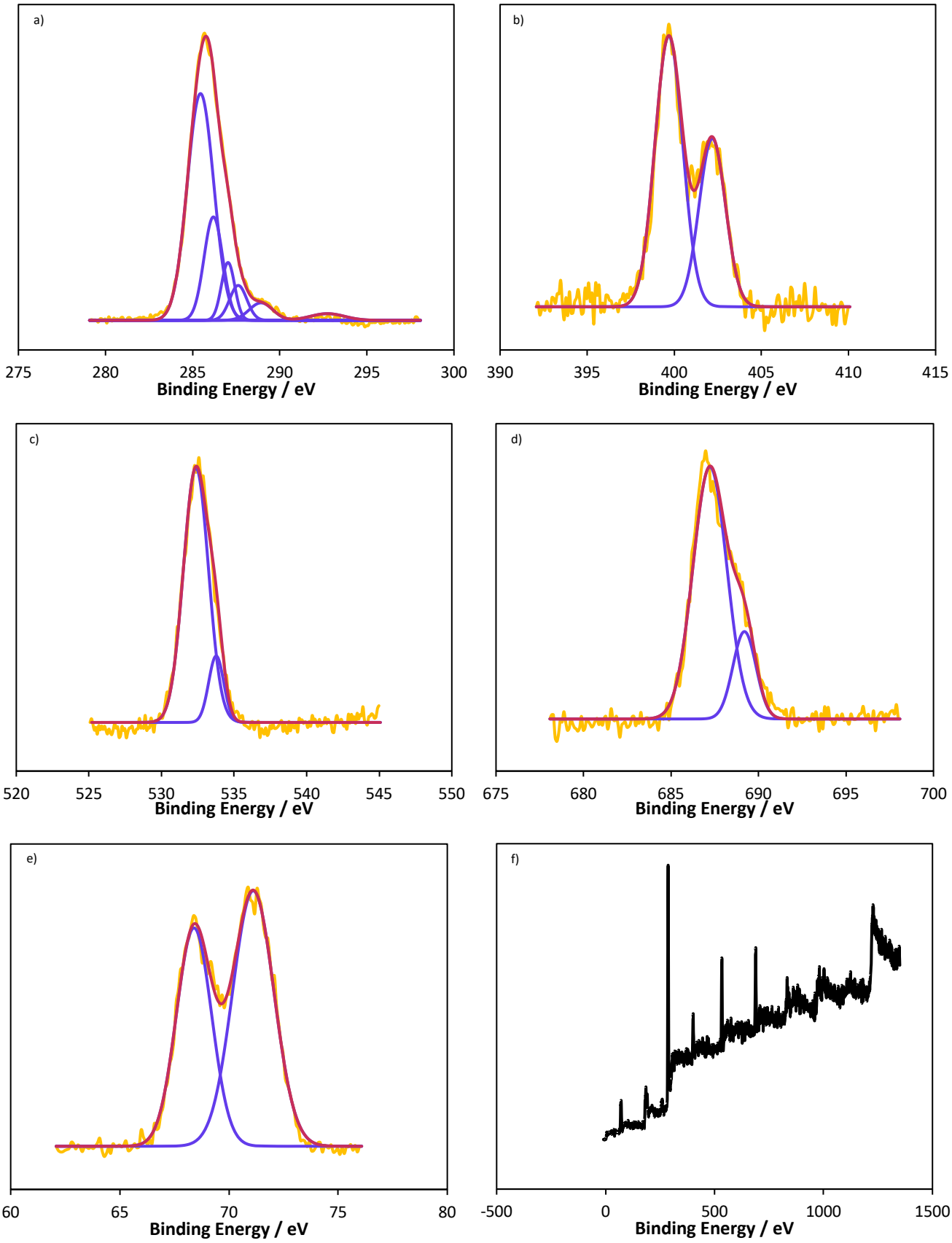

C6: XPS data of a carbon electrode modified from trifluoroacetyl-3- methylpyridinium showing the a) C1s region; b) N1s region; c) O1s region; d) F1s region; e) Br3d region; f) survey spectrum. Red line – cumulative fit; blue line – individual peaks; yellow line – raw

Carbon Electrode Modified with Trifluoroacetylpyridinium then Base-Treated

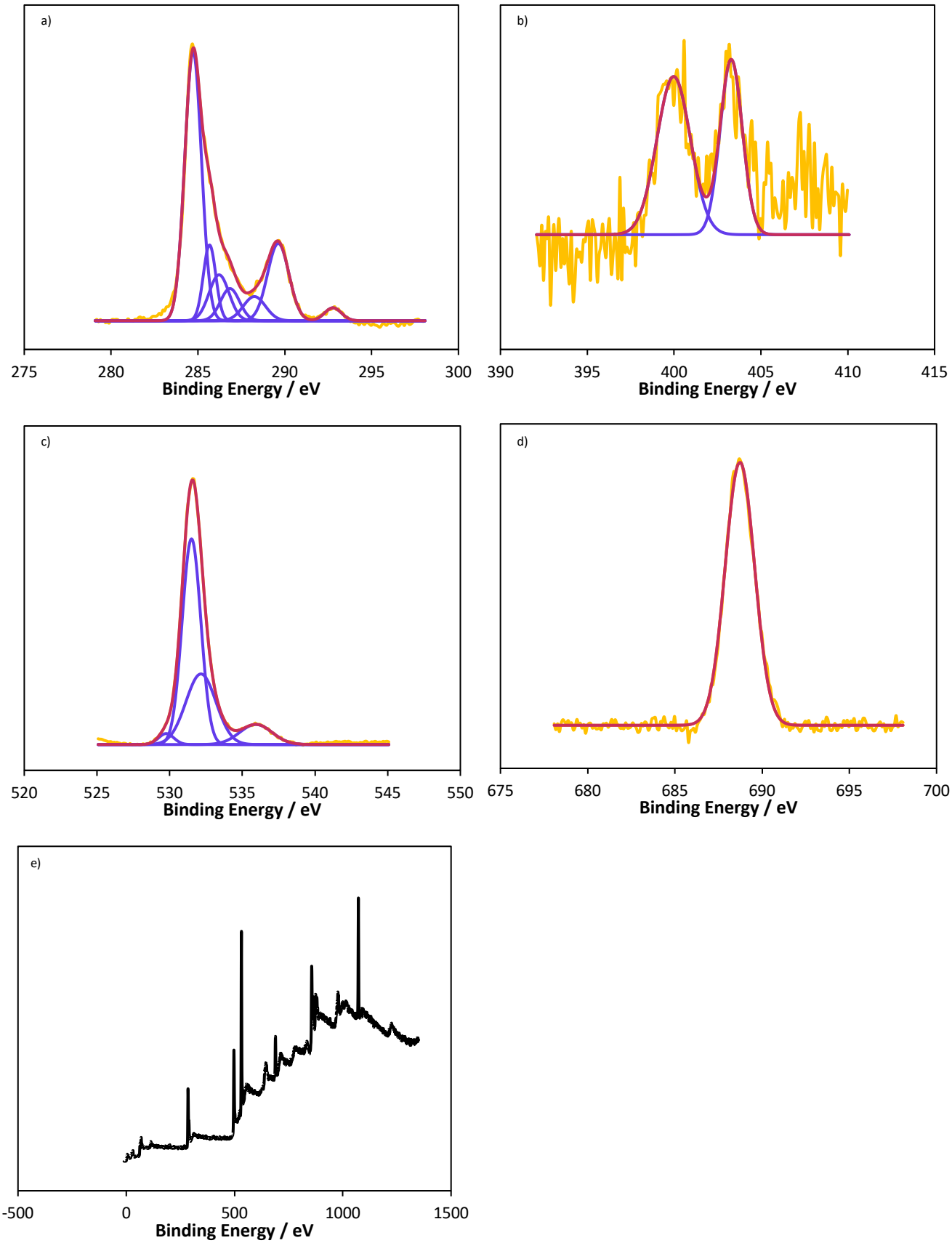

C7: XPS data of a carbon electrode modified from trifluoroacetylpyridinium, then base-treated, showing the a) C1s region; b) N1s region; c) O1s region; d) F1s region; e) survey spectrum. Red line – cumulative fit; blue line – individual peaks; yellow line – raw data.

Carbon Electrode Modified with Trifluoroacetylpyridinium then Acid-Treated

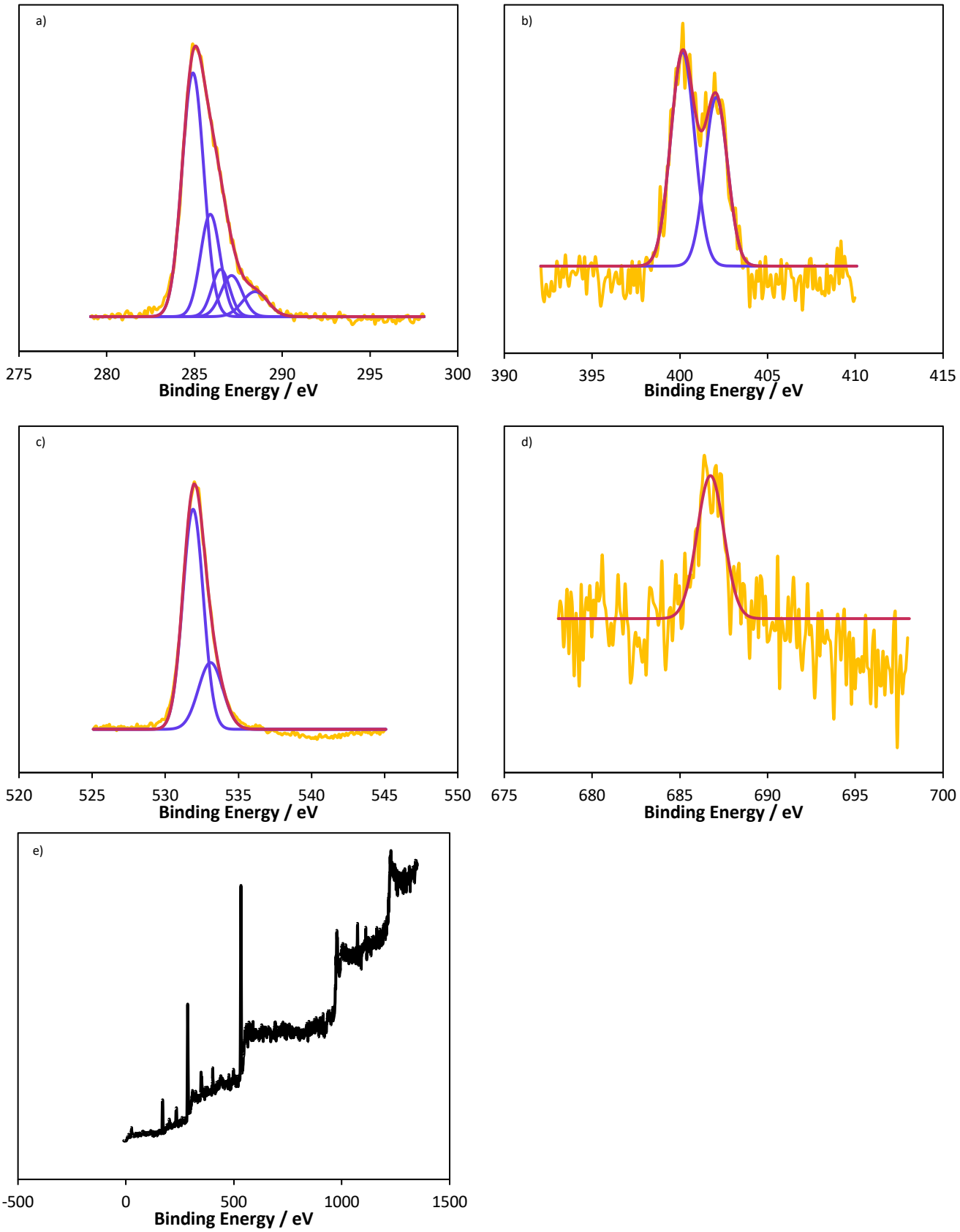

C8: XPS data of a carbon electrode modified from trifluoroacetylpyridinium, then acid treated, showing the a) C1s region; b) N1s region; c) O1s region; d) F1s region; e) survey spectrum. Red line – cumulative fit; blue line – individual peaks; yellow line – raw data.

Carbon Electrode Modified with Trifluoroacetylpyridinium with $LiClO_4$ Electrolyte

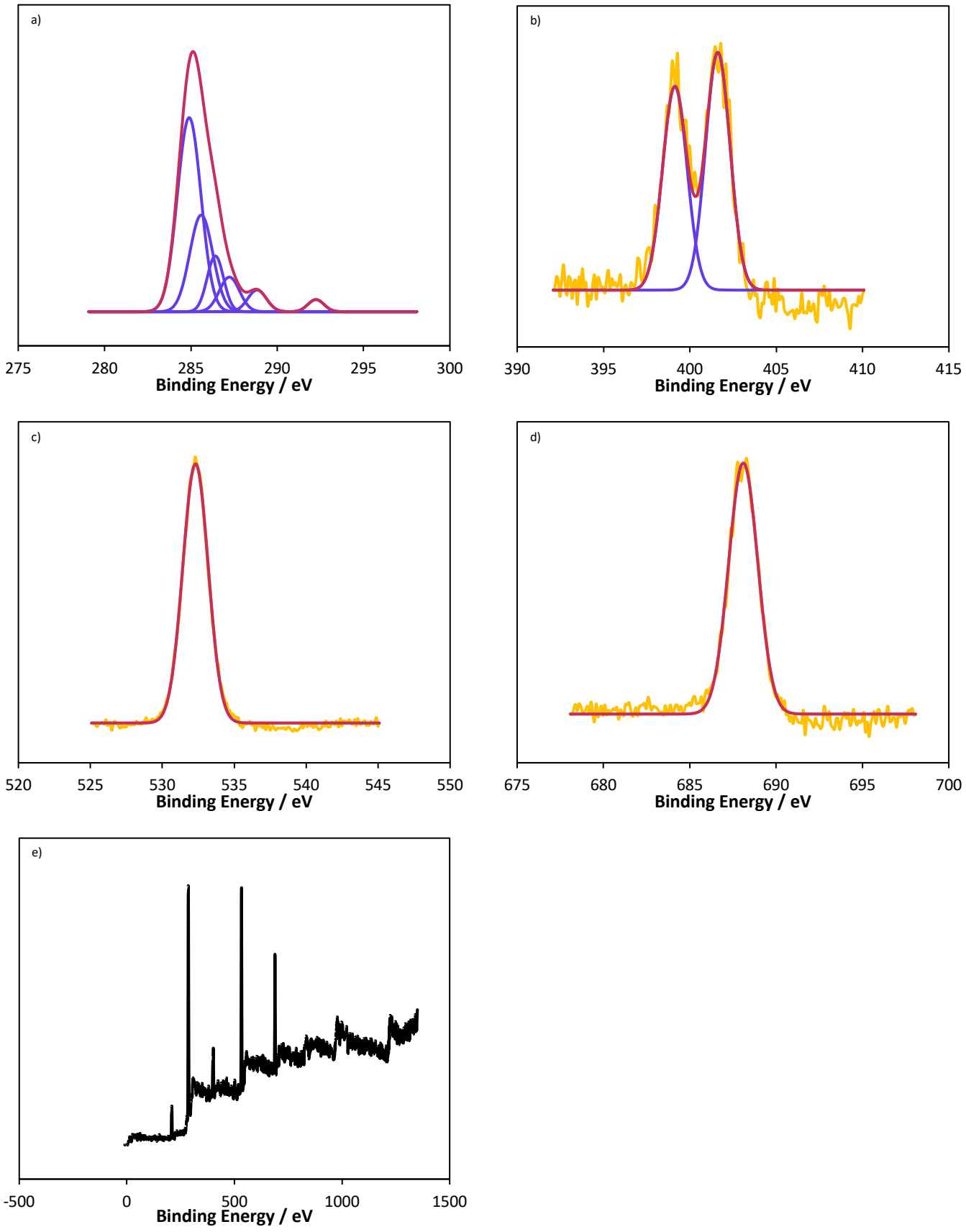

C9: XPS data of a carbon electrode modified from trifluoroacetylpyridinium with $LiClO_4$ electrolyte, showing the a) C1s region; b) N1s region; c) O1s region; d) F1s region; e) survey spectrum. Red line – cumulative fit; blue line – individual peaks; yellow line – raw data.

Carbon Electrode Modified with Trifluoroacetylpyridinium with No Electrolyte

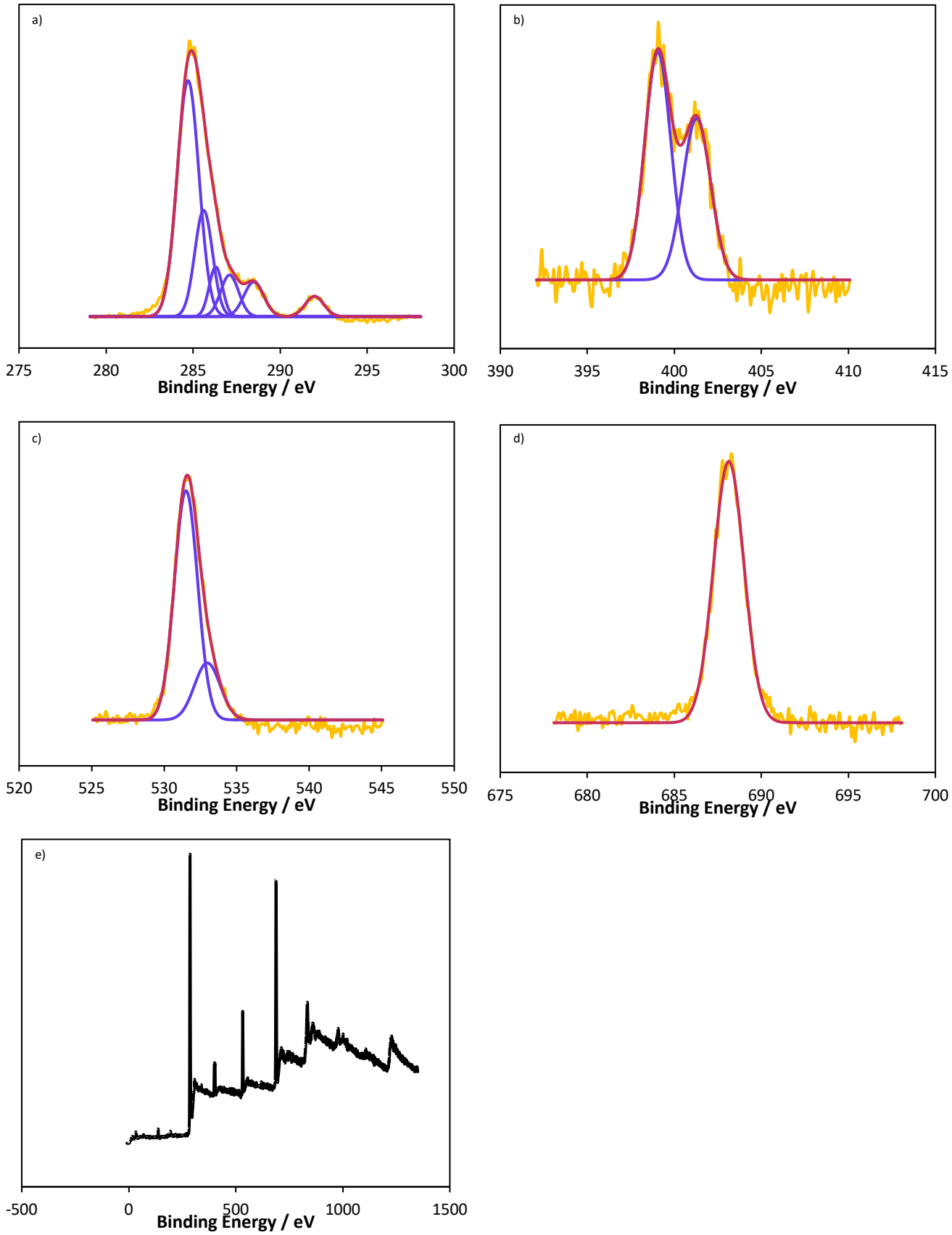

C10: XPS data of a carbon electrode modified from trifluoroacetylpyridinium with $LiClO_4$ electrolyte, showing the a) C1s region; b) N1s region; c) O1s region; d) F1s region; e) survey spectrum. Red line – cumulative fit; blue line – individual peaks; yellow line – raw data.

Carbon Electrode Modified with Trifluoroacetylpyridinium at -0.96 V, Degassed Solution

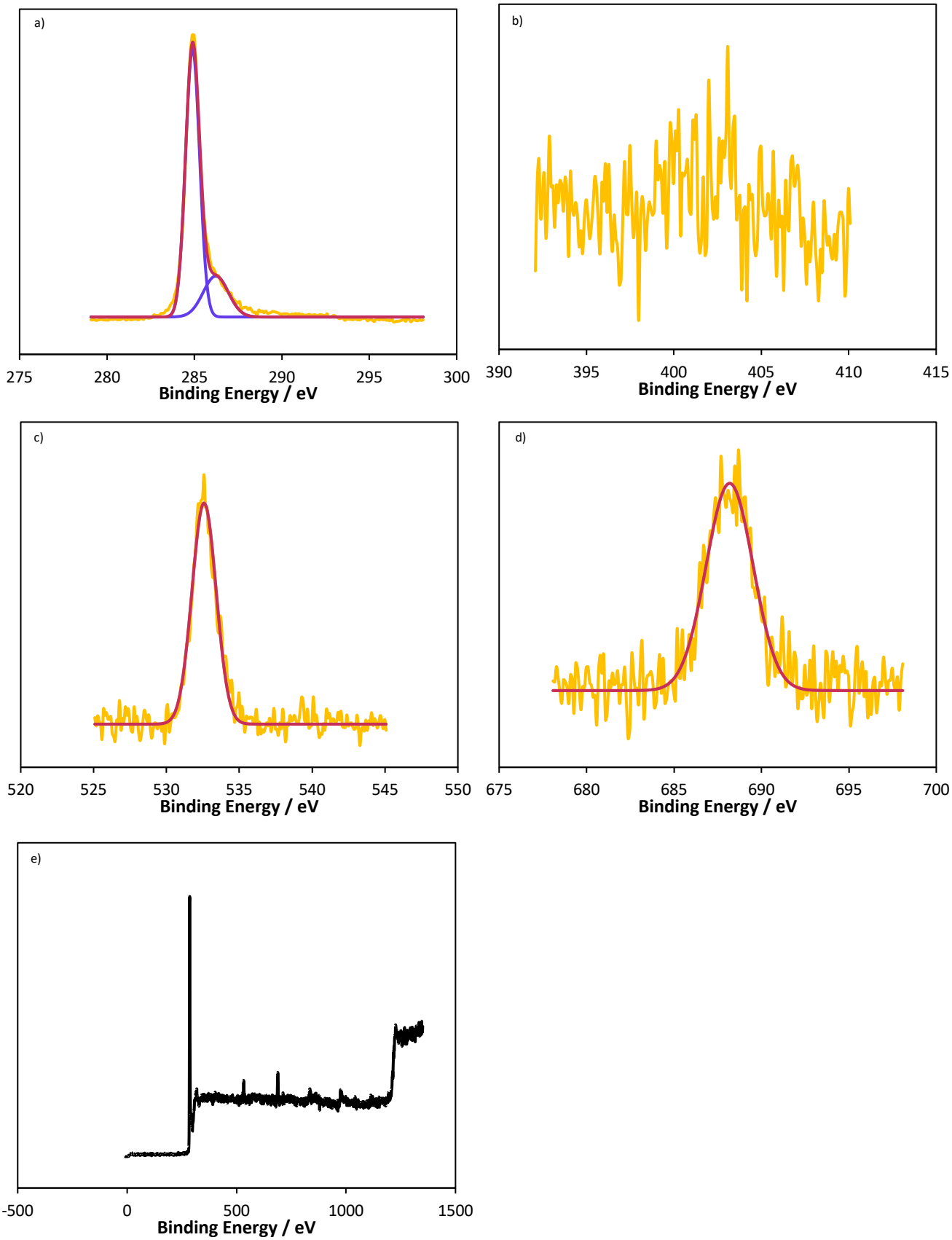

C11: XPS data of a carbon electrode modified from trifluoroacetylpyridinium, at -0.96 V with a degassed solution, showing the a) C1s region; b) N1s region; c) O1s region; d) F1s region; e) survey spectrum. Red line – cumulative fit; blue line – individual peaks; yellow line – raw data.

Carbon Electrode Modified with Trifluoroacetylpyridinium at -0.96 V, Not Degassed

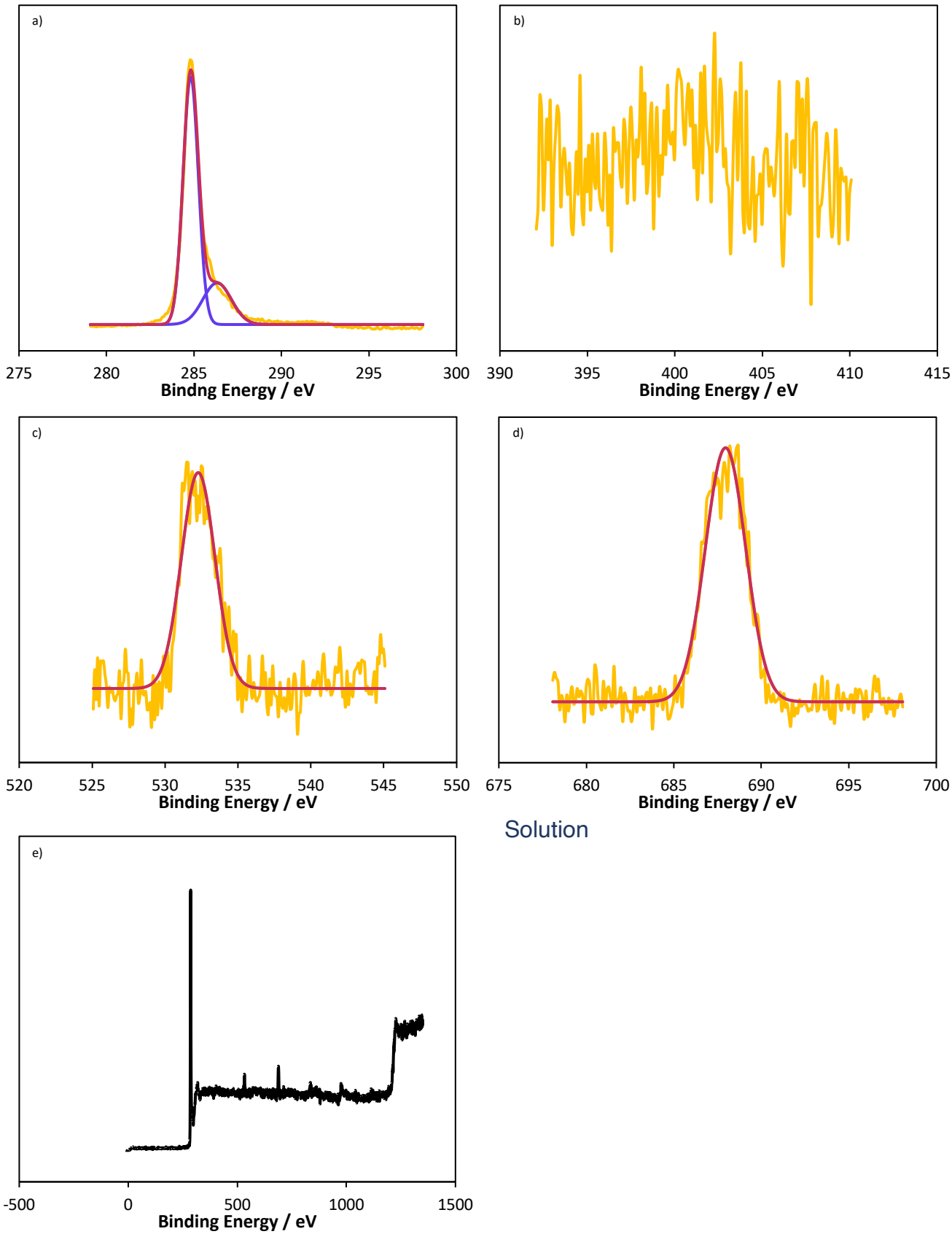

C12: XPS data of a carbon electrode modified from trifluoroacetylpyridinium, at -0.96 V with a non-degassed solution, showing the a) C1s region; b) N1s region; c) O1s region; d) F1s region; e) survey spectrum. Red line – cumulative fit; blue line – individual peaks; yellow line – raw data.

Carbon Electrode Modified with Trifluoroacetylpyridinium at -1.52 V, Degassed

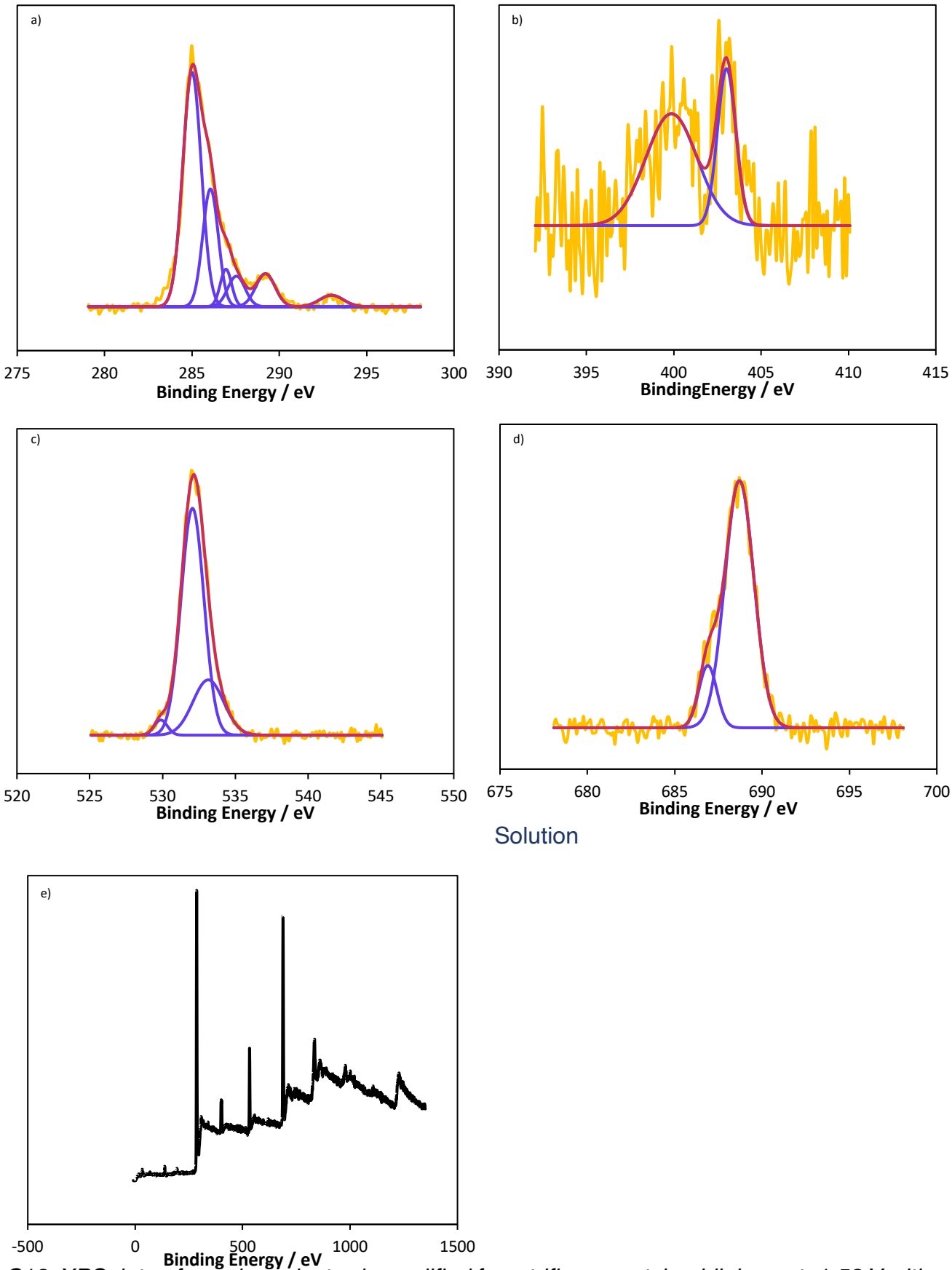

C13: XPS data of a carbon electrode modified from trifluoroacetylpyridinium, at -1.52 V with a degassed solution, showing the a) C1s region; b) N1s region; c) O1s region; d) F1s region; e) survey spectrum. Red line – cumulative fit; blue line – individual peaks; yellow line – raw data.

Carbon Electrode Modified with Trifluoroacetylpyridinium at -1.52 V, Not Degassed Solution

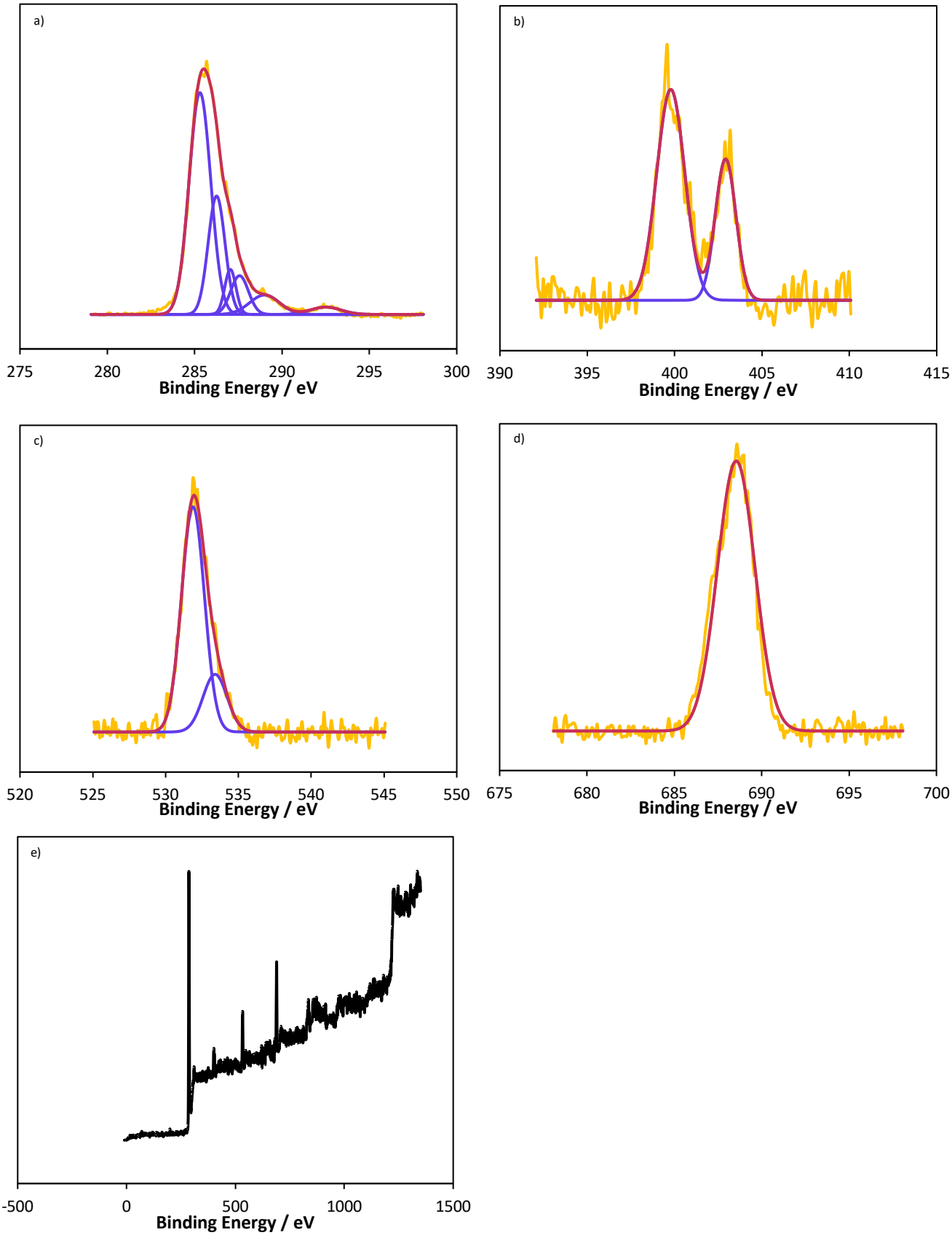

C14: XPS data of a carbon electrode modified from trifluoroacetylpyridinium, at -1.52 V with a non-degassed solution, showing the a) C1s region; b) N1s region; c) O1s region; d) F1s region; e) survey spectrum. Red line – cumulative fit; blue line – individual peaks; yellow line – raw data.

Appendix D

Oxytrifluoromethylation of Styrene(s) Experimental

Chapter six detailed the experiments undertaken to develop a successful electrosynthetic oxytrifluoromethylation reaction. The work below describes the refined procedure along with full characterisation of the products formed. The identities of these products were confirmed via NMR, IR and mass spectrometry data that matched with those found in the literature.[150, 156, 157, 158]

General Procedure

All reactions were carried out in a 20 ml sample tube that had been dried in an oven overnight. The sample tube was fitted with a plastic lid with 4 holes, one for each electrode and an air inlet. The electrodes used were: glassy carbon working electrode, nickel counter electrode, silver wire reference electrode.

$TBAPF_6$ (0.5811g, 1.5 mmol) was dissolved in MeCN (15 ml) to make up a 0.1 M solution, in a 20 ml sample tube equipped with a stir bar. This was used as the reaction cell. Pyridine (0.80 ml, 10 mmol) and styrene (0.12 ml, 1 mmol) were then added to the cell. Under constant mixing, TFAA (2.10 ml, 15 mmol) was added slowly to the solution. The cell was then connected to an air cylinder via a needle. Air was gently bubbled through the solution for the entire reaction. The electrodes were then added to the cell and connected to the potentiostat. The potential of the working electrode was set to -1.55 V for 9 h using an Autolab potentiostat (EcoChemie, Netherlands), controlled by GPES version 4.7. After 9 h the potentiostat was turned off and the solution was diluted with EtOAc and washed with water. The organic layer was collected and condensed. The final product was purified via column chromatography (6% EtOAc/hexane).

NMR, IR and mass spectrometry were used to characterise the final products. To do this, small amounts of each sample (~1-2 mg) were dissolved in an appropriate

solvent. For NMR this was deuterated chloroform ($CDCl_3$), for IR this was petroleum ether (PET, which was allowed to evaporate from the IR prism before the spectrum was collected) and for mass spectrometry this was MeCN. For mass spectrometry, samples were submitted and run by the mass spectrometry team at UCL, on a Thermo Orbitrap Exactive Plus mass spectrometer. NMR samples were run on a Bruker NMR Avance Neo 700 or Avance III 400. The spectra were referenced to the solvent peak ($CHCl_3$ in $CDCl_3$ at 7.24 ppm for ^1H NMR and 77.0 ppm for ^{13}C NMR). The signals are noted as s = singlet, d = doublet, dd = doublet of doublets , t = triplet, dt = doublet of triplets, q = quartet. Coupling constants (J) are reported in Hz. IR samples were run on an ALPHA Bruker ATR using OPUS software. For IR spectroscopy a drop of the dissolved sample was placed on the IR prism and time was allowed for the PET to evaporate before the data was acquired.

Materials

The reaction was carried out in MeCN collected from the UCL Chemistry anhydrous solvent system (dried over alumina). EtOAc was used straight from the bottle. $TBAPF_6$ was used as the supporting electrolyte and was purchased from Merck Life Science UK and used without purification and was kept in a desiccator to ensure a dry environment when not in use. The starting materials were purchased from ACROS Organics, Alfa Aesar, Fisher Scientific Ltd. and Merck Life Science UK. The styrenes used were passed through a pipette of aluminium oxide before use, to remove any radical inhibitors in the solution. All other starting materials were used without purification. The air cylinder used was purchased from BOC.

3,3,3-trifluoro-1-phenylpropan-1-one **70a**

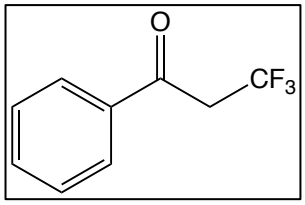

General procedure yielded a white solid, 70a (85 mg, 45%); IR ν_{max} (neat) 2924 (C-H), 1700 (C=O), 1598 (Ar-H) cm^{-1}; ^{1}H NMR (400 MHz, $CDCl_3$) δ_H 7.94 (2H, d, *J* 8.4, Ar*H*), 7.64 (1H, tt, *J* 1.29, 7.4, Ar*H*), 7.51 (2H, t, *J* 7.4, Ar*H*), 3.8 (2H, q, *J* 10, CH_2) ppm; ^{13}C NMR (176 MHz, $CDCl_3$) δ_C 189.8 (*C*=O), 136.0 (Ar*C*), 134.3 (Ar*C*), 129.1 (Ar*C*), 128.5 (Ar*C*), 124.1 (q, *J* 278, *C*F_3), 42.3 (q, *J* 28, *C*H_2) ppm; ^{19}F NMR (400 MHz, $CDCl_3$) δ_F -62.0 (C*F*$_3$) ppm; *m/z* expected M^+ ($C_9H_7OF_3$) 189.0521, found 189.0519.

3,3,3-trifluoro-1-(4-methylphenyl)propan-1-one **70b**

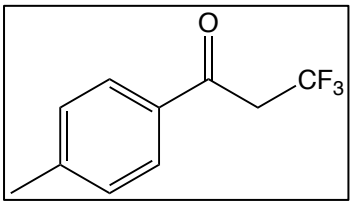

General procedure, but with 4-methylstyrene (0.13 ml, 1 mmol) yielded a white solid, **70b** (40 mg, 20%); IR ν_{max} (neat) 2925 (C-H), 1694 (C=O), 1606 (Ar-H) cm^{-1}; ^{1}H NMR (400 MHz, $CDCl_3$) δ_H 7.83 (2H, d, *J* 8.3, Ar*H*), 7.30 (2H, d, *J* 8.3, Ar*H*), 3.76 (2H, q, *J* 10, CH_2), 2.43 (3H, *s*, CH_3) ppm; ^{13}C NMR (176 MHz, $CDCl_3$) δ_C 189.4 (*C*=O), 145.5 (Ar*C*), 133.6 (Ar*C*), 129.7 (Ar*C*), 128.6 (Ar*C*), 124.2 (q, *J* 277, *C*F_3), 42.2 (q, *J* 28, *C*H_2), 21.8 (*C*H_3) ppm; ^{19}F NMR (400 MHz, $CDCl_3$) δ_F -62.0 (C*F*$_3$) ppm; *m/z* expected M^+ ($C_{10}H_9OF_3$) 203.0678, found 203.0675.

1-(4-fluorophenyl)-3,3,3-trifluoropropan-1-one **70c**

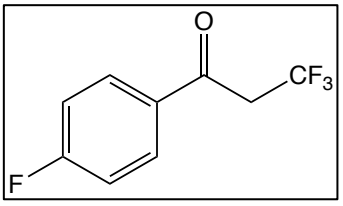

General procedure, but with 4-fluorostyrene (0.11 ml, 1 mmol) yielded a white solid, **70c**, (76 mg, 37%); IR ν_{max} (neat) 1699 (C=O), 1600 (Ar-H), cm^{-1}; ^{1}H NMR (400 MHz, $CDCl_3$) δ_H 7.97 (2H, dd, *J* 8.9, 5.3, Ar*H*), 7.18 (2H, t, *J* 8.6, Ar*H*), 3.77 (2H, q, *J* 10, CH_2), ppm; ^{13}C NMR (100 MHz, $CDCl_3$) δ_C 188.3 (*C*=O), 166.5 (d, *J* 256, Ar*C*F), 132.4 (Ar*C*), 131.2 (d, *J* 9, Ar*C*), 123.7 (q, *J* 277, *C*F_3), 116.3 (d, *J*

22, Ar*C*), 42.2 (q, *J* 28, *C*H$_2$), ppm; ^{19}F NMR (400 MHz, CDCl$_3$) δ_F -62.0 (C*F*$_3$), 102.9 (C*F*) ppm.

1-(4-(*tert*-butyl)phenyl)-3,3,3-trifluoropropan-1-one **70d**

General procedure, but with 4-tert-butylstyrene (0.18 ml, 1 mmol) yielded a white solid, **70c**, (73mg, 30%). IR ν_{max} (neat) 2967 (C-H), 1695 (C=O), 1605 (Ar-H) cm^{-1}; ^{1}H NMR (400 MHz, CDCl$_3$) δ_H 7.88 (2H, dt, *J* 8.5, 2.05, Ar*H*), 7.52 (2H, dt, *J* 8.6, 2.05 Ar*H*), 3.77 (2H, q, *J* 10.1, C*H*$_2$), 1.35 (9H, s, C*H*$_3$) ppm; ^{13}C NMR (100 MHz, CDCl$_3$) δ_C 189.4 (*C*=O), 158.2 (Ar*C*), 133.4 (Ar*C*), 128.5 (Ar*C*), 126.0 (Ar*C*), 124.2 (q, *J* 277, *C*F$_3$), 42.1 (q, *J* 28, *C*H$_2$), 35.3 (Ar*C*(CH$_3$)$_3$), 31.1 (*C*H$_3$) ppm; ^{19}F NMR (400 MHz, CDCl$_3$) δ_F -62.0 (C*F*$_3$) ppm.

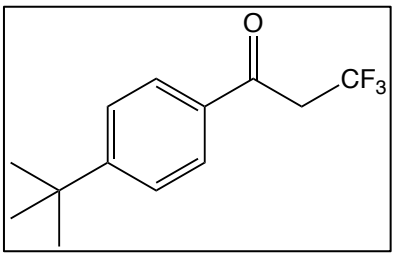

Spectroscopic Data for 3,3,3-trifluoro-1-phenylpropan-1-one **70a**

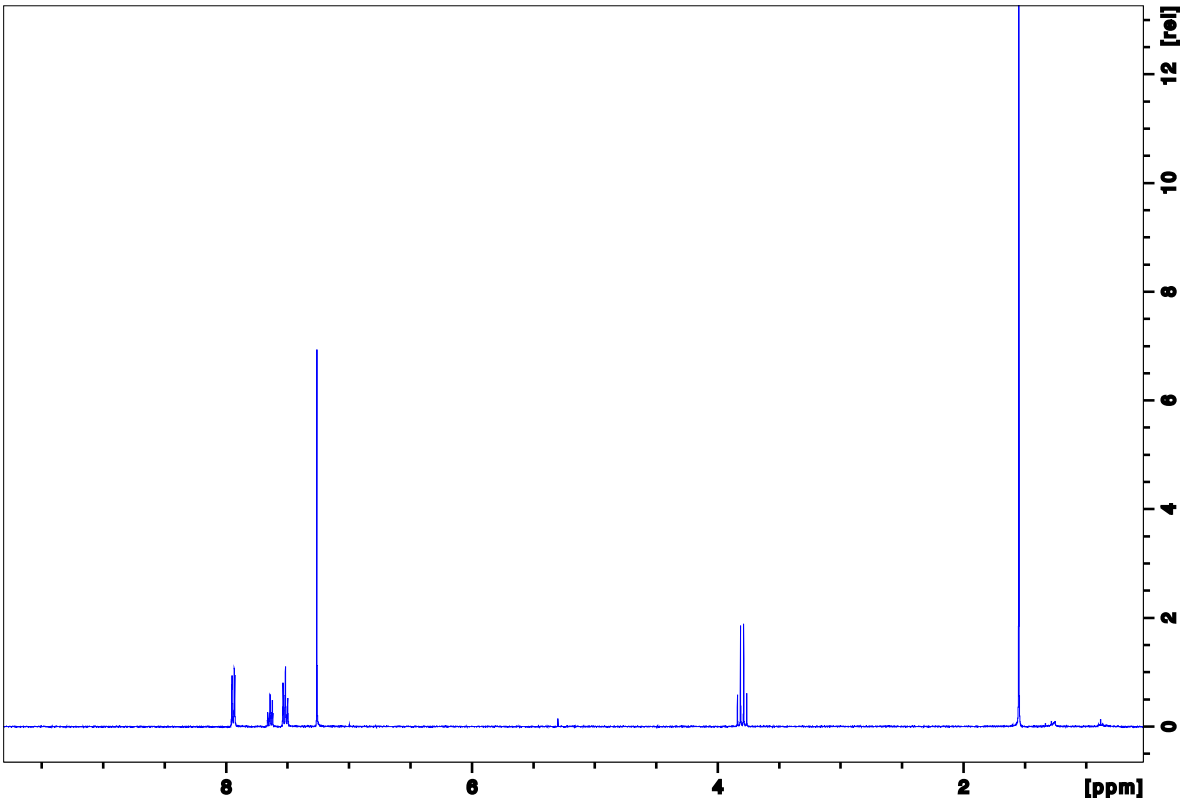

D1: ^{1}H NMR spectrum for 3,3,3-trifluoro-1-phenylpropan-1-one 70a

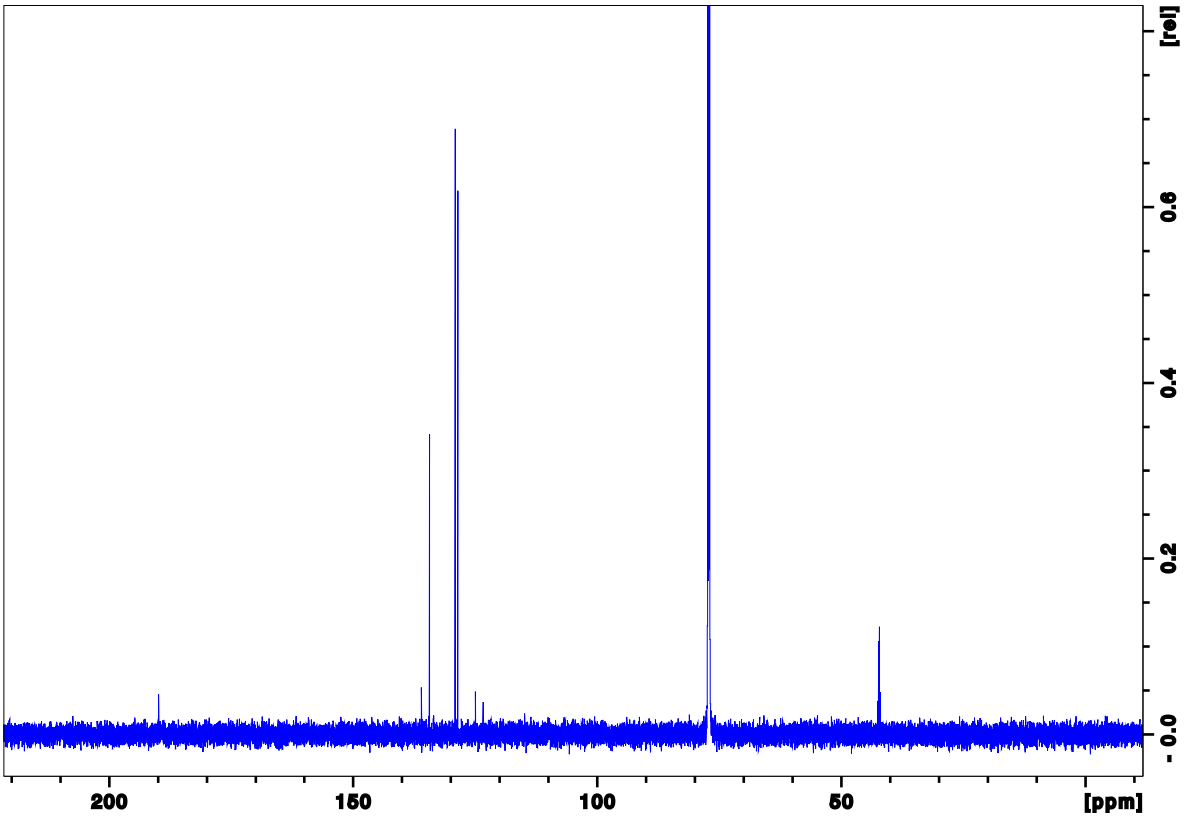

D2: ^{13}C NMR spectrum for 3,3,3-trifluoro-1-phenylpropan-1-one 70a

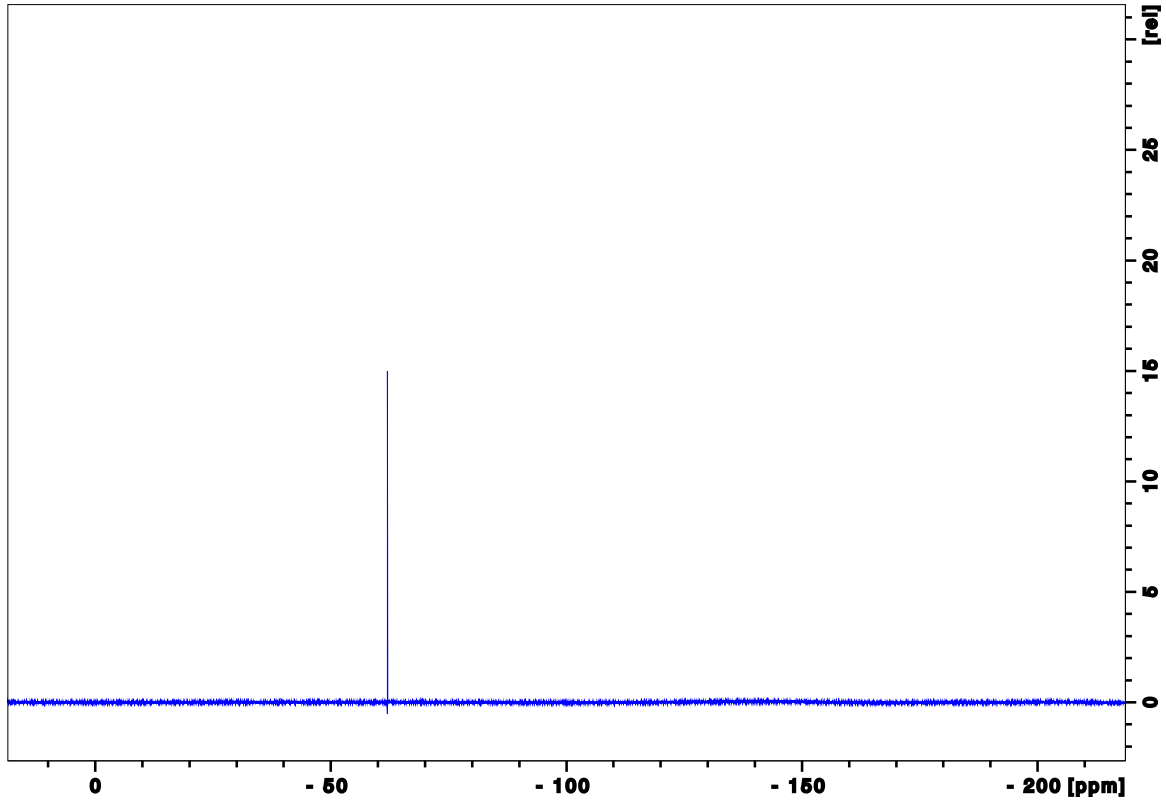

D3: [19]F NMR spectrum for 3,3,3-trifluoro-1-phenylpropan-1-one 70a

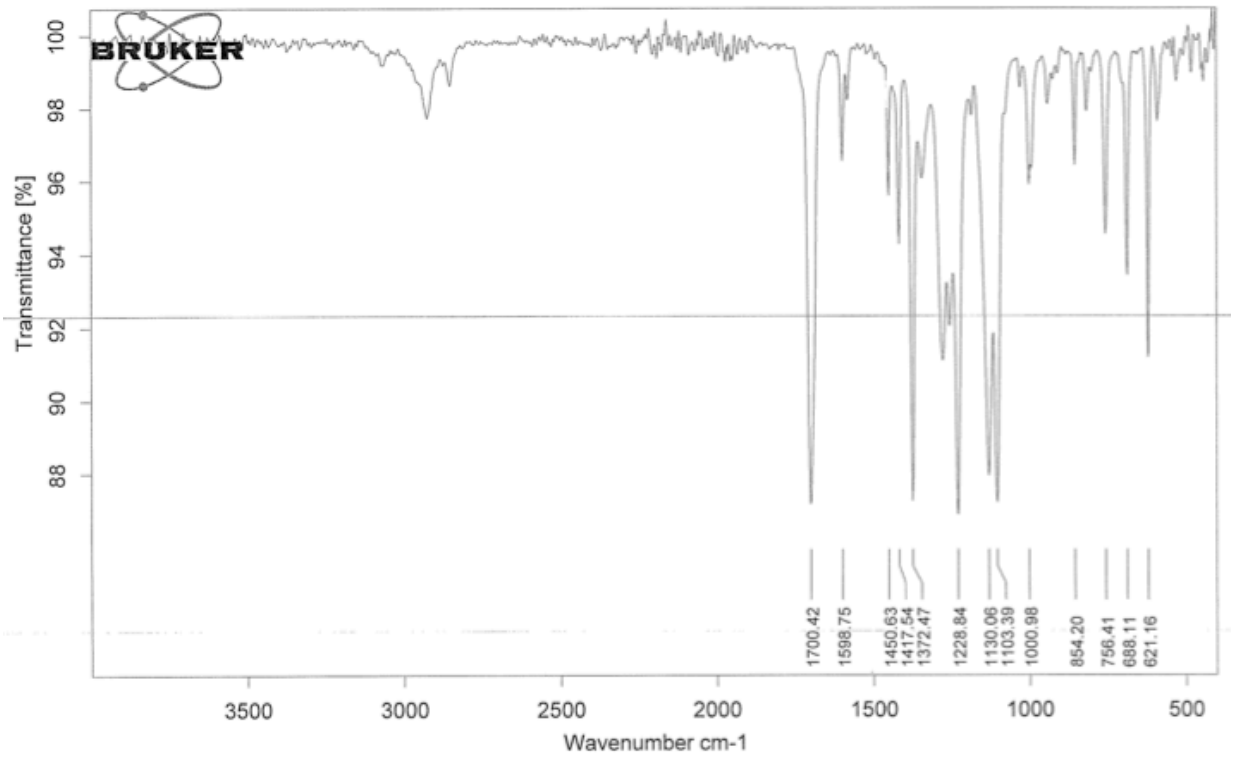

D4: IR spectrum for 3,3,3-trifluoro-1-phenylpropan-1-one 70a

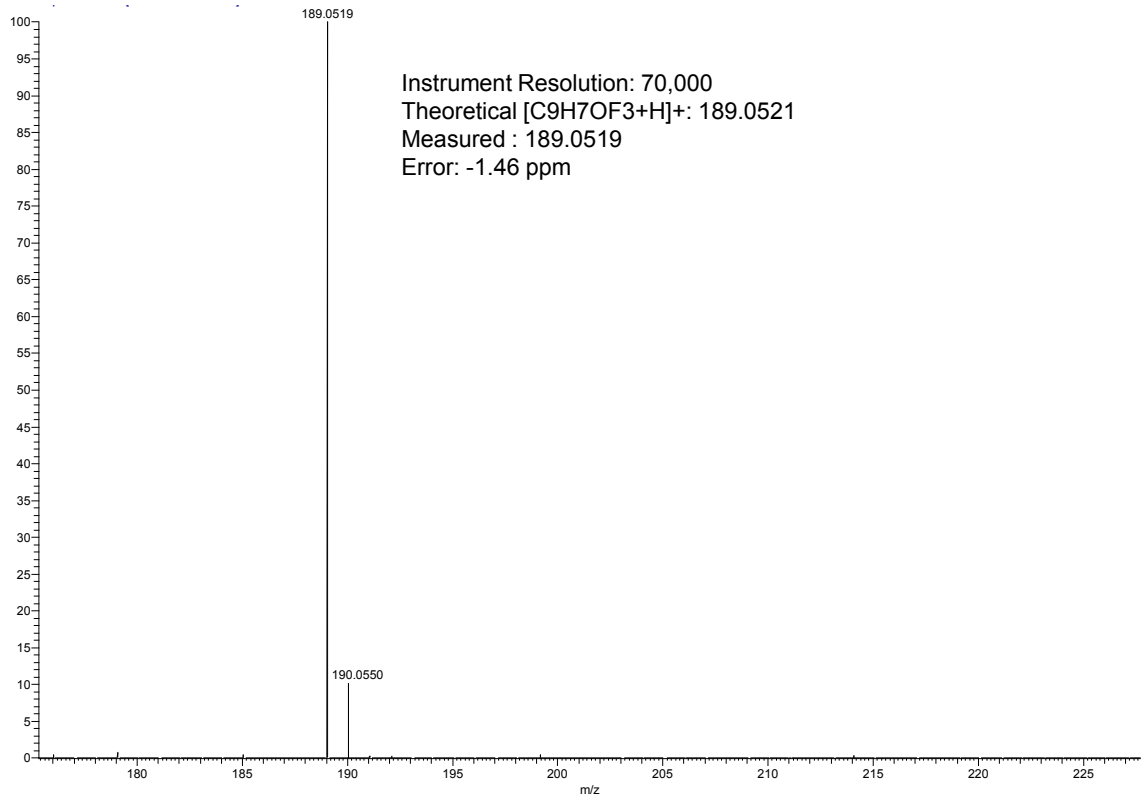

D5: Mass spectrum for 3,3,3-trifluoro-1-phenylpropan-1-one 70a

Spectroscopic Data for 3,3,3-trifluoro-1-(4-methylphenyl)propan-1-one **70b**

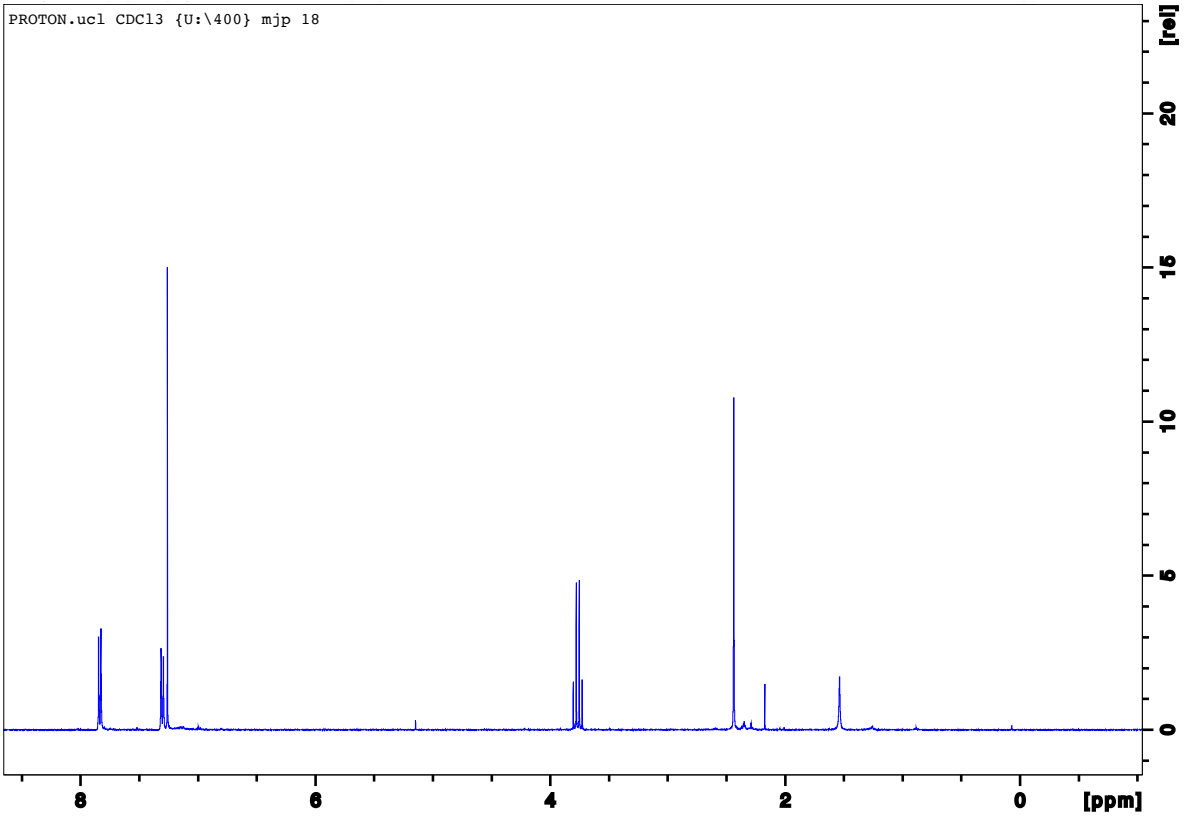

D6: ^{1}H NMR spectrum for 3,3,3-trifluoro-1-(4-methylphenyl)propan-1-one 70b

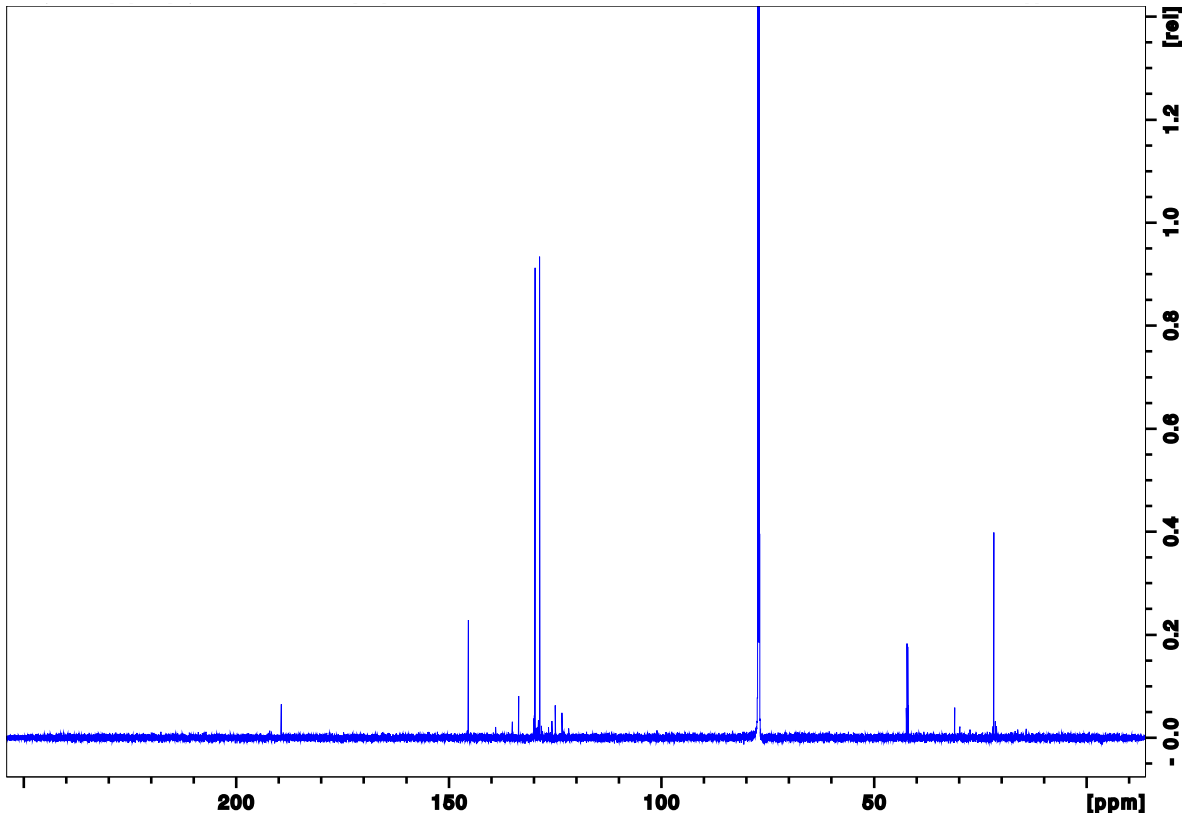

D7: ^{13}C NMR spectrum for 3,3,3-trifluoro-1-(4-methylphenyl)propan-1-one 70b

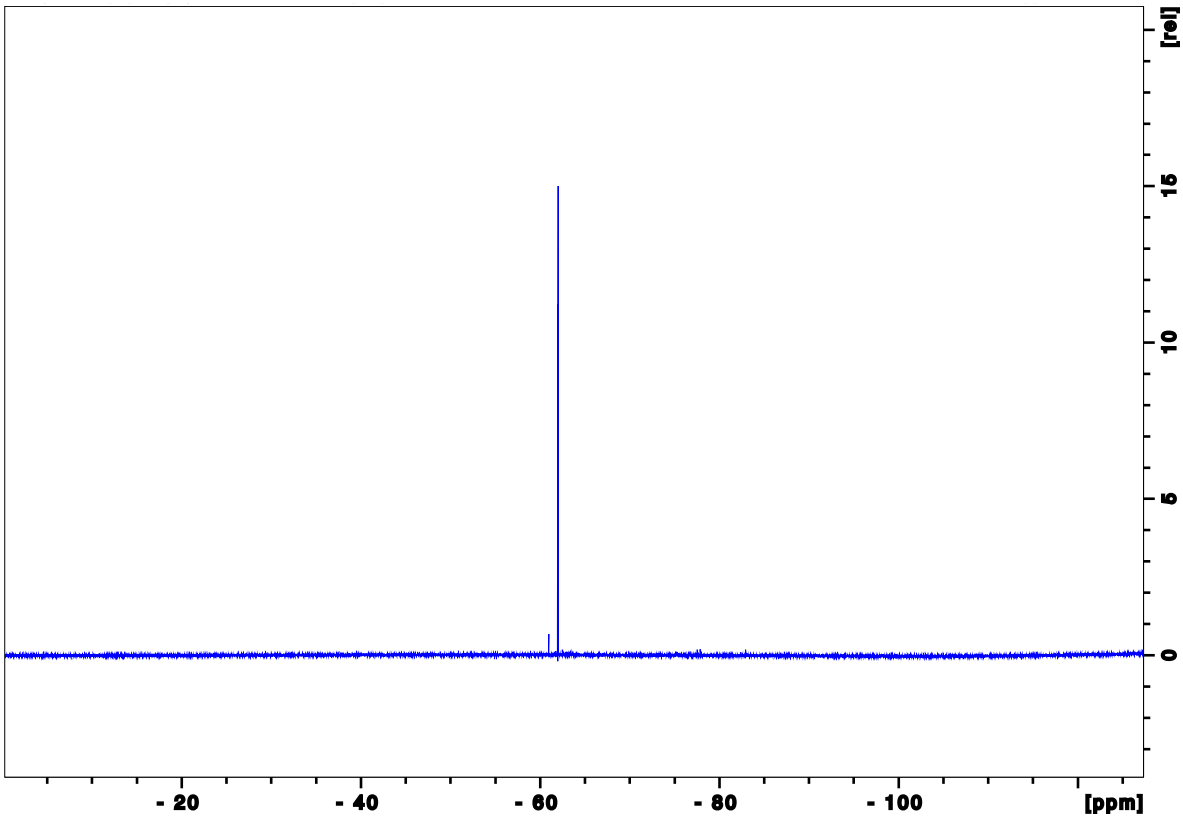

D8: ^{19}F NMR spectrum for 3,3,3-trifluoro-1-(4-methylphenyl)propan-1-one 70b

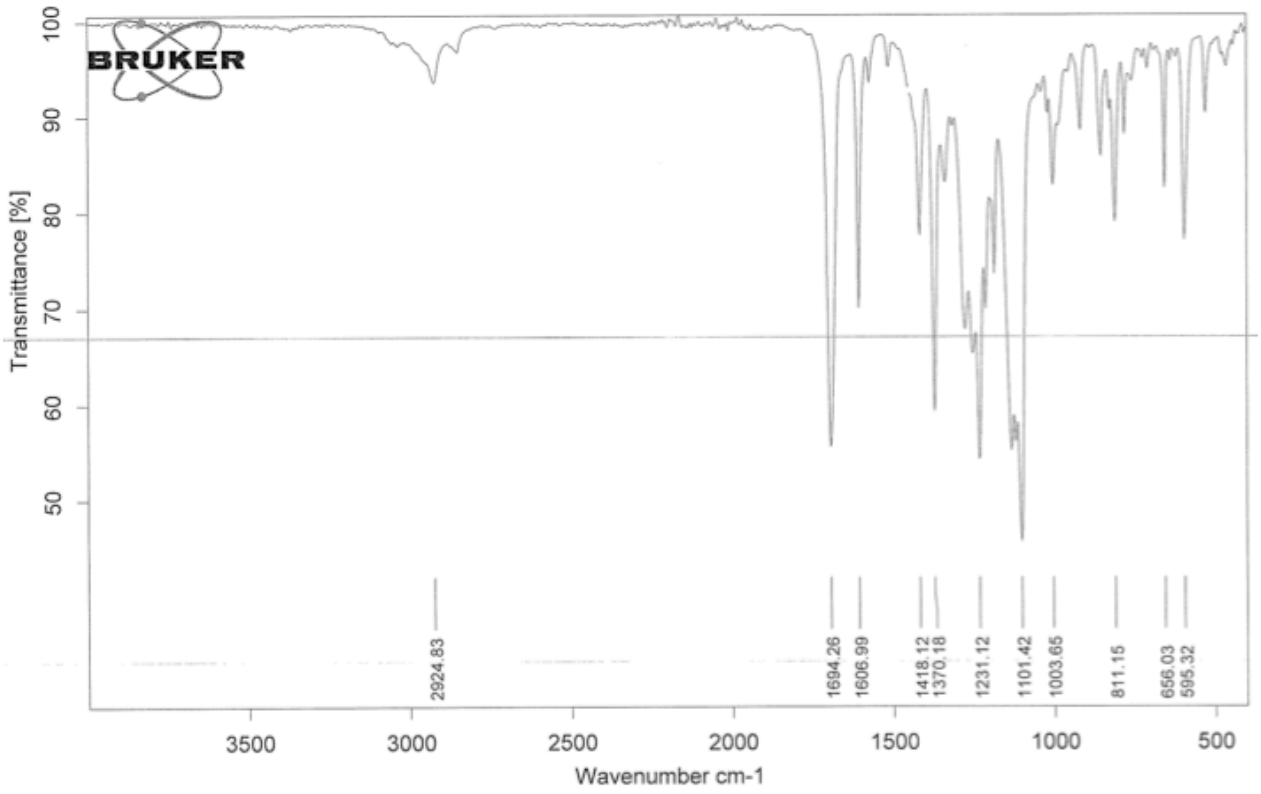

D9: IR spectrum for 1-(4-methylphenyl)-3,3,3-trifluoropropan-1-one 70b

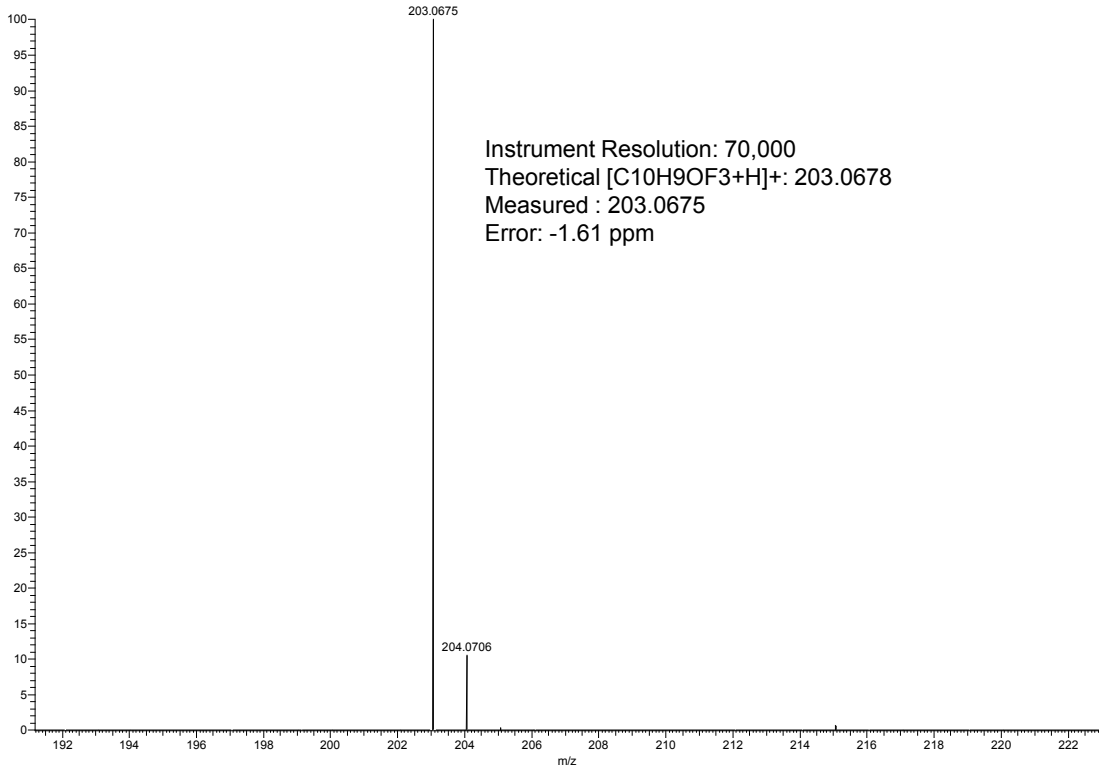

D10: Mass spectrum for 3,3,3-trifluoro-1-(4-methylphenyl)propan-1-one 70b

Spectroscopic Data for 1-(4-fluorophenyl)-3,3,3-trifluoropropan-1-one **70c**

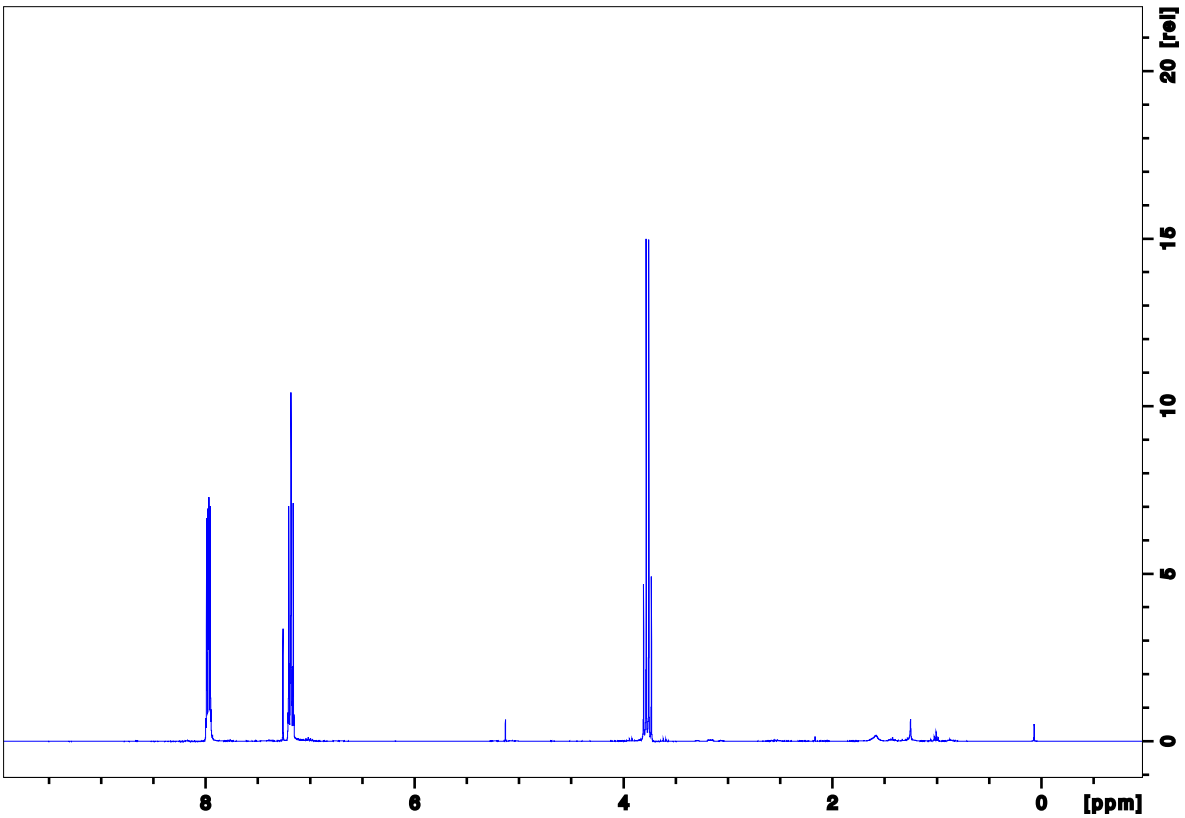

D11: ^{1}H NMR spectrum for 1-(4-fluorophenyl)-3,3,3-trifluoropropan-1-one 70c

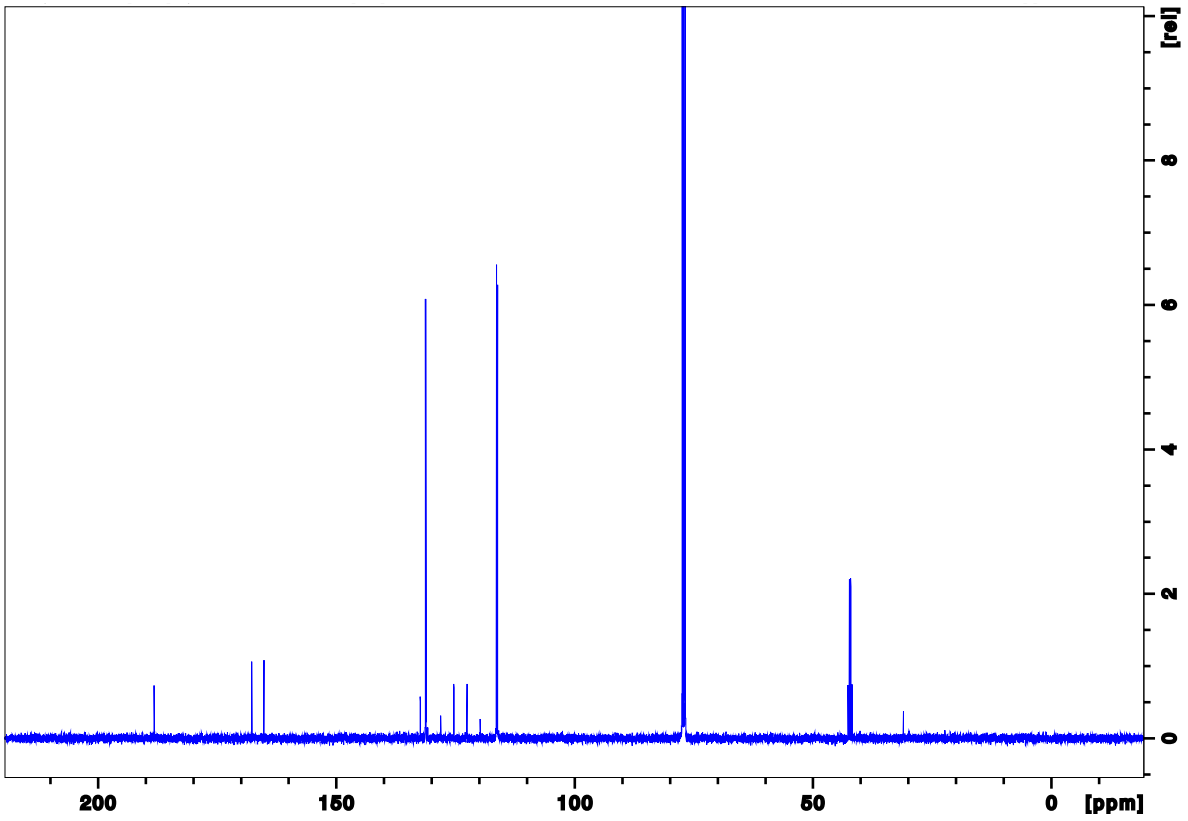

D12: ^{13}C NMR spectrum for 1-(4-fluorophenyl)-3,3,3-trifluoropropan-1-one 70c

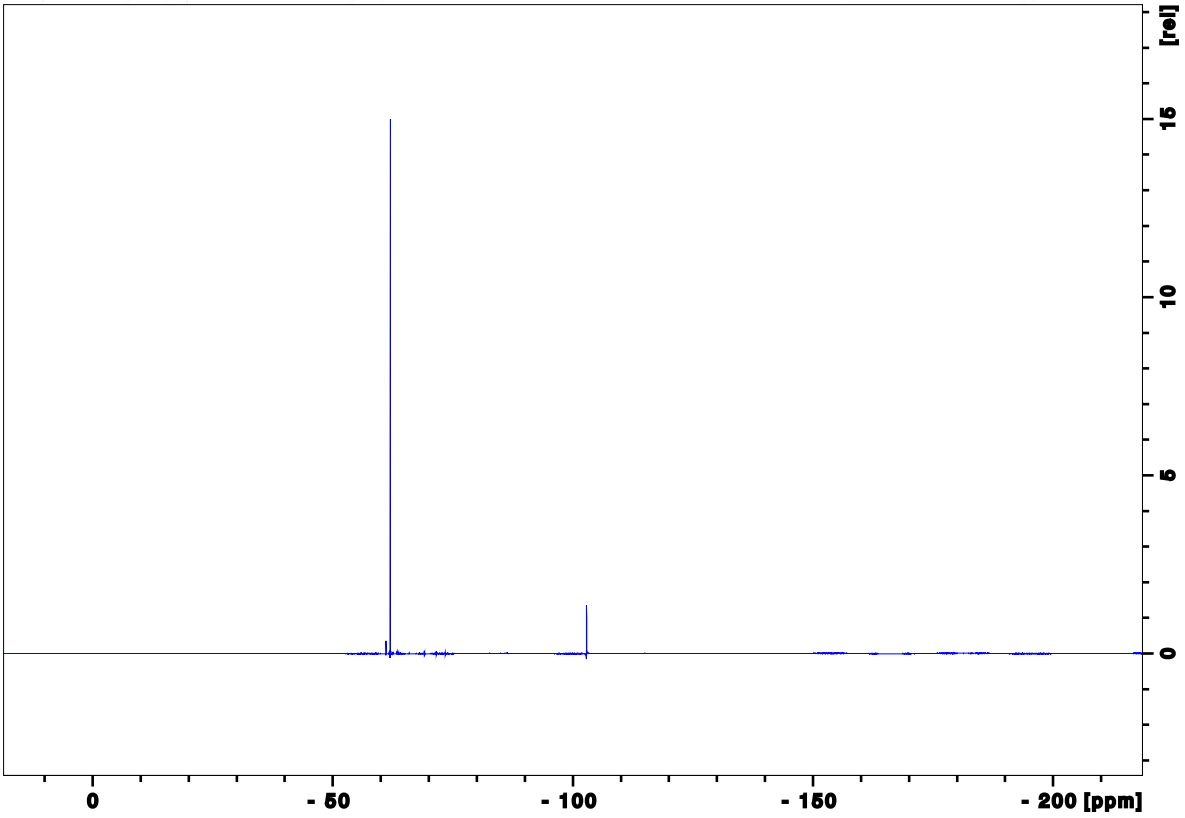

D13: ^{19}F NMR spectrum for 1-(4-fluorophenyl)-3,3,3-trifluoropropan-1-one 70c

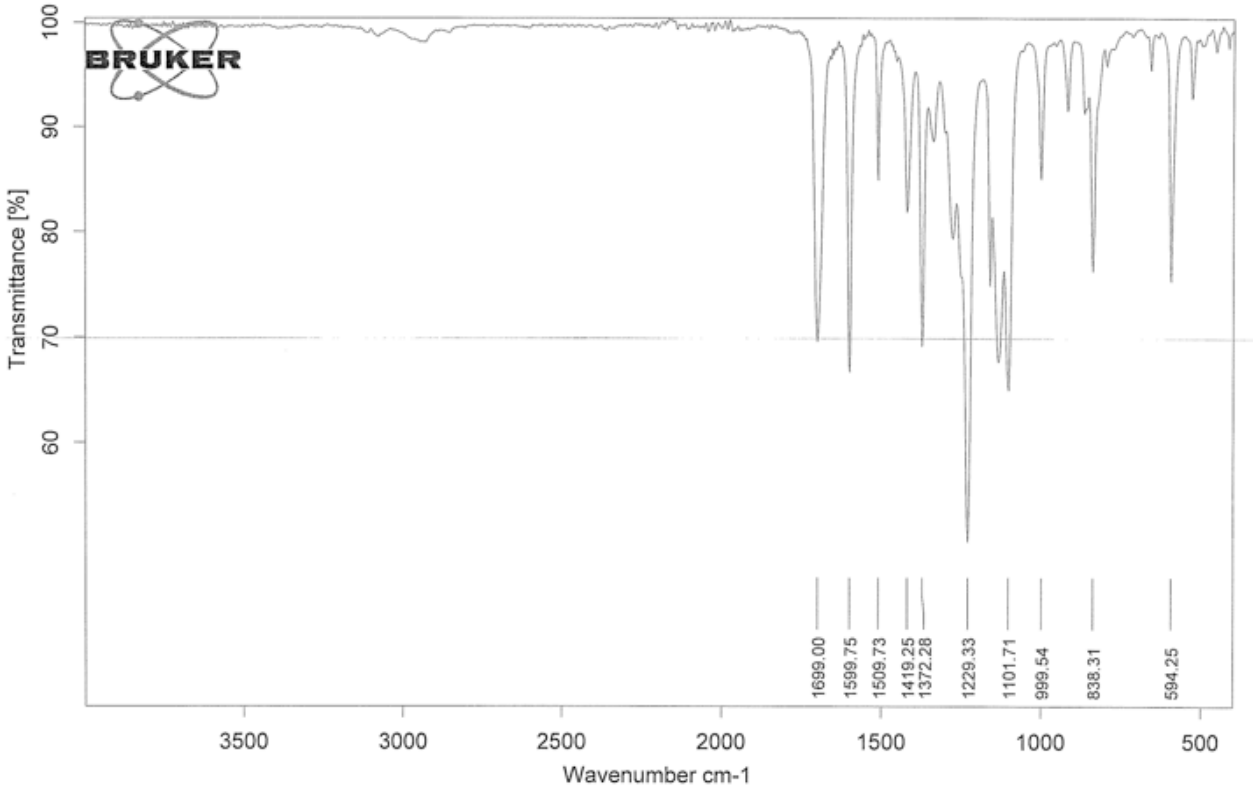

D14: IR spectrum for 1-(4-fluorophenyl)-3,3,3-trifluoropropan-1-one 70c

Spectroscopic Data for 1-(4-(tert-butyl)phenyl)-3,3,3-trifluoropropan-1-one **70d**

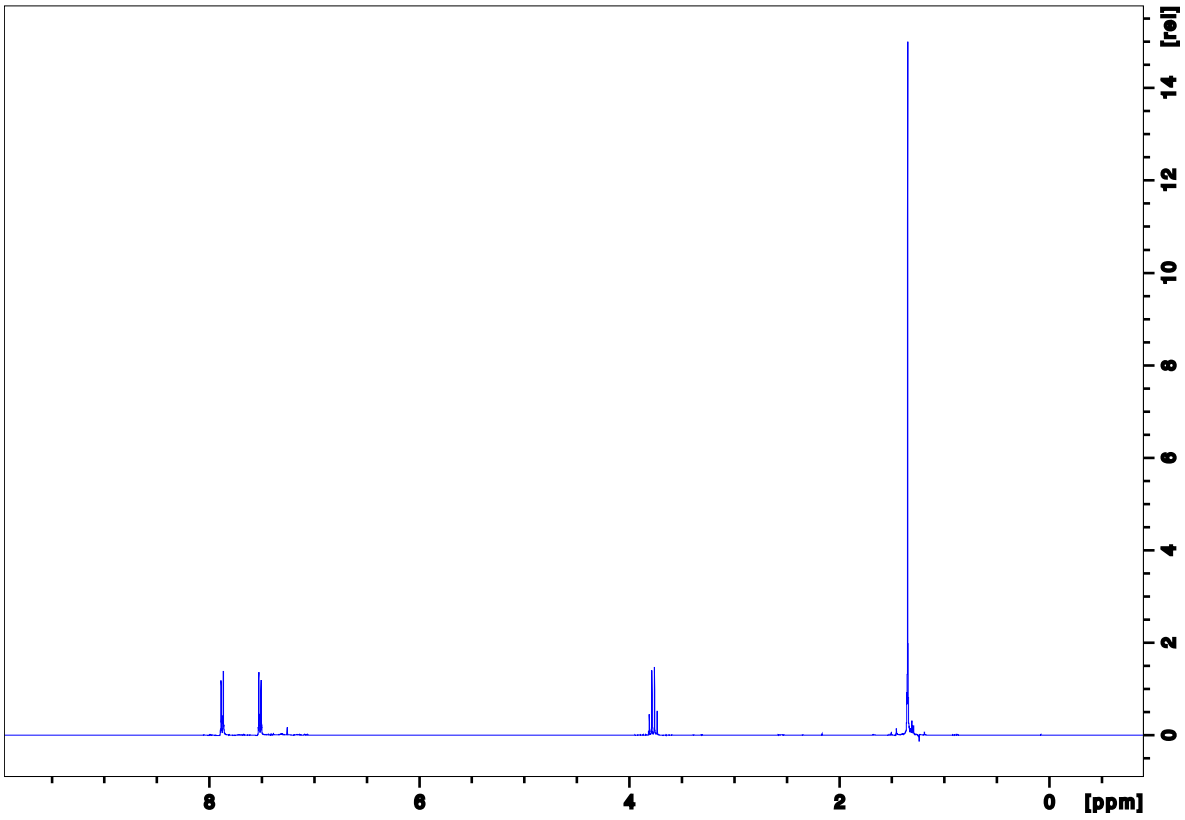

D15: ^{1}H NMR spectrum for 1-(4-(tert-butyl)phenyl)-3,3,3-trifluoropropan-1-one

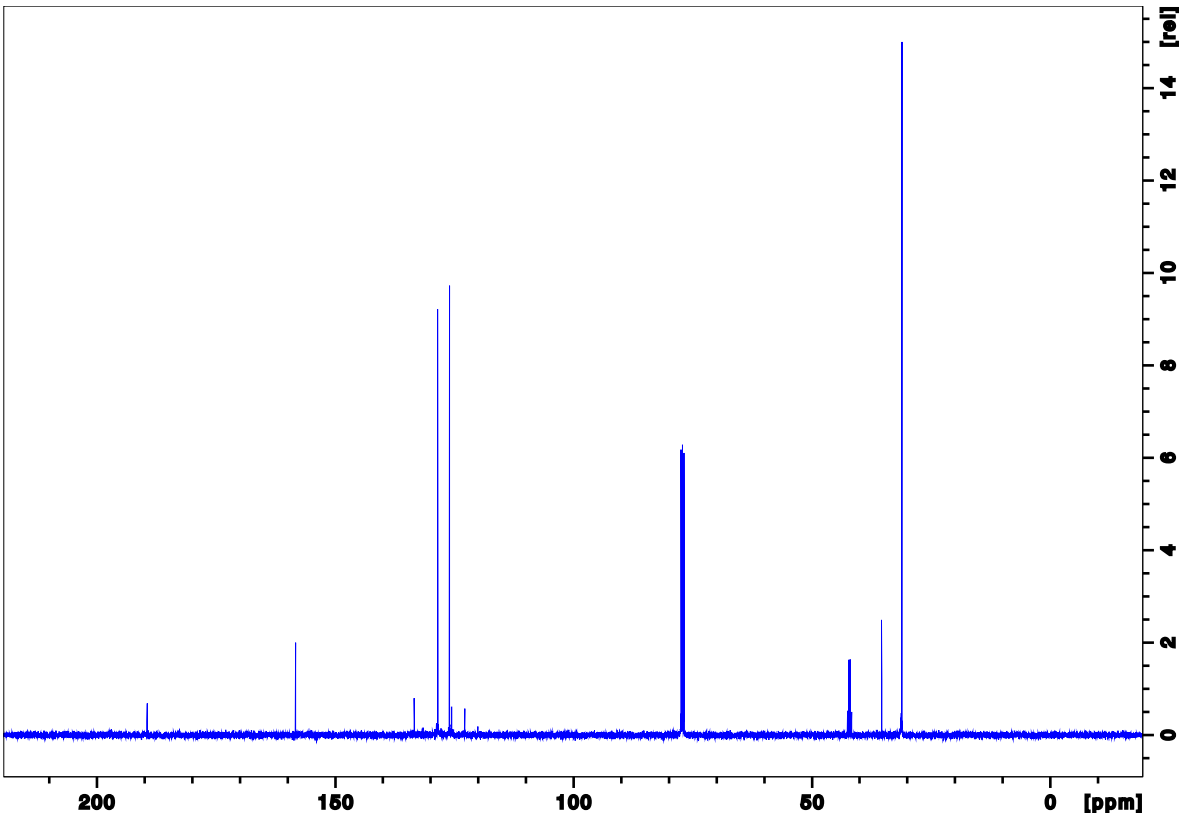

D16: ^{13}C NMR spectrum for 1-(4-(tert-butyl)phenyl)-3,3,3-trifluoropropan-1-one

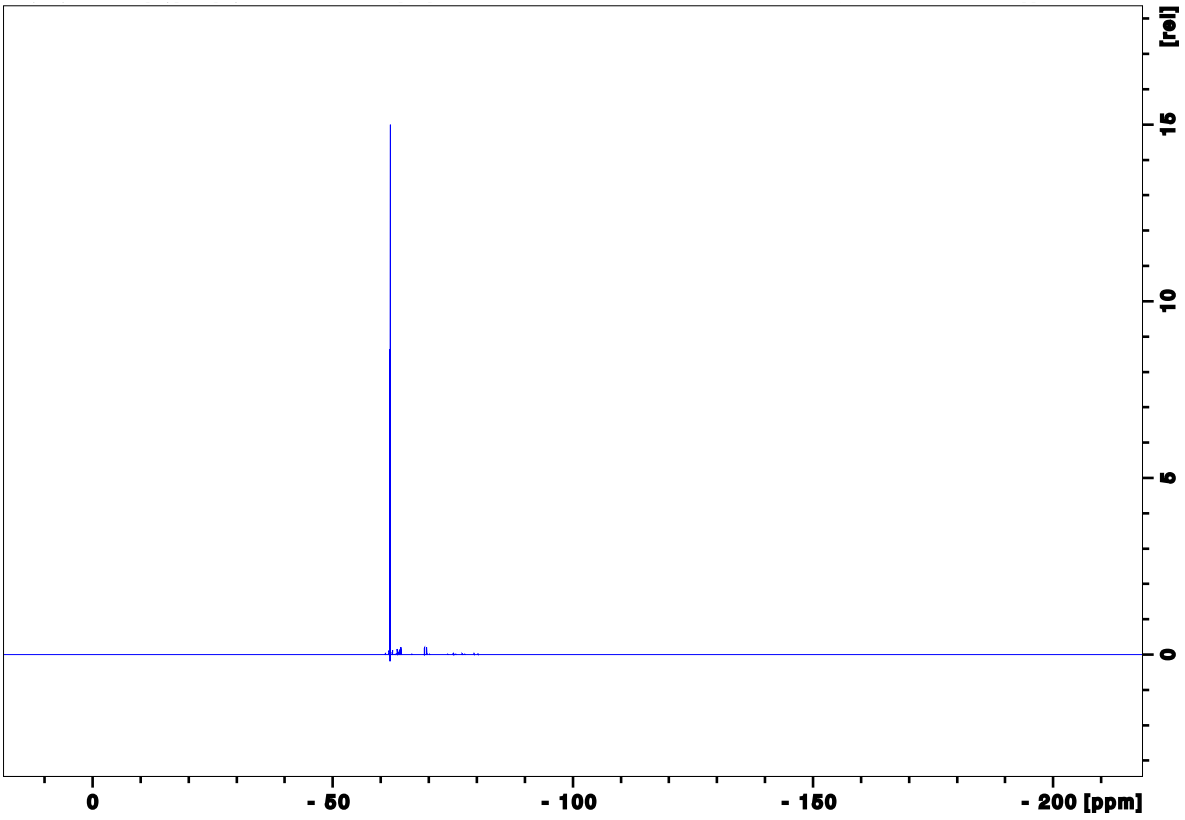

D17: ^{19}F NMR spectrum for 1-(4-(tert-butyl)phenyl)-3,3,3-trifluoropropan-1-one

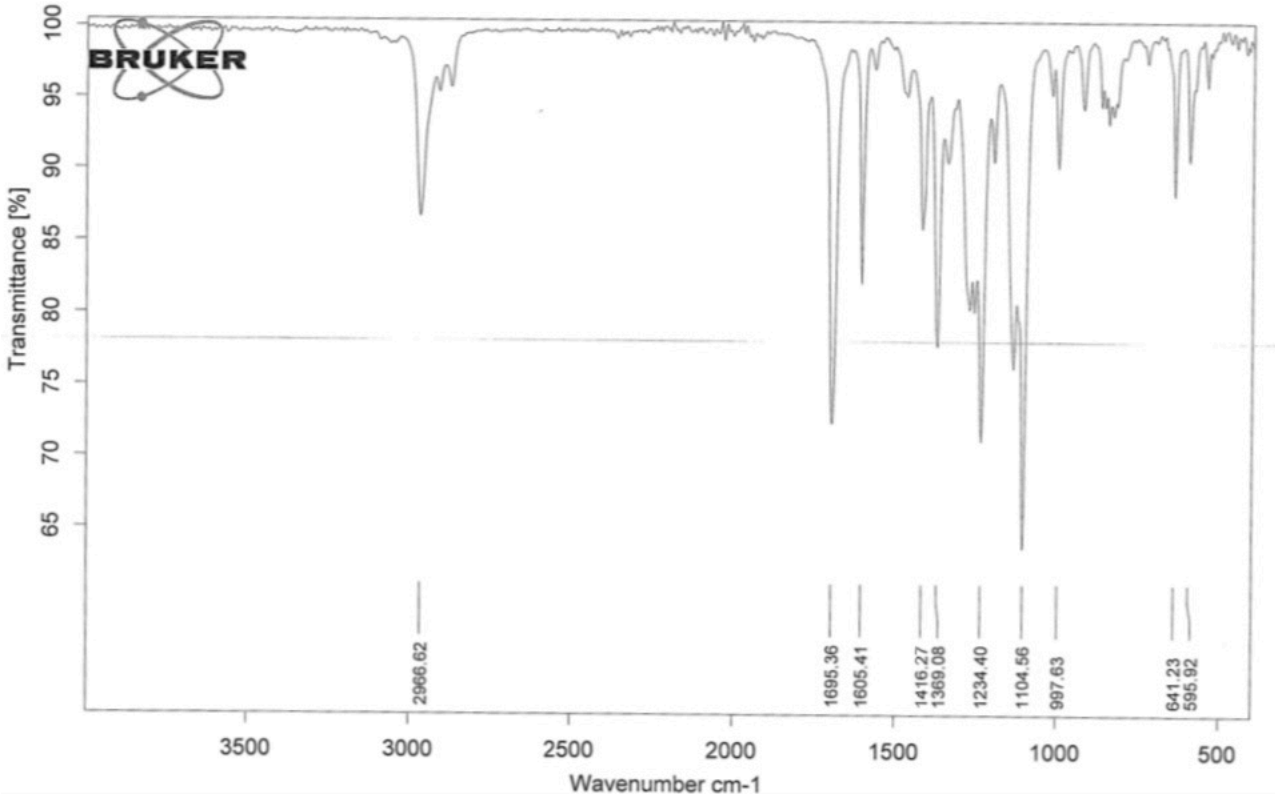

D18: IR spectrum for 1-(4-(tert-butyl)phenyl)-3,3,3-trifluoropropan-1-one 70d